

**Faculty of Science and Engineering
Department of Chemical Engineering**

**Modeling of Liquid-Solid Circulating Fluidised Bed for Continuous Purification
of Kafirin**

Pei Wen Lau

**This thesis is presented for the Degree of
Doctor of Philosophy
of
Curtin University**

March 2014



DECLARATION

To the best of my knowledge and belief this thesis contains no material previously published by any other person except where due acknowledgement has been made. This thesis contains no material which has been accepted for the award of any other degree or diploma in any university.

Signature of Student Pei Wen Lau

Date 18 March 2014

ABSTRACT

Kafirin is a prolamin protein of value for novel biomaterial development. Kafirin is recoverable from sorghum grain seeds, but its hydrophobicity currently limits its industrial production in a food-compatible form. A liquid-solid circulating fluidised bed (LSCFB) system may allow high throughput kafirin purification to be possible by simultaneously performing its adsorption and desorption allowing for a continuous operation. A typical LSCFB ion-exchange system consists of a downer and a riser, integrating adsorption and desorption operations simultaneously. The LSCFB system dynamics are complex and influenced by many parameters. A computational model to quantitatively describe such a system is thus highly desirable.

In this study, the concept of LSCFB was introduced and applied for continuous purification of kafirin using ion exchanger matrices. A general purpose, extensible and dynamic model based on the tanks-in-series framework was developed. The model was validated with previously published data on the extraction of bovine serum albumin as the model protein. Studies regarding the kinetics and equilibrium characteristics of kafirin adsorption onto the ion exchangers have been conducted to better understand the mass transfer, adsorption capacity and affinity of kafirin adsorption onto ion exchangers. The parameters derived from equilibrium and kinetic experiments, and from empirical correlations were incorporated into the model validated earlier. Model predictions for kafirin purification in the LSCFB ion-exchange system were conducted under different operating conditions, including the degree of mixing, the solids circulation rate, the liquid velocities in circulating fluidised beds, and the feed concentration. The kafirin production rate, the fraction of kafirin recovered, and the resin inventory required, were indicative of the LSCFB performance.

A close scrutiny of the sensitivity study revealed that some of the operating parameters tested previously acted in a conflicting manner in which none of the system performance rating could be raised without degrading some of the other performance ratings. With these parameters influencing the LSCFB differently, it can be expected that the system to have discontinuous, or non-smooth performance ratings. The elitist non-dominated sorting genetic algorithm was used to optimize the two most important LSCFB ratings, the production rate and overall recovery. The Pareto frontier solution was generated to capture the interaction between the system parameters, and to provide some insight of their operability range, amongst which a suitable operating point could be selected based on the specific requirements in the LSCFB system.

CO-AUTHORSHIP STATEMENT

Title: Modeling and Numerical Simulation of Liquid-Solid Circulating Fluidised Bed System for Protein Purification.

Authors: Lau, P.W., R. Utikar, V. Pareek, S. Johnson, S. Kale, and A. Lali.

Publication: Chem. Eng. Res. Des. 91(9): 1660-1673.

Relevance: Thesis, Chapter 3.

Contribution: All computational tasks were carried out by P.W. Lau, under the supervision of Dr. R. Utikar. All the drafts were written by P.W. Lau. Modifications were done under the supervision of the supervisors.

Title: Kafirin Adsorption on Ion-Exchange Resins: Isotherm and Kinetic Studies.

Authors: Kumar, P., P.W. Lau, S. Kale, S. Johnson, V. Pareek, R. Utikar, and A. Lali.

Publication: Paper accepted by J. Chromatogr. A.

Relevance: Thesis, Chapter 4.

Contribution: All computational tasks were carried out by P.W. Lau, under the supervision of Dr. R. Utikar. All experiments were carried out under the assistance of P.W. Lau. All the drafts were co-written by P. Kumar and P.W. Lau. Modifications were done under the supervision of the supervisors.

Title: Investigations in Adsorption-Desorption Phenomena of Kafirin on Ion-Exchange Matrix

Authors: Kumar, P., P.W. Lau, S.B. Kale, A.M. Lali, V. Pareek, S. Johnson, and R.P. Utikar.

Publication: Paper submitted to Prep. Biochem. Biotechnol.

Relevance: Thesis, Chapter 4.

Contribution: All experiments were designed and carried out under the assistance of P.W. Lau. Part of the results and discussion were also contributed by P.W. Lau.

Title: Modeling and Simulation of LSCFB for Large Scale Purification of Kafirin

Authors: Lau, P.W., P. Kumar, R.P. Utikar, V.K. Pareek, S.B. Kale, A.M. Lali, S.K. Johnson.

Publication: Paper to be submitted to Chemical Engineering Journal

Relevance: Thesis, Chapter 5.

Contribution: All computational tasks were carried out by P.W. Lau, under the supervision of Dr. R. Utikar. All the drafts were written by P.W. Lau. Modifications were done under the supervision of the supervisors.

Title: Multi-Objective Optimisation (MOO) of Liquid-Solid Circulating Fluidised Bed (LSCFB) for Continuous Kafirin Purification using Ion-Exchange Chromatography.

Authors: Lau, P.W., P. Kumar, V. Pareek, S. Johnson, S. Kale, and A. Lali.

Publication: Paper accepted for oral presentation at Chemeca 2014

Relevance: Thesis, Chapter 6.

- Contribution:** All computational tasks were carried out by P.W. Lau, under the supervision of Dr. R. Utikar. All the drafts were written by P.W. Lau. Modifications were done under the supervision of the supervisors.
- Title:** Modelling and Numerical Simulation of Liquid-Solid Circulating Fluidised Bed Systems
- Authors:** Lau, P.W., R. Utikar, V. Pareek, S. Johnson, S. Kale, and A. Lali. 2012.
- Publication:** Chemeca 2012: Quality of Life Through Chemical Engineering, Wellington, New Zealand, 23-26 September 2012, 139-149. Barton, A.C.T.: Engineers Australia. (Conference Oral Presentation)
- Relevance:** Thesis, Chapter 3.
- Contribution:** All computational tasks were carried out by P.W. Lau, under the supervision of Dr. R. Utikar. All the drafts were written by P.W. Lau. Modifications were done under the supervision of the supervisors.
- Title:** Kinetics of Kafirin Sorption and Desorption using Chromatography.
- Authors:** Lau, P.W., P. Kumar, R. Utikar, V. Pareek, S. Kale, and S. Johnson.
- Publication:** Chemeca 2013: Challenging Tomorrow 2013, Brisbane Convention and Exhibition Centre, Queensland/ Chemical College, Engineers Australia, 29 September – 2 October 2013, 30342. Brisbane, Q.L.D.: Chemeca 2013. (Conference Poster Presentation)
- Relevance:** Thesis, Chapter 4.
- Contribution:** All computational tasks were carried out by P.W. Lau, under the supervision of Dr. R. Utikar. All the drafts were written by P.W. Lau. Modifications were done under the supervision of the supervisors.
- Title:** Modeling Continuous Kafirin Purification in LSCFB.
- Authors:** Lau, P.W., P. Kumar, R. Utikar, V. Pareek, S. Kale, A. Lali, and S. Johnson.
- Publication:** Bioprocessing India 2013, Indian Institute of Technology Delhi, India, 5-7 December 2013. New Delhi, India. (Conference Poster Presentation)
- Relevance:** Thesis, Chapter 4.
- Contribution:** All computational tasks were carried out by P.W. Lau, under the supervision of Dr. R. Utikar. All the drafts were written by P.W. Lau. Modifications were done under the supervision of the supervisors.

ACKNOWLEDGEMENTS

First, I want to express my heartfelt gratitude to my supervisor, Dr. Ranjeet P. Utikar. It has been an honour to be his first Ph.D. student. He has supported, helped and become a role model for me, without whom this Ph.D. work could not culminate in such a result. His joy and enthusiasm for his research has fostered and fortified mine, even during tough times in the Ph.D. pursuit.

The members of the kafirin purification group have contributed immensely to my Ph.D. time at Curtin. I am especially grateful to Prashant Kumar who was here as a university associate a couple of years ago. I very much appreciated his guidance on the kafirin purification experiments, which contributed much to the success of this Ph.D. work. My appreciation extends to Professor Vishnu K. Pareek, Dr. Stuart K. Johnson and Dr. Sandeep B. Kale for their encouragements and constructive advices.

I would also like to thank my examiners, Dr. Potumarthi and Dr. P. R. Naren, who provided encouraging and constructive comments. To the many anonymous reviewers at the various conferences, thank you for helping to shape and guide the direction of the work with your careful and instructive comments.

I gratefully acknowledge the funding sources that made my Ph.D. work possible. The Department of Chemical Engineering, Curtin University has funded my study. The Australian Department of Industry, Innovation, Climate Change, Science, Research and Tertiary Education also provided funding for the kafirin purification project.

To the staff and students at Curtin whom I have had the privilege to interact past working constraints and become good friends with, thank you all for making my time at Curtin enjoyable.

I would not have contemplated this journey if not for my loving parents, who instilled within me a passion for learning new knowledge. To my parents, thank you.

Last, but not least, to Augustine, with love. Without you, I would not have succeeded.



TABLE OF CONTENTS

DECLARATION	i
ABSTRACT	ii
CO-AUTHORSHIP STATEMENT	iii
ACKNOWLEDGEMENTS	v
TABLE OF CONTENTS	vi
LIST OF TABLES	ix
LIST OF FIGURES	xi
NOMENCLATURE	xiv
CHAPTER 1 GENERAL INTRODUCTION	1
1.1 Introduction	1
1.2 Significance and Objectives	3
1.3 Thesis Structure	4
CHAPTER 2 LITERATURE REVIEW	7
2.1 Introduction	7
2.1.1 Sorghum Seed Protein Kafirin	7
2.1.2 Kafirin Extraction	7
2.1.3 Uses of Kafirin	12
2.2 Preparative Ion Exchange Chromatography	17
2.2.1 Principles of Ion Exchange Chromatography	18
2.2.2 Characteristics of Ion Exchangers	22
2.3 Continuous Adsorption Based Chromatographic Systems	26
2.3.1 Fixed-Bed Chromatography	27
2.3.2 Fluidised-Bed Chromatography	30
2.3.3 Simulated Moving Bed Chromatography	31
2.3.4 Continuous Annular Chromatography	34
2.3.5 Liquid-Solid Circulating Fluidised Bed Chromatography	35
2.4 Modeling Continuous Chromatographic Systems	37
2.4.1 Mass Transport Models	39
2.4.2 Fluid Dynamic	43
2.5 Conclusion	48
CHAPTER 3 LIQUID-SOLID CIRCULATING FLUIDISED BED SYSTEM: DESCRIPTION AND MODELING	49
3.1 Introduction	49
3.2 LSCFB Chromatographic System	49
3.2.1 Standard Protein and Ion Exchanger	52
3.2.2 Fluidised Beds	53
3.2.3 Distributors	53
3.2.4 Liquid-Solids Separator and Washing Sections	55
3.2.5 Solids Return Pipes	56
3.3 LSCFB Hydrodynamic Regions and Transitions	59
3.3.1 Downer Hydrodynamics	59
3.3.2 Riser Hydrodynamics	60
3.4 Model Development	64
3.4.1 Model Assumptions	65
3.4.2 Formulation of Downer	65



3.4.3 Formulation of Riser	69
3.5 Numerical Simulation	72
3.6 Model Validation	74
3.7 Results and Discussion	74
3.7.1 Effects of Solids Circulation Rate	76
3.7.2 Effects of Superficial Liquid Velocity in Downer	78
3.7.3 Effects of Superficial Liquid Velocity in Riser	78
3.7.4 Effects of Feed Concentration	81
3.8 Conclusion	81
CHAPTER 4 KAFIRIN ADSORPTION CHROMATOGRAPHY: ISOTHERM AND KINETIC ANALYSIS	83
4.1 Introduction	83
4.2 Experimental	83
4.2.1 Materials	83
4.2.2 Adsorption Equilibrium Experiments	84
4.2.3 Kinetic Uptake Experiments	87
4.2.4 Model Fitting Routine	88
4.3 Results and Discussion	89
4.3.1 Equilibrium Adsorption Analysis	89
4.3.2 Langmuir Isotherm Model	93
4.3.3 Freundlich Isotherm Model	94
4.3.4 Ion Exchanger Selection	95
4.3.5 Uptake Kinetic Analysis	96
4.4 Conclusion	104
CHAPTER 5 LIQUID-SOLID CIRCULATING FLUIDISED BED SYSTEM: MODELING CONTINUOUS KAFIRIN PURIFICATION	105
5.1 Introduction	105
5.2 Simulation of Continuous Kafirin Purification in LSCFB	105
5.2.1 Modeling Basis	105
5.2.2 Model Equations and Solutions	106
5.2.3 Isotherm and Kinetic Data	109
5.3 Results and Discussion	110
5.3.1 Selection of Ion Exchangers	110
5.3.2 Estimation of Model Parameters	111
5.3.3 Performance of Different Ion Exchangers in LSCFB Operation	115
5.3.4 Start-Up Dynamics of LSCFB	117
5.3.5 LSCFB Flow Configuration	118
5.3.6 Effects of LSCFB Operating Parameters	122
5.4 Conclusion	128
CHAPTER 6 LIQUID-SOLID CIRCULATING FLUIDISED BED SYSTEM: MULTIOBJECTIVE OPTIMISATION FOR CONTINUOUS KAFIRIN PURIFICATION	130
6.1 Introduction	130
6.2 Formulation of Multiobjective Problems	130
6.3 Elitist Non-Dominated Sorting Genetic Algorithm Solver	133
6.3.1 Input Parameters	134
6.3.2 Flow Diagram	136



6.4 Results and Discussion	138
6.5 Conclusion	143
CHAPTER 7 CONCLUSIONS AND RECOMMENDATIONS	144
7.1 Conclusions	144
7.1.1 Liquid-Solid Circulating Fluidised Bed System: Description and Modeling	144
7.1.2 Kafirin Adsorption Chromatography: Isotherm and Kinetic Analysis	145
7.1.3 Liquid-Solid Circulating Fluidised Bed System: Modeling Continuous Kafirin Purification	146
7.1.4 Liquid-Solid Circulating Fluidised Bed System: Multiobjective Optimisation for Continuous Kafirin Purification	147
7.2 Recommendations for Future Work	147
REFERENCES	149
CURRICULUM VITAE	169

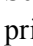

LIST OF TABLES

Table 2.1	United States sorghum production and utilization statistics.	8
Table 2.2	World sorghum production and consumption statistics by different countries.	9
Table 2.3	Kafrin extraction procedures and solvents used.	14
Table 2.4	Adsorption based chromatographic principles and uses.	19
Table 2.5	Commonly used ion exchangers for proteins separation.	20
Table 2.6	Continuous chromatographic systems and their characteristics.	29
Table 2.7	Mass transport models of chromatographic protein separation.	42
Table 2.8	Drag correlations and proposed range of applicability.	46
Table 2.9	Bed expansion correlations of chromatographic systems.	47
Table 3.1	Liquid-solid circulating fluidised bed dimensions and design specifications.	51
Table 3.2	Liquid-solid circulating fluidised bed operating parameters.	69
Table 3.3	Simulation results under different solids circulation rate, G_s ($c_{od}=2\text{kg/m}^3$; $U_{ld}=0.6\text{m/s}$; $U_{lr}=11.3\text{mm/s}$; $S=3\text{kg}$).	77
Table 3.4	Simulation results under different downer liquid superficial liquid velocity, U_{ld} ($c_{od}=2\text{kg/m}^3$; $G_s=1.24\text{kg/m}^2/\text{s}$; $U_{lr}=11.3\text{mm/s}$; $S=3\text{kg}$).	79
Table 3.5	Simulation results under different riser superficial liquid velocity, U_{lr} ($c_{od}=2\text{kg/m}^3$; $G_s=1.24\text{kg/m}^2/\text{s}$; $U_{ld}=0.60\text{mm/s}$; $S=3\text{kg}$).	80
Table 3.6	Simulation results under different initial protein concentration, c_{od} ($G_s=1.24\text{kg/m}^2/\text{s}$; $U_{ld}=0.60\text{mm/s}$; $U_{lr}=11.3\text{mm/s}$; $S=3\text{kg}$).	82
Table 4.1	Specifications of ion exchangers.	85
Table 4.2	Summary of results from Langmuir and Freundlich isotherm models.	90
Table 4.3	Summary of results from film-pore diffusion model for adsorption kinetics experiments.	103
Table 5.1	Characteristics of the commercial ion exchangers evaluated.	112
Table 5.2	Parameter estimates used in the isotherm and second-order equations.	114
Table 5.3	Process conditions for base case steady-state simulation runs.	115
Table 5.4	Steady-state liquid-solid circulating fluidised bed performance of different ion exchangers at base case conditions.	116
Table 5.5	Steady-state liquid-solid circulating fluidised bed performance of UNOsphere Q at different hydraulics of downer dense region.	119
Table 5.6	Steady-state liquid-solid circulating fluidised bed performance of UNOsphere Q at different hydraulics of riser distributor region.	120
Table 5.7	Steady-state liquid-solid circulating fluidised bed performance of UNOsphere Q at different hydraulics of riser upper dilute region.	121
Table 5.8	Steady-state liquid-solid circulating fluidised bed performance of UNOsphere Q at various solids circulation rate, G_s ($c_{od}=2\text{kg/m}^3$; $U_{ld}=0.6\text{mm/s}$; $U_{lr}=5.28\text{mm/s}$; $h_{d,\text{eff}}=0.8\text{m}$).	123
Table 5.9	Steady-state liquid-solid circulating fluidised bed performance of UNOsphere Q at various downer liquid velocity, U_{ld} ($c_{od}=2\text{kg/m}^3$; $G_s=1.24\text{kg/m}^2/\text{s}$; $U_{lr}=5.28\text{mm/s}$; $h_{d,\text{eff}}=0.8\text{m}$).	125
Table 5.10	Steady-state liquid-solid circulating fluidised bed performance of UNOsphere Q at various riser liquid velocity, U_{lr} ($c_{od}=2\text{kg/m}^3$; $G_s=1.24\text{kg/m}^2/\text{s}$; $U_{ld}=0.60\text{mm/s}$; $h_{d,\text{eff}}=0.8\text{m}$).	126
Table 5.11	Steady-state liquid-solid circulating fluidised bed performance of UNOsphere Q at various initial feed concentration, c_{od} ($G_s=1.24\text{kg/m}^2/\text{s}$; $U_{ld}=0.60\text{mm/s}$; $U_{lr}=5.28\text{mm/s}$; $h_{d,\text{eff}}=0.8\text{m}$).	127
Table 6.1	Parameters used in elitist non-dominated sorting genetic algorithm solver and their values.	134



Table 6.2	Decision variables and objective functions for point A to C in the Pareto-optimal frontier plot.	138
Table 6.3	Process conditions for base case steady-state simulation runs.	142

LIST OF FIGURES

Figure 1.1	Flow diagram of research methodology	5
Figure 2.1	Macroscopic schematic of protein molecules in bulk solution showing the locations of mass transfer and dispersive mechanisms. 1. liquid transport; 2. film diffusion, 3a. pore diffusion; 3b. surface diffusion; 4. surface reaction at phase boundary.	24
Figure 2.2	Schematic diagrams of (a) fixed-bed chromatography, and (b) fluidised-bed chromatography.	28
Figure 2.3	Schematic diagram of simulated moving bed chromatography.	32
Figure 2.4	Schematic diagram of simulated moving bed chromatography principle.  slow-moving liquid flow,  fast-moving liquid flow.	32
Figure 2.5	Schematic diagram of rotating annular chromatography.	34
Figure 2.6	Schematic diagram of liquid-solid circulating fluidised bed chromatography.	36
Figure 3.1	Schematic of the liquid-solid circulating fluidised bed system containing ion exchange particles.	50
Figure 3.2	Schematic of the distributors in the liquid-fluidised beds system. (a) downer distributor; (b) riser distributor.	54
Figure 3.3	Schematic of the dynamic seals in a liquid-solid circulating fluidised beds system. (a) liquid-solids separator, top washing section and dynamic seal; (b) bottom washing section and dynamic seal.	57
Figure 3.4	Flow diagram of the liquid-solid circulating fluidised beds. Segregation of the downer in M_d number of solid phase tanks and N_d number of liquid phase sub tanks per solid tank.	61
Figure 3.5	Flow diagram of the liquid-solid circulating fluidised beds. Segregation of the riser in M_{r1} number of solid phase tanks and N_{r1} number of liquid phase sub tanks per solid tank in freeboard region, and M_{r2} number of solid phase tanks and N_{r2} number of liquid phase sub tanks per solid tank in upper dilute region.	63
Figure 3.6	Schematic representations of liquid-phase (a) i_d -th sub tank, (b) 1st sub tank, and (c) $M_d N_d$ -th sub tank in the downer.	66
Figure 3.7	Schematic representations of solid-phase (a) j_d -th tank, (b) 1st tank, and (c) M_d -th tank in the downer.	67
Figure 3.8	Schematic representations of liquid-phase (a) i_r -th sub tank, (b) 1st sub tank, and (c) $M_r N_r$ -th sub tank in the riser.	70
Figure 3.9	Schematic representations of solid-phase (a) tank- j_r , (b) tank-1, and (c) tank- M_r in the riser.	71
Figure 3.10	Algorithm for simulating the liquid-solid circulating fluidised bed system by tanks-in-series model.	73
Figure 3.11	Experimental and theoretical liquid phase protein concentration profiles under different (a) solids circulation rate, G_s , (b) superficial liquid velocity in the downer, U_{ld} , (c) superficial liquid velocity in the riser, U_{lr} . Symbols and solid lines correspond to experimental and predicted curves, respectively.	75
Figure 3.12	Liquid phase protein concentration profile in (a) the downer, and (b) the riser under different solids circulation rate, G_s ($c_{od}=2\text{kg/m}^3$; U_{ld}	77

	$=0.6\text{mm/s}$; $U_{lr}=11.3\text{mm/s}$; $S=3\text{kg}$).	
Figure 3.13	Liquid phase protein concentration profile in (a) the downer, and (b) the riser under different superficial liquid velocity in the downer, U_{ld} ($c_{od}=2\text{kg/m}^3$; $G_s=1.24\text{kg/m}^2/\text{s}$; $U_{lr}=11.3\text{mm/s}$; $S=3\text{kg}$).	79
Figure 3.14	Liquid phase protein concentration profile in (a) the downer, and (b) the riser under different superficial liquid velocity in the riser, U_{lr} ($c_{od}=2\text{kg/m}^3$; $G_s=1.24\text{kg/m}^2/\text{s}$; $U_{ld}=0.60\text{mm/s}$; $S=3\text{kg}$).	80
Figure 3.15	Liquid phase protein concentration profile in the downer under different feed concentration, c_{od} ($G_s=1.24\text{kg/m}^2/\text{s}$; $U_{ld}=0.60\text{mm/s}$; $U_{lr}=11.3\text{mm/s}$; $S=3\text{kg}$).	82
Figure 4.1	Experimental and theoretical results for kafirin adsorption equilibrium on (a) UNOsphere Q, (b) ReliSorb QA-400, (c) Tulsion A-36MP, (d) Toyopearl QAE-550C, (e) Toyopearl SuperQ-650M, (f) Toyopearl SP-550C, (g) Toyopearl SP-650M. Symbols and solid lines correspond to experimental and isotherm curves, respectively.	92
Figure 4.2	Experimental results for kafirin adsorption equilibrium on ion exchangers at different initial kafirin solution concentrations.	95
Figure 4.3	Experimental and theoretical results for kafirin adsorption to (a) UNOsphere Q, (b) ReliSorb QA-400, (c) Tulsion A-36MP, (d) Toyopearl QAE-550C, (e) Toyopearl SuperQ-650M, (f) Toyopearl SP-550C, (g) Toyopearl SP-650M. Symbols and solid line correspond to experimental and theoretical curve, respectively.	100
Figure 4.4	Pore-liquid concentration profiles for kafirin adsorption at different radial position in UNOsphere Q particle.	102
Figure 4.5	Pore-liquid concentration profiles for kafirin adsorption on UNOsphere Q at different time step.	102
Figure 5.1	Flow diagram of the liquid-solid circulating fluidised beds. Segregation of the downer in M_d number of solid phase tanks and N_d number of liquid phase subtanks per solid tank.	107
Figure 5.2	Flow diagram of the liquid-solid circulating fluidised beds. Segregation of the riser in M_{r1} number of solid phase tanks and N_{r1} number of liquid phase subtanks per solid tank in freeboard region, and M_{r2} number of solid phase tanks and N_{r2} number of liquid phase subtanks per solid tank in upper dilute region.	108
Figure 5.3	Concentration profiles analysis of the kafirin purification data on UNOsphere Q (a) equilibrium data, (b) desorption data. Symbols and solid line correspond to experimental and predicted curve, respectively.	113
Figure 5.4	Dynamic profiles of kafirin concentration during liquid-solid circulating fluidised bed start-up. (a) Downer dynamic profile of dimensionless kafirin concentration for UNOsphere Q. (b) Riser dynamic profile of dimensionless kafirin concentration for UNOsphere Q.	118
Figure 5.5	Concentration profiles analysis of (a) downer steady-state adsorption profile, (b) riser steady-state desorption profile for UNOsphere Q on the effects of changes in the solids circulation rate, G_s ($c_{od}=2\text{kg/m}^3$; $U_{ld}=0.6\text{mm/s}$; $U_{lr}=5.28\text{mm/s}$; $h_{d,\text{eff}}=0.8\text{m}$).	123
Figure 5.6	Concentration profiles analysis of (a) downer steady-state adsorption	125

	profile, (b) riser steady-state desorption profile for UNOsphere Q on the effects of changes in the downer liquid velocity, U_{ld} ($c_{od}=2\text{kg/m}^3$; $G_s=1.24\text{kg/m}^2/\text{s}$; $U_{lr}=5.28\text{mm/s}$; $h_{d,\text{eff}}=0.8\text{m}$).	
Figure 5.7	Concentration profiles analysis of (a) downer steady-state adsorption profile, (b) riser steady-state desorption profile for UNOsphere Q on the effects of changes in the riser liquid velocity, U_{lr} ($c_{od}=2\text{kg/m}^3$; $G_s=1.24\text{kg/m}^2/\text{s}$; $U_{ld}=0.60\text{mm/s}$; $h_{d,\text{eff}}=0.8\text{m}$).	126
Figure 5.8	Concentration profiles analysis of (a) downer steady-state adsorption profile, (b) riser steady-state desorption profile for UNOsphere Q on the effects of changes in the initial feed concentration, c_{od} ($G_s=1.24\text{kg/m}^2/\text{s}$; $U_{ld}=0.60\text{mm/s}$; $U_{lr}=5.28\text{mm/s}$; $h_{d,\text{eff}}=0.8\text{m}$).	127
Figure 6.1	Flowchart explaining the multiobjective optimisation process by elitist non-dominated sorting genetic algorithm solver.	137
Figure 6.2	Results for maximisation of P and R . (a) Set of Pareto-optimal solutions, (b-f) Values of decision variables corresponding to the Pareto-optimal solutions shown in (a). Symbol \times indicates base case operating point.	140
Figure 6.3	Calculated amount of the solids inventory required corresponding to the Pareto-optimal solutions for maximization of kafrin production rate and overall recovery. Kafrin production rate (o) and recovery (Δ) against amount of the solids required.	143



NOMENCLATURE

LATIN LETTERS

a	Specific surface area, L^2/L^3
A_b	Bottom solids return pipe cross sectional area, L^2
A_d	Downer cross-sectional area, L^2
A_t	Top solids return pipe cross-sectional area, L^2
Ar	Archimedes number, $Ar=d_p^3 \rho_l g (\rho_p - \rho_l) / \mu^2$, dimensionless
A_r	Riser cross-sectional area, L^2
A_{sep}	Liquid-solids separator cross-sectional area, L^2
Bi	Biot number, $Bi=r_p k_f / D_p$, dimensionless
C_D	Drag coefficient, dimensionless
c_e	Equilibrium liquid phase concentration, M/L^3
c_{ed}	Downer raffinate protein concentration, M/L^3
c_{eq}	Liquid-phase equilibrium concentration, M/L^3
c_{er}	Riser extract liquid-phase concentration, M/L^3
c_i	Bulk-liquid phase concentration at i -th time or tank number, M/L^3
$c_{i,d}$	Downer i -th subtank protein liquid-phase concentration, M/L^3
$c_{i,r}$	Riser i -th tank protein liquid-phase concentration, M/L^3
c_o	Initial bulk phase concentration, M/L^3
c_{od}	Downer entering liquid-phase concentration, M/L^3
c_{or}	Riser entering liquid-phase concentration, M/L^3
$c_{p,i}$	Pore-liquid phase concentration at i -th time or tank number, M/L^3
$c_{p,o}$	Initial pore-liquid phase concentration, M/L^3
D	Column diameter, L
D_{ax}	Axial dispersion coefficient, L^2/T
D_b	Bottom solids return pipe diameter, L
D_c	Column diameter, L
D_m	Molecular dispersion coefficient, L^2/T
D_p	Pore diffusion coefficient, L^2/T
d_p	Particle diameter, L
D_t	Top solids return pipe diameter, L
D_r	Riser diameter, L
D_s	Surface diffusion coefficient, L^2/T
D_{sep}	Liquid-solids separator diameter, L
F	Force exerting on a particle, LM/T^2
F_s	Force exerting on a sphere, LM/T^2
G	Gravitational acceleration, L/T^2
Ga	Galileo number, $Ga=d_p^3 g (\rho_p - \rho_l) / \mu^2$, dimensionless
G_s	Solids circulation rate, $M/L^2/T$
$h_{d,eff}$	Downer effective bed height, L
h_{ld}	Downer liquid-phase subtank height, L
h_{lr}	Riser liquid-phase subtank height, L



H_r	Riser height, L
h_{r1}	Riser distributor region height, L
h_{r2}	Riser upper dilute region height, L
h_{sd}	Downer solid-phase tank height, L
h_{sep}	Liquid-solids separator height, L
h_{sr}	Riser solid-phase tank height, L
k_1	First-order kinetic mass transfer coefficient, 1/T
k_2	Second-order kinetic mass transfer coefficient, L ³ /M/T
$k_{1,ps}$	Pseudo-first-order kinetic mass transfer coefficient, 1/T
$k_{2,ps}$	Pseudo-second-order kinetic mass transfer coefficient, L ³ /M/T
k_{ads}	Reversible kinetic adsorption coefficient, L ³ /M/T
K_d	Langmuir dissociation coefficient, M/L ³
k_{des}	Reversible kinetic desorption coefficient, 1/T
k_f	Film mass transfer coefficient, L/T
K_L	Lumped mass transfer coefficient, L/T
k_r	Riser desorption coefficient, L/T
k_{r1}	Riser distributor region desorption coefficient, L/T
k_{r2}	Riser upper dilute region desorption coefficient, L/T
L_b	Bottom solids return pipe length, L
L_t	Top solids return pipe length, L
M_d	Downer number of solid tanks, dimensionless
M_r	Riser number of solid tanks, dimensionless
M_{r1}	Riser distributor region number of solid tanks, dimensionless
M_{r2}	Riser upper dilute region number of solid tanks, dimensionless
n	Bed expansion index, dimensionless
N_d	Downer number of liquid subtanks, dimensionless
n_f	Freundlich binding coefficient, dimensionless
N_r	Riser number of liquid subtanks, dimensionless
N_{r1}	Riser distributor region number of liquid subtanks, dimensionless
N_{r2}	Riser upper dilute region number of liquid subtanks, dimensionless
P	Protein production rate, M/T
pI	Isoelectric point, dimensionless
q_e	Equilibrium solid phase concentration, M/L ³
q_{ed}	Downer exiting solid-phase protein concentration, M/L ³
q_{er}	Riser exiting solid-phase protein concentration, M/L ³
q_f	Freundlich adsorption capacity, M/L ³
q_i	Adsorbent phase concentration at i -th time or tank number, M/L ³
$q_{j,d}$	Downer j -th tank protein solid-phase concentration, M/L ³
$q_{j,r}$	Riser j -th tank protein solid-phase concentration, M/L ³
q_m	Langmuir adsorption capacity, M/L ³
q_o	Initial solid phase concentration, M/L ³
q_{od}	Downer entering solid-phase protein concentration, M/L ³
q_{or}	Riser entering solid-phase protein concentration, M/L ³
R	Overall fraction of protein recovery, dimensionless



r	Radial distance along the adsorbent radius, L
R^2	Coefficient of determination, dimensionless
Re_p	Particle Reynolds number, $Re_p = U_{slip} d_p \rho / \mu$, dimensionless
Re_t	Particle terminal Reynolds number, $Re_t = U_t d_p \rho / \mu$, dimensionless
R_L	Langmuir equilibrium constant, $R_L = 1/(1 + bc_o)$, dimensionless
r_p	Particle radius, L
S	Solid particles inventory, M
Sc	Schmidt number, $Sc = \mu / \rho D_m$, dimensionless
t	Time, T
U_i	Superficial liquid velocity at $\varepsilon=1$, L/T
U_l	Superficial liquid-phase velocity, L/T
U_{ld}	Downer superficial liquid velocity, L/T
U_{lr}	Riser superficial liquid velocity, L/T
U_r	Relative velocity between the particle and the bulk liquid, L/T
U_{sd}	Downer superficial solid velocity, L/T
U_{slip}	Superficial slip velocity, L/T
U_{sr}	Riser superficial solid velocity, L/T
U_t	Terminal velocity, L/T
V	Volume per tank, L ³
\dot{V}	Volumetric flowrate, L ³
V'	Total volume of solid pipes and separator, L ³
V_s	Particle volume, L ³
z	Axial distance along the column, L

GREEK LETTERS

ε	Voidage, dimensionless
ε'	Total voidage of solid pipes and separator, dimensionless
ξ	Time, $\xi = r / r_p$, dimensionless
ε_d	Downer voidage, dimensionless
ε_p	Particle porosity, dimensionless
ε_b	Bottom solids return pipe voidage, dimensionless
ε_t	Top solids return pipe voidage, dimensionless
ε_r	Riser voidage, dimensionless
ε_{sd}	Downer solids holdup, dimensionless
ε_{sep}	Liquid-solids separator voidage, dimensionless
ε_{sr1}	Riser distributor region solids holdup, dimensionless
ε_{sr2}	Riser upper dilute region solids holdup, dimensionless
φ	Bulk liquid concentration, $\varphi = c_l / c_o$, dimensionless
φ_m	Langmuir isotherm parameter, $\varphi_m = q_m / c_o$, dimensionless
φ_p	Pore liquid concentration, $\varphi_p = c_p / c_o$, dimensionless
ρ	Bulk solution density, M/L ³
ρ_a	Particle apparent density, M/L ³
ρ_l	Density of bulk liquid, M/L ³
ρ_p	Particle density, M/L ³



ρ_w	Particle wet density, M/L ³
μ	Bulk solution viscosity, M/L/T
τ	Time, $\tau=D_p t/r_p^2$, dimensionless
Γ	Linearized equation, Eq. 4.14, dimensionless
ω	Langmuir isotherm parameter, $\omega=K_d/c_o$, dimensionless
χ	Partial radial position, $\chi=r^2/r_p^2$, dimensionless

ACRONYMS

BSA	Bovine serum albumin
CAC	Continuous annular chromatography
GA	Genetic algorithm
LSCFB	Liquid-solid circulating fluidised bed
LYS	Lysozyme
MOO	Multiobjective optimisation
NSGA-II	Elitist non-dominated sorting genetic algorithm
SAC	Strong acidic cation exchanger
SBA	Strong basic anion exchanger
SMB	Simulated moving bed
WAC	Weak acidic cation exchanger
WBA	Weak basic anion exchanger

CHAPTER 1

GENERAL INTRODUCTION

1.1 INTRODUCTION

The sorghum grain protein, kafirin, has potential as a biomaterial for coatings, biodegradable films, bioplastics, and controlled-release microspheres for food and medical purposes (Buchner 2006, 88; da Silva and Taylor 2005, 9; Elkhalfifa et al. 2009, 159; Park et al. 2002, 318; Pérez-Gago 2012, 13; Taylor et al. 2009, 7523). Kafirins which are highly cross-linked hydrophobic prolamins, account for more than 68% of the total protein content of whole sorghum grains, and no less than 77% of the endosperm (de Mesa-Stonestreet, Alavi and Bean 2010, 91; Hamaker et al. 1995, 583). Under reducing conditions, the individual polypeptides of kafirin range in size from 15 to nearing 30 kDa and are classified into α -, β -, and γ -kafirins by differences in molecular weight, solubility, and structure (Belton et al. 206, 272; Lasztity 1996, 227). Reports of kafirin separation date back as far as 1916 when Johns and Brewster (1916, 59) first extracted kafirin using aqueous ethanol from the sorghum variety Dwarf kafir. Since then kafirins have been separated from sorghum grains, brans, and endosperms by aqueous ethanol at elevated temperature or tertiary butanol at ambient temperature (Johns and Brewster 1916, 59; Taylor, Schüssler, and van der Walt 1984, 151). Until present, most extraction studies on kafirin have focused primarily on batch laboratory-scale separation, for the kafirin hydrophobicity having restrained the establishment of an economical, food-compatible, and non-toxic industrial-scale extraction process.

From a practical viewpoint, studies carried out on aqueous ethanol extraction of kafirin can serve as framework to establish kafirin production at industrial scale. A batch semi-industrial kafirin extraction process has been modified from an existing laboratory-scale process by the Council for Scientific and Industrial Research, South Africa (Kaser 2003). In this process, aqueous ethanol plus sodium metabisulphite and sodium hydroxide were used as the solvent (Erasmus 2003; Kaser 2003). This semi-industrial batchwise process, although simple and easy to control, suffered from two major drawbacks. Firstly, although the process adapts conditions which are effective

when used in laboratory scale extractions, the process is not considered effective since large amounts of fresh solvent is required and the final kafirin solution is very dilute and necessitates downstream solvent evaporation and precipitation to further separate the kafirin. Secondly, the extraction process does not yield kafirin of high purity. In addition, the complex batch process involving multiple steps is difficult to optimize leading to increased production costs and affect the final product quality. Therefore, a continuous system is highly preferable for industrial-scale kafirin production. Liquid-solid circulating fluidised bed (LSCFB) using ion exchangers may be a potential approach for large scale kafirin purification, which can overcome the drawbacks of the previously reported batch process. In addition to the generic benefits of fluidisation, including low and stable pressure drops across the fluidised beds, LSCFB has extra advantages. These include higher throughput, higher heat and mass transfer rates, enhanced interfacial contact, reduced backmixing and improved handling of particles of different sizes and densities, all of which lead to a much more effective production.

The LSCFB systems have emerged in recent years as one of the most promising mass contactor of industrial importance due to their wide applications in processing technology, such as in wastewater treatment, phenol polymerization and lactic acid production (Cui et al. 2004, 699; Trivedi, Bassi and Zhu 2006, 61; Patel et al. 2008, 821). The arrangement and recirculation connections of the LSCFB reactor used were fabricated such that the two fluidised beds were interconnected and were running as anoxic and aerobic beds for simultaneous nitrification and denitrification processes (Cui et al. 2004, 699). Feng et al. (2003, 235) studied caesium separation from high radioactive liquid waste in LSCFB system wherein the riser operated in circulating fluidising region and the downer in the state of slow-moving packed bed. The effects of system dimension on the hydrodynamics behaviour of the LSCFB were also investigated. LSCFB was used in the continuous polymerization reaction of phenol by Trivedi, Bassi and Zhu (2006, 61). In the riser polymerization reaction was carried out and in the downer the regeneration of immobilised enzyme particles (Trivedi, Bassi and Zhu 2006, 61). Reliability and commercial viability analysis on a pilot-scale LSCFB were conducted for a leachate treatment process, and the study result proved that the LSCFB has effectively removed biological nutrients from landfill leachate (Eldyasti et al. 2010, 289). Patel et al. (2008, 821) have conducted

simultaneous fermentative and extractive production of lactic acid from whey. The production and adsorption of lactic acid was carried out in the downer, while recovery or desorption was carried out in the riser.

As mentioned earlier the current semi-industrial kafirin production suffered from low product production volume and purity issues. Therefore a purification method that produces kafirin of high purity consistently, such as the LSCFB, would be highly desirable. The LSCFB adapting ion-exchange chromatography and adsorption have been satisfactorily used for recovery of a variety of plant and animal proteins such as bovine serum albumin (BSA), whey and soy protein indicating that it might be a suitable for purification of kafirin. The research group established by Professor Zhu at the University of Western Ontario studied the effects of important operating parameters on the hydrodynamic behaviour of LSCFB and potential applications for the continuous recovery of BSA, whey and soy protein (Lan et al. 2000, 858; Lan et al. 2001, 157; Mazumder et al. 2009a, 111; Prince et al. 2012, 157). However, a systematic understanding of adsorption and desorption mass transfer processes from a phenomenological perspective is required for successful application of LSCFB for process design and scale-up.

1.2 SIGNIFICANCE AND OBJECTIVES

Kafirin extraction and purification processes are important when considering kafirin-based product commercialization, which not only targets at production at large quantities of purified kafirin but also with high purity for desired applications as biomaterial for coatings, biodegradable films, bioplastics, and controlled-release microspheres for food and medical purposes. Critical to kafirin separation process and the subject of most protein extraction studies are presence of biological broth (Lan et al. 2000, 858; Lan et al. 2001, 157; Nfor et al. 2008, 124). Inefficient protein elicitation from such feed liquor could result in low product yield and increase the potential risks of fouling and plugging in downstream operations. Furthermore, large volumes of sorghum grains must be treated for industrial kafirin purification, implicating domination of the operating expenditure over the overall production cost. Therefore, development of a highly efficient kafirin purification process is of genuine commercial interests. A highly efficient continuous process like the LSCFB

has obviously offered an attractive approach for industrial scale kafirin purification from sorghum grains. The essential concept is that sorghum protein adsorption and desorption processes are conducted in continuous mode.

It is the objective of this study to introduce the concepts of recovering sorghum protein using viable protein extraction and purification process scheme on LSCFB system. Specifically phenomenological modeling and optimisation methods are applied to simulate and optimise the continuous purification process on LSCFB. The LSCFB comprises of two fluidised beds, integrating adsorption (in the downer) and desorption (in the riser) simultaneously. A comprehensive model based on the tanks-in-series framework is developed considering the hydrodynamics, mass transfer, and kinetics. Both sensitivity analysis of process operating parameters and optimisation for multiple objective functions is carried out to gain insight and improve process understanding. Therefore the specific objectives of this study are model development, mass transfer and kinetics, model adaptation, followed by sensitivity studies and optimisation. The flow of the study is clearly presented in Figure 1.1.

1.3 THESIS STRUCTURE

A comprehensive literature review is presented in Chapter 2. In particular, sorghum literature data on seed protein kafirin regarding its properties, uses and processes implemented for its extraction is presented. After this, a review of adsorption-based ion exchange chromatography and its principles are given. Continuous systems adapting ion exchange chromatography are also reviewed, with the emphasis on the applications of these systems in continuous kafirin purification. A brief review of phenomenological modeling of ion exchange chromatography systems along with the fluid dynamic correlations for these systems is also presented.

In Chapter 3, a general purpose, extensible, and dynamic model for LSCFB is presented. The model is written based on the tanks-in-series framework. The model allows for adjusting the backmixing degree in the liquid phase and solid phase for the fluidised beds in the system. The model is validated with the literature data on BSA extraction as the model protein. The interaction between the fluidised beds is captured with the sensitivity analysis using the validated model.

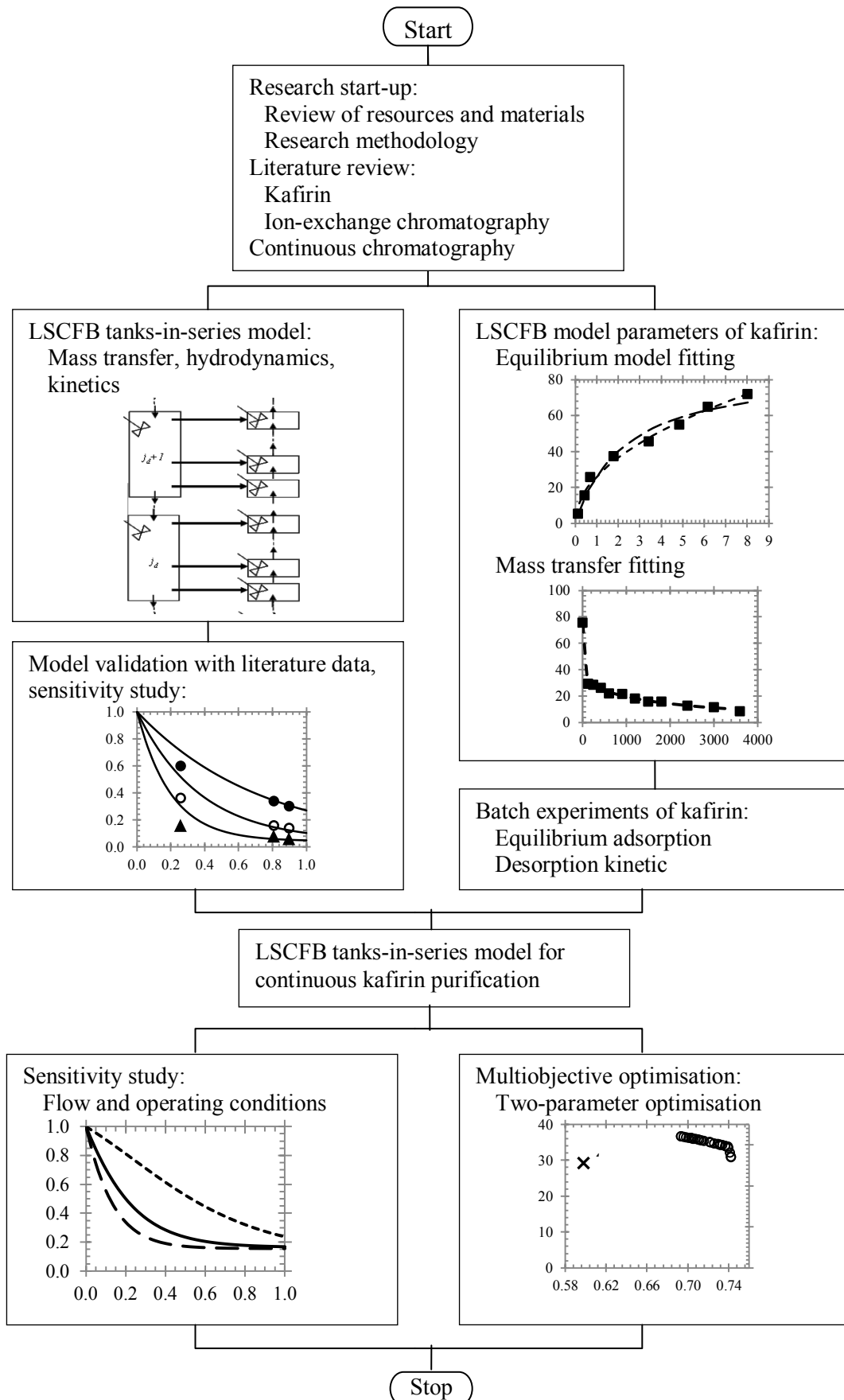


Figure 1.1 Flow diagram of research methodology.

In Chapter 4, the isotherm and kinetic studies of kafirin adsorption on anion- and cation exchangers for practical applications in preparative-scale chromatography are presented. Isotherm parameters such as adsorbent loading capacity and dissociation constant are determined for Langmuir isotherm, and adsorptive capacity and affinity constant for Freundlich isotherm. Batch uptake kinetics for kafirin adsorption on these ion exchangers are also carried out and critical parameters including the diffusion coefficient, film mass transfer coefficient, and Biot's number for diffusion model are calculated. Both the isotherm and the kinetic parameters are considered for selection of appropriate ion exchanger for kafirin purification.

In Chapter 5, the validated model described in Chapter 3 using LSCFB is simulated to predict the behaviour of the system for continuous purification of kafirin. Appropriate modifications are carried out to adopt the model for kafirin purification. Simplified mass transfer models are used, particularly, the lumped adsorption model and second-order desorption model. Continuous kafirin purification in the LSCFB ion exchange system is simulated out under different degree of mixing and operating conditions.

In Chapter 6, multiobjective optimisation study is reported to optimize two performance indicators of the LSCFB model. Important process conditions are chosen as the process decision variables in the study. The controlled elitist genetic algorithm is used in order to obtain a set of Pareto optimal solutions capturing the trade-off between the objective functions over a wide range of non-dominated solutions. The Pareto set solution offers useful insights in deciding the optimal solution for the LSCFB model operation.

Finally, Chapter 7 summarizes the major findings of this study and presents some recommendations for continuous improvement of this novel technology.

CHAPTER 2

LITERATURE REVIEW

2.1 INTRODUCTION

2.1.1 Sorghum Seed Protein Kafirin

Sorghum is an important staple food for the human population. Details of the world sorghum consumption and sorghum utilization of United States are listed in Table 2.1 and Table 2.2, accordingly (USDA 2014a, 2014b). The use of sorghum thus far has been limited in feed and food products. Few value-added applications have been derived for sorghum in other areas. Grain sorghum (*Sorghum bicolor* (L.) Moench) has protein content varying from 6-18%, averaged at 11% (Park and Bean 2003, 7050). Kafirin, the major storage protein in sorghum, is classified as prolamin, and as such, contains high levels of proline and glutamine and is soluble in nonpolar solvents such as aqueous alcohols (Shewry and Tatham 1990, 1). Kafirin account for 68-73% of total protein in whole sorghum grain and 77-82% in sorghum endosperm, whereas non-prolamin proteins such as albumins, globulins, and glutelins account for 30% of total proteins (Belton et al. 2006, 272). The relative molecular mass and isoelectric point (pI) is $M_r \sim 23,000$ and $pI \sim 6.0$ for kafirin (Shull, Watterson, and Kirleis 1991, 83; Anyango, de Kock, and Taylor 2011, 2126). Kafirin have been categorised into different subclasses, namely α -, β -, and γ -kafirins, on basis of the molecular weight, solubility, and structure. Sorghum endosperm constitute of about 66-84% α -kafirin, 8-13% β -kafirin, and 9-21% γ -kafirin (Park and Bean 2003, 7050). Overall, kafirin subclasses are usually loaded with glutamic acid and nonpolar amino acids namely proline, leucine, and alanine, but almost absent with the essential amino acid lysine (Belton et al. 2006, 272).

2.1.2 Kafirin Extraction

Prolamin separations from sorghum have been difficult due to insolubility of prolamins. Aqueous alcohol was first used to extract the prolamin, named as kafirin soon after, from the sorghum variety Dwarf kafir (Johns and Brewster 1916, 59). Virupaksha and Sastry (1968, 199) firstly separated proteins from sorghum endosperms, corresponding to a modification of the classic Osborne and Mendel

Table 2.1 United States sorghum production and utilization statistics.

	Supply (Million Bushels)				Disappearance (Million Bushels)						
	Begin. stocks	Production	Imports	Total supply	Food, alcohol, and industrial	Seed use	Feed and resid. use	Total domestic use	Exports	Total disp.	
2011/12	Q1 Sep-Nov	27	214	0.00	242	25		44	69	22	91
	Q2 Dec-Feb	151		0.05	151	26		6	31	12	43
	Q3 Mar-May	108		0.05	108	26	0.59	15	42	8	50
	Q4 Jun-Aug	59		0.01	59	8	0.19	5	14	22	36
2012/13	MY Sep-Aug	27	214	0.11	242	84	0.77	71	156	63	219
	Q1 Sep-Nov	23	247	1.09	271	25		79	104	27	131
	Q2 Dec-Feb	140		0.06	140	25		4	29	19	48
	Q3 Mar-May	92		5.52	97	25	0.47	17	42	14	56
2013/14	Q4 Jun-Aug	41		2.91	44	19	0.42	-7	13	16	29
	MY Sep-Aug	23	247	9.57	279	94	0.89	93	188	76	264
	Q1 Sep-Nov	15	389	0.01	404	45		94	139	33	173
	Q2 Dec-Feb	231		0.01	231	10		2	12	44	56
2014/15	Q3 Mar-May	176		0.01	176	12	0.41	5	17	66	83
	MY Sep-Aug	15	389	0.02	404	78	0.70	95	174	205	379
	MY Sep-Aug	25	429		455	119	0.70	110	230	190	420

Table 2.2 World sorghum production and consumption statistics by different countries.

	Production (Thousand Metric Tons)					Consumption (Thousand Metric Tons)				
	2011/12	2012/13	2013/14	2014/15 Sep		2011/12	2012/13	2013/14	2014/15 Sep	
Argentina	4,200	4,700	4,200	4,200	Argentina	1,900	2,300	2,700	2,800	
Australia	2,239	2,230	1,107	2,000	Australia	1,105	1,105	805	1,205	
Brazil	2,222	2,102	2,400	2,400	Brazil	2,175	2,300	2,300	2,300	
Burkina	1,500	1,924	1,940	1,900	Burkina	1,500	1,900	1,900	1,900	
Cameroon	1,150	1,100	1,150	1,150	Cameroon	1,175	1,110	1,175	1,175	
Chad	648	1,172	745	900	Chad	650	1,150	850	900	
China	2,051	2,556	2,700	2,800	China	2,200	3,200	6,800	6,500	
Ethiopia	3,951	3,604	4,000	4,000	Ethiopia	3,700	3,700	4,100	4,000	
India	6,030	5,300	5,250	5,300	India	6,000	5,150	5,200	5,200	
Mali	1,191	1,212	1,200	1,200	Japan	1,475	1,900	1,100	1,500	
Maxico	6,425	6,174	7,170	7,000	Mali	1,300	1,200	1,200	1,200	
Niger	807	1,376	1,287	1,200	Maxico	8,100	8,100	7,400	7,300	
Nigeria	6,900	5,943	6,500	6,500	Niger	950	1,200	1,300	1,300	
Sudan	4,605	4,524	2,249	3,800	Nigeria	6,800	5,900	6,450	6,500	
United States	5,447	6,272	9,882	10,926	Sudan	4,500	4,700	2,550	4,100	
Tanzania	807	839	800	800	United States	3,953	4,775	8,698	5,589	
Others	7,072	6,905	7,108	7,106	Others	9,501	9,338	4,293	8,919	
World Total	57,245	57,933	59,688	63,182	World Total	58,488	57,804	59,144	62,628	

(1914, 1) procedure hitherto used for extraction of maize proteins. This method separated proteins into water-soluble albumins, salt-soluble globulins, alcohol-soluble prolamins, and acid- or base-soluble glutelins (Virupaksha and Sastry 1968, 199; Taylor, Schüssler, and van der Walt 1984, 149). This sequential technique, however, has resulted in significant overlapping of protein fractions due to the inefficient separation. Significantly small kafirin amounts were yielded using the same Osborne-Mendel method by Skogh et al. (1970, 472), indicating the insolubility issue of sorghum prolamins when the classic Osborne-Mendel solvent systems and techniques were used. Using the same method, gelling issues that caused the failure to work with sorghum prolamins were reported (Jones and Beckwith 1970, 33; Haikerwal and Mathieson 1971, 142).

A systematic protein separation scheme first suggested for corn maize by Landry and Moureaux (1970, quoted in Taylor, Schüssler and van der Walt 1984, 149) was later adapted for sorghum prolamins. This procedure separated the prolamins into Prolamin I that is extractable in aqueous alcohol alone and Prolamin II that is extractable in aqueous alcohol plus a reducing agent (Taylor, Schüssler, and van der Walt 1984, 149; de Mesa-Stonestreet, Alavi, and Bean 2010, 96). Since then reducing agents such as 2-mercaptoethanol and dithiothreitol, were often employed to assist kafirin separation from sorghum (Jambunathan and Mertz 1973, 692; Paulis and Wall 1979, 20; Wu and Wall 1980, 455).

These changes improved the prolamins extraction from sorghum significantly and enhanced the kafirin yield from Landry-Moureaux method compared to the Osborne-Mendel (Skogh et al. 1970, 480; Jambunathan and Mertz 1973, 692). Hamaker et al. (1995, 584), though, adapted a more efficient extraction method used to extract maize proteins previously by Wallace et al. (1990, 192). Higher kafirin yield in whole grain flours and endosperms was obtained from this method. It circumvents the complicated and cumbersome classification procedures used beforehand wherein sorghum prolamins are divided into different solubility fractions, despite that there is no obvious reasoning for the prolamins subdivision based on solubility differences. Non-prolamins are differentiated from prolamins in this simple method, through the use of a basic buffer, plus additives such as detergent and reducing agent (Hamaker et al. 1995, 586; Park and Bean 2003, 7050).

Kafirin extraction process from different sorghum fractions such as whole sorghum grains, sorghum endosperms, sorghum brans, and sorghum distillers dried grains and solubles has been reported. Sorghum bran is a byproduct of sorghum dry-milling, while sorghum distillers dried grains and solubles is the dried byproduct of alcohol manufacture from sorghum grains (Wang et al. 2009, 8366). Extraction buffer in the presence of additives has been used to extract kafirin from sorghum. While most of the kafirin extraction procedures developed proved that for effective separation either aqueous alcohols at elevated temperature (ethanol) or ambient temperature (tertiary butanol) (Jambunathan and Mertz 1973, 693; Taylor, Schüssler, and van der Walt 1984, 151), or basic buffer containing sodium metabisulphite followed by aqueous tertiary butanol (Hamaker et al. 1995, 584) are needed. While most of the kafirin separation procedures performed up until now has been developed based on the conventional techniques discussed earlier, there have been some advances in the solvent systems used for kafirin separation recently. For example, efforts have been made to replace solvents that may not be suitable for consumption or required extreme process conditions with food-compatible solvents with moderate operation conditions. Pioneering work in this area has been done by Taylor et al. (2005, 485) and Bean et al. (2006, 99). Glacial acetic acid was suggested to replace tertiary butanol, while food-compatible reducing agents such as sodium metabisulphite, glutathione, and cysteine were tested to replace dithiothreitol and 2-mercaptoethanol. The solvent systems functioned as expected, except that to improve kafirin yield, pre-soaking step is required for the combined glacial acetic acid and SMS system.

Sonication has been utilised to improve kafirin extraction. Bean et al. (2006, 99) investigated the effects of various extraction and precipitation conditions, including the use of ultrasound, on recovery and purity of kafirins. Ethanol extraction was performed on whole ground sorghum flour, with and without reducing agents, and with 4 min sonication. Park et al. (2006, 611) also used sonication for extraction of kafirin from sorghum flour. Various extraction buffers containing sodium borate buffer, SDS and different reducing agents were mixed with the sorghum flour, and then sonicated. It is thought that sonication helped to reduce the molecular weight of large proteins by reducing covalent bonds through shear degradation (de Mesa-Stonestreet, Alavi, and Bean 2010, 96). Zhao et al. (2008, 946) also used sonication

to extract kafirin from sorghum. Sorghum meal slurry containing sodium borate and SDS was sonicated for 30 sec to obtain the kafirin. A summary of all the extraction procedures discussed above is shown in Table 2.3.

2.1.3 Uses of Kafirin

Application of kafirin is limited, apart from the difficulty of a consistent kafirin supply. Nevertheless, over the past decade, some potential applications of kafirin have been demonstrated. The narrow range of applicability concerning kafirin may be due to the difficulty in extracting kafirin hence the limited work in finding possible applications for this prolamin. Thus far the kafirin extraction procedures developed and applied in laboratories operate at batch scale, and are particularly cumbersome and difficult to scale up. These consequently results in considerable investment in terms of time and money, with little or no return at all. Nonetheless, kafirin may be considered as a possible substitute for some applications of zein, a maize prolamin homologous to kafirin. Kafirin is much similar to zein in molecular weight, solubility, structure, and amino acid composition (DeRose et al. 1989, 245; Shull, Watterson, and Kirleis 1991, 83; Belton et al. 2006, 272). In fact, kafirin is more hydrophobic and less digestible than zein, so kafirin may be a better biomaterial compared to zein (Taylor, Belton and Minnaar 2009, 7523). This section focuses on major kafirin uses that originated from zein, namely biopolymer films and coatings, and kafirin microparticles, (Buffo, Weller, and Gennadios 1997, 473; Da Silva and Taylor 2005, 9; Taylor et al. 2005, 491; Elkhalfifa et al. 2009, 159; Taylor, Belton and Minnaar 2009, 7523).

Biopolymer Films and Coatings

The film forming properties of plant proteins, particularly zein of maize, have been used in the industries since early in the last century to address deficiency of shellac in lacquers, varnishes, and coatings in industries after the start of World War II (Lawton 2002, 1). Kafirin, being the most hydrophobic of the cereal prolamins, with low digestibility and non-allergenic, may be an alternative to zein in making biopolymers (Duodu et al. 2003, 117; Belton et al. 2006, 272). The terms “coatings” and “films” are often used interchangeably because there is no distinct difference between these two terms. Still, Gennadios and Weller (1990, 63) defined the two separately in which edible coatings are thin layers of edible material directly applied and formed

on the substance surface, while edible films are thin sheet preformed from edible materials before applied to the substance (Gennadios and Weller 1990, 63).

Buffo, Gennadios, and Weller (1997, 473) casted biopolymer films from sorghum gluten meal, a byproduct obtained from wet-milling of sorghum, using the formulation described by Park et al. (1994, 916). Ethanol was used as solvent, while glycerol and polyethylene glycol are plasticizers used to impart adequate flexibility and to obtain free-standing kafirin films (Buffo, Gennadios and Weller 1997, 473). The kafirin films water vapour permeability (WVP) values did not differed much from commercial zein films made plasticised in similar manner. The WVP is a measure of ease with which a film or coating can be permeated by water vapour. A lower WVP value indicates better film performance (McHugh and Krochta 1994, 139). Sorghum dry milling fractions such as flour and bran fractions also used to cast films by da Silva and Taylor (2005, 9). Taylor et al. (2005, 401) suggested glacial acetic acid to replace aqueous ethanol as kafirin film casting solvent in which the films casted from both solvents were decent and with identical mechanical properties (Cuq, Gontard, and Guillbert 1998, 1). Other studies on the kafirin film modification were done by chemical cross-linking with condensed tannins, and by microwaving to improve the kafirin films functional properties (Emmambux, Stading and Taylor 2004, 127; Byaruhanga et al. 2007, 167).

Table 2.3 Kafirin extraction procedures and solvents used.

	Solvent system	Function	Proteins
Ethanol extraction (Johns and Brewster 1916)	70% ethanol, 70°C	Breaks hydrophobic interactions & solubilizes prolamins	Total proteins
Osborne procedure (Jones and Beckwith 1970; Skogh 1970; Haikerwal and Methieson 1971; Taylor et al. 1984; Virupaksha and Sastry 1968)	i) Distilled water, 1% NaCl solution ii) Aqueous alcohols (e.g., 70% ethanol, 60% tertiary butanol, 70% isopropanol) iii) Acidic or basic solution	Breaks non-covalent electrostatic interactions Reduces hydrophobic interactions Reduces non-covalent electrostatic interactions	Albumins; globulins Prolamins Glutelins
Landry-Moureaux sequential extraction procedure (Jambunathan and Mertz 1973; Paulis and Wall 1979; Wu and Wall 1980; Taylor et al. 1984)	i) 0.5M NaCl solution ii) Aqueous alcohols, (e.g., 70% ethanol, 60% tertiary butanol, 70% isopropanol) iii) 60% tertiary butanol + 0.5% 2-mercaptoethanol iv) 12.5 mM basic borate buffer + 0.5% 2-mercaptoethanol v) 12.5 mM basic borate buffer + 2% sodium dodecyl sulphate	Breaks hydrophilic interactions Reduces hydrophobic interactions 2-mercaptoethanol (reducing agent) cleaves covalent disulphide bonds Breaks non-covalent electrostatic interactions and disulphide bonds Sodium dodecyl sulphate (detergent) cleaves hydrogen bonds and hydrophobic interactions	Albumins; globulins Kafirin-I Kafirin-II/ cross-linked kafirin Alcohol-soluble glutelins Alcohol-insoluble reduced glutelins

Table 2.3 Kafirin extraction procedures and solvents used (continued).

	Solvent system	Function	Proteins
Sequential extraction (Hamaker et al. 1995; Park and Bean 2003)	<ul style="list-style-type: none"> i) 12.5mM basic borate buffer + 1% sodium dodecyl sulphate + 2% 2-mercaptoethanol ii) 60%tertiary butanol 	<p>Breaks non-covalent electrostatic interactions, hydrogen & disulphide bonds</p> <p>Precipitates non-prolamin</p>	Total proteins Kafirin; non-kafirin
Glacial acetic acid extraction (Taylor et al. 2005)	<ul style="list-style-type: none"> i) Pre-soak for 16 h in 0.5% sodium metabisulphite, 25°C ii) Glacial acetic acid iii) NaOH for adjusting to pH 5 	<p>Cleaves disulphide bonds</p> <p>Breaks hydrophobic interaction</p> <p>Precipitates kafirin</p>	Kafirin
Sonication with ethanol (Bean et al. 2006)	<ul style="list-style-type: none"> i) 70% ethanol (+sonication) + food-safe reducing agent (e.g, cysteine, glutathione, sodium metabisulphite) ii) Distilled water to dilute ethanol to 60% 	<p>Sonication breaks large protein aggregates; ethanol breaks hydrophobic interactions and solubilizes prolamins</p> <p>Precipitates lipids</p>	Kafirin monomer; cross-linked kafirin
Sonication with sodium borate and SDS (Park et al. 2006; Zhao et al. 2008)	<ul style="list-style-type: none"> i) 12.5mM sodium borate buffer, pH 10 + 2% SDS (+ sonication; 10W, 30s) ii) 12.5mM sodium borate buffer, pH10 + 2% sodium dodecyl sulphate + 2% 2-mercaptoethanol 	<p>Buffer breaks non-covalent electrostatic interactions; sodium dodecyl sulphate cleaves hydrogen bonds and hydrophobic interactions; sonication breaks large protein aggregates</p> <p>Buffer and sodium dodecyl sulphate function as mentioned previously ; 2-mercaptoethanol cleaves disulphide bonds</p>	<p>Kafirin monomer; cross-linked kafirin; lipids</p> <p>Detergent-extractable proteins; cross-linked proteins</p> <p>Detergent-extractable proteins; cross-linked proteins</p>

From previous section, it can be realised that kafirin has the potential to cast edible films and coatings. These kafirin products are not only biodegradable, they are also effective inhibitors of moisture, oxygen, aroma and oil, carriers of antioxidants, antimicrobials, flavours, colours and nutrients, while improving mechanical integrity and sensory quality of the products (Krochta 2002, 4). Khan (2004, 23) and Buchner et al. (2006, 110) demonstrated that kafirin coatings were effective in preserving the quality of pears, litchi and cashew nuts. The kafirin coatings were found to be highly functional, low detectability and acceptable by consumer test panels that were used to fresh fruits and nuts.

Kafirin Microparticles

Microparticles of plant proteins have been studied since the last two decades, particularly for zein. Predominant uses for prolamin microparticles are in the pharmaceutical field with some success reported for zein, soy protein isolates, whey proteins microparticles to deliver pharmaceuticals (Parris, Cooke and Hicks 2005, 4788; Chen, Remondetto, and Subirade 2006, 272; Chen et al. 2008, 3750; Zhong and Jin 2009, 2886; Lau et al. 2012, 706; Lau et al. 2013, 277). Prolamin microparticles have been popular in this field for their high specificity and potency, and that almost any ingredient can be encapsulated, despite of its hydrophobic, hydrophilic, or even microbial nature.

Taylor et al. (2009a, 99) reported a novel approach to prepare microparticles from kafirin by phase separation. Different solvents were tested for use as the solvent, and results showed that organic acids such as glacial acetic acid, lactic acid, and propionic acid formed many internal holes or vacuoles on kafirin microparticles. The larger internal surface areas of these organic acid derived microparticles were believed to be useful to encapsulate pharmaceuticals. Comparison with microparticles formed by similar manner using aqueous ethanol has shown few internal holes. The surface properties of the microparticles explained that the holes were formed from air bubbles entrapped in the microparticles during formation since ethanol is known as a powerful degasser. Using kafirin microparticles made by phase separation from organic acid, Taylor et al. (2009b, 7523) proved the potential to encapsulation of phenolic antioxidants within these microparticles. Experimental results suggested progressive release profiles for these microparticles. This

observation was supported by the other sustained release application of kafirin microparticles caffeine as a model drug, with the drug release being observed progressively for a few hours (Elkhalifa et al. 2009, 159).

2.2 PREPARATIVE ION EXCHANGE CHROMATOGRAPHY

A major disadvantage of Kafirin extraction processes discussed in Section 2.1.2 is the low purity of the different kafirin preparations, which often affected the properties of the kafirin products. For example, kafirin films were reported to have different thickness which is unquestionably due to low purity kafirin preparations which casted films with higher levels of total solids, compared to films from high purity kafirin preparations (Da Silva 2003, 7). Besides this, films and coatings casted from lower purity kafirin preparations were usually slightly cloudy because of the impurities co-extracted with kafirin (Taylor and Taylor 2013). This will undoubtedly affect the applications of kafirin products previously discussed in Section 2.1.3. For example, kafirin films and coatings to preserve fruits and nuts must be transparent so that the sensory quality of the products is not affected. Kafirin microparticles used to encapsulate pharmaceutical products also require high purity of kafirin for human consumption. Therefore the need arises to design a purification method that produces kafirin of high purity with high consistency, which is the focus of this section.

In 1903, Tswett first described the fundamentals of chlorophyll substances separation technique which linked to the term “chromatography” in his article (McNaire and Miller 1998, 1). Protein separation may be preparative, or analytical. Preparative separation, which is also the focus of this research, is carried out to obtain high throughput of purified protein for subsequent uses (Ward 2012, 3). Analytical purification produces a relatively small amount of desired protein for a variety of research or analytical purposes. Protein separation has been dominated by adsorption based chromatography since the early history of chromatography (Pfund 1987; Bonnerjea et al. 1988, 357). Details about several common separation methods that can be applied to protein purification are listed in Table 2.4 (Polykarpon 2011; GE Healthcare 2013; Pall Corporation 2013). Of these, the ion exchange adsorption and chromatography, based on net surface charges between the ion exchangers and molecules from aqueous solution, is the most widely accepted techniques for protein

purification, for both laboratory and process scales (Bonnerjera et al. 1986, 954 quoted in Khan 2012, 331). The ion exchange chromatography is most commonly used for protein purification due to the many advantages associated with it. First of all, the ion exchange chromatography is controllable by the buffer pH, salt concentration and the ion exchanger, thus serving as a concentration step for recovering proteins from a dilute solution (Stanton 2004, 23). This is a useful characteristic in instances where demands on protein quality are robust particularly for intended use in pharmaceutical applications. Besides, the ion exchange chromatography offers high throughput and high selectivity attributable to its high resolving ability for molecules with small charge differences. Furthermore, this technique is non-denaturing which is often compatible with processes coupled with further downstream chromatographic systems.

2.2.1 Principles of Ion Exchange Chromatography

Some commonly used ion exchangers and their properties are listed in Table 2.5. Most commercial ion exchangers can be classified according to their solid support types into cellulose, dextran, agarose, and polystyrene based ion exchangers. The cellulose, dextran, and agarose ion exchangers are derived from natural polymers, and used for protein separation for their low, non-specific adsorption. These ion exchangers are extremely hydrophilic and proteins do not adhere to them (Jungbauer and Machold 2004, 669). The advantage of dextran and agarose ion exchangers over cellulose is the better flow behaviour since the loose structure of cellulose ion exchangers often limits the flowrate achievable in column chromatography. The polystyrene based ion exchangers are made of synthetic polymer to sustain pH extremes and oxidizing environments. The accessibility of the charged functional groups and stability of ion exchangers are determined by the structure of the matrix (Roos 1999, 3).

Negatively or positively charged functional groups are covalently bound to matrix supports to produce either a cation or anion exchanger, respectively (Ahmed 1959, 150). Cation and anion exchangers are classified in terms of their ability to exchange positively or negatively charged species. Strongly acidic cation (SAC) and strongly basic anion (SBA) exchangers are ionised and thus are effective at nearly all pH values. Weakly acidic cation (WAC) exchangers are typically effective in the

Table 2.4 Adsorption based chromatographic principles and uses.

Separation principle	Loading/ elution condition	Uses
<p>Ion exchange chromatography</p> <p>Interaction of separation based on electrostatic attraction between opposite charges on chromatography adsorbents and target molecules.</p>	<p>Elution requires gradient to higher salt concentrations or pH change.</p>	<p>Removal of charged contaminant; Sample concentration.</p>
<p>Hydrophobic interaction chromatography</p> <p>Interaction of separation based on reversible interaction between hydrophobic surface of chromatography adsorbents and target molecules.</p>	<p>Loading requires: high concentrations of structure-enhancing salt. Elution requires gradient down to lower ionic strength buffer.</p>	<p>Removal of hydrophobic contaminant; Sample concentration.</p>
<p>Reversed-phase chromatography</p> <p>Interaction of separation based on reversible interaction between hydrophobic surfaces of chromatography adsorbents and target molecules.</p>	<p>Loading requires water or low solvent concentrations. Elution requires gradient to higher solvent concentrations.</p>	<p>Removal of hydrophobic contaminant; Sample concentration and removal of peptides; Separation of complex peptide samples.</p>
<p>Affinity chromatography</p> <p>Interaction of separation based on reversible interaction between specific ligands attached to chromatography adsorbents and target molecules.</p>	<p>Elution requires competitive ligand, or changing pH, ionic strength or polarity.</p>	<p>Removal of specific contaminant; One step purification of target molecules from complex samples; Purification of tagged recombinant proteins.</p>
<p>Size exclusion chromatography</p> <p>No interaction; physical separation based on difference in molecule size.</p>	<p>No specific condition required during loading and elution.</p>	<p>Removal of contaminant in specific size range; Sample desalting and buffer exchange; Separation of complex samples.</p>

Table 2.5 Commonly used ion exchangers for proteins separation.

Type	Matrix	Functional group	Protein	Reference
Amberlite IRC-50	Polyacrylic acid	Carboxyl	Cytochrome	Boardman and Partridge 1955
CM-Sepharose HP	Crosslinked 6% agarose	Carboxymethyl	Whey protein	Yamamoto and Ishihara 1999
CM-Toyopearl 650S	Crosslinked 6% agarose	Carboxymethyl	Whey protein	Yamamoto and Ishihara 1999
Source 15S	Crosslinked PS/DVB	Sulphonate	Whey protein	Yamamoto and Ishihara 1999
SP-Sepharose HP	Crosslinked PS/DVB	Sulphopropyl	Whey proteins; PEG-linked proteins	Yamamoto and Ishihara 1999; Seely and Richey 2001
Streamline SP	Crosslinked 6% agarose	Sulphopropyl	LYS	Bruce and Chase 2002; Tong, Xue and Sun 2003; Yun et al.
DEAE Sephacel	Cellulose	Diethylamino-ethyl	Antibodies	Sober et al. 1956
DEAE Sephadex A-50	Crosslinked dextran	Diethylamino-ethyl	Plant protein	Haq et al. 1999
DEAE-Sepharose FF	Crosslinked 6% agarose	Diethylamino-ethyl	Whey proteins	Yamamoto and Ishihara 1999
SP-Sepharose HP	Crosslinked 6% agarose	Sulphopropyl	PEG-linked proteins	Seely and Richey 2001
DEAE-Trisacryl M	Polystyrene	Diethylamino-ethyl	Antibody	Corthier et al. 1984

Table 2.5 Commonly used ion exchangers for proteins separation (continued).

Type	Matrix	Functional group	Protein	Reference	
Streamline DEAE	WBA	Crosslinked 6% agarose	Diethylamino-ethyl	BSA	Karau et al. 1997; Bruce and Chase 2002; Tong et al. 2003;
Diaion HPA25	SBA	Crosslinked PS/DVB	Quaternary alkyamine	BSA; Whey protein	Lan et al. 2000; Lan et al. 2002a
Q-Sepharose FF	SBA	Crosslinked 6% agarose	Quaternary amine	BSA; Whey protein	Draeger and Chase 1990; Gerberding and Byers 1998
Q-Sepharose HP	SBA	Crosslinked 6% agarose	Quaternary amine	Whey proteins	Yamamoto and Ishihara 1999
Source 15Q	SBA	Crosslinked PS/DVB	Quaternary amine	Whey proteins	Yamamoto and Ishihara 1999

range of pH 5 to 14, and weakly basic anion (WBA) exchangers are effective in the range of pH 0 to 9. The differences in the binding affinity and effective pH ranges of ion exchangers are strongly affected by their functional groups. For example, SAC and SBA usually carry sulfonic acid groups and quaternary amine groups, or corresponding salts, respectively (Wheaton and Lefevre 1981, 678). While WAC contains acrylic or methacrylic acid groups, WBA with primary-, secondary, or tertiary-amine groups (Wheaton and Lefevre 1981, 678; Thermax 2013). Charged protein molecules are adsorbed and retained by an oppositely charged ion exchanger, while molecules with neutral or similar charge as the ion exchanger flow through the void volume and elute from the feed solution. Ion exchange chromatography is primarily affected by the pH and salt concentration of buffer solutions. The binding of charged molecules is reversible, and elution is achieved by selectively decreasing the affinity of the molecules for the charged functional groups on the ion exchangers by continuously changing either the buffer pH or ionic strength, which is termed as the gradient elution. The *pI* of a molecule is the pH at which the molecules are neutral or with net zero surface charge. The molecules are negatively charged at a pH above their *pI* value, and vice versa. Subsequently, anion exchange chromatography is applied above the *pI* of the protein in order to promote elution of bound protein molecules, whereas cation exchange chromatography is carried out with pH below the *pI* value.

2.2.2 Characteristics of Ion Exchangers

Adsorption Equilibrium

The adsorption isotherm, which describes the phase equilibrium relationship, is of interests of many researchers. Study on the equilibrium behaviour of an ion exchange chromatography provides important information associated to the adsorption mechanism and equilibrium parameters required for process-scale chromatography modeling. A variety of isotherm models has been developed, and can be grouped into linear and nonlinear models, depending on the protein loading state. Protein samples used in analytical chromatographic runs are typically very dilute, and hence the chromatographic parameters generally remained within the linear isotherm range and independent of the sample loading (Jonsson 1996, 1591). In contrast to the dilute sample loading associated to linear isotherms, the nonlinear isotherms are usually used to characterise preparative chromatography which operate

under overloaded conditions. Nonlinear isotherm models commonly used to represent protein ion exchange equilibrium are Langmuir isotherm (Lan et al. 2000a, 858; Özdural et al. 2004, 77; Li et al. 2007, 2419; Chen et al. 2008, 3750; Mazumder et al. 2009a, 111) and Freundlich isotherm models (Boyer and Hsu 1990, 61; Finette, Mao and Hearn 1997, 71; Bayramoğlu et al. 2007, 68).

The Langmuir isotherm is the first theoretically developed adsorption isotherm by Langmuir (1916, 2221; 1917, 1848) to describe gas-solid phase adsorption onto activated carbon. Several assumptions were made in the derivation of the isotherm model. Firstly, the adsorption can only occur at finite number of definite localised sites. Second, each site accommodates only one adsorbed molecule. Thirdly, the energy state of each molecule is similar at all adsorption sites on the surface independent of the surface coverage. Therefore, the Langmuir isotherm model, also called localised model, assumes uniform and homogeneous adsorption surface and negligible lateral interactions between the adsorbed molecules. The Langmuir isotherm can be expressed in terms of adsorption capacity of adsorbent, q_m (Eq. 2.1) and dissociation coefficient related to the binding affinity, K_d (Kinniburgh 1986, 895; Ho 2006, 81; Foo and Hameed 2010, 2). An essential feature of the Langmuir isotherm may be expressed in terms of a dimensionless equilibrium constant, R_L (Eq. 2.2) to indicate the favourability of the adsorption nature (Weber and Chakravorti 1974, 228; Chairat et al. 2005, 231). The values of R_L indicate the type of isotherm to be irreversible ($R_L=0$), favourable ($0<R_L<1$), linear ($R_L=1$), or unfavourable ($R_L>1$).

$$q_e = \frac{q_m c_e}{K_d + c_e} \quad (2.1)$$

$$R_L = \frac{1}{1 + (c_o / K_d)} \quad (2.2)$$

The Freundlich isotherm, which is an empirical correlation between adsorbent loading and liquid concentration, is a limiting form of the Langmuir isotherm at medium pressures (Freundlich 1906, 385). Similar to the Langmuir isotherm, the Freundlich isotherm (Eq. 2.3) is expressed in terms two constants, the dimensionless exponent n_f and the adsorbent adsorption capacity, q_f . $1/n_f$ is a function of adsorption intensity. The values of $1/n$ indicate normal adsorption ($1/n_f < 1$), cooperative

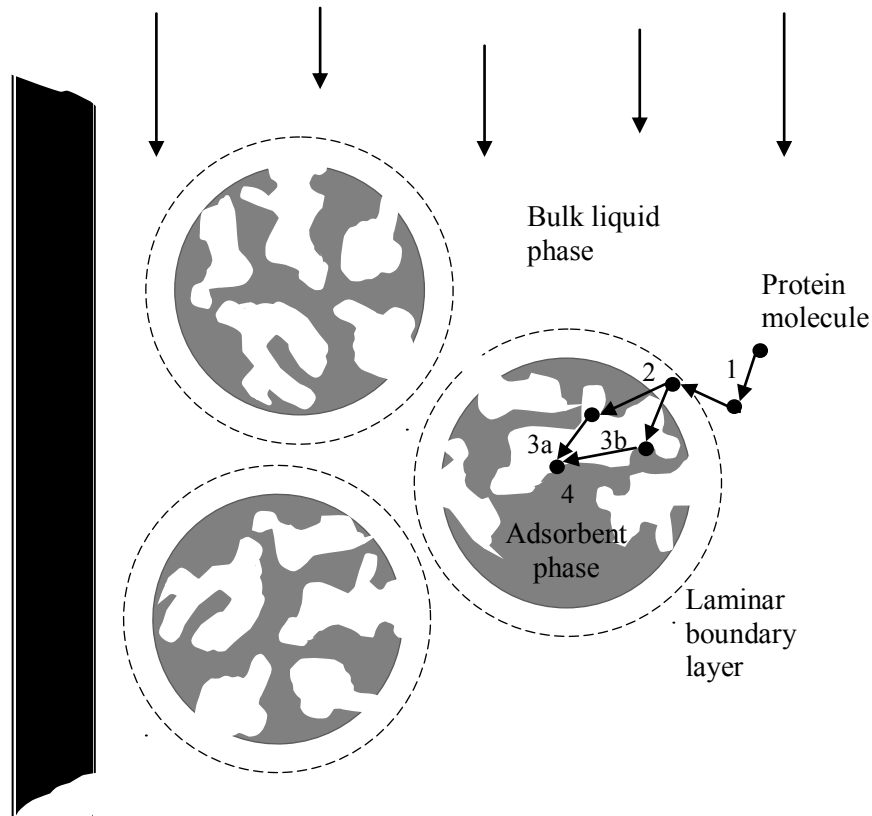


Figure 2.1 Macroscopic schematic of protein molecules in bulk solution showing the locations of mass transfer and dispersive mechanisms. 1. liquid transport; 2. film diffusion, 3a. pore diffusion; 3b. surface diffusion; 4. surface reaction at phase boundary.

adsorption ($1/n_f > 1$), and negligible effects of liquid concentration ($1/n_f = 1$) (Haghseresht and Lu 1998, 1100).

$$q_e = q_f c^{1/n_f} \quad (2.3)$$

Ion Exchange Mass Transfer

For large molecules like proteins, the mass transport process might be much slower than smaller molecules because of the resistances limiting the mass transport of proteins inside and outside the ion-exchange particles. Protein mass transport onto the binding sites of a chromatographic adsorbent entails the following macroscopic steps which are, the transport of protein molecule in bulk liquid (liquid dispersion and convection), diffusion from bulk liquid across the laminar boundary layer around the adsorbent particle (liquid film transport), diffusion within the pores (pore and surface diffusions), and, the interaction at the surface site (adsorption equilibrium or adsorption kinetics), as illustrated in Figure 2.1 (Crittenden and Weber 1978, 185;

Crittenden et al. 1986, 271). A number of theoretical models have been developed based on the assumption that one specific step limits the mass transport while the effects of other steps are negligible. These include the kinetic rate models and diffusion based models.

Diffusion resistances such as pore diffusion, surface diffusion or a combination of both have been considered in theoretical models of ion exchange chromatography. For example, Hunter and Cartar (2000, 81) predicted the recovery of bovine serum albumin (BSA) and proactive enzyme uptake on BRX-Q and BRX-QP anion exchangers, and BRX-S cation exchanger considering both surface and pore diffusion effects in the adsorbent particle mass balance. Bruce and Chase (2002, 3087), though, accounted the sole effect of pore diffusion on Streamline DEAE and Streamline SP on BSA and lysozyme (LYS) recovery, respectively. Differential mass balance with both pore and surface diffusions (Eq. 2.4) and pore diffusion of particle phase (Eq. 2.5), are showed below (Masamune and Smith 1964, 246; Masamune and Smith 1965, 41; Xu, Cai and Pan 2013, 155).

$$\frac{\partial q_i}{\partial t} = \frac{1}{r^2} \frac{\partial}{\partial r} \left[r^2 \left(\varepsilon_p D_p \frac{\partial c_{p,i}}{\partial r} + (1 - \varepsilon_p) D_s \frac{\partial q_i}{\partial r} \right) \right] \quad (2.4)$$

$$\frac{\partial q_i}{\partial t} = \frac{1}{r^2} \frac{\partial}{\partial r} \left(r^2 D_p \frac{\partial c_{p,i}}{\partial r} \right) \quad (2.5)$$

Though the assumption of a rate-determining kinetic step might seem unrealistic for some adsorption chromatography since this step is generally much faster than other influencing effects, when considering ion exchange chromatography, this simplification may be justified due to the fast mass transports (Ruthven 1984, 255; Lan et al. 2000b, 858; Guiochon et al. 2006, 295). For instance, the desorption mass transport in separations of BSA and whey protein using Diaion HPA25 anion exchanger were rapid and represented well by the simple forward first-order kinetic model (Lan et al. 2000a, 858; Mazumder 2009a, 111). Kinetic mass transports of protein are usually well represented by first- and second-order rate models, such as the forward first-order, forward second-order, reversible, pseudo-first-order, pseudo-second-order kinetic models. The first-order (Eq. 2.6), second-order (Eq. 2.7) and reversible (Eq. 2.8) kinetic models are the simplest forms of rate model. The pseudo-first-order kinetic model (Eq. 2.9) was suggested by Lagergren (1898, 1), expressed

in terms of a pseudo-first-order adsorption coefficient. The pseudo-second-order model (Eq. 2.10) assumed a second-order ion exchange interaction between the protein molecule and adsorbent particle (Ho and McKay 2000, 189).

$$\frac{\partial q_i}{\partial t} = k_1 q_i \quad (2.6)$$

$$\frac{\partial q_i}{\partial t} = k_2 q_i^2 \quad (2.7)$$

$$\frac{\partial q_i}{\partial t} = k_{ads} c_i (q_e - q_i) - k_{des} q_i \quad (2.8)$$

$$\frac{\partial q_i}{\partial t} = k_{1,ps} (q_e - q_i) \quad (2.9)$$

$$\frac{\partial q_i}{\partial t} = k_{2,ps} (q_e - q_i)^2 \quad (2.10)$$

2.3 ADSORPTION BASED CHROMATOGRAPHY SYSTEMS

Kafirin hydrophobicity restrains the establishment of an economical, food-compatible, and non-toxic industrial-scale extraction process. From a practical viewpoint, studies done on aqueous ethanol extraction of kafirin could serve as framework to establish process-scale kafirin production. A batch semi-industrial scale kafirin extraction has been modified from an existing laboratory-scale process by the Council for Scientific and Industrial Research, South Africa (Kaser 2003). Aqueous ethanol plus SMS and sodium hydroxide have been used in the solvent system (Erasmus 2003; Kaser 2003). The semi-industrial batch process, although simple and easy to control, suffers from several inherent disadvantages associated with batch processing. Despite its proximity to laboratory conditions, the batch process is ineffective after upscale for the excessive increase in solvent evaporation temperature and waiting time before freeze drying (Erasmus and Taylor 2003, Kaser 2003). One essential consideration for any process-scale production is the procedures and time required. The batch approach involves a series of cumbersome, time-consuming batch procedures. The complicated process steps incur significant capital and recurrent expenditures. Besides these, significant kafirin yield loss and quality deterioration might happen during the batch-to-batch transfer. Further losses of kafirin might also occur due to denaturation due to prolonged operation time.

Adsorptive, preparative ion exchange chromatography of protein, discussed in Section 2.2.2, may be performed in either fed-batch, semi-continuous, or continuous processes. As interest undergoes a transition from research bench towards product commercialization, cost reductions in process development and process-scale protein purification are emerging as major factors for commercial success. In a protein purification process development, the overall process economics is typically dominated by the protein purification cost. Consistent with the above mentioned objectives are continuous protein purification process. Continuous processes inherently provide higher throughput, more consistent quality, smaller equipment, and reduced cost than that possible with corresponding batch processes. Besides, continuous processes are commonly more flexible both for controlling and optimisation, two essential attributes for process-scale applications. Also, continuous purification processes are more naturally integrated into full continuous process systems. These benefits allowed continuous processes to become the norm rather than the exception in the process industry. Some examples and their characteristics are discussed below, and summarised as in Table 2.6.

2.3.1 Fixed-Bed Chromatography

Conventional fixed bed operating format is a stationary bed of chromatographic adsorbents. Fixed-bed chromatography, commonly known as column chromatography, is ubiquitous in the preparative chromatography of proteins (Chase 1994, 296; Przybycien, Pujar and Steele 2004, 469). A schematic representation of the fixed bed is shown in Figure 2.2a. In late 1970s, column chromatography was introduced for proteins separation in the industry (de Wit 2001, 30). Process scale column chromatography of whey protein from milk was carried out continuously using anion exchanger, with the patent licensed to Rhone-Poulenc Industries (1980). The license holder also patented IEC of other common proteins (Rhone-Poulenc Industries 1978). From then, research on column chromatography of protein has been continuing, for both cation and anion exchange chromatography. For example, McCreath et al. (1977, 73) recovered LYS from egg white and homogenate enzyme protein from clarified yeast using SP-PVA-FEP cation exchanger and Q-PVA-FEP anion exchanger, respectively. Hahn et al. (1998, 277) used Macro-Prep High S, S-Sepharose FF, S-HyperD-F, and Fracogel EMD SO_3^- 650 cation exchangers on preparative purification of bovine whey protein from cow milk. Other

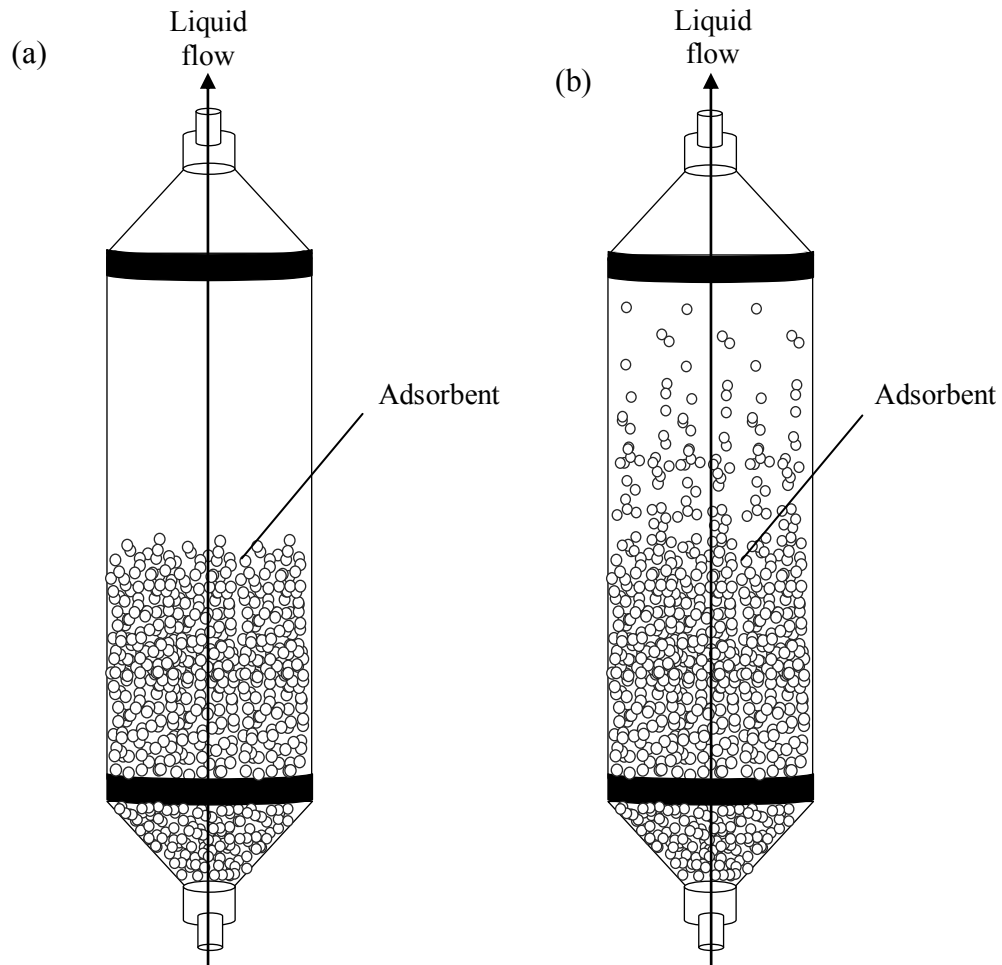


Figure 2.2 Schematic diagrams of (a) fixed-bed chromatography, and (b) fluidised-bed chromatography.

examples of fixed-bed based anion exchange chromatography using include Q and S HyperD for purification of *Escherichia coli* and BSA (Horvath et al. 1994, 11). Rodrigues et al. (1995, 233) also conducted separation of BSA on fixed bed with POROS Q/M and Q HyperD. Couriol et al. (2000, 465) purified a protein mixture to meet human consumption requirements on a preparative scale fixed bed of Q HyperD/F.

All these studies showed that the fixed bed chromatography is effective for protein recovery. However, this system is not suitable to process feedstocks with suspended particulates, as particulates become trapped in the voids of the bed (Chase 1994, 296). This results in the formation of trapped solids near the bed inlet and eventually to a complete clogging of the bed, often after bed compression. Even though most downstream processing is equipped with solid clarification operation,

Table 2.6 Continuous chromatographic systems and their characteristics.

	Ability to handle particulates	Ability to regenerate adsorbents	Comments	Reference
Fixed-bed chromatography	No	No	Validated method; subject to bed clogging problem when feed contains particulates	Chase 1994; Przybycien, et al. 2004
Fluidised-bed chromatography	Yes	No	Subject to particulate-adsorbent interaction that reduces efficiency.	Chase and Draeger 1992; Feuser et al. 1999
Simulated moving bed chromatography	Yes, limited to medium feed flowrate	Yes	Two-component separation; subject to excessive pressure drop and bed closing problems at high solute flowrate.	Silva et al. 2007; Liang et al. 2013
Continuous annular chromatography	No	No	Multi-component separation; complex operation; subject to fouling problem easily.	Buchacher et al. 2001; Uretschlager et al. 2001; Gordon et al. 1990
Liquid-solid circulating fluidised bed chromatography	Yes	Yes	High velocity operation; validated for unclarified whole broth protein recovery	Grace 1990; Yang et al. 1993; Lan et al. 2000; Lan et al. 2001

this incurs extra capital and recurrent expenditure. Besides the effectiveness depends on the nature of suspended solids, for instance some might be extremely difficult to remove by centrifugation and filtration. Also, all these might result in considerable product yield reduction, and further product losses through denaturation due to time spent on the mandatory pretreatment of feedstocks. Finally, a separated unit operation is required to regenerate the chromatographic adsorbents. Such a system is similar to the liquid-solid circulating fluidised bed, discussed later.

2.3.2 Fluidised-Bed Chromatography

Fluidised bed circumvents the need for the compulsory feedstock preclarification of fixed-bed chromatography (Chase 1994, 296; Anspach et al. 1999, 129). A subset of fluidised bed, the expanded bed, addresses situations with low superficial velocities close to the minimum fluidisation velocity. For most chromatographic adsorbents the expanded-bed adsorption is typically applicable only to bed expansions of less than two times the settled bed height. Nevertheless, the expanded-bed and fluidised-bed adsorption chromatography uses the similar setup as fixed-bed chromatography with minor difference in bed expansion characteristics. Thus, for protein chromatography adsorption over a large range of bed expansions, including high expansions, the term “fluidised-bed chromatography” includes those of expanded-bed as well. In fluidised-bed system, the adsorbents are allowed to rise from their settled state, which increases the space in between the adsorbents to allow unwanted suspended solids from crude feedstock to pass through without the risk of blocking the bed. The difference between fluidised bed and fixed bed expansion is clearly illustrated in Figure 2.2. For its advantages of direct purification of proteins, the fluidised-bed chromatography has been used for proteins of different origins and applications. For example, a pilot-scale purification of recombinant human placental anticoagulant protein from *Escherichia coli* homogenate was carried out using fluidised-bed chromatography packed with Streamline DEAE anion exchanger (Barnfield Frej, Hjorth, and Hammarstrom 1994, 922). And, scale-up of fluidised bed based chromatography was applied on phycobiliprotein purification utilizing Streamline DEAE (Bermejo, Ruiz, and Acien 2007, 927).

However, the presence of suspended particulate matter during operation was found to have a potential impact on the operation of the fluidised bed. Sometimes,

the particulate-adsorbent interactions led to a deteriorated stability of the fluidised bed and in turn to a reduced chromatographic efficiency. For example, Chase and Draeger (1992, 2021) studied Q-Sepharose FF anion exchanger and S-Sepharose FF cation exchanger on purification of BSA. The experiment results suggested that the fluidised bed efficiency was affected by the particulate-adsorbent interaction, with the anion exchanger affected the most. Feuser et al. (1999, 99) performed the same study, and similar observation was stated. The particulates, therefore, have to be treated as an integral part of the system and potential interactions between suspended solids and expanded adsorbents should be evaluated carefully. Other studies were carried out for assessing the fluidised-bed chromatography efficiency. Johansson, Jagersten, and Shiloach (1996, 9), for example, performed process-scale purification of recombinant protein from *Escherichia coli* homogenate was tested on fluidised bed packed with Streamline DEAE, with final protein three times more concentrated. This was supported by separation of extracellular inulinase purification with final product ten times more concentrated (Kalil, Maugeri-Filho, and Rodrigues 2005, 581). A seven-fold increase in the antibody concentration was achieved from recovery of whole mammalian cell culture broth as well (Balt, Yabannavar, and Singh 1995, 41).

2.3.3 Simulated Moving Bed Chromatography

Simulated moving bed (SMB) chromatography is of rising interest in protein separation. The SMB offers a promising solution to the adsorbent circulation problems associated with fixed-bed and fluidised-bed systems (Silva, Gandi, and Rodrigues 2007, 82). The SMB is also much more suitable to process-scale production due to its reduced solvent consumption, high productivity and final purities. The SMB as its name indicates, the movement of the stationary adsorbent phase is simulated. This is achieved by connecting multiple fixed beds to make a circulation loop, and periodically switching the feed and withdrawal points from one bed to the other. A schematic representation of an SMB is portrayed in Figure 2.3. The SMB typically consists of four different sections, the first section is located between the eluent and extract streams, the second section between the extract and feed streams, the third section between the feed and raffinate streams, and the fourth section between the raffinate and eluent (Silva, Gandi, and Rodrigues 2007, 82; Suvarov, Wouwer, and Kienle 2012). The principles of SMB based chromatography

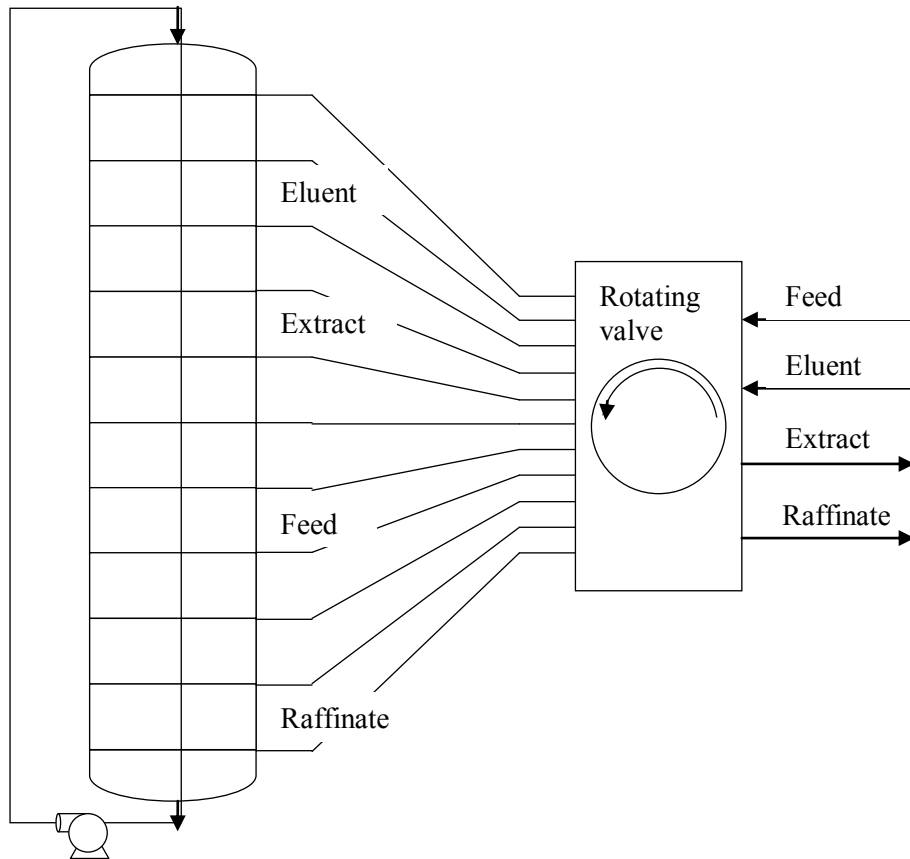


Figure 2.3 Schematic diagram of simulated moving bed chromatography.

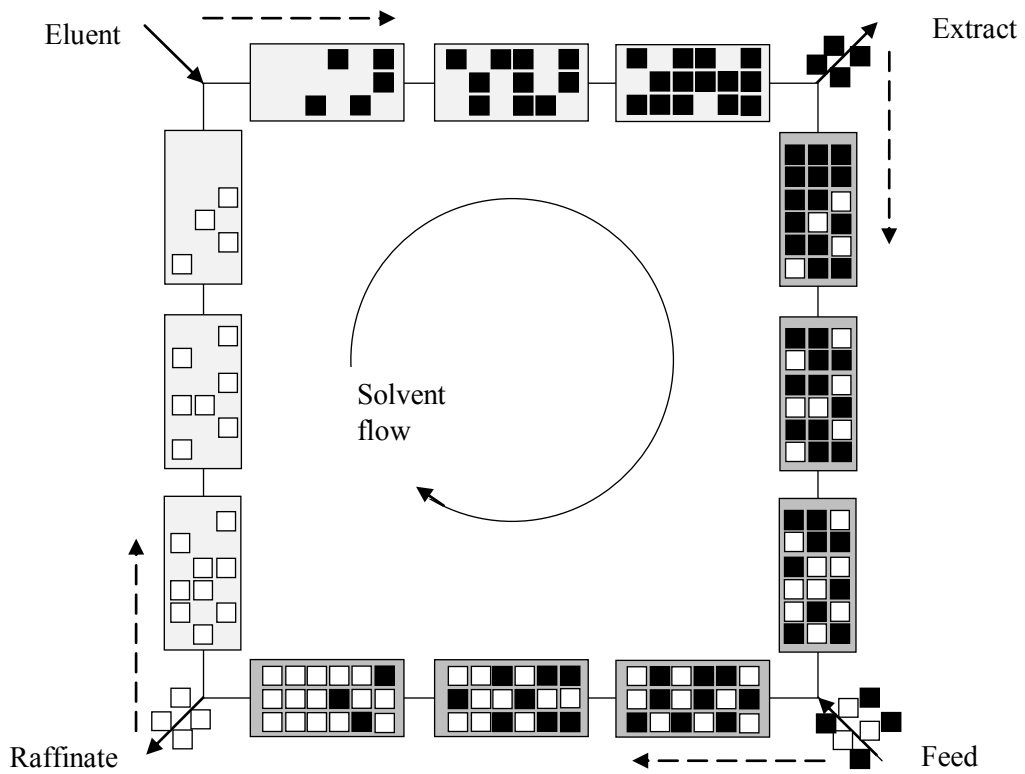


Figure 2.4 Schematic diagram of simulated moving bed chromatography principle. slow-moving liquid flow, fast-moving liquid flow.

is as shown in Figure 2.4. The feedstock containing two components to be separated is injected between the second and third section. The less adsorbed component is collected at the raffinate port and the more adsorbed component at the extract port. The separations of components are performed in the second and third sections, whereas the first and fourth sections are dedicated to adsorbent regeneration and solvent recycling, respectively.

Current applications of the SMB originated from Universal Oil Products (Broughton 1968, 60; Broughton 1984, 723). The first patent of SMB application was licensed as the Sorbex process and issued for a number of process-scale separations in the chemical process industry (Universal Oil Products 1962). Purifications of protein on SMB have, to date, only rarely been carried out. Huang et al. (1986, 291) first attempted to isolate trypsin enzyme from an extract of porcine pancreas by devising an SMB made of six affinity beds. Another example is the separation of human serum albumin on two SMB connected in series, with the removals of less adsorbent components and more strongly adsorbed components carried out in the first and second SMB, respectively (Houwing 1996 quoted in Blehaut and Nicoud 1998, 60). The results were validated experimentally by Li, Xiu, and Rodrigues (2007, 2419) on a four-section SMB packed. Myoglobin and LYS proteins were also separated on an eight-staged SMB (Nicoud 1996). In addition, SMB has also been applied to recover monoclonal antibodies from *Escherichia coli*, by adding two extra purge steps the two-section SMB managed to achieve greater yield (Gottschlich and Kasche 1996, 201). Gueorguieva et al. (2011, 6402) also tested recombinant streptokinase protein separation on a three-section open loop SMB, with some experiment runs reported relatively high purity. Besides, in separation of bovine milk proteins from whey protein concentrate, pilot-scale SMB gave higher productivity, and higher product purity while consuming less solvent in comparison to column chromatography (Andersson and Mattiasson 2006, 88). An ion exchanger typically used in packed beds, Streamline-SP, was used in these experiments. Despite all these, SMB suffers from pressure drop problems associated with packed beds. High effluent flows in the first section can result in excessive pressure drops and the SMB can be clogged by suspended solids in the feed (Liang et al. 2013, 1).

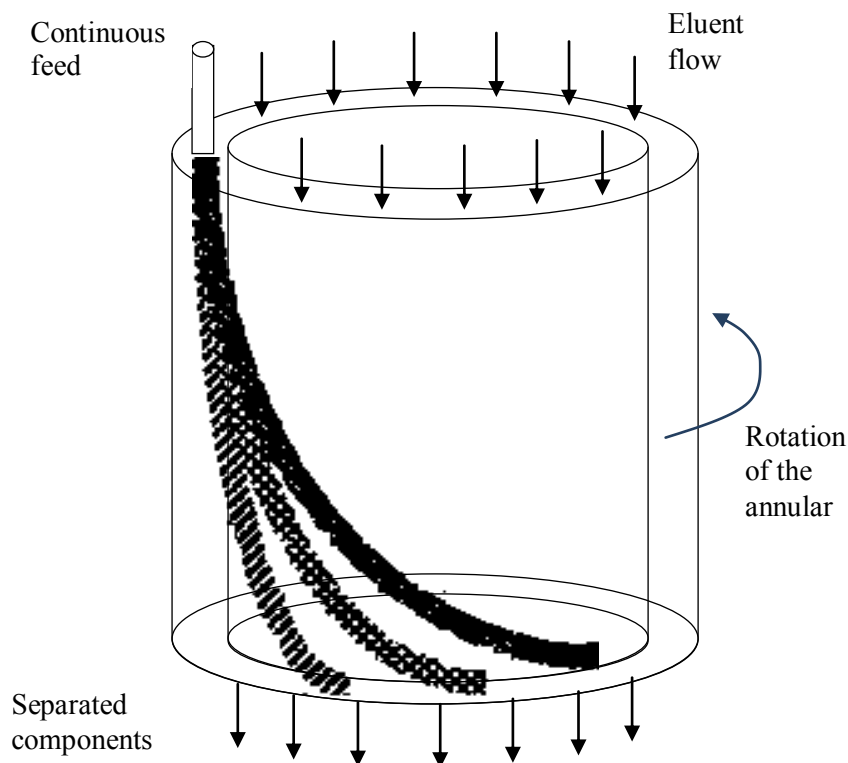


Figure 2.5 Schematic diagram of rotating annular chromatography.

2.3.4 Continuous Annular Chromatography

Continuous annular chromatography (CAC) has been developed for preparative multi-components separation (Byers et al. 1989, 635). The schematic of a CAC is portrayed in Figure 2.5. The CAC consists of two packed concentric annulus gradually rotating along a stationary feed and solvent ports (Sengupta and Sengupta 2001, 89; Silveston, Hashimoto, and Kawase 2012, 590). Such as system accepts a continuous feed at one rotating point and separate it into a series of constituent streams that appear as separate helical bands in the annulus. The retention time differences of the components of the feed based on interaction with the stationary adsorbent phase, resulting in individual withdrawal of each component. Between 1970s and 1990s most of the research on CAC was performed in the Oak Ridge National Laboratories (Begovich and Sisson 1981; Begovich and Sisson 1981, 11; Byers et al. 1989, 635). More recently, S-Sepharose, a strong acidic cation exchanger was used in the CAC for separation of a mixture of albumin, haemoglobin, and cytochrome c (Bloomingburg et al. 1991, 1061). Other than that, the use of CAC for separation of myoglobin and hemoglobin proteins was also studied by others (Takahashi and Goto 1992, 403). Reissner et al. (1997, 49) desalted BSA from a

mixture of phosphate, sodium chloride, and potassium chloride, and gained highly purified final product.

While CAC is promising continuous chromatographic process, its operation is complex. Though the CAC is capable of resolving multi-component from continuous feedstocks, in most process-scale separations, recovery of only one product is needed. Additionally, CAC faces fouling problems easily. A study by Buchacher et al. (2001, 14) reported fouling for separation of concentrated immunoglobulin concentration, which have prohibited the continuous CAC based chromatography. Other than that, the performance of CAC reduced to that of a batch chromatography when dealing with crude protein feed, such as the green fluorescent protein (Uretschlager, Einhauer, and Jungbauer 2001, 243). All these necessitate pretreatment of the feedstocks. The CAC system is continuous only in applications where cycling between feed application, adsorption, elution and regeneration is not required. Since most IEC separations require a change of elution conditions, the advantages of continuous separation cannot be realised using CAC (Gordon, Moore, and Cooney 1990, 741).

2.3.5 Liquid-Solid Circulating Fluidised Bed Chromatography

Liquid-solid circulating fluidised bed (LSCFB) chromatography may be a potential approach for process-scale protein separation, which could overcome the drawbacks of the other chromatographic systems discussed earlier. Given the advantages of fluidised beds for these systems have included such factors as the capability of operating with small adsorbents which in turn leads to better utilization of the surface area of the particles hence high effectiveness factors, increased contact efficiency between the adsorbents surface area and the carrying fluid due to increased slip between the adsorbent and solvent phase, and ability to withdraw and input adsorbents continuously (Grace 1990, 1956; Yang et al. 1993, 85). The high velocities operations also gave higher throughput of product and rapid mass transport between different phases (Grace 1990, 1956). Liquid-solid circulating fluidised bed (LSCFB) has been rapidly applied in adsorption based chromatographic processes recently. These processes are primarily used industrially in metal recovery from hydrometallurgical leach liquors, and decontamination of water, aqueous solutions and petroleum products (Liang et al. 1995, 98; Cui et al. 2004, 699; Trivedi, Bassi,

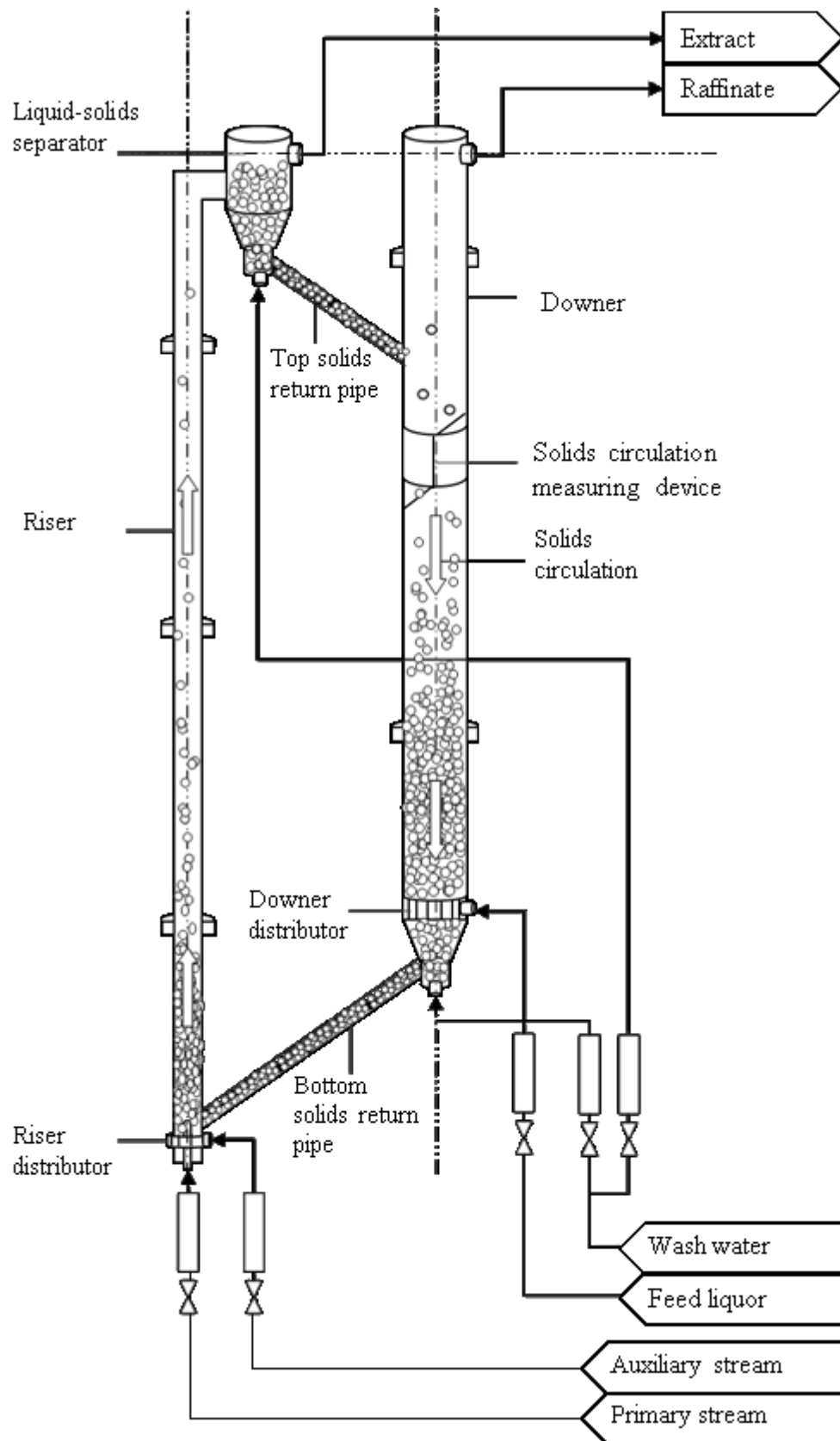


Figure 2.6 Schematic diagram of liquid-solid circulating fluidised bed chromatography.

and Zhu 2006, 61; Patel et al. 2008, 821). These continuous systems must be coupled with regeneration of chromatographic adsorbent, and often with washing as well. Washing for removal of residual solution within the intraparticle pores and the intraparticle voids of the adsorbents can be attained quite effectively by fluidisation of the adsorbents with the required solvent.

Current applications of the LSCFB based protein purification originated from a pilot-scale of such system fabricated at the University of Western Ontario, schematically shown in Figure 2.6. The LSCFB consists of two liquid-solid fluidised beds, downer and riser, to carry out protein adsorption and elution, respectively. These fluidised beds are connected to circulate chromatographic adsorbents so that continuous process is made possible. Lan et al. (2000a, 859; 2002, 252) demonstrated the ability of LSCFB to separate BSAs using Diaion HPA25 anion exchanger. Results showed that the LSCFB chromatography is excellent for recovery of proteins, with high throughput and end product recovery. Other than that, the LSCFB is also capable of handling unclarified feedstocks. Lan et al. (2001, 157) successfully separated whey proteins from whole broth, and reported high overall protein recovery and yield. Overall the LSCFB offers advantage of economy. Considering all these, it is concluded that the LSCFB chromatography is suitable for continuous protein separation. More details associated to the LSCFB are discussed in Chapter 3.

2.4 MODELING CONTINUOUS CHROMATOGRAPHIC SYSTEMS

Several theoretical models have been developed to describe chromatographic protein in in continuous chromatographic columns. For example, Wiblin et al. (1995, 81) adapted the well-established packed bed simple kinetic model by Cowan, Gosling and Sweetenham (1989, 187) to simulate the antibody separation in expanded- and fluidised beds, taking into account the liquid film transport, axial dispersion and pore diffusion effects. In fact, the stirred tank model was applied wherein the continuous beds were discretised into a number of tanks of equal volume to predict the process performance. Owen and Chase (1998, 3771) consulted to identical models of McCreath et al. (1992, 189) and Gordon and Cooney (1990, 120)

in development of the stirred tank model for protein purification. The theoretical model, considered the lumped mass transfer with an artificially decreased liquid film coefficient, required seventeen tanks to simulate performance of expanded bed chromatography. Later, Bruce and Chase (2002, 3087) used the same software package reported by Wiblin et al. (1995, 81) to predict breakthrough curves of LYS and BSA by including the liquid dispersion, pore diffusion and liquid film transport. Deviations between the experimental and simulated results were observed and were attributed to the negligence of axial variation in particle size, bed void fraction, liquid dispersion and film transport. Hunter and Cartar (2000, 81) conducted experiments on BSA and proactive enzyme uptake and used the general rate model to compare the transport rates for adsorbents having different structures as well as their adsorption equilibrium characteristics. Wright and Glasser (2001, 474) developed a model for protein recovery in fluidised bed and investigated the effect of operating parameters on the process dynamic. Axial dispersion and mass transport effects were accounted for in the model, and close estimations for both pore and surface diffusion models were obtained for experiment results. Tong et al. (2002, 117) considered the pore diffusion effect to predict the LYS breakthrough performance in expanded bed. The theoretical model was modified to consider the axial particle size distribution and discovered less axial dispersion for the small-sized, dense adsorbent used in the expanded bed. Li, Xiu and Rodrigues (2004, 3838) proposed a three-zone mathematical model for estimating the breakthrough curves from literature. The simulation results closely approximated experimental data in the literature by accounting for the bed voidage and particle size axial distribution other than pore diffusion, film transport, and axial dispersion in the phases. Other than these adsorption chromatographic models, some theoretical models have also been developed for continuous adsorption and elution processes and agreed well with the experimental data on purification of BSA (Lan et al. 2000, 858; Mazumder et al. 2009a, 111).

It can be seen that the literature on the theoretical studies of protein chromatographic based adsorption and elution have significantly evolved over the past decade. Therefore this effort is made to summarize different models applied in continuous bed chromatography contributed in this field. In these chromatographic columns, the variation of the protein amount loaded to the column over a period of

time is known as the breakthrough curve. Prediction of the breakthrough curve gives one of the solutions to modeling the continuous bed dynamics and effects of process parameters on the overall performance, which needs knowledge of the equilibrium behaviour as described by adsorption isotherm and mass transport characteristics from the bulk liquid to the adsorbent particles. A summary of some of the modeling studies mentioned above are presented in Table 2.7.

2.4.1 Mass Transport Models

Typically, the theoretical models describing chromatographic mass transport processes consists of the bulk liquid phase and the stationary adsorbent phase, which have to be accounted for separately. Amongst the different model approaches for chromatography, the general rate models, the lumped rate models, and the stirred tank models are most commonly applied for continuous protein separations on chromatographic beds. These are discussed in detail as follow.

General Rate Models

The general rate models are the most detailed models. In addition to axial dispersion, D_{ax} they are characterised by a minimum of two other parameters describing mass transport effects in chromatographic columns. These two parameters may combine mass transfer in the liquid film, k_f and inside the pores, D_p as well as surface diffusion, D_s and adsorption kinetics in various kinds. Radial mass transport inside the particle pores of stationary adsorbent phase is also taken into account, which results in concentration $\partial c_p/\partial r$ and loading distributions $\partial q/\partial r$ along the particle radius. The mass transfer in the bulk liquid phase (Eq. 2.11) includes accumulation within the bulk liquid, convection, axial dispersion, and external film transport outside the particles (Hunter and Carta 2000, 81). The differential mass balance of adsorbent phase accounts for the intraparticle diffusion resistances such as pore diffusion (Eq. 2.12), surface diffusion or a combination of both (Eq. 2.13).

$$\varepsilon D_{ax} \frac{\partial^2 c_i}{\partial z^2} = \varepsilon \frac{\partial c_i}{\partial t} + U_l \frac{\partial c_i}{\partial z} + (1 - \varepsilon) \frac{\partial q_i}{\partial t} \quad (2.11)$$

$$\varepsilon_p \frac{\partial c_{p,i}}{\partial t} + (1 - \varepsilon_p) \frac{\partial q_i}{\partial t} = \frac{1}{r^2} \frac{\partial}{\partial r} \left[r^2 \left(\varepsilon_p D_p \frac{\partial c_{p,i}}{\partial r} + (1 - \varepsilon_p) D_s \frac{\partial q_i}{\partial r} \right) \right] \quad (2.12)$$

$$\varepsilon_p \frac{\partial c_{p,i}}{\partial t} + (1 - \varepsilon_p) \frac{\partial q_i}{\partial t} = \varepsilon_p \frac{1}{r^2} \frac{\partial}{\partial r} \left(r^2 D_p \frac{\partial c_{p,i}}{\partial r} \right) \quad (2.13)$$

Boundary conditions for the stationary adsorbent phase are necessary in addition to the conditions of the chromatographic column inlet and outlet. The following is restricted to the form of the boundary condition derived by Ma et al. (1996, 1244) for a general rate model. Owing to particle symmetry, the concentration and loading gradients vanish at the centre of the particle (Eq. 2.14). The links between liquid, pore and solid phase are given by mass balances at the particle boundary (Eq. 2.15).

$$\left. \frac{\partial c_{p,i}}{\partial r} \right|_{r=0} = \left. \frac{\partial q_i}{\partial r} \right|_{r=0} = 0 \quad (2.14)$$

$$k_f \left[c_i - c_{p,i} \right]_{r=r_p} = \varepsilon_p D_p \left. \frac{\partial c_{p,i}}{\partial r} \right|_{r=r_p} + (1 - \varepsilon_p) D_s \left. \frac{\partial q_i}{\partial r} \right|_{r=r_p} \quad (2.15)$$

A system of partial differential and algebraic equations is obtained for all models. For the solution of these systems initial and boundary conditions for the chromatographic column are essential. The initial conditions and concentration as well as the loading specify their values at the onset of simulation run, $t=0$ (Eq. 2.16). Generally, zero values are assumed.

$$c_i = c_i|_{t=0,z} = 0 \quad (2.16)$$

$$c_{p,i} = c_{p,i}|_{t=0,z,r} = 0$$

$$q_i = q_i|_{t=0,z,r} = 0$$

Lumped Rate Models

The lumped rate models characterised by a second parameter describing rate limitations apart from axial dispersion, D_{ax} were applied in studies on continuous chromatography of a variety of proteins. The second parameter subdivides the models into those where either mass transport or kinetic terms are rate limiting. In the mass transport limiting lumped rate models, the concentration inside the adsorbent pores is identical to the bulk liquid phase concentration, $c_p=c$. A lumped film transfer coefficient, k_f is used to denote the internal and external mass transport

resistances. The mass transport term is also defined by the linear driving force approach, which described the external mass transfer as a linear function of the concentration difference between the concentration in the bulk liquid phase and on the adsorbent surface separated by a film boundary layer (Xu, Cai and Pan 2013, 155). Therefore, the lumped rate model consists of the balance equations in the bulk liquid phase written with the pore concentration (Eq. 2.17) as well as in the stationary adsorbent phase (Eq. 2.18).

$$\varepsilon D_{ax} \frac{\partial^2 c_i}{\partial z^2} = \varepsilon \frac{\partial c_i}{\partial t} + U_l \frac{\partial c_i}{\partial z} + (I - \varepsilon) \left[\varepsilon_p \frac{\partial c_{p,i}}{\partial t} + (I - \varepsilon_p) \frac{\partial q_i}{\partial t} \right] \quad (2.17)$$

$$\varepsilon_p \frac{\partial c_{p,i}}{\partial t} + (I - \varepsilon_p) \frac{\partial q_i}{\partial t} = k_f \frac{3}{r_p} (c_i - c_{p,i}) \quad (2.18)$$

Like the mass transfer coefficient in the transport lumped rate models, the adsorption, k_{ads} and desorption, k_{des} rate constants are considered as effective lumped parameters. Though the assumption of a rate-determining kinetic step might seem unrealistic for some adsorption chromatography since this step is generally much faster than other influencing effects, when considering ion exchange chromatography this simplification may be justified due to the fast mass transport rates (Guiochon et al. 2006, 295; Ruthven 1984, 255; Lan et al. 2000, 858). Since no film transfer resistance exists, concentration inside the particle pores is the same as the bulk liquid phase concentration, $c_p = c$. The model can be described by the bulk liquid phase (Eq. 2.19) and adsorbent phase (Eq. 2.20) mass balances (Lan et al. 2000, 858). Shown here is a simple reversible kinetic model. Other kinetic rate models are discussed in Section 2.2.2.

$$\varepsilon D_{ax} \frac{\partial^2 c_i}{\partial z^2} = \varepsilon \frac{\partial c_i}{\partial t} + U_l \frac{\partial c_i}{\partial z} + (I - \varepsilon) \left[\varepsilon_p \frac{\partial c_i}{\partial t} + (I - \varepsilon_p) \frac{\partial q_i}{\partial t} \right] \quad (2.19)$$

$$\varepsilon_p \frac{\partial c_i}{\partial t} + (I - \varepsilon_p) \frac{\partial q_i}{\partial t} = k_{ads} c_i (q_e - q_i) - k_{des} q_i \quad (2.20)$$

Tanks-In-Series Models

An entirely different approach to describe a chromatographic column dynamics leads to the stirred tanks-in-series models. Instead of dynamic microscopic balance, the continuous chromatographic column is modelled as a sequence of a finite number

Table 2.7 Mass transport models of chromatographic protein separation.

	Bulk model	Adsorption phase model	Local equilibrium	Solution	Reference
Antibody	Lumped rate model	Solid diffusion inherent in effective film transfer constant	Nonlinear (Langmuir)	Numerical	Özdural et al. 2004.
Antibody	Stirred tank model	Pore diffusion	Not mentioned	Numerical	Wiblin et al. 1995
BSA	Lumped rate model	Intraparticle diffusion inherent in effective film transport	Nonlinear (Langmuir)	Numerical	Chen et al. 2008
BSA; proactive enzyme	General rate model	Pore diffusion; surface diffusion	Linear	Numerical; analytical	Hunter and Carta 2000
BSA; whey	Lumped rate model	Intraparticle diffusion inherent in effective film transport	Nonlinear (Langmuir)	Analytical	Lan et al. 2000, 2001
BSA	Lumped rate model	Intraparticle diffusion inherent in effective film transport	Nonlinear (Langmuir)	Numerical	Mazumder et al. 2009a
LYS; BSA	General rate model	Pore diffusion	Not mentioned	Numerical	Bruce and Chase 2002
LYS	Lumped rate model	Intraparticle diffusion inherent in effective film transport	Nonlinear (Langmuir)	Numerical; analytical	Guerrero-German et al. 2012
LYS	General rate model	Pore diffusion	Nonlinear (Langmuir)	Numerical	Li et al. 2007; Tong et al. 2002
LYS	Lumped rate model; stirred tank model	Intraparticle diffusion inherent in effective film transport	Linear	Numerical	Owen and Chase 1999
LYS	General rate model	Pore diffusion; surface diffusion	Nonlinear (Langmuir)	Numerical	Wright and Glasser 2001
BSA; whey	Lumped rate model	First-order kinetic; elution	Non-equilibrium	Analytical	Lan et al. 2000, 2001
BSA	Lumped rate model	First-order kinetic; elution	Non-equilibrium	Numerical	Mazumder et al. 2009a

N of similar tanks. Each tank is filled with liquid and solid that is completely mixed. The tanks-in-series model was introduced by Martin and Synge (1941, 1358) and is equal to the concept of stirred tank in series typically used in reaction processes. A constant flow of bulk liquid through a cascade of N ideally stirred tanks is assumed, each tank having a total volume equal to the total volume divided by N , $V=V_{sys}/N$. Inside each tank, a fraction is occupied by the solid phase and the concentration inside the liquid is similar in the bulk phase and in the pore phase. This leads to the following mass balance (Eq. 2.21) for the i -th tank, where accumulation is equal to difference between the inlet and the outlet stream. The adsorbent phase mass balance including mass transport resistance can also be developed (Eq. 2.22) as follow (Schmidt-Traub and Strube 1996, 641).

$$\varepsilon \frac{\partial c_i}{\partial t} + (1-\varepsilon) \frac{\partial q_i}{\partial t} = \frac{\dot{V}}{V} (c_{i-1} - c_i) \quad (2.21)$$

$$\frac{\partial q_i}{\partial t} = k_f \frac{3}{r_p} (c_i - c_{p,i}) \quad (2.22)$$

2.4.2 Fluid Dynamics

Fluid dynamics of the chromatographic fluidised beds can be expected to play important roles in predicting breakthrough curves and performance of such systems. Once the mass transport and equilibrium aspects have been analysed, the key concepts of particle and fluidised bed hydrodynamics are explored.

Particle Drag Coefficient

The drag coefficient, C_D is defined as the ratio of the force on the particle and the fluid dynamic pressure caused by the fluid times the area projected by the particles (Eq. 2.23). Stokes (1851, 8) first derived an expression for drag force describing the motion of a spherical particle moving through a viscous fluid. The equation is based primarily on the radius of particle, r_p and the viscosity of fluid, μ . For creeping flow conditions, where the Navier-Stokes inertial effects were assumed to be negligible, the drag correlation for steady state spherical particle motion was derived (Eq. 2.24). The drag equation is a function of the particle Reynolds number, Re_p (Eq. 2.25). However, the Stokes law is only valid for Reynolds number less than 0.1.

$$C_D = \frac{F}{(1/2)\rho_f U_r^2 A_p} \quad (2.23)$$

$$C_D = 24 \left(\frac{\mu}{d_p U_r \rho_f} \right) = \frac{24}{Re_p} \quad (2.24)$$

$$Re_p = \frac{U_r d_p \rho_f}{\mu} \quad (2.25)$$

Stokes drag correlation showed no wake through disregarding of inertial effects. Oseen (1910, 1) considered these effects approximately and derived a correction to the Stokes drag correlation. The improvement in predictions due to the correction of Oseen motivated further formulations to be added to the traditional Oseen (1910, 1) approximation. These drag correlations were mainly proposed by Schiller and Naumann (1933, 318), Fair and Geyer (1954.), Proudman and Pearson (1957, 237), Clift, Grace and Weber (1978, 33), Flemmer and Banks (1986, 217), Turton and Levenspiel (1986, 83), Khan and Richardson (1987, 135) and Haider and Levenspiel (1989, 63). These are summarised in Table 2.8 (Eqs. 2.2 to 2.34), respectively, along with the range of applicability claimed by the authors.

Particle Terminal Velocity

The upper limit for operating a fluidised bed is given by the terminal (settling) velocity of the particles, U_t . The terminal velocity is defined as the velocity reached by a free-falling particle in a stagnant fluid under steady-state conditions. The terminal velocity depends primarily on the physical properties of the fluid and particle. The calculation of the particle terminal velocity used to be an iterative process. Further development allowed for direct calculations without trial-and-error. Many of terminal velocity formulations were based on the well-accepted terminal settling velocity known as the Stokes settling velocity (Eq. 2.35), which is valid for Reynolds numbers less than 0.1 (Stokes 1851, 8). This correlation was derived by equating the drag force and the gravitational force for a spherical particle (Eqs. 2.36 to 2.37).

$$U_r = U_t = \sqrt{\frac{4 d_p (\rho_p - \rho_l) g}{3 \rho_p C_D}} \quad (2.35)$$

$$F_s = \frac{\pi}{8} C_D \rho_l U_r^2 d_p^2 = \frac{\pi d_p^3}{6} (\rho_p - \rho_l) g \quad (2.36)$$

$$C_D = \frac{4 d_p (\rho_p - \rho_l) g}{3 \rho_p U_r^2} \quad (2.37)$$

Nonetheless, Eq. 2.35 was valid for describing free-falling velocity of spherical particles. Other forms of terminal velocity correlations can be applied to the specific range of applicability by combining Eq. 2.35 and the recommended drag coefficient correlations listed in Table 2.8.

Fluidised Bed Expansion

Many studies have been carried out to study the extension properties of fluidised beds (Richardson and Zaki 1954, 35; Rowe 1961, 175; Wen and Yu 1966, 100; Garside and Al-Dibouni 1977, 206; Khan and Richardson 1989, 111). Experimental data demonstrate that the voidage and terminal velocity relationship is independent of the total mass of solid particles in a liquid-solid fluidised bed. The different relationships between the superficial fluid velocity, U_l , the terminal velocity, U_t and the bed voidage, ϵ_l have been developed. Richardson and Zaki (1954, 35), based on a dimensional analysis, proposed the fluidised bed expansion correlation (Eq. 2.38). The correlation was derived in terms of voidage and the superficial fluid velocity as the bed voidage approaches unity (Eq. 2.39) (Karamanev and Nikolov 1992, 1916). The bed expansion index, n in the correlation is a function of terminal Reynolds number of particles, Re_t based on bed expansion data and can be defined into four separate equations with each spanning over a limited range of Reynolds number.

$$\frac{U_l}{U_t} = \epsilon^n \quad (2.38)$$

$$\log U_l = \log U_t - \frac{d_p}{D} \quad (2.39)$$

The Richardson and Zaki correlation is generally applicable to voidage around 0.8 to 0.9, except for heavy and/or large particles. A better correlation for the bed expansion index (Eq. 2.37) than the Richardson-Zaki correlation was developed by Khan and Richardson (1989, 111). Similar to the former correlation, this correlation

Table 2.8 Drag correlations and proposed range of applicability.

Range of Re_p	Correlation	Ref.	Eq.
$Re_p \leq 1$	$C_D = \frac{24}{Re_p} \left(1 + \frac{3 Re_p}{16} \right)$	Oseen 1910	2.26
$0.1 < Re_p < 1000$	$C_D = \frac{24}{Re_p} \left(1 + 0.15 Re_p^{0.687} \right)$	Schiller and Naumann 1933	2.27
$Re_p < 10^4$	$C_D = \frac{24}{Re_p} + \frac{3}{\sqrt{Re_p}} + 0.34$	Fair and Geyer 1954	2.28
$Re_p \leq 1$	$C_D = \frac{24}{Re_p} \left(1 + \frac{3}{16} Re_p - \frac{9}{160} Re_p^2 \ln Re_p \right)$	Proudman and Pearson 1957	2.29
$Re_p < 0.01$	$C_D = \frac{24}{Re_p} + \frac{3}{16}$	Clift et al. 1978	2.30
$0.01 < Re_p \leq 20$	$C_D = \frac{24}{Re_p} \left(1 + 0.1315 Re_p^{0.82-0.05 \log_{10} Re_p} \right)$		
$20 \leq Re_p \leq 260$	$C_D = \frac{24}{Re_p} \left(1 + 0.1935 Re_p^{0.6305} \right)$		
$260 \leq Re_p \leq 1500$	$\log_{10} C_D = 1.6435 - 1.1242 \log_{10} Re_p - 0.9295 Re_p^2 + 0.1558 (\log_{10} Re_p)^2$		
$1.5 \leq Re_p \times 10^{-3} \leq 12$	$\log_{10} C_D = 2.4571 + 2.5558 \log_{10} Re_p + 0.1049 (\log Re_p)^3$		
$1.2 \leq Re_p \times 10^{-4} \leq 4.4$	$\log_{10} C_D = -1.9181 + 0.6370 \log_{10} Re_p - 0.0636 (\log_{10} Re_p)^2$		
$4.4 \leq Re_p \times 10^{-4} \leq 33.8$	$\log_{10} C_D = -4.3390 + 1.5809 \log_{10} Re_p - 0.1546 (\log_{10} Re_p)^2$		
$Re_p < 8.6 \times 10^4$	$C_D = \frac{24}{Re_p} 10^{\frac{0.261 Re_p^{0.369} - 0.105 Re_p^{0.431} - 0.124}{1 + (\log_{10} Re_p)^2}}$	Flemmer and Banks 1986	2.31
$Re_p < 2.6 \times 10^5$	$C_D = \frac{24}{Re_p} \left(1 + 0.173 Re_p^{0.657} \right) + \frac{0.413}{1 + 16.3 Re_p^{1.09}}$	Turton and Levenspiel 1986	2.32
$0.01 < Re_p < 3 \times 10^5$	$C_D = \left(2.25 Re_p^{0.31} + 0.36 Re_p^{0.06} \right)^{3.45}$	Khan and Richardson 1989	2.33
$Re_p < 2.6 \times 10^5$	$C_D = \frac{24}{Re_p} + 3.3643 Re_p^{0.3471} + \frac{0.4607 Re_p}{Re_p + 2682.5}$	Haider and Levenspiel 1989	2.34

Table 2.9 Bed expansion correlations of chromatographic systems.

Expansion correlation	Voidage correlation	Range	Ref.	Eq.
$n = 4.65 + 19.5 \frac{d_p}{D}$		$Re_t < 0.2$		2.40
$n = \left(4.35 + 17.5 \frac{d_p}{D} \right) Re_t^{-0.03}$	Richardson and Zaki 1954	$0.2 < Re_t < 1$	Richardson 1871	
$n = \left(4.45 + 18 \frac{d_p}{D} \right) Re_t^{-0.1}$		$1 < Re_t < 200$		
$n = 4.45 Re_t^{-0.1}$		$200 < Re_t < 500$		
$n = 2.39$		$Re_t > 500$		
$\frac{4.7 - n}{n - 2.35} = 0.175 Re_t^{0.75}$	Richardson and Zaki 1954	Entire flow range	Rowe 1987	2.41
$\frac{4.8 - n}{n - 2.4} = 0.043 Ga^{0.57}$	Khan and Richardson 1989	$10^{-2} < Ar < 10^{10}$ $10^{-3} < \frac{d}{D} < 0.2$	Khan and Richardson 1989	2.42
$\frac{5.1 - n}{n - 2.7} = 0.1 Re_t^{0.9}$	Richardson and Zaki 1954	Entire flow range	Garside and Al-Dibouni 1977	2.43
$Ga = \left(18 Re^{1.687} \right) \epsilon^{-4.7}$	Richardson and Zaki 1954	Entire flow range	Wen and Yu 1966	2.44
$Ga = \left(20 Re + 1.44 Re^{1.8} \right) \epsilon^{4.73}$	Richardson and Zaki 1954	Entire flow range	Hartman et al., 1992	2.45

is valid in certain range of applicability as well. These two correlations and other popular correlations for spherical particles are summarised in Table 2.9 (Eqs.2.40 to 2.45). Some correlations are expressed as a function of dimensionless parameters, such as the Galileo, Ga and Archimedes, Ar numbers (Eqs. 2.46 to 2.47).

$$\frac{U_i}{U_t} = 1 - 1.15 \left(\frac{d_p}{D} \right)^{0.6} \quad (2.37)$$

$$Ar = \frac{d_p^3 \rho_l g (\rho_p - \rho_l)}{\mu^2} \quad (2.46)$$

$$Ga = \frac{d_p^3 g (\rho_p - \rho_l)}{\mu^2} \quad (2.47)$$

2.5 CONCLUSION

In this chapter, the sorghum seed protein kafirin was reviewed, regarding its physical properties, applications, and methods applied for its extraction. The batch extractions of kafirin were limited by low kafirin yield and purity, therefore requiring for kafirin purification. Ion exchange adsorption and chromatography was selected for purification of kafirin due to its wide application in protein purification, for both laboratory and industrial purposes. The principles of ion exchange chromatography were discussed, followed by a review of the different applications of ion exchange processes. Different adsorption based ion exchange systems were reviewed, with the emphasis on the application of the systems in continuous kafirin purification. Phenomenological modeling work done on ion exchange chromatographic systems were also summarised, followed by a review on the correlations to represent the fluid dynamics of these systems.

CHAPTER 3

LIQUID-SOLID CIRCULATING FLUIDISED BED SYSTEM: DESCRIPTION AND MODELING

3.1 INTRODUCTION

The inability of current generation processes to produce purified kafirin is clearly illustrated in the last chapter. Therefore, further purification using ion exchange chromatography can prove to be ideal. Continuous liquid solid circulating bed (LSCFB) offers distinct advantages over other ion exchange systems.

In order to develop a protein purification system based on the LSCFB, it is important to understand the effect of various operating parameters on its operations. A phenomenological model can ideally provide such understanding. A typical LSCFB system consists of downer and riser, integrating two different operations simultaneously. This chapter presents a general purpose, extensible, and dynamic model based on the tanks-in-series framework. The model allows adjusting the degree of backmixing in each phase for both fluidised beds. The model is validated with previously published data on extraction of BSA as model protein. Detailed dynamic analysis is performed on the ion exchange chromatographic based protein recovery. The interaction between the riser and downer are captured. Parametric studies on protein recovery in LSCFB system are carried out using the validated model to better understand the system behaviour.

3.2 LSCFB CHROMATOGRAPHIC SYSTEM

A typical LSCFB system is shown in Figure 3.1. The LSCFB systems consists of a pair of fluidised beds, liquid-solids separator, washing section below the separator, top solids return pipe between the separator and the downer, washing section below the downer, and bottom solids return pipe between the riser and the downer at the bottom (Lan et al. 2000, 858; Zhu et al. 2000, 83; Lan et al. 2002b, 252). Details of the dimensions and design characteristics of the whole LSCFB chromatographic system are reported in Table 3.1, and served as the foundation in this study.

Table 3.1 Liquid-solid circulating fluidised bed dimensions and design specifications.

Dimension	Design specifications
Downer fluidised bed.	Used for adsorption chromatography. Cylindrical vertical, circular cross section fluidised bed made of acrylic. Particles enter below raffinate outlet to create freeboard free of particles below
Riser fluidised bed.	Used for regeneration (elution) of adsorbent or ion exchange particles. Cylindrical vertical, circular cross section fluidised bed made of Plexiglas.
Downer distributor	Used mainly for radial velocity distribution. Tubular ring of perforated stainless steel pipe.
Riser primary distributor	Used mainly for radial velocity distribution. Primary stream and solids enter at the same elevation at base of riser.
Riser auxiliary distributor	Used mainly for radial velocity distribution. Auxiliary perforate plate distributor covered with stainless steel mesh.
Liquid-solids separator.	Hydraulic cyclone made of acrylic; stainless steel mesh on extract outlet. Extract outlet at same level as raffinate outlet on top of downer.
Riser washing section	Large-top, small-bottom funnel; wash water discharged at extract outlet.
Downer washing section	Funnel bottom of downer and vertical pipe; wash water discharged at raffinate outlet
Top solids return pipe	Inclined pipe connecting liquid-solids separator and top of downer. Maintained at moving packed bed region; essential for dynamic seal.
Bottom solids return pipe	Inclined pipe connecting downer and riser at the bottom. Maintained at moving packed bed region; essential for dynamic seal.

The first liquid-fluidised bed is a conventional counter-current flow downer fluidised bed in which the ion exchange particles enter through the inlet adjacent to the top of the downer by gravitational force from top solids return pipe and move downward to the bottom of the downer. The first fluidising liquid, the feed solution, enters the downer at the bottom end and flows upward in counter current with the particles. The second fluidised bed is a riser wherein the particles settle at the bottom of downer fluidised bed fall to the inlet adjacent to the bottom of riser from the bottom solid return pipe, after being rinsed by the washing section below the downer fluidised bed, and flow upward in co-current relation with a second fluidising liquid, the extracting buffer, which enters the riser from the bottom and flows upward through the riser carrying the particles along its flow.

3.2.1 Standard Protein and Ion Exchanger

Most chromatographic systems require the use of a reference standard. BSA is most commonly used as a standard for the determination of protein concentration as well as for other analytical methods (Lundblad 2012, 83). A number of researchers therefore used BSA as the model protein for the development of continuous processes involving ion exchange chromatography. Hunter and Cartar (2000, 81) used the BSA as a standard for comparison of proactive enzyme uptake on BRX-Q and BRX-QP anion exchangers, and BRX-S cation exchanger. Bruce and Chase (2002, 3087) used it as a model protein together with lysozyme (LYS) for evaluating performance of Streamline DEAE and Streamline SP, respectively. The molecular mass and isoelectric point is $M_r \sim 65000$ and $pI \sim 5$ for BSA (Righetti and Tudor 1981, 115).

Diaion HPA25, a strongly basic highly porous anion exchanger, is selected as the most suitable for use in the pilot-scale LSCFB chromatographic system (Lan et al. 2000, 858; Lan et al. 2002b, 252). The BSA adsorption capacity of Diaion HPA25 is 94.93 kg/m^3 , which is satisfactory for the LSCFB process. The average diameter of Diaion HPA25 particles is $320 \text{ }\mu\text{m}$, and the wet density 1.08 g/ml , which makes the terminal velocity of Diaion HPA 25 in water equivalent to 4.5 mm/s , sufficient for the LSCFB ion exchange chromatography. Anion exchange chromatography with Diaion HPA25 allows the recovery of BSA from neutral solution with a pH around 7.0, therefore giving a mild pH condition to maintain the BSA integrity. Also, Diaion

HPA25 is economical amongst other commercial ion exchangers, which is very important for process-scale applications.

3.2.2 Fluidised Beds

Liquid-solids adsorptive chromatographic systems are used for proteins recovery for decades. For the ion exchange chromatographic system of this study, cylindrical vertical circulating fluidised beds with circular cross section are applied. Hydrodynamics of these fluidised beds are the major interest of Section 3.3, so this section presents only the dimension and design specifications of these fluidised beds. The downer fluidised bed is made from Plexiglass with the height being 2.5 m and inner diameter of 120 mm (Lan et al. 2000, 858; Zhu et al. 2000, 83; Lan et al. 2002b, 252). Ion exchange particles are introduced into the downer about 0.82 m below the raffinate outlet so sufficient residence time is provided for the transfer of regenerated ion exchange particles, from the washing section below the liquid-solids separator into the bottom solids return pipe, by gravity, and to provide a part of the downer wherein a freeboard free of the particles is maintained under the raffinate outlet of sufficient height to substantially eliminate carryover of particles through the outlet while the raffinate is drained.

The riser is an acrylic column with the height being 3 m and inner diameter of 38 mm (Lan et al. 2000, 858; Zhu et al. 2000, 83; Lan et al. 2002b, 252). The extract outlet on the liquid-solids separator connected to the riser is at the equivalent elevation as that of the raffinate outlet on the top of the downer fluidised bed. Such design stabilizes the LSCFB within a satisfactory range by maintaining the pressure balance between these circulating fluidised beds.

3.2.3 Distributors

Distributors are installed in the circulating fluidised beds with intentions to induce as radially uniform and stable liquid velocity distribution across the entire fluidised beds cross sections as possible, in conjunction with the calming or homogenizing regions usually located upstream of the distributors, thus eliminating or at least minimising any tendency toward channelling or bulk circulation. Other functions of the distributors are to prevent non-fluidised regions upstream of the distributors, and to support the fluidised beds during system start-up and shutdown.

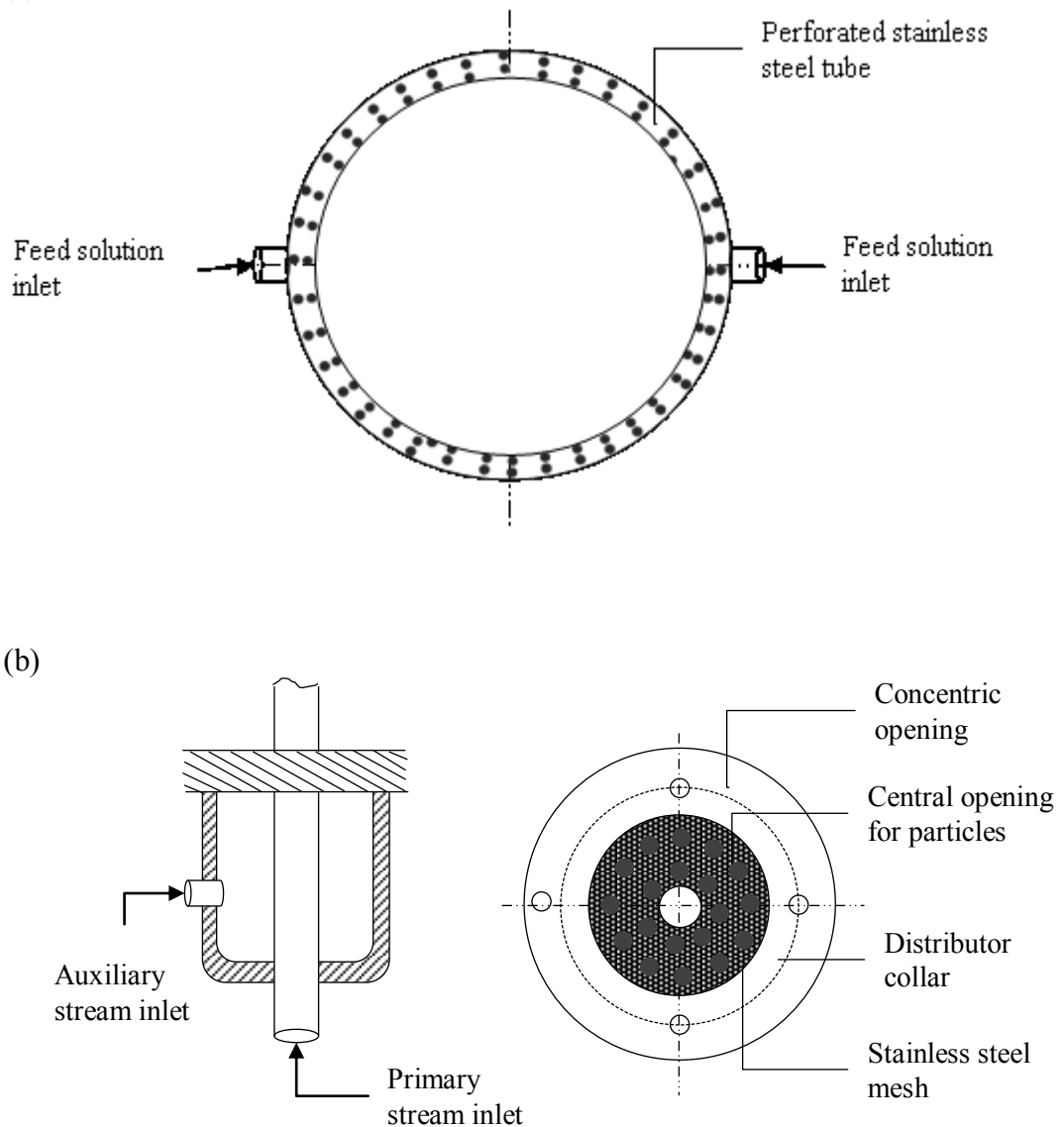


Figure 3.2 Schematic of the distributors in the liquid-fluidised beds system. (a) downer distributor; (b) riser distributor.

A schematic representation of the downer distributor is as shown in Figure 3.2(a). The distributor is a tubular ring of perforated stainless steel pipe, in which the particles are allowed to fall through the bottom solids return pipe while the feed liquor is introduced to the lower of the bed (Lan et al. 2000, 858; Zhu et al. 2000, 83; Lan et al. 2002b, 252). Also, for prevention of direct loss of solid particles while the extract is withdrawn, a stainless steel mesh is used to cover the extract outlet.

The distributor of the riser fluidised bed divides the entering extracting buffer into the primary stream and the auxiliary stream, as shown in Figure 3.2(b) (Lan et al. 2000, 858; Zhu et al. 2000, 83; Lan et al. 2002b, 252). The primary stream enters through a tubing of 11 mm inner diameter extending 36 mm into the riser, and therefore at the same elevation as that of the ion exchange particles entrance adjacent to the bottom of the riser through the bottom solids return pipe. This design helps to increase the pressure drop across the bottom solids return pipe and the stability of the system through the dynamic seal between the circulating fluidised beds. Description about the dynamic seal is covered in a later section. The auxiliary stream, on the other hand, is introduced to the lower of the riser through a perforated plate inlet covered by a stainless steel mesh. The auxiliary stream functions to induce stirring of particles settled at the bottom of the riser to be entrained upward to the top by the combination of the primary and auxiliary streams.

3.2.4 Liquid-Solids Separator and Washing Sections

A hydraulic cyclone connects directly to the riser fluidised bed functions as the liquid-solids separator for separation of the ion exchange particles from the extract outlet (Lan et al. 2000, 858; Lan et al. 2002b, 252). The cyclone has the advantages for not having any internal rotating parts, its low construction and maintenance costs, and low pressure drops. The separator has a liquid-solids inlet that was much larger than that of the riser to reduce the liquid velocity to lower than the particles terminal velocity to let gravity assist in the particles separation by differences in density and particle size, an axial liquid outlet, a solids outlet for the collected solid particles, and a stainless steel mesh covering the extract outlet. The mesh is necessary to avoid blockages of ion exchange particles circulation when the liquid-solids separator operated at relatively high liquid velocity.

Ion exchange and regeneration (elution) of ion exchange particles are coupled with washing of the particles before the particles are transferred from one bed to the other. Residual liquid trapped within the intraparticle pores and the intraparticle voids of the particles is removed for preventing the residual liquid from one column to contaminate the main stream in the other column. The top washing section is configured by the funnel bottom of the liquid-solids separator discussed earlier and the solids return pipe made of acrylic with diameter being 40 mm and height of 200

mm (Lan et al. 2000, 858; Lan et al. 2002b, 252). A schematic illustration of the combined separator and top washing section is depicted in Figure 3.3(a). Wash water is introduced at an elevation slightly higher than the top solids return pipe, and went upward. The wash water slows down the falling particles, created a solids layer in the funnel bottom of the separator, and rinses the particles before their falling into the top solids return pipe. The wash water also minimises the intermixing between the extract in the riser and the deionised feed solution at the top of the downer. The wash water combines with the extract at the top of the riser, and exits from the extract outlet with minimal dilution effect due to substantial flowrate differences between these liquids. This design nonetheless simplifies the control of the LSCFB system.

The bottom washing section of the downer is comprised of the funnel bottom of the bed and a vertical pipe of 40 mm inner diameter and 200 mm height wherein the wash water enters from the base of the bed. A schematic diagram of the washing section is shown in Figure 3.3(b). The upward wash water travels counter current to and washes the ion exchange particles before they leave to the riser. The wash water dilutes the deionised feed solution and exits from the top of the downer through the raffinate outlet.

3.2.5 Solids Return Pipes

Two main streams with different properties, the feed solution of low ionic strength and high concentration of solute, and the pure extract of high ionic strength and low concentration of solute, are involved in the downer and the riser, separately. Thus a dynamic seal between these fluidised beds to prevent intermixing of these main streams while allowing for a stable circulation of particles is critical for smooth operation of the LSCFB system. The dynamic seal is achieved by keeping the particles in the solids return pipes operating as packed moving beds to form a particle plug splitting the two primary streams of different properties (Lan et al. 2000, 858; Lan et al. 2001, 159; Lan et al. 2002b, 252).

Formation and maintenance of the particle plugs in the whole liquid-solid system of interest depends on the flow of particles within the solids returning pipes. Control of the latter is accomplished by the butterfly valve. Butterfly valves are quarter-turn valves used to regulate flow, incorporating a rotational disk to control the flowing

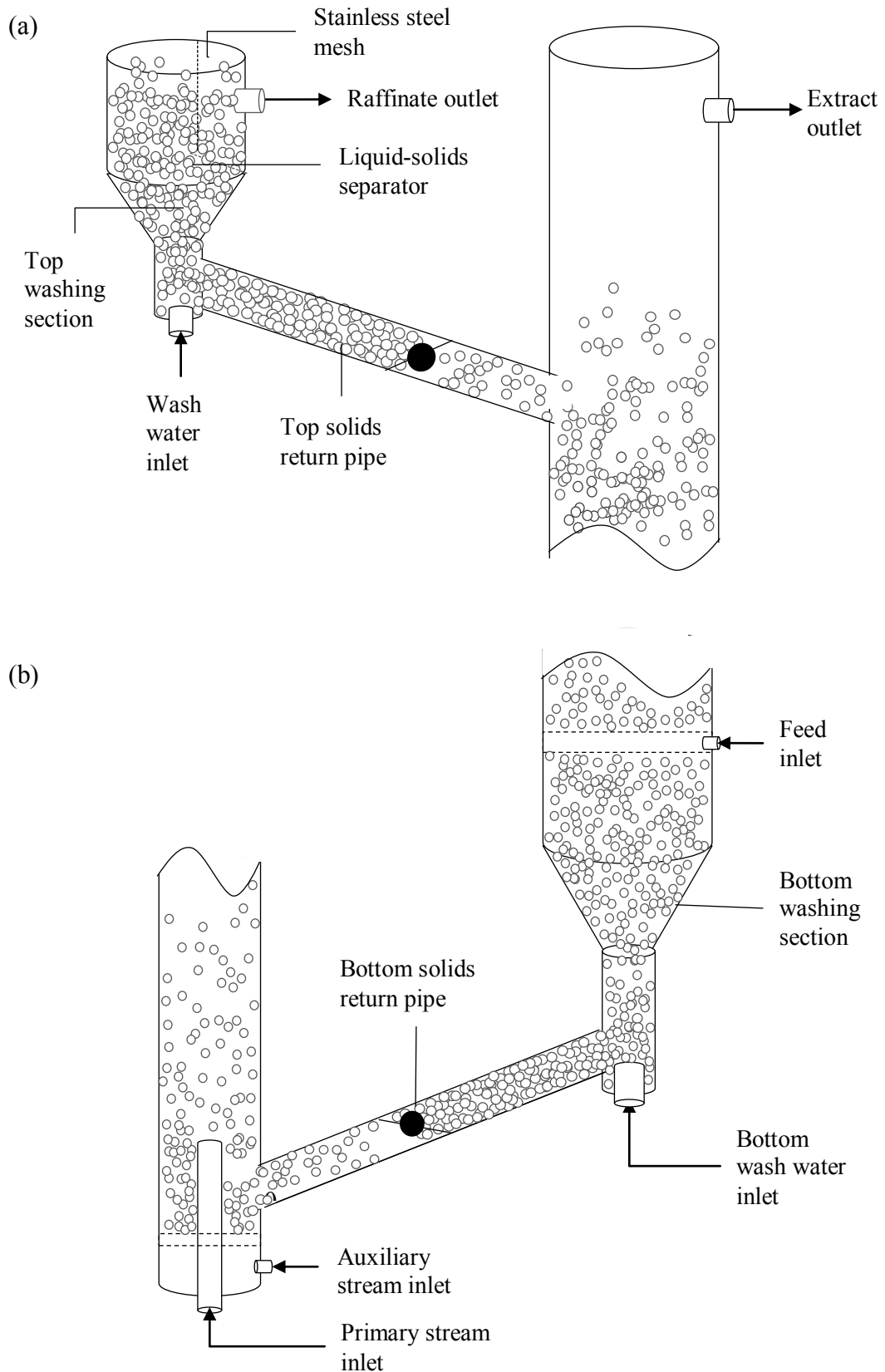


Figure 3.3 Schematic of the dynamic seals in a liquid-solid circulating fluidised beds system. (a) liquid-solids separator, top washing section and dynamic seal; (b) bottom washing section and dynamic seal.

fluid in the process. The disk is positioned perpendicular to the flow in the closed position, and rotates one quarter of a turn to be parallel to the flow in the fully opened position. Intermediate rotations allow regulation of the fluid flow. The butterfly valve is preferred over other valves because of the low density of ion exchange particles which proves to be difficult for some valves. Another credit to the butterfly valve is that it enhanced the pressure drop across the solids return pipe, which is critical for forming and maintaining the dynamic seal between the fluidised beds and the stabilization of the whole system.

The dynamic seal introduced through the top solids return pipe, 500 mm long and 35 mm in diameter, in between the liquid-solids separator and the top of downer is shown in Figure 3.3(a) (Mazumder et al. 2009a, 113). Mixing of the de-ionised feed solution and extract is prevented wherein the wash water introduced from the bottom of the separator is forced upward to the top washing section. Complete mixing is initiated by the system design comprised of a smaller wash water inlet than the separator bottom pipe and the pipe is smaller than the funnel bottom. When the top solids return pipe works in the packed moving bed region, when particle plug is maintained, mixing between the deionised feed solution and the extract is successfully avoided. The wash water exits via the extract outlet, slightly diluting the extract but not enough to affect the carrying fluid velocity in the riser fluidised bed.

The bottom solids return pipe is 800 mm long and 35 mm in diameter, between the bottoms of the downer and the riser fluidised beds, is based on similar ideals as the bottom solids return pipe, as discussed above (Mazumder et al. 2009a, 113). A schematic diagram of the bottom solids return pipe and washing section to illustrate the dynamic seal is shown in Figure 3.3(b) (Lan et al. 2000, 858; Lan et al. 2001, 159; Lan et al. 2002b, 252). Wash water introduced from the base of the downer is forced upward into the bottom washing section to initiate perfect mixing of the phases due to the smaller wash water pipe compared to the lower of the washing section in addition to the large top, small bottom-funnel to help deliver different velocities in different parts, and thus the efficiency of mixing and rinsing of particles. The wash water is discharged from the raffinate outlet with minor dilution effect to simplify the LSCFB system control for not requiring for a dynamic seal between the downer and the bottom washing section.

3.3 LSCFB HYDRODYNAMIC REGIONS AND TRANSITIONS

3.3.1 Downer Hydrodynamics

In the downer, a counter-current flow of liquid and solid phases is attained as the feed solution moves upward and ion exchange particles flow downward. Fluidisation region and flow characteristics in the LSCFB determine the particles residence time and mass transport essential in LSCFB hydrodynamic modeling. There is a common agreement in many simulation and modeling studies which divides the downer into three hydrodynamically differing regions based on solids holdup distribution. These are called the freeboard at the top, the dilute region in the middle, and the dense phase region at the bottom of the downer (Lan et al. 2000, 858). The freeboard is essential to prevent loss of particles into the raffinate while the dense phase region is the most vital region for adsorption in the downer as the solids holdup in this region is much higher than the freeboard and dilute regions. Liquid phase protein concentration in the more dilute regions at upper section of the downer is found to be very low. So the extent of protein adsorption in this region is assumed to be negligible. The effective downer bed height, $h_{d,eff}$ (Eqs. 3.1 and 3.2) investigated is therefore the height of the dense phase region calculated from solids holdups from different parts of the LSCFB system (Zheng et al. 1999, 284; Lan et al. 2000, 858; Lan et al. 2002b, 252).

$$h_{d,eff} \varepsilon_{sd} A_d = \frac{S}{\rho_a} - A_r (h_{r1} \varepsilon_{sr1} + h_{r2} \varepsilon_{sr2}) - V' (1 - \varepsilon') \quad (3.1)$$

$$V' (1 - \varepsilon') = \frac{4}{3} h_{sep} \varepsilon_{sep} A_{sep} - L_t A_t (1 - \varepsilon_t) - L_b A_b (1 - \varepsilon_b) \quad (3.2)$$

Downer dense phase region operates in conventional fluidisation region, where the particles are in full suspension and uniformly distributed within this region (Kwauk, 1963, 587; Lan et al. 2000, 858). Figure 3.4 shows the counter-current contact between the two phases in the dense phase region. The modified Richardson and Zaki equation (Eq. 3.3), as proposed by Kwauk (1963, 587), has been employed to compute for bed voidage, ε_d . This model is valid for conventional liquid-solid particulate fluidisation, in other words, there is uniform flow structure distribution.

$$U_{ld} + \frac{U_{sd} \varepsilon_d}{1 - \varepsilon_d} = U_i \varepsilon_d^n \quad (3.3)$$

The bed expansion index, n (Eq. 3.4) in the correlation is expressed as a function of terminal Reynolds number of particles, Re_t (Eq. 3.5) based on bed expansion data (Lan et al. 2002b, 252). The terminal settling velocity, U_t correlation employed is known as the Stokes settling velocity (Eq. 3.6), derived by equating the drag and gravitational forces for a spherical particle, and valid for Re_t between 1 and 200 (Stokes 1851, 8).

$$n = Re_t^{-0.01} \left(4.4 + \frac{18d_p}{D_c} \right) \quad (3.4)$$

$$Re_t = \frac{U_t d_p \rho}{\mu} \quad (3.5)$$

$$U_t = \frac{gd_p^2(\rho_w - \rho)}{18\mu} \quad (3.6)$$

The correlation proposed by Khan and Richardson (1989, 111), Eq. 3.7, is applied to obtain U_i , the superficial liquid velocity at bed voidage, $\varepsilon = 1$.

$$\frac{U_i}{U_t} = 1 - 1.15 \left(\frac{d_p}{D_c} \right)^{0.6} \quad (3.7)$$

Entrained particles from the liquid-solids separator then transfer into the downer through the return pipe by gravity. Assuming the solids velocity, U_{sd} equivalent to the particles terminal settling velocity, U_t , the voidage in the top solids return pipe and separator, ε_t (Eq. 3.8) and ε_{sep} (Eq. 3.9), can be estimated (Zheng et al. 1999, 284).

$$1 - \varepsilon_t = \left(\frac{D_r}{D_t} \right)^2 \frac{G_s}{\rho_p U_t} \quad (3.8)$$

$$1 - \varepsilon_{sep} = \left(\frac{D_r}{D_{sep}} \right)^2 \frac{G_s}{\rho_p U_t} \quad (3.9)$$

3.3.2 Riser Hydrodynamics

The riser operates in liquid-solid circulating fluidisation region, and provides excellent interfacial mass transfer between the two phases above and beyond that of conventional fluidisation. To maintain fast fluidisation region, the superficial liquid

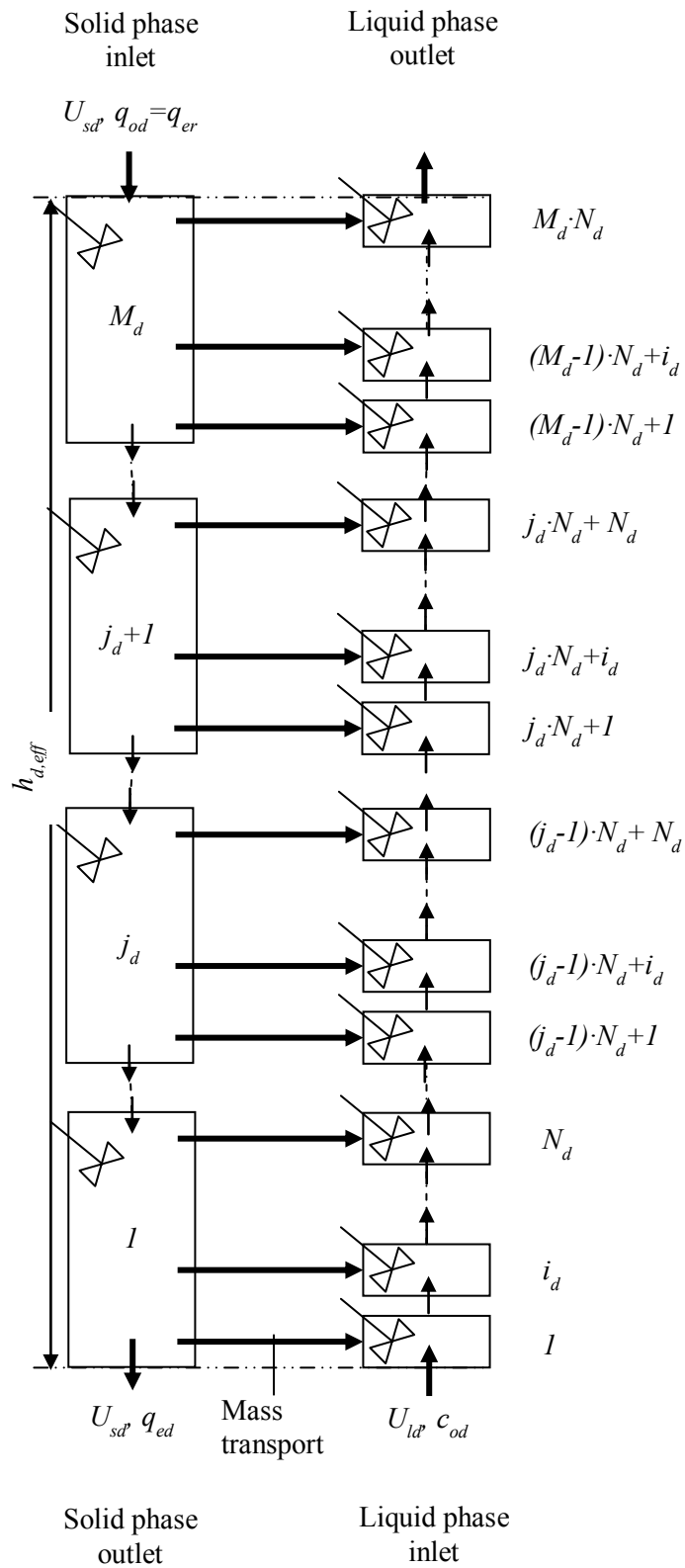


Figure 3.4 Flow diagram of the liquid-solid circulating fluidised beds. Segregation of the downer in M_d number of solid phase tanks and N_d number of liquid phase subtanks per solid tank.

velocity U_{lr} must exceed particle terminal velocity U_t , so that significant amount of the particles is entrained upwards to the top of the riser, and separated by a liquid-solids cylindrical separator. Co-current contact between the liquid and solid phase is shown in Figure 3.5.

Existence of a lower distributor region of an extensively higher solids holdup and an upper region in the dilute-phase flow are common in fast fluidised beds (Karri and Knowlton 1991, 67; Zheng et al. 1999, 284; Monazam and Shadle 2004, 89). The solids holdup distribution described the extent of different regions. Despite its comparatively little height, the distributor region is of importance because of the higher solids holdup distribution and thus assumed to obey Richardson-Zaki correlation (Richardson and Zaki 1952, 35). Hydrodynamics of the riser distributor region is well defined by the voidage by the voidage, ε_{rl} acquired by the modified correlation of Richardson and Zaki by Kwauk (1963, 587), Eq. 3.10, for co-current flows. The bed expansion index, n and the superficial liquid velocity, U_i at $\varepsilon = 1$ in the distributor region are obtained from Eqs. 3.4 to 3.7.

$$U_{lr} - \frac{U_{sr}\varepsilon_{rl}}{1-\varepsilon_{rl}} = U_i\varepsilon_{rl}^n \quad (3.10)$$

A transition from conventional fluidisation region in the distributor region into circulating fluidisation region in the upper dilute region has been observed for low density ion-exchange particles (Zheng et al. 1999, 284; Monazam and Shadle 2004, 89). This transition happens so sharply for ion-exchange particles with low densities that the transition is hardly over a range, but a single point in the liquid velocity. The upper dilute region is described by a uniform axial voidage, ε_{r2} profile along the riser (Liang et al. 1995, 259; Zheng et al. 1999, 284; Zhu et al. 2000, 82; Monazam and Shadle 2004, 89). An empirical correlation for solids holdup in the upper dilute region, ε_{sr2} is proposed by Mazumder et al. (2009a, 111) as a function of superficial liquid velocity and solids circulation rate (Eq. 3.11). The use of this correlation has obtained good agreement between the predicted and experimentally obtained results reported by Lan et al. (2002, 252).

$$\varepsilon_{sr2} = 2.64 \times 10^{-14} U_{lr}^{-5.343} + 2.57 \times 10^{-5} G_s U_{lr}^{-1.578} \quad (3.11)$$

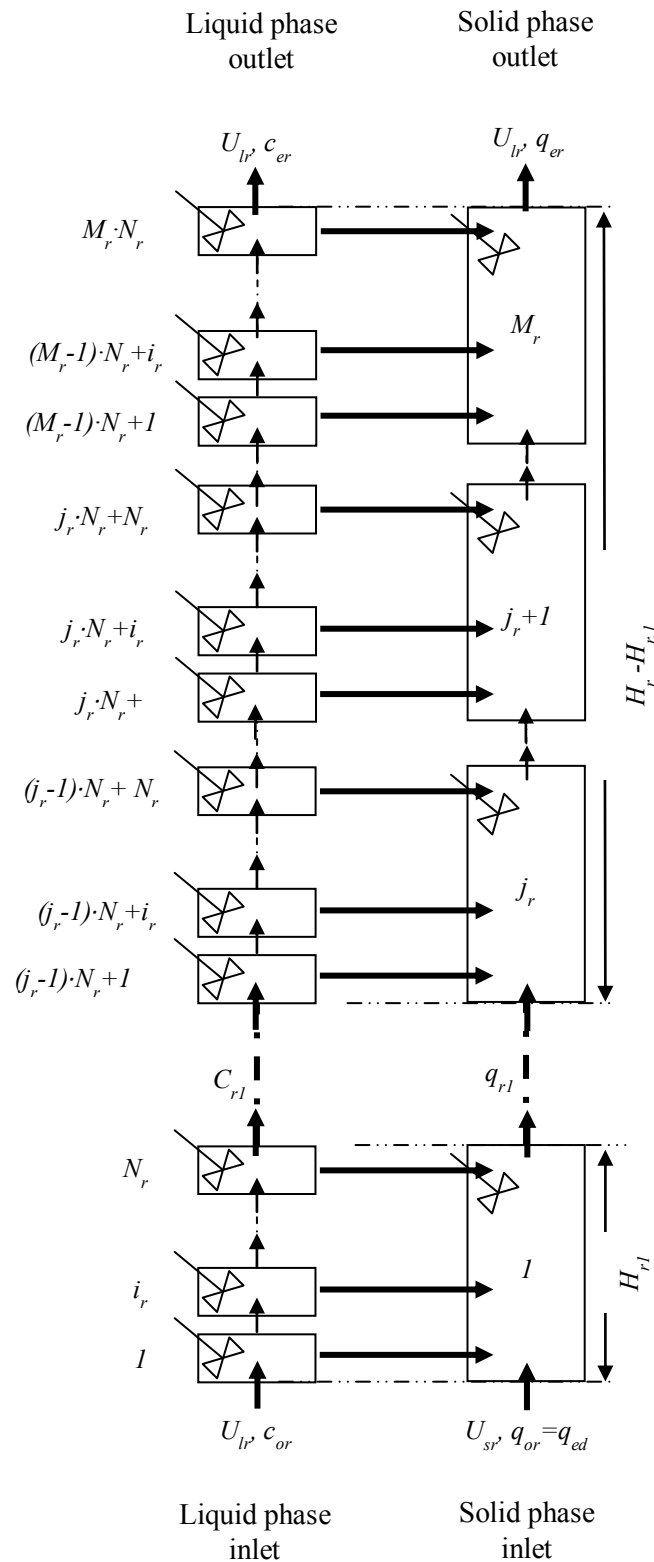


Figure 3.5 Flow diagram of the liquid-solid circulating fluidised beds. Segregation of the riser in $M_{r,l}$ number of solid phase tanks and $N_{r,l}$ number of liquid phase sub-tanks per solid tank in freeboard region, and $M_{r,2}$ number of solid phase tanks and $N_{r,2}$ number of liquid phase sub-tanks per solid tank in upper dilute region.

3.4 MODEL DEVELOPMENT

The performance of the LSCFB depends closely on the hydrodynamics and the distribution of different phases in the downer and riser. Therefore, a model that allows describing the hydrodynamics in a flexible manner is desirable. The tanks-in-series framework allows adjusting the backmixing degree in each of the phase independently. Additionally it allows flexibility in adjusting the residence time distribution of different phases. Therefore, it is chosen as the basis of the model.

A schematic diagram of the LSCFB system is shown in Figure 3.1. The mixing patterns in these fluidised beds are represented by a series of ideally mixed tanks. The tank-in-series framework is chosen because it not only allowed easy integration with the mass transport model, but also offered a straightforward comparison of the tanks-in-series system performance with that of a plug flow system reported previously (Lan et al. 2000, 858; Mazumder et al. 2009a, 111). Each of the fluidised beds in the LSCFB is divided into two series of ideally mixed stirred tanks, illustrated schematically in Figure 3.4 and Figure 3.5; one corresponding to liquid phase, while the other to solid phase. Diaion HPA25 anion exchanger is referred to as the solid phase in the diagram. In the current model, the solid phase is formed by M equally size ideally mixed stirred tanks, arranged in series, and each solid tank is then further subdivided into a series of N ideally mixed subtanks of liquid phase.

The predicted results have been examined for fitting with reported data in Lan et al. (2000, 858) and Mazumder et al. (2009a, 111) by performing the simulation with different numbers of M and N for downer and riser. Optimum fitting results are found for the case with downer dense phase region $M_d=20$ and $N_d=1$, riser upper dilute phase region $M_{r1}=1$ and $N_{r1}=3$, and riser distributor region $M_{r2}=9$ and $N_{r2}=3$. In the LSCFB, entrained ion exchange particles do not flow convectively through the downer and riser in contrast to liquid flows. Subsequently, mixing in solid phase is relatively extensive than that in liquid phase. Thus, the solids phase is represented by fewer tanks than the liquid phase. The tanks-in-series model for the various phases in the LSCFB fluidised beds are numbered upwards.

3.4.1 Model Assumptions

Governing equations for recovery of protein in LSCFB system are derived on basis of the research results on equilibrium isotherm and hydrodynamics of the various phases (Lan et al. 2000, 858; Lan et al. 2002b, 252; Mazumder et al. 2009a, 111). In deriving the model equations, some assumptions are made and listed as followed:

- Adsorption rate is limited by intra-particle diffusional resistance and mass transfer resistance in the laminar boundary layer surrounding an individual particle.
- Surface adsorption is instantaneous and thus a local equilibrium is established at the particle surface between protein concentrations in the two existing phases. The equilibrium adsorption behaviour is well-described by the Langmuir isotherm.
- Ion exchange particles are spherical and uniform in size with a mean particle radius. These particles are relatively immobile.
- Protein concentrations in liquid solution of the freeboard and dilute phase region in downer are very low, thus adsorption in these regions are negligible compared to that of the dense region.
- Uniform distributions of particle concentration and solids holdup in the system.
- Effects of liquid axial dispersion and solid backmixing in each tank are negligible.
- Thermal effects are negligible, i.e., the system operates isothermally.

On the basis of these assumptions, transient model equations for the downer and riser are derived. In order to close the model equations, information on various hydrodynamic parameters are required. The framework is flexible in selecting correlations for these parameters. The correlations used in this study are previously discussed in Section 3.3.

3.4.2 Formulation of Downer

Protein mass balance in liquid and solids phase is applied to develop ordinary different equations to describe protein concentrations in different phase. The effective downer height investigated is the height of dense phase region due to negligible protein adsorption in the dilute phase region. For i_d -th subtank represented by Figure 3.6(a), where $1 < i_d < M_d N_d$, the protein mass transfer balance (Eq. 3.12) is derived. Corresponding mass transfer balance for solid phase (Eq. 3.13) is also developed, for $1 < j_d < M_d$ as described in Figure 3.7(a).

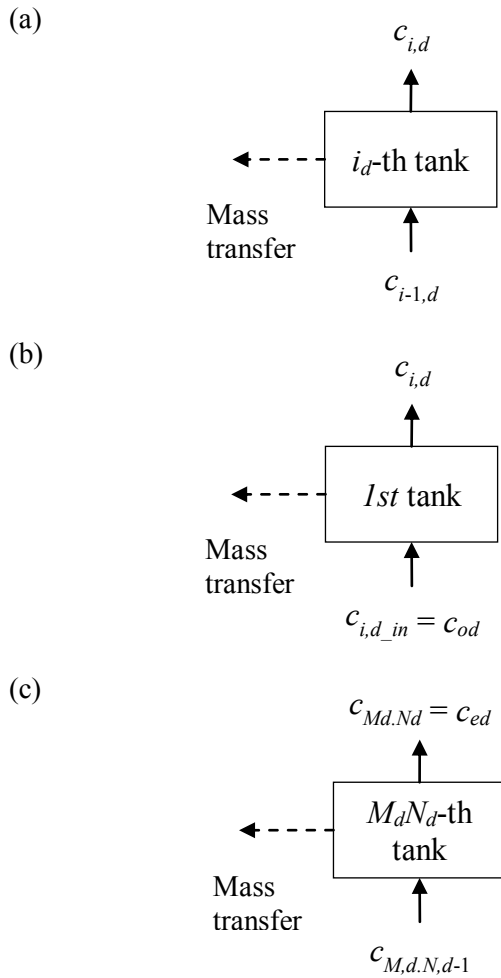


Figure 3.6 Schematic representations of liquid-phase (a) i_d -th subtank, (b) 1st subtank, and (c) $M_d N_d$ -th subtank in the downer.

$$\frac{dc_{i,d}}{dt} = \frac{U_{ld}(c_{i-1,d} - c_{i,d})}{h_{ld}\varepsilon_d} - \frac{K_L a(1 - \varepsilon_d)(c_{i,d} - c_{eq})}{\varepsilon_d} \quad (3.12)$$

$$\frac{dq_{j,d}}{dt} = \frac{U_{sd}(q_{j+1,d} - q_{j,d})}{h_{sd}(1 - \varepsilon_d)} + \sum_{i,d} \frac{K_L a(1 - \varepsilon_d)(c_{i,d} - c_{eq})}{\varepsilon_d} \quad (3.13)$$

The feed solution, with protein concentration, c_{od} enters the 1st liquid subtank in Figure 3.6(b), and exits the system at c_{ed} from $M_d N_d$ -th subtank described in Figure 3.6(c). Liquid phase mass balance (Eq. 3.12) is rewritten as Eq. 3.15.

$$c_{1,d_in} = c_{od} \quad (3.14)$$

$$c_{M_d N_d} = c_{ed}$$

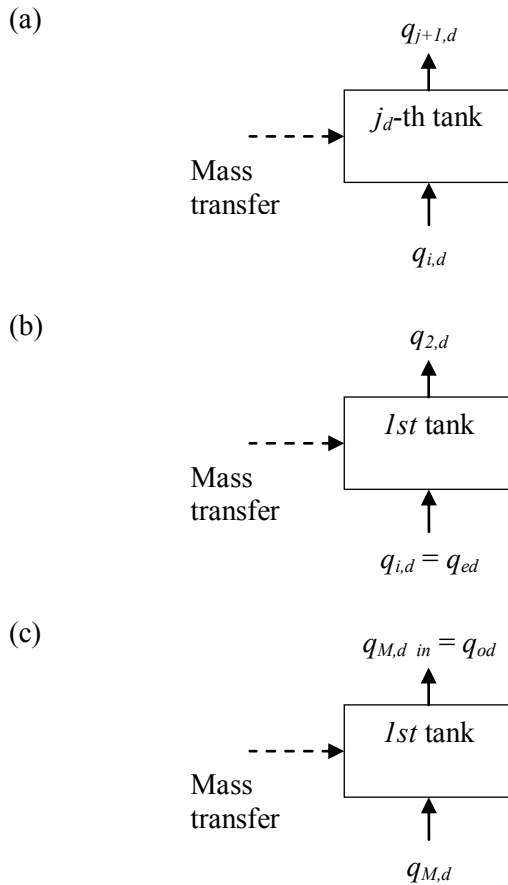


Figure 3.7 Schematic representations of solid-phase (a) j_d -th tank, (b) 1st tank, and (c) M_d -th tank in the downer.

$$\frac{dc_{1,d}}{dt} = \frac{U_{1d}(c_{od} - c_{1,d})}{h_{1d}\varepsilon_d} - \frac{K_L a(1 - \varepsilon_d)(c_{1,d} - c_{eq})}{\varepsilon_d} \quad (3.15)$$

$$\frac{dc_{M_d(N_d)}}{dt} = \frac{U_{1d}(c_{M_d(N_d)} - c_{M_d(N_d)})}{h_{1d}\varepsilon_d} - \frac{K_L a(1 - \varepsilon_d)(c_{M_d(N_d)} - c_{eq})}{\varepsilon_d}$$

In writing the solid phase mass balance for protein, the dynamic seal between the riser and downer is considered, as intermixing does not occur between the two phases in the solids feed pipe meaning no adsorption has taken place. Mass balances for the solid phase are then written so as to make the protein concentration at the outlet of downer, q_{ed} equivalent to that at the inlet of riser, q_{or} . The corresponding boundary conditions (Eq. 3.16) are as described. Solid phase balance of downer is therefore rewritten in Eq. 3.17.

$$q_{1,d} = q_{ed} \quad (3.16)$$

$$\begin{aligned}
 q_{M,d_in} &= q_{od} = q_{er} \\
 \frac{dq_{1,d}}{dt} &= \frac{U_{sd}(q_{2,d} - q_{ed})}{h_{sd}(1 - \varepsilon_d)} + \sum_{i,d} \frac{K_L a(1 - \varepsilon_d)(c_{i,d} - c_{eq})}{\varepsilon_d} \\
 \frac{dq_{M,d}}{dt} &= \frac{U_{sd}(q_{er} - q_{M,d})}{h_{sd}(1 - \varepsilon_d)} + \sum_{i,d} \frac{K_L a(1 - \varepsilon_d)(c_{i,d} - c_{eq})}{\varepsilon_d}
 \end{aligned} \tag{3.17}$$

To solve the coupled mass balances, initial and boundary conditions are required. In the beginning, zero protein concentration and loading (Eq. 3.18) are assumed in the downer liquid subtanks and solid tanks.

$$\begin{aligned}
 c_{i,d} \Big|_{t=0} &= 0 \\
 q_{j,d} \Big|_{t=0} &= 0
 \end{aligned} \tag{3.18}$$

It is reasonable to simplify the system by assuming that the downer operates in plug flow, since liquid-solid system is fluidised homogeneously. As the downer operates at very low liquid velocity, the effect of liquid dispersion and solids backmixing are negligible. Again, the lumped mass transfer rate coefficient, K_L can be expressed as a product of the film mass transfer coefficient, k_f and a constant factor considering intraparticle diffusion effect, ψ (Eq. 3.19).

$$K_L = \psi k_f \tag{3.19}$$

The k_f in the downer dense phase region (Eq. 3.20) is calculated as a function of solids holdup, ε_{sd} and particle Reynolds number, Re_p in the downer using the correlation reported by Fan, Yang and Wen (1960, 482).

$$k_f = \frac{D_m}{d_p} \left[2 + 1.03 (\varepsilon_{sd} Re_p)^{0.5} (Sc)^{0.33} \right] \tag{3.20}$$

In the downer of the LSCFB system, both the liquid and solid phases are moving and Re_p is expressed in terms of the superficial slip velocity, U_{slip} in the downer (Eq. 3.21). For counter-current flow arrangement, the actual slip velocity accounts for both the feed solution and particles superficial velocities (Eq. 3.22) (Mazumder et al. 2009a, 111).

$$Re_p = \frac{d_p U_{slip} \rho}{\mu} \tag{3.21}$$

Table 3.2 Liquid-solid circulating fluidised bed operating parameters.

	Value
Constant factor for intraparticle diffusion, ψ	0.003944 ^{3.9336 Gs}
Langmuir dissociation constant, K_d (kg/m ³)	0.25
Desorption rate constant of riser distributor region, k_{r1} (m/s)	0.005253
Desorption rate constant of riser upper dilute region, k_{r2} (m/s)	0.0006
Feed concentration, c_{od} (kg/m ³)	2
Solids circulation rate, G_s (kg/m ² /s)	1.24
Downer superficial liquid velocity, U_{ld} (m/s)	0.0006
Riser superficial liquid velocity, U_{lr} (m/s)	0.0113
Solid particles inventory, S (kg)	3

$$U_{slip} = \frac{U_{ld}}{\varepsilon_d} + \frac{U_{sd}}{1-\varepsilon_d} \quad (3.22)$$

BSA adsorption onto the anion exchanger Diaion HPA25 obeys the Langmuir isotherm model. This experimental observation has been stated in literature (Lan et al. 2000, 858). Therefore, the equilibrium liquid-phase protein concentration at the liquid-solids interface, c_{eq} is predicted (Eq. 3.23).

$$c_{eq} = \frac{K_d q_d}{q_m - q_d} \quad (3.23)$$

3.4.3 Formulation of Riser

Protein mass balances in liquid (Eq. 3.24) and solid phase (Eq. 3.25) are written, for the flow arrangement shown in Figure 3.8(a) and Figure 3.9(a). Elution in riser is very fast. The riser is composed of two distinct regions, the distributor region and upper dilute region. From experiment, protein elution rate from ion exchange particles surface is higher in the distributor region due to the higher solids holdup in this region. In the distributor region k_{r1} differs from that of the upper dilute region k_{r2} , as presented in Table 3.2.

$$\frac{dc_{i,r}}{dt} = \frac{U_{lr}(c_{i-1,r} - c_{i,r})}{h_{lr}\varepsilon_r} + \frac{k_r q_{j,r}(1-\varepsilon_r)}{\varepsilon_r} \quad (3.24)$$

$$\frac{dq_{j,r}}{dt} = \frac{U_{sd}(q_{j-1,r} - q_{j,r})}{h_{sr}(1-\varepsilon_r)} - \sum_{i,r} \frac{k_r q_{j,r}(1-\varepsilon_r)}{\varepsilon_r} \quad (3.25)$$

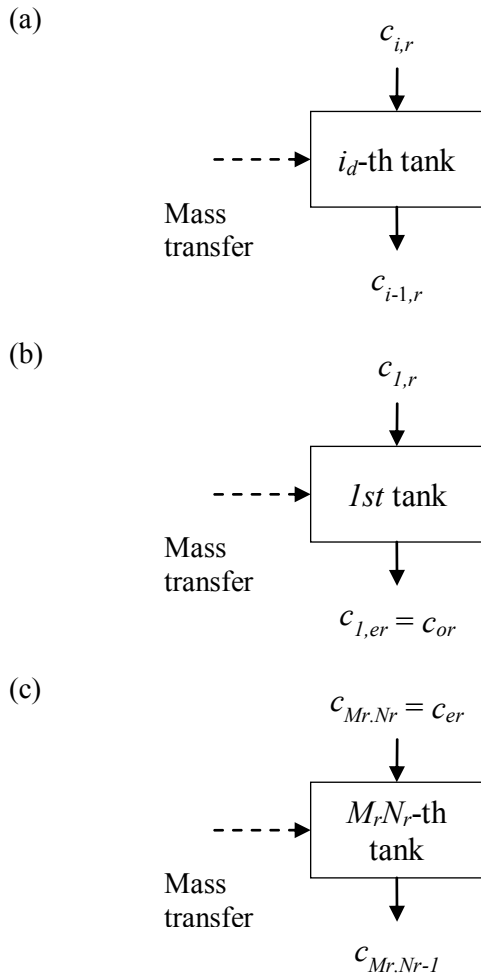


Figure 3.8 Schematic representations of liquid-phase (a) i_r -th subtank, (b) 1st subtank, and (c) $M_r N_r$ -th subtank in the riser.

The extracting buffer with initial protein concentration c_{or} enters the 1st liquid subtank shown in Figure 3.8(b), and then exits the system at c_{er} from $M_r N_r$ -th subtank described by Figure 3.8(c).

Liquid phase mass balance (Eq. 3.24) is rewritten as Eq. 3.27.

$$c_{1,r_in} = c_{or} \quad (3.26)$$

$$c_{M_r N_r} = c_{er}$$

$$\frac{dc_{1,r}}{dt} = \frac{U_{lr}(c_{or} - c_{1,r})}{h_{lr}\epsilon_r} + \frac{k_r q_{j,r}(1 - \epsilon_r)}{\epsilon_r} \quad (3.27)$$

$$\frac{dc_{M_r(N_r)}}{dt} = \frac{U_{lr}(c_{M_r(N_r)-1} - c_{er})}{h_{lr}\epsilon_r} + \frac{k_r q_{j,r}(1 - \epsilon_d)}{\epsilon_r}$$

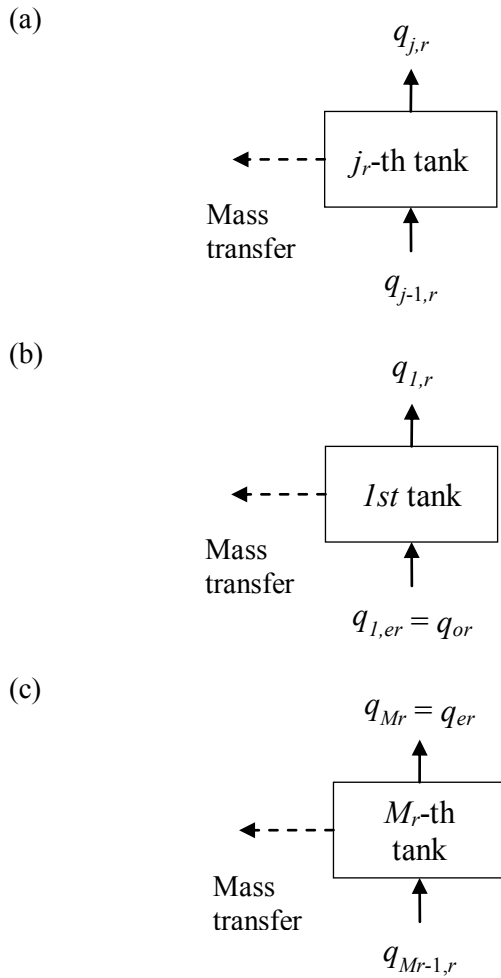


Figure 3.9 Schematic representations of solid-phase (a) tank- j_r , (b) tank-1, and (c) tank- M_r in the riser.

The corresponding boundary conditions (Eq. 3.28) as described by the dynamic seal, is incorporated into the solid phase balance rewritten in Eq. 3.29.

$$q_{1,r_in} = q_{od} = q_{ed} \quad (3.28)$$

$$q_{M,r} = q_{er}$$

$$\frac{dq_{1,r}}{dt} = \frac{U_{sr}(q_{ed} - q_{1,r})}{h_{sr}(1 - \varepsilon_r)} - \sum_{i,r} \frac{k_r q_{1,r}(1 - \varepsilon_r)}{\varepsilon_r} \quad (3.29)$$

$$\frac{dq_{M,r}}{dt} = \frac{U_{sr}(q_{er} - q_{M,r})}{h_{sr}(1 - \varepsilon_r)} - \sum_{i,r} \frac{k_r q_{M,r}(1 - \varepsilon_r)}{\varepsilon_r}$$

To solve the coupled mass balances, initial and boundary conditions are required. Similar assumptions are made in the riser, in which zero protein concentration and loading (Eq. 3.30) are assumed in the riser liquid sub tanks and solid tanks.

$$c_{i,r}|_{t=0} = 0 \quad (3.30)$$

$$q_{j,r}|_{t=0} = 0$$

3.5 NUMERICAL SIMULATION

Figure 3.10 presents the schematic diagram of LSCFB, while Table 3.2 summarizes the parameters used in the current numerical simulation. Computational algorithm outlined in Figure 3.10 is a step-by-step procedure for solving the initial value problem in coupled ordinary differential equations for simulating the system performance. MATLAB[®] R2010a code is incorporated into this model. Two model parameters specified at the outset of the simulation are, the number of tanks-in-series in each phase used to assemble the two entrained fluidised beds. The mixing behaviour in particles is considerably extensive than liquid phase, thus the former is represented by fewer tanks than the latter. Initially, the liquid phase superficial velocities and solid circulation rate are given, and the particle superficial velocities are calculated. Bed voidage in the downer dense region ε_d , riser distributor region ε_{r1} , and upper dilute region ε_{r1} are solved (Eqs. 3.3, 3.10, and 3.11) accordingly. Effective height of the downer $h_{d,\text{eff}}$ is computed as a function of the solids holdup in different LSCFB sections (Eqs. 3.8 and 3.9), from Eqs. 3.1 and 3.2. At time $t=0$, the system initial conditions are set (Eqs. 3.18 and 3.30).

In this study, the built-in numerical solver ODE45 in MATLAB[®] R2010a is used to solve the system ordinary differential equations. The set of coupled ordinary differential equations (Eqs. 3.12 and 3.13) that integrated the liquid and solid phase mass transfer interaction in downer are solved simultaneously using the initial values of $c_{i,d}$ and $q_{j,d}$ in the tanks. The calculated protein concentration profile along the downer is assigned to $c_{i,d}$ and $q_{j,d}$. Protein concentration in the solid phase leaving at the bottom of the downer q_{ed} is calculated, which equivalent to that entering the riser q_{or} . Next, using the value of q_{or} , the coupled ordinary differential equations for the riser (Eqs. 3.24 and 3.25) are solved simultaneously, to find the protein concentration profile along the riser regions. As mentioned previously, a dynamic seal is maintained between the columns. The concentration in solid particles at the top of the riser q_{er} is thus used as the new value of q_{od} as no adsorption occurred inside solids feed pipe. Subsequently, the second cycle commences with the calculated

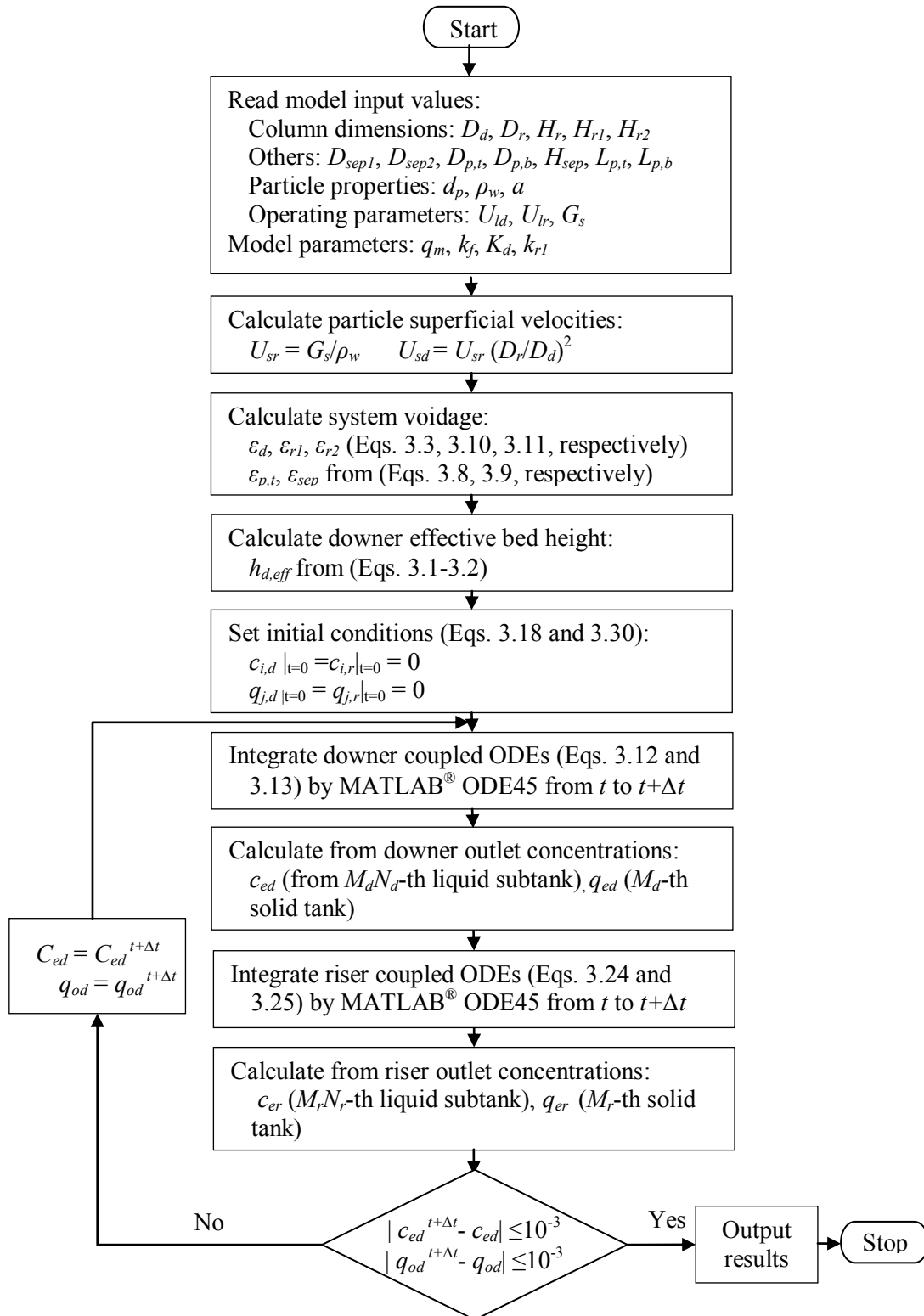


Figure 3.10 Algorithm for simulating the liquid-solid circulating fluidised bed system by tanks-in-series model.

values of c_{ed} and q_{od} , and the set of ordinary differential equations are solved repeatedly in similar manner. Based on this iteration, the ODE45 solver iterates over the next time step until c_{ed} and q_{od} have arrived to convergence.

3.6 MODEL VALIDATION

Model predicted results are compared against experimental data for the liquid phase protein concentration profiles reported in the literature (Lan et al. 2000, 858; Lan et al. 2002b, 252), with variations in some critical operating parameters, e.g., solids circulation rate, G_s represented by Figure 3.11(a), superficial liquid velocity in the downer, U_{ld} in Figure 3.11(b), and superficial liquid velocity in the riser, U_{lr} in Figure 3.11(c). Other parameters are kept at their base case values, as listed in Table 3.2. It can be observed that both magnitude and trends of the model predictions are in reasonably good agreement with the reported data over almost all the range. One clear difference however, is that the predicted values are slightly higher than experimental data at lower end of the downer, i.e., less than 30% of $h_{d,eff}$. The main reason for this difference is probably due to the rapid initial particles acceleration upon entering the system, because of the fluid drag forces interaction with other particles in the entrance near to the distributors, and then more gradually further down the downer. At the same time, the flow structure develops accordingly from non-uniform distribution into a more uniform distribution. Rapid initial solids acceleration has brought to higher tendencies of solids backmixing in regions near to the liquid distributors. While this could be adapted into the current modeling framework by altering the number of tanks in the section near to the solids entrance, no special effort is made to adjust it as residence time distribution profiles are not available.

3.7 RESULTS AND DISCUSSION

With the numerical model validated, parametric sensitivity analysis of some key parameters is conducted to obtain a better understanding of mass transfer and hydrodynamics in the system. At a given inventory of solid particles, the simultaneous adsorption and elution behaviour of protein at steady state depends primarily on: solids circulation rate G_s , superficial liquid velocity in downer U_{ld} , superficial liquid velocity in riser U_{lr} , and entering feed solution concentration c_{od} .

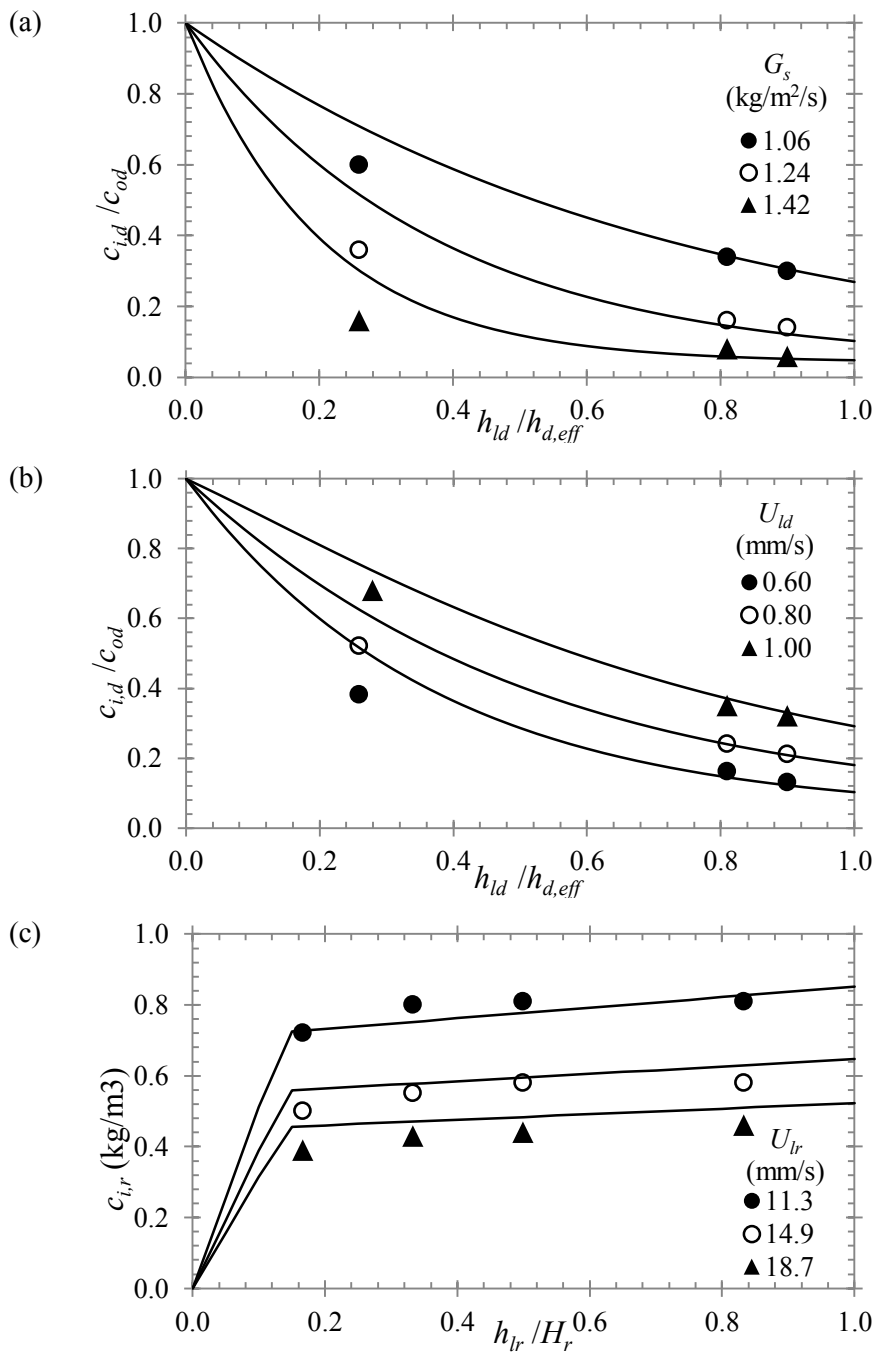


Figure 3.11 Experimental and theoretical liquid phase protein concentration profiles under different (a) solids circulation rate, G_s , (b) superficial liquid velocity in the downer, U_{id} , (c) superficial liquid velocity in the riser, U_{ir} . Symbols and solid lines correspond to experimental and predicted curves, respectively.

Since many key parameters are interrelated, individual contributions of each parameter could not be uncoupled in the simulation setup. A way to uncouple and study the contribution of each parameter on the LSCFB system is through a parametric analysis where an individual effect is changed, whereas the other

parameters are kept constant at base case values. In this study, the base case conditions are the experimental conditions used in model validation, as the predicted protein concentration profiles demonstrated relatively good agreement with the experimental results reported by Lan et al. (2000, 858; 2002, 252). This parametric study allowed ratings of the protein production rate, P (Eq. 3.26) and overall protein recovery, R (Eq. 3.27) of the system.

Protein production rate, P

$$= \text{Extract flowrate} \times \text{Protein concentration in extract} = U_{lr} A_r c_{er} \quad (3.26)$$

Overall protein recovery, R

$$= \text{Protein production rate} / \text{Protein loading rate} = U_{lr} A_r c_{er} / U_{ld} A_d c_{od} \quad (3.27)$$

3.7.1 Effects of Solids Circulation Rate

Effects of solids circulation rate, G_s in the downer are shown in Figure 3.12(a). The auxiliary liquid velocity is adjusted to yield variations in G_s . As shown in Figure 3.12(a), protein concentration in the raffinate, c_{ed} decreases with G_s , results in a decreasing concentration gradient. Table 3.3 verifies that the effective bed height of downer $h_{d,eff}$ increases with G_s , indicating an enhanced dynamic adsorption capacity, as more interfacial contact area become available. Furthermore, higher G_s increase the liquid-solid slip velocity; thereby, high liquid-solid interfacial contact efficiency is expected for improved mass transfer coefficient $K_L a$ in the dense phase region. At the same time, the solids holdup ε_{sd} decreases with G_s , as higher auxiliary liquid flow rate yields higher particle velocity, and the solid phase residence time in the downer is reduced. Therefore, steeper concentration profiles are observed at higher G_s values.

Figure 3.12(b) shows the expected riser concentration profiles at different G_s . Solid phase is denser in the distributor region and relatively dilute further down the riser. Even so, non-uniformity of solids distribution increases with G_s , results in a slight drop of solids holdup gradient and reduced riser elution capacity. The flow structure characteristic suggested that the liquid-solid mixing along the riser is more likely to be non-uniform near the distributor but developed uniformly further down the riser. Referring to Table 3.3, protein production rate increases from 37.68 g/h to 41.54 g/h, and protein recovery from 77.19% to 85.10%. It can thus be assured that higher G_s is useful for system performance.

Table 3.3 Simulation results under different solids circulation rate, G_s ($c_{od} = 2\text{kg/m}^3$; $U_{ld} = 0.6\text{m/s}$; $U_{lr} = 11.3\text{mm/s}$; $S = 3\text{kg}$).

Solids circulation rate, G_s ($\text{kg/m}^2/\text{s}$)	1.06	1.24	1.42
Downer solids holdup, ε_{sd}	0.3249	0.3167	0.3083
Riser distributor region solids holdup, ε_{sr1}	0.1026	0.1158	0.1284
Riser upper dilute region solids holdup, ε_{sr2}	0.0328	0.0383	0.0438
Downer effective bed height, $h_{d,eff}$ (m)	0.7683	0.7942	0.8225
Molecular dispersion constant, $10^{11} D_m$ (m^2/s)	6.13	6.13	6.13
Lumped mass transfer constant, $10^3 K_L a$ (s^{-1})	3.70	7.50	15.10
Downer raffinate concentration, c_{ed} (kg/m^3)	0.5379	0.205	0.0962
Riser extract concentration, c_{er} (kg/m^3)	0.8197	0.8509	0.9037
Downer solid outlet concentration, q_{ed} (kg/m^3)	49.93	44.79	41.53
Riser solid outlet concentration, q_{er} (kg/m^3)	27.39	25.21	24.03
Protein production rate, P (g/h)	37.68	39.11	41.54
Fraction of protein recovery, R	0.7719	0.8013	0.8510

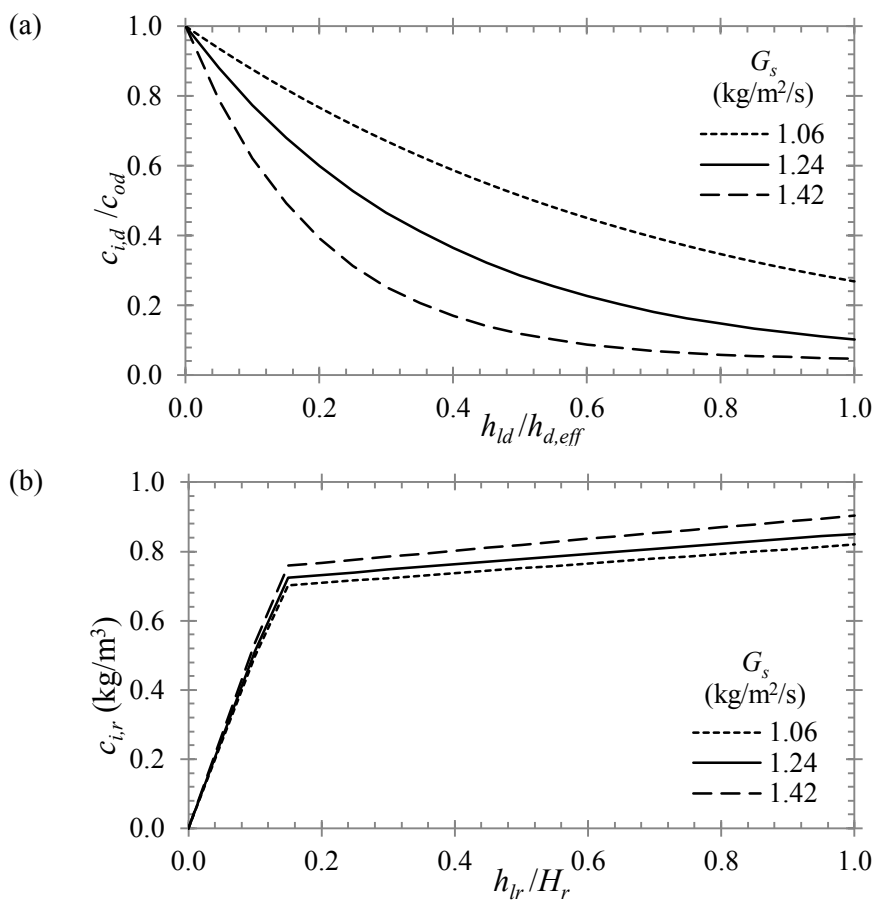


Figure 3.12 Liquid phase protein concentration profile in (a) the downer, and (b) the riser under different solids circulation rate, G_s ($c_{od} = 2\text{kg/m}^3$; $U_{ld} = 0.6\text{mm/s}$; $U_{lr} = 11.3\text{mm/s}$; $S = 3\text{kg}$).

3.7.2 Effects of Superficial Liquid Velocity in Downer

Significant effects of superficial liquid velocity in the downer, U_{ld} are shown in Figure 3.13. Protein concentration in the raffinate, c_{ed} are found to increase steeply with increasing U_{ld} , suggesting more protein is lost at higher U_{ld} . This could be explained by shorter liquid phase residence time in the downer due to increasing U_{ld} , and hence reduced time for protein adsorption. From Table 3.4, it can be observed that $h_{d,eff}$ increases with U_{ld} , and thereby reduced solids holdup in the downer. The mass transfer coefficient K_La increases slightly with U_{ld} . One possibility to this trend may be the increase in solid-liquid slip velocity. Despite that, the effect of mass transfer is small compared to those by liquid phase residence time and solids holdup.

Since the protein loading rate and downer dense region height increase with U_{ld} , significantly higher amount of adsorbed protein are being carried along with the particles into the riser, as indicated by increasing q_{ed} . Referring to Table 3.4, increase in both production rate, i.e., from 14.43 g/h to 67.06 g/h, and protein recovery, i.e., from 80.13% to 82.42% are accomplished. It should be noted, however, that when U_{ld} is too high, the total amount of protein in the liquid phase will eventually exceed the adsorption capacity of the solid particles, causing more protein lost into the raffinate.

3.7.3 Effects of Superficial Liquid Velocity in Riser

Results of the variation of both adsorption and elution capacities of LSCFB with change in the superficial liquid velocity in the riser, U_{lr} are shown in Figure 3.14. With the solids circulation rate kept constant, it is realised that the higher the U_{lr} , the lesser the protein concentration in extract, c_{er} . Drag force exerted by the upward flowing liquid increases with U_{lr} , reducing the residence time available for elution. Consequently, the riser elution capacity deteriorated. More particles are transferred into the downer at higher U_{lr} , reducing the solids holdup in riser and therefore increase in the effective height of the downer $h_{d,eff}$. Nonetheless, increase in $h_{d,eff}$ is compensated by decrease of downer adsorption capacity due to relegation in riser elution capacity as more protein remained in the regenerated particles. Referring to Table 3.5, a slight improvement can be noticed in the protein production, i.e., from 39.11 g/h to 39.77 g/h, and recovery, i.e., from 80.13% to 81.47%.

Table 3.4 Simulation results under different downer liquid superficial liquid velocity, U_{ld} ($c_{od}=2\text{kg/m}^3$; $G_s=1.24\text{kg/m}^2/\text{s}$; $U_{lr}=11.3\text{mm/s}$; $S=3\text{kg}$).

Downer superficial liquid velocity, U_{ld} (mm/s)	0.60	0.80	1.00
Downer solids holdup, ε_{sd}	0.3167	0.2749	0.2390
Riser distributor region solids holdup, ε_{sr1}	0.1158	0.1158	0.1158
Riser upper dilute region solids holdup, ε_{sr2}	0.0383	0.0383	0.0383
Downer effective bed height, $h_{d,eff}$ (m)	0.7942	0.9151	1.0523
Molecular dispersion constant, $10^{11} D_m$ (m ² /s)	6.13	6.13	6.13
Lumped mass transfer constant, $10^3 K_L a$ (s ⁻¹)	14.5	14.9	15.2
Downer raffinate concentration, c_{ed} (kg/m ³)	0.2050	0.3600	0.5824
Riser extract concentration, c_{er} (kg/m ³)	0.8509	1.1649	1.4588
Downer solid outlet concentration, q_{ed} (kg/m ³)	44.79	61.14	76.05
Riser solid outlet concentration, q_{er} (kg/m ³)	25.21	34.46	43.00
Protein production rate, P (g/h)	39.11	53.55	67.06
Fraction of protein recovery, R	0.8013	0.8227	0.8242

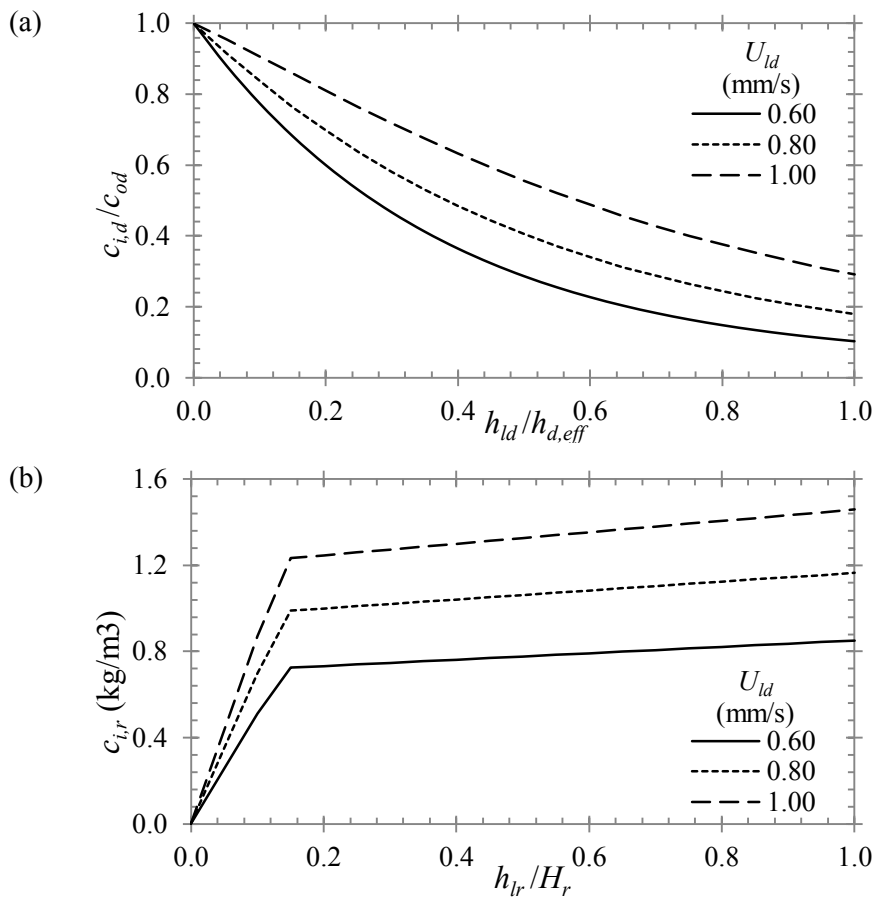


Figure 3.13 Liquid phase protein concentration profile in (a) the downer, and (b) the riser under different superficial liquid velocity in the downer, U_{ld} ($c_{od}=2\text{kg/m}^3$; $G_s=1.24\text{kg/m}^2/\text{s}$; $U_{lr}=11.3\text{mm/s}$; $S=3\text{kg}$).

Table 3.5 Simulation results under different riser superficial liquid velocity, U_{lr} ($c_{od}=2\text{kg/m}^3$; $G_s=1.24\text{kg/m}^2/\text{s}$; $U_{ld}=0.60\text{mm/s}$; $S=3\text{kg}$).

Riser superficial liquid velocity, U_{lr} (mm/s)	11.3	14.9	18.7
Downer solids holdup, ε_{sd}	0.3167	0.3167	0.3167
Riser distributor region solids holdup, ε_{sr1}	0.1158	0.0875	0.0690
Riser upper dilute region solids holdup, ε_{sr2}	0.0383	0.0245	0.0170
Downer effective bed height, $h_{d,eff}$ (m)	0.7942	0.8088	0.8169
Molecular dispersion constant, $10^{11} D_m$ (m ² /s)	6.13	6.13	6.13
Lumped mass transfer constant, $10^3 K_L a$ (s ⁻¹)	14.5	14.5	14.5
Downer raffinate concentration, c_{ed} (kg/m ³)	0.2050	0.2615	0.3723
Riser extract concentration, c_{er} (kg/m ³)	0.8509	0.6466	0.5228
Downer solid outlet concentration, q_{ed} (kg/m ³)	44.79	54.70	66.60
Riser solid outlet concentration, q_{er} (kg/m ³)	25.21	35.79	48.00
Protein production rate, P (g/h)	39.11	39.19	39.77
Fraction of protein recovery, R	0.8013	0.8028	0.8147

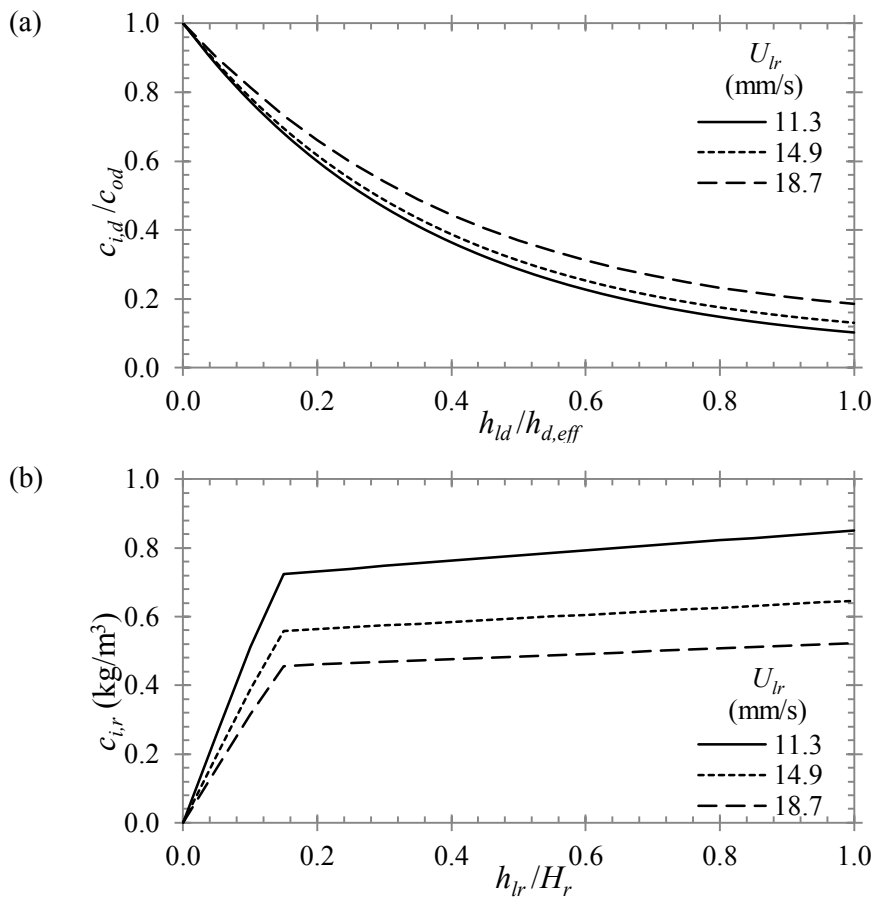


Figure 3.14 Liquid phase protein concentration profile in (a) the downer, and (b) the riser under different superficial liquid velocity in the riser, U_{lr} ($c_{od}=2\text{kg/m}^3$; $G_s=1.24\text{kg/m}^2/\text{s}$; $U_{ld}=0.60\text{mm/s}$; $S=3\text{kg}$).

3.7.4 Effects of Feed Concentration

Effects of protein concentration in feed solution, c_{od} are studied and the results are shown in Figure 3.15. When maintaining other parameters at fixed values, protein concentration in raffinate c_{ed} increases with c_{od} as presented in Table 3.6. Higher c_{od} signifies higher protein loading rate onto the solid particles. Despite the constant solids circulation rate G_s , protein concentration in the extract c_{er} increases steeply with c_{od} . Referring to Table 3.6, increases in both the protein production rate, i.e., from 17.01 g/h to 59.90 g/h, and overall recovery, i.e., from 69.69% to 81.81%, have been obtained with increase in c_{od} .

3.8 CONCLUSION

A general purpose, extensible, and dynamic theoretical compartmental model based upon a tanks-in-series framework incorporating the equilibrium and hydrodynamics of liquids and solid particles has been developed for continuous protein recovery in LSCFB systems. The model is used to simulate the recovery of aqueous BSA solution onto Diaion HPA25 anion exchanger. The model allows adjusting for the degree of backmixing in each phase for the riser and the downer, while make possible easy integration with the kinetics model and offer a straightforward comparison of the reactor performance with that of a plug flow reactor. The simulated results compare well with the experimental results obtained from the laboratory-scale BSA recovery. A systematic study of the effect of several key operating parameters is performed. The analysis revealed that both the BSA production rate and recovery increase with increasing solids circulation rate while both decrease with increasing superficial liquid velocity in the riser. With the increase in superficial liquid velocity in the downer and feed BSA concentration, the rate of BSA production increases, but the overall recovery decreases. The model derived in this work is flexible and can use different forms of ion exchange mass transport models and can simulate different hydrodynamic behaviour in order to gain insight into protein recovery processes. The very nature of the model makes it a useful tool in learning other protein recovery operations for plant and animal proteins. It can also be utilised for further multi-objective optimisation studies to optimize LSCFB systems.

Table 3.6 Simulation results under different initial protein concentration, c_{od} ($G_s = 1.24 \text{ kg/m}^2/\text{s}$; $U_{ld} = 0.60 \text{ mm/s}$; $U_{lr} = 11.3 \text{ mm/s}$; $S = 3 \text{ kg}$).

Initial feed concentration, c_{od} (kg/m^3)	1.00	2.00	3.00
Bulk solution density, ρ (kg/m^3)	999.6	999.2	998.8
Bulk solution viscosity, μ	0.9471	0.9526	0.9582
Molecular dispersion constant, $10^{11} D_m$ (m^2/s)	6.13	6.13	6.13
Lumped mass transfer constant, $10^3 K_{La}$ (s^{-1})	14.5	14.5	14.5
Downer raffinate concentration, c_{ed} (kg/m^3)	0.0870	0.2050	0.3597
Riser extract concentration, c_{er} (kg/m^3)	0.3700	0.8509	1.3031
Downer solid outlet concentration, q_{ed} (kg/m^3)	19.74	44.79	68.35
Riser solid outlet concentration, q_{er} (kg/m^3)	11.04	25.21	38.54
Protein production rate, P (g/h)	17.01	39.11	59.90
Fraction of protein recovery, R	0.6969	0.8013	0.8181

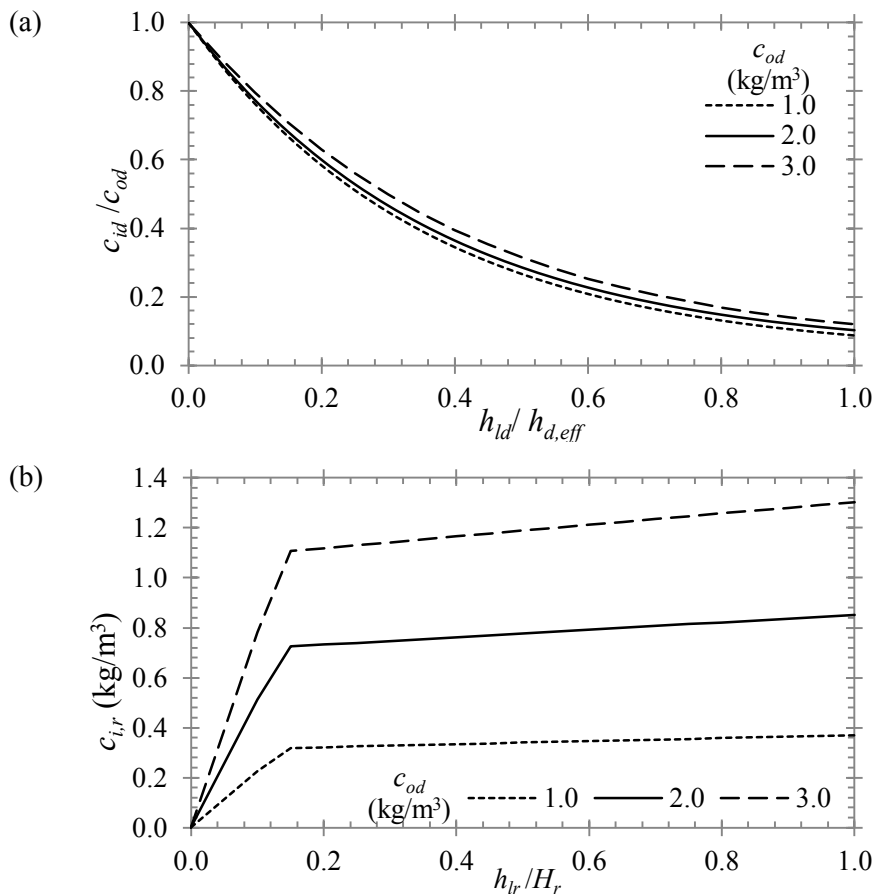


Figure 3.15 Liquid phase protein concentration profile in the downer under different feed concentration, c_{od} ($G_s = 1.24 \text{ kg/m}^2/\text{s}$; $U_{ld} = 0.60 \text{ mm/s}$; $U_{lr} = 11.3 \text{ mm/s}$; $S = 3 \text{ kg}$).

CHAPTER 4

KAFIRIN ADSORPTION CHROMATOGRAPHY: ISOTHERM AND KINETIC ANALYSIS

4.1 INTRODUCTION

In order to use the model developed in previous chapter, it is important that equilibrium and kinetic data on kafirin adsorption onto various adsorbents is available. Such data is not available in the literature; therefore, experiments are carried out to determine the adsorption behaviour of kafirin onto various ion exchangers. This study is the first scientific insight into the isotherm and kinetic studies of kafirin adsorption on basic anion- and acidic cation-exchangers for practical applications in preparative-scale chromatography. Adsorption isotherms are determined for a total of five anion-exchangers and two cation-exchangers in batch systems with different kafirin initial concentrations at a constant temperature. Isotherm parameters such as adsorbent loading capacity and dissociation constant are determined for Langmuir isotherm, and adsorptive capacity and affinity constant for Freundlich isotherm. Both these isotherms are found to fit the adsorption equilibrium data well. Batch uptake kinetics for kafirin adsorption on these ion exchangers are also carried out and critical parameters including the diffusion coefficient, film mass transfer coefficient, and Biot's number for diffusion model are calculated. Both the isotherm and the kinetic parameters are considered for selection of appropriate ion exchangers for kafirin purification. Bio-Rad UNOsphere Q and Toyopearl SuperQ-650M are found to offer better kafirin adsorption capacities and interaction strength with excellent uptake kinetics under moderate operating conditions. The data presented in this chapter is valuable for designing process-scale preparative adsorptive chromatographic kafirin purification systems such as liquid-solid circulating fluidised bed.

4.2 EXPERIMENTAL

4.2.1 Materials

The ion exchangers used in this adsorption equilibrium study consists of five base anion exchangers UNOsphere Q, ReliSorb QA400, Tulsion A-36MP, Toyopearl

QAE-550C, and Toyopearl SuperQ-650M, and two acidic cation exchangers Toyopearl SP-550C and Toyopearl SP-650M. UNOsphere Q is purchased from Bio-Rad Laboratories (Gladesville, New South Wales, Australia). ReliSorb QA-400 is purchased from Mitsubishi Chemical (Gurgaon, Haryana, India). Tulsion A-36MP is purchased from Thermax (Pune, India). All Toyopearl ion exchangers are purchased from Tosoh Bioscience (Redland Bay, Queensland, Australia). Specifications of these ion exchangers are summarised in Table 4.1 (Resindion 2011; Tosoh Bioscience 2011a; Tosoh Bioscience 2011b; Tosoh Bioscience 2011c; Bio-Rad 2014; Thermax 2014). Strong ion exchangers are used because kafirin has higher solubility in acidic range of 0.5 to 2.0, and in basic pH range of 9.0 and above (Kumar et al. 2014). All aqueous solutions are made from distilled water. All other chemicals used are analytical-grade and purchased from Sigma Aldrich (Castle Hill, New South Wales, Australia).

Sorghum endosperm is obtained by steeping and fractionation of sorghum seeds (De Mesa-Stonestreet, Alavi, and Bean 2010, 90). Kafirin extract is prepared from sorghum endosperm as described by Emmambux and Taylor (2003, 402). The extracted kafirin is further purified to 99% on dry weight basis by multiple precipitations followed by hexane extraction to remove oil fraction. A sample feed solution of 20 mg/ml is prepared by dissolving pure kafirin in 100 ml 65% (v/v) aqueous ethanol. Solution pH is adjusted to 9.0 with 1.0 M NaOH as necessary. Kafirin is left to solubilize at 50°C with mild shaking until solubilisation is complete, which took approximately 2 hours. The solution is then centrifuged at 12000 x g for 20 min at room temperature to remove any suspended particulate matter. Soluble kafirin in the clear supernatant is used for adsorption equilibrium studies on anion exchangers. The feed solution for cation exchangers is prepared using similar method, but with pH adjusted to 1.5 using 1.0 M HCl.

4.2.2 Adsorption Equilibrium Experiments

All ion exchangers are pre-treated prior to experiments. The ion exchangers are washed with distilled water to remove all traces of preservative agents. All washed ion exchangers are degassed and equilibrated. For anion exchangers, equilibration is carried out using 65% (v/v) aqueous ethanol (pH 9.0) solution under mild stirring condition for 15 min. The same equilibration solution at pH 1.5 is used for cation

Table 4.1 Specifications of ion exchangers.

	UNOsphere Q	ReliSorb QA-400	Tulsion A-36MP	Toyopearl QAE-550C	Toyopearl SuperQ-650M	Toyopearl SP-550C	Toyopearl SP-650M
Type	SBA	SBA	SBA	SBA	SBA	SAC	SAC
Matrix structure	Crosslinked polystyrene divinylbenzene	Crosslinked poly-methacrylate	Crosslinked polystyrene	Crosslinked poly-methacrylate	Crosslinked poly-methacrylate	Crosslinked poly-methacrylate	Crosslinked poly-methacrylate
Functional group	Quaternary amine	Quaternary amine	Quaternary amine type-II	Quaternary amine	Quaternary amine	Quaternary amine	Quaternary amine
Particle size (μm)	120	120	750	100	65	100	65
Intraparticle porosity	0.60	0.55	0.65	0.50	0.55	0.60	0.55
Pore size (Å)	>2000	4500	n.a.	500	400	500	1000
Ion exchange capacity ($\mu\text{eq/ml}$)	120	300	1200	360	240	130	120
Dynamic binding capacity (mg BSA/ml)	125-180	n.a.	n.a.	60-80	105-155	120-140	40-60
Operable pH range	1-14	1-14	0-14	2-13	2-13	2-13	2-13

exchangers. The equilibrated ion exchangers are kept in the respective equilibration solutions until use.

For anion exchangers, adsorption equilibrium experiments are carried out by batch adsorption method in 65% (v/v) aqueous ethanol (pH 9.0). Fixed amount (500 μ L) of pre-equilibrated anion exchangers are transferred into each of the falcon tubes and contacted with 3 ml of kafirin solution with different initial bulk phase concentrations (1-20 mg/ml). The falcon tubes are then kept on rocker shaker to attain equilibrium for 3 h at 25°C, which is confirmed by kinetic adsorption studies for all ion exchangers used to be sufficient to reach adsorption equilibrium under all the conditions studied. Upon reaching the equilibrium, the ion exchanger is allowed to settle and the supernatants from each tube are sampled and analysed by spectrophotometry at 276 nm. For cation exchangers, similar steps are followed in which kafirin extract (pH1.5) at different bulk phase concentrations (1-20 mg/ml) are loaded into each of the ion exchangers in falcon tubes, followed by analysis of supernatant after equilibrium is attained.

For the batch equilibrium experiments, the measurement of kafirin concentration in the supernatant solutions before and after adsorption is carried out by means of modified Landry method using ultraviolet-visible spectrophotometry (Landry, Paulis, and Wall 1987, 51). The kafirin content in 65% (v/v) aqueous ethanol is determined at its maximum absorbance wavelength (λ) of 276 nm. All experiments are performed in triplicate and the mean values are reported. The ion exchangers loading at the equilibrium are calculated by a simple mass balance for batch system (Eq. 4.1). The isotherms of kafirin adsorption on anion- and cation-exchangers are analysed using Langmuir isotherm (Eq. 4.2) and Freundlich isotherm (Eq. 4.3) models. All the constants in the isotherm models are evaluated by nonlinear regression using MATLAB R2011a (MathWorks, Inc.).

$$q_e = \frac{V(c_o - c_e)}{V_s} \quad (4.1)$$

$$q_e = \frac{q_m c_e}{K_d + c_e} \quad (4.2)$$

$$q_e = q_f c^{1/n_f} \quad (4.3)$$

4.2.3 Kinetic Uptake Experiments

All ion exchangers are pre-treated prior to experiments. The ion exchangers are washed with distilled water to remove all traces of preservative agents. All washed ion exchangers are degassed and equilibrated. For anion exchangers, equilibration is carried out using 65% (v/v) aqueous ethanol (pH 9.0) solution under mild stirring condition for 15 min. The same equilibration solution at pH 1.5 is used for cation exchanger. The equilibrated ion exchangers are kept in the respective equilibration solutions until use.

Kafirin uptake kinetic experiments are conducted in 65% (v/v) aqueous ethanol using the stirred batch adsorption method. A fixed amount (5 ml) of pre-equilibrated ion exchanger is placed in a 50 ml glass beaker and then contacted with 25 ml of kafirin solution with initial concentration of 20 mg/ml. The beaker is kept under mild stirring condition at 25°C to suspend the ion-exchange particles. Fixed-volume (100 μ l) of samples are withdrawn at specified time intervals using micropipette and diluted to appropriate concentration with equilibration solution of pH 9.0 for anion exchangers and pH 1.5 for cation exchanger. These samples are then centrifuged at 12000 x g for 20 min before analysis by spectrophotometry. The total reduction in solution volume due to sampling is less than 5% for all experiments, so that adsorption rates are essentially measured under constant batch volume.

For uptake kinetic experiments, a similar approach as the adsorption equilibrium experiments is adopted to measure the kafirin concentration in the supernatant solutions. The ion exchangers loading at the anytime during the adsorption are calculated by a simple mass balance for batch system (Eq. 4.4).

$$q_i = \frac{V(c_o - c_i)}{V_s} \quad (4.4)$$

The diffusion model is used to model the kafirin uptake kinetics by the ion exchangers. The pore diffusion model assumed that the radial diffusion in ion-exchange particles occurs in liquid-filled pores, which could be expressed in terms of the pore-liquid concentration gradient (Wright, Muzzio, and Glasser 1998, 913; Chu and Hung 2010, 351). Generally, the dual-resistance models are insensitive to the film diffusion effects in almost all well-mixed, batch systems (Do and Rice 1990,

1419; Pignatello and Xing 1996, 1; Wright, Muzzio, and Glasser 1998, 913). The following discussion assumes that the pore diffusion governs the rates of solute adsorption interaction with the particles. Some typical assumptions made in this model include: spherical particles, isothermal conditions and fast intrinsic adsorption kinetics, resulting in the adsorbed solute to be in equilibrium with the pore-liquid at each radial position within the particle, represented by an equilibrium isotherm relationship (Chu and Hung 2010, 351). For the adsorption of solute, under transient conditions, the mass transport balance over a volume element of a particle yields the Fick's second law in spherical geometry (Eq. 4.5).

$$(1 - \varepsilon_p) \frac{\partial q_i}{\partial t} + \varepsilon_p \frac{\partial c_{p,i}}{\partial t} = \frac{D_p}{r^2} \frac{\partial}{\partial r} \left(r^2 \frac{\partial c_{p,i}}{\partial r} \right) \quad (4.5)$$

The mass transport balance (Eq. 4.5) can be simplified by differentiating the equilibrium isotherm mathematical expression and substituting for $q_{s,i}$ term representing the intraparticle solute concentration on a pore-free basis. This substitution is valid if the rate of dissociation at the pore wall is fast in relative to the rate of diffusion through the pore-liquid, i.e., if the local equilibrium between adsorbed solute and pore-liquid is valid at each radial position inside the particle. The equilibrium relationship is described using the nonlinear Langmuir isotherm model (Eq. 4.2).

An external boundary condition for Eq. 4.5 comprising a well-mixed, bulk liquid of fixed volume will produce an initial adsorption rate equivalent to the early stages of particle surface boundary conditions. Nonetheless, as the liquid phase solute concentration approaches equilibrium, the pore-liquid concentration gradient, and therefore the overall adsorption rate, is greatly reduced in relative to the initial conditions. The bulk-liquid concentration for a stirred, batch system (Eq. 4.6) can be evaluated at the particle surface, i.e. $r=r_p$ in constant batch liquid volume.

$$\frac{\partial c}{\partial t} = \varepsilon \frac{3D_p V_s}{r_p V} \frac{\partial c_{p,i}}{\partial t} \Bigg|_{r=r_p} \quad (4.6)$$

4.2.4 Model Fitting Routine

The parameter estimations are based on the nonlinear least-squares method. The method minimises the sum of the squares of the residuals between the experimental

data and model predictions. Convergence on the residual sum of squares is selected because studies have shown that convergence criterion which accounted for squares residual returned much smaller standard deviation of the average error compared to convergence based on parameters (McCullough 2012, 149). To obtain the model predictions, in order to calculate the residuals between the model result and experimental data, the models are simulated. Only theoretical data points c_i corresponding to the sample intervals of the experimental data points \hat{c}_i are used. All estimations are made with nonlinear least-squares fitting algorithm, LSQCURVEFIT, in MATLAB[®]. The LSQCURVEFIT algorithm requires an initial estimate for model from which the local minima is estimated. To increase the likelihood of locating the global minimum, the MATLAB[®] MULTISTART approach is employed where a set of starting points is initiated and LSQCURVEFIT algorithm is called to locate the corresponding local minima. The data point with the lowest objective value and is feasible is chosen to be the global minimum.

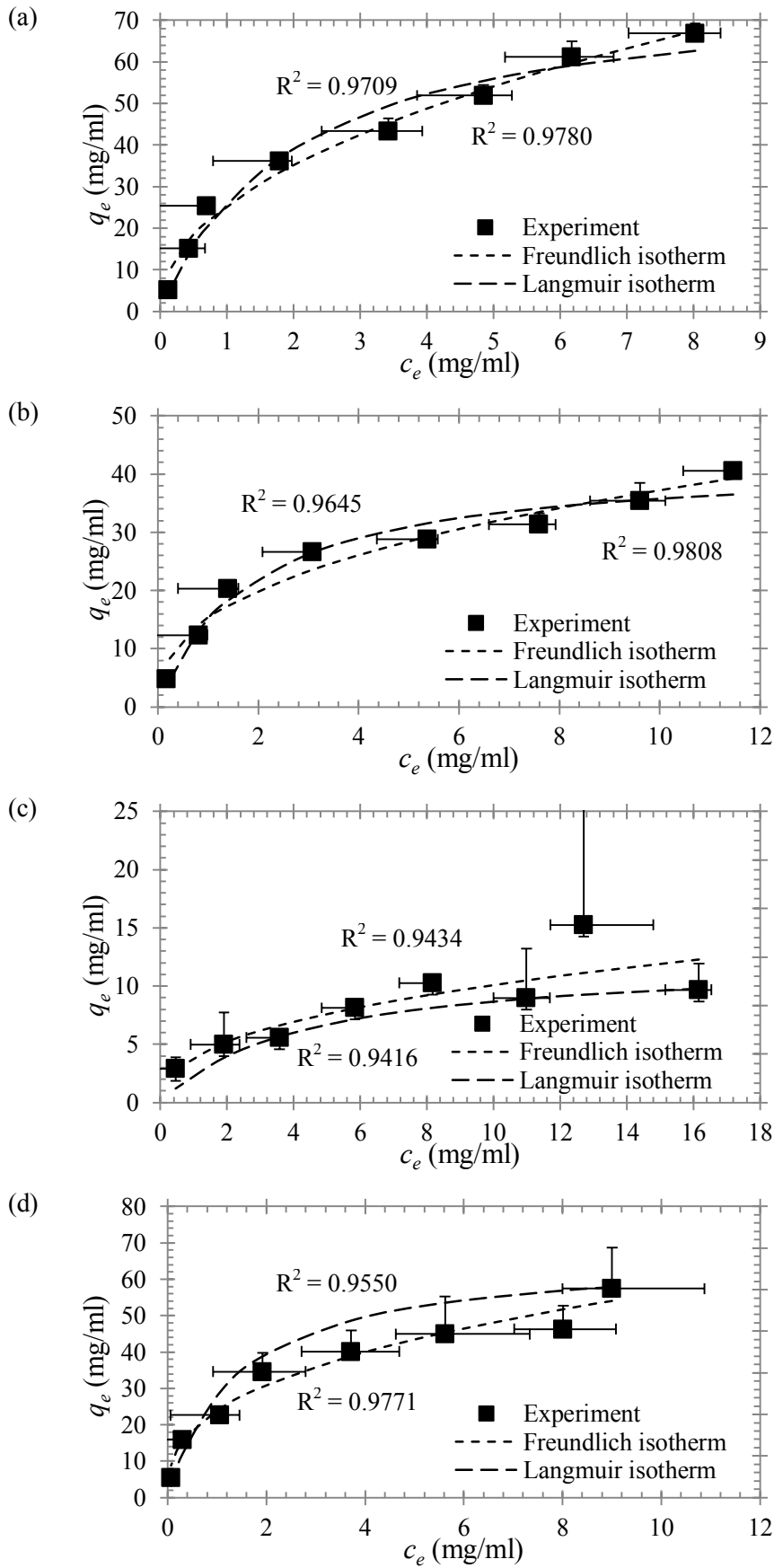
4.3 RESULTS AND DISCUSSION

4.3.1 Equilibrium Adsorption Analysis

The equilibrium data from batch adsorption equilibrium experiments of kafirin at different initial bulk phase concentrations are plotted for each of the ion exchangers in Figure 4.1. According to the classification of Giles et al. (1960, 3973), it can be observed from the adsorption isotherm for ion exchangers follows the Langmuir-type, indicating a non-competitive adsorption (Hinz 2001, 225). For comparison of single-solute isotherm results in a quantitative manner, the isotherms are described by the Langmuir isotherm (Eq. 4.2) and the Freundlich isotherm (Eq. 4.3) models. Best-fitting values according to these isotherm models are listed in Table 4.2. The coefficient of determination gives the variance explained by a model, so it is used to evaluate the goodness of fit. High values of coefficients of determination shows that both models are suitable to describe the adsorption behaviour of kafirin. Further analysis of the isotherm coefficients is done to emphasize their physical significance, such as the maximum adsorption capacities which are useful for ion exchanger selection. Polymeric ion exchangers such as UNOsphere Q, ReliSorb QA-400, Toyopearl QAE-550C, Toyopearl SuperQ-650M, Toyopearl SP-550C, and Toyopearl SP-650M are found to more mechanically stable compared to Tulsion A-

Table 4.2 Summary of results from Langmuir and Freundlich isotherm models.

	UNOsphere Q	ReliSorb QA-400	Tulsion A-36MP	Toyoparl QAE-550C	Toyoparl SuperQ-650M	Toyoparl SP-550C	Toyoparl SP-650M
Langmuir isotherm							
Adsorption capacity, q_m (mg/ml)	87.08	58.20	48.21	71.27	78.57	81.36	71.75
Dissociation constant, K_d (M)	1.073×10^{-4}	1.272×10^{-5}	6.402×10^{-4}	8.205×10^{-5}	7.776×10^{-5}	4.275×10^{-4}	7.641×10^{-4}
R_L at $c_0 = 1$ mg/ml	0.7116	0.7452	0.9364	0.6536	0.6414	0.9077	0.9462
R_L at $c_0 = 20$ mg/ml	0.11098	0.1276	0.424	0.0862	0.0821	0.3296	0.4677
Coefficient of determination, R^2	0.9709	0.9645	0.9416	0.9550	0.9929	0.9958	0.9401
Freundlich isotherm							
Adsorption capacity, q_f (mg/ml)	26.11	16.15	4.372	24.94	27.95	8.427	4.699
Adsorption intensity inverse, $1/n$	0.4877	0.4571	0.6284	0.4145	0.4151	0.6885	0.7435
Coefficient of determination, R^2	0.9780	0.9808	0.9434	0.9771	0.9479	0.9943	0.9470



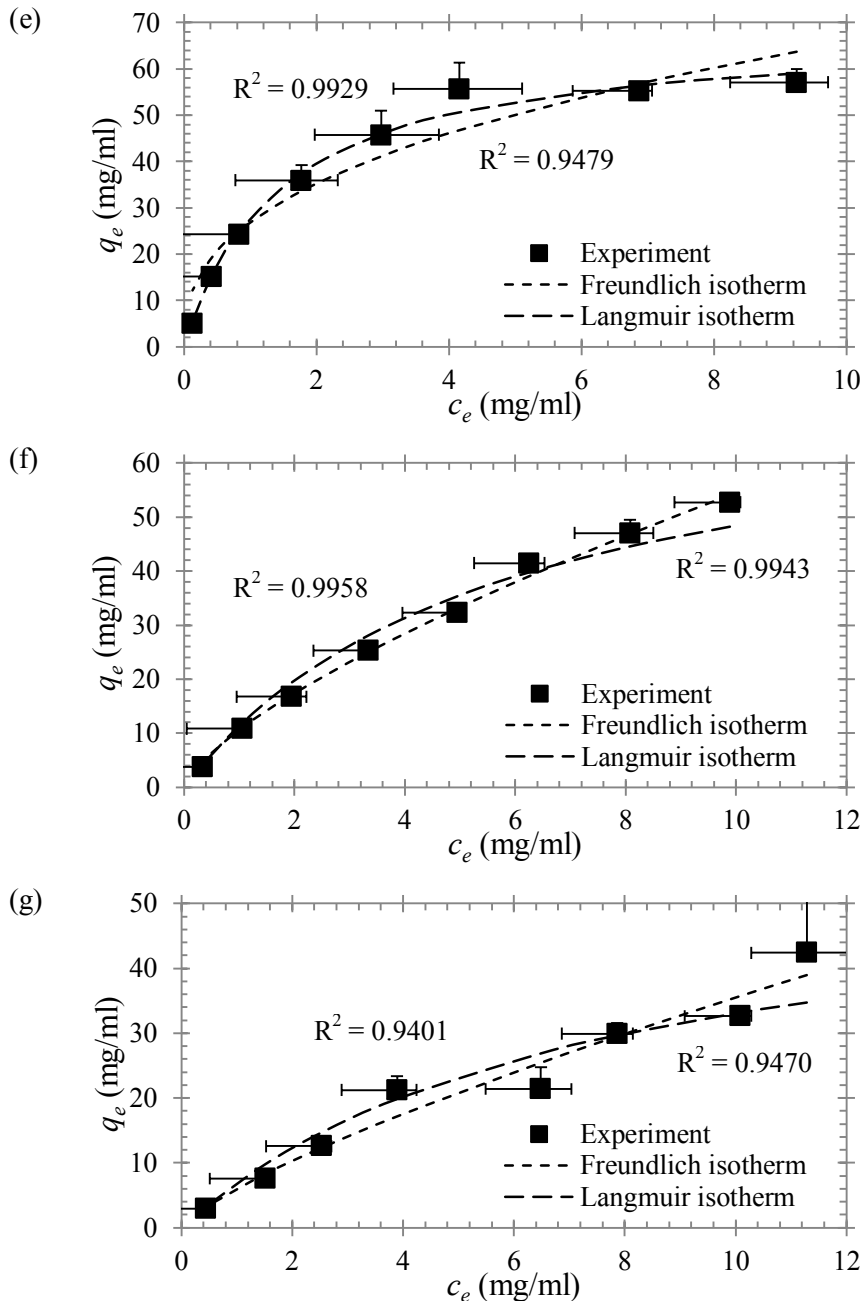


Figure 4.1 Experimental and theoretical results for kafirin adsorption equilibrium on (a) UNOsphere Q, (b) ReliSorb QA-400, (c) Tulsion A-36MP, (d) Toyopearl QAE-550C, (e) Toyopearl SuperQ-650M, (f) Toyopearl SP-550C, (g) Toyopearl SP-650M. Symbols and solid lines correspond to experimental and isotherm curves, respectively.

36MP which easily disintegrated due to attrition during adsorption experiments thus producing fine particles. The particle fines also interfere with the spectrophotometric method for kafirin analysis thereby necessitating their removal from analytical samples using microfiltration or high speed centrifugation.

4.3.2 Langmuir Isotherm Model

The Langmuir equilibrium constant, $R_L = 1/(1 + c_o/K_d)$ (Eq. 4.7), a critical parameter of the Langmuir isotherm model is calculated to decide the nature of kafirin adsorption on the ion exchangers (Weber and Chakravorti 1974, 228; Chairat et al. 2005, 231). The R_L constants obtained from the equilibrium results are in the range of zero to one over the entire range of initial bulk phase concentration investigated, indicating favourable adsorption. The Langmuir adsorbent loading capacity, q_m indicates the quantity of kafirin required for formation of a single monolayer on the ion exchanger surface, and it is relatively proportional to the ion exchanger specific surface area. It is thus anticipated that ion exchangers with higher specific surface area provide more adsorption sites for monolayer adsorption of the kafirin. The ion exchangers have been arranged in an order of magnitude based on their calculated Langmuir binding capacities, q_m (Table 4.2), in which the resulting sequence matches with adsorption of BSA (Table 4.1). This confirms that monolayer adsorption is the most probable mechanism involved in the kafirin adsorption process. The adsorption capacity of ReliSorb QA-400 and Tulsion A-36MP are not found in the literature thus far. Significantly lower q_m values are found for these ion exchangers compared to others used in the batch equilibrium experiments. This might be due to the lower specific surface area of ion exchanger available for kafirin adsorption, hence the lower adsorption capacity.

The dissociation coefficient, K_d is another important Langmuir constant, indicative of the interaction affinity between kafirin and the interacting ligands on ion exchanger surface. K_d values for ion exchangers are typically between 10^{-8} M and 10^{-2} M (Yang 2008, 78). K_d higher than this range indicates the interaction may be too weak for chromatography purpose and is not suitable for equilibrium analysis. Smaller K_d shows that the binding interaction could be too strong to be disrupted in elution process (Hooper 1999, 217). Ideally, the binding should be reversible so that the adsorbed kafirin can be eluted without denaturation. From the equilibrium analysis, fitted K_d values are within the operating window stated above. K_d values calculated for anion exchangers are comparatively less than those of the cation exchangers, showing stronger binding strength of kafirin with the former. This is desirable for kafirin adsorption because impurities in kafirin extract can be effectively removed by washing without disrupting the specific binding between

kafirin and ion exchanger. The higher binding affinity with anion exchangers could be described by the higher electrostatic potentials developed on kafirin due to pH difference. More specifically, adsorption is conducted at pH 9.0 for anion exchangers and pH 1.5 for cation exchangers, which is 3 and 4.5 pH units above and below the isoelectric point of kafirin respectively. In such environment it can be argued that at pH 9.0 more intense surface charges are developed on kafirin to interact with the oppositely charged adsorption sites on the anion exchangers, resulting into higher amount and affinity of kafirin adsorbed. Also, pH 9.0 is relatively near-neutral pH as compared to pH 1.5, giving a mild condition to maintain kafirin integrity for practical chromatographic purpose in kafirin purification.

4.3.3 Freundlich Isotherm Model

The dimensionless constant, n_f , in the Freundlich isotherm model, is calculated to obtain the adsorption favourability of kafirin on the ion exchangers. It is suggested that a smaller value of $1/n_f$ is a sign of a better adsorption and formation of stronger binding interaction (Freundlich 1906, 385). $1/n_f$ values, listed in Table 4.2, further supports that the adsorption of kafirin on the ion exchangers are indeed favourable with the $1/n_f$ of more than zero and less than unity. Relatively smaller $1/n_f$ values are found for anion exchangers compared to that of the cation exchangers, suggesting greater affinity of binding between the former and kafirin. This observation is consistent with the analysis using Langmuir isotherm model.

The Freundlich loading capacity coefficient, q_f is another important parameter in the Freundlich isotherm model which implies the loading capacity of ion exchangers on either monolayer (chemisorption) or multilayer (physisorption) heterogeneous surface. In contrast to the Langmuir loading capacity, the calculated q_f for the ion exchangers when arranged in the order of magnitude, disagrees with those reported for the BSA adsorption on same ion exchangers. The disagreement between the predicted q_f and the reported loading capacity sequence suggests that kafirin adsorption on the ion exchangers is probably not as well described by the Freundlich isotherm model compared to the Langmuir isotherm model, despite the high values of coefficient of determination. Also, the values of the interaction affinity factor, n_f , deduced from $1/n_f$, for all ion exchangers are found to be greater than unity stating that kafirin adsorption on these ion exchangers used is a monolayer-chemisorption

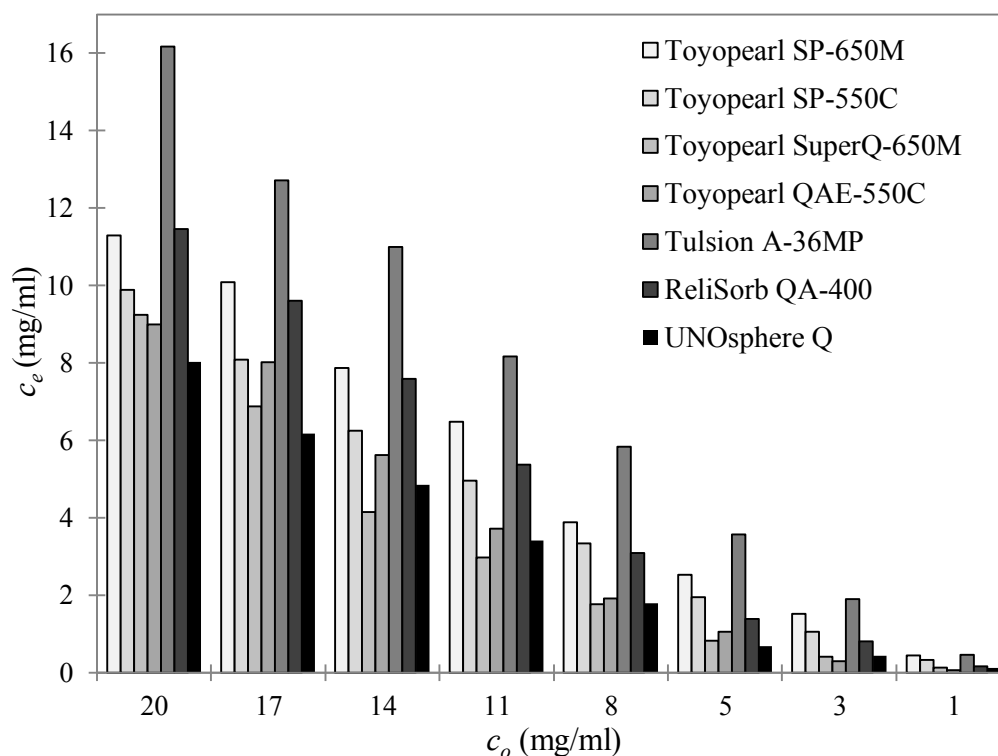


Figure 4.2 Experimental results for kafirin adsorption equilibrium on ion exchangers at different initial kafirin solution concentrations.

process. This further validates the use of Langmuir isotherm model for describing adsorption equilibrium for kafirin purification with chromatographic method.

4.3.4 Ion Exchanger Selection

Equilibrium concentration of kafirin at different initial bulk phase concentrations is plotted in Figure 4.2. Lower equilibrium concentration indicates higher adsorption on the ion exchanger. Overall, the anion exchangers, i.e., UNOsphere Q, Toyopearl QAE-550C, and Toyopearl SuperQ-650M showed relatively good performance in terms of adsorption efficiency compared to cation exchangers across the entire range of concentrations studied. Although cation exchangers have comparatively larger adsorption capacities than some of anion exchangers, other factors determining adsorption efficiency of kafirin cannot be neglected. The primary factor would be the solvent pH which intensified the surface charge on kafirin as well as cation exchangers leading to better adsorption efficiency at pH 9.0, a milder condition for upholding kafirin integrity. Other contributing factors are the ion-exchange particle size, solid support, functional group, and pH stability range. Of all exchangers studied, UNOsphere Q and Toyopearl SuperQ-650M showed higher adsorption

efficiency followed by Toyoparl QAE-550C, Toyoparl SP-550C, and least by Toyoparl SP-650M. The other anion exchangers, namely, ReliSorb QA-400 and Tulsion A-36MP are thought to be unviable for this purpose due to their low adsorption capacities.

4.3.5 Uptake Kinetic Analysis

For the adsorption of kafirin to ion exchangers, the Langmuir equilibrium parameter, R_L values (Eq. 4.7), previously calculated in Section 4.3.2, are in the range of zero to one over the solute concentration range used, which supports favourable adsorption (Chairat et al. 2005, 231). Taking the Langmuir isotherm expressed on a pore-free volume basis, the mass transport model is in terms of the pore-liquid concentration (Eq. 4.8).

$$\frac{\partial c_{p,i}}{\partial t} = \frac{D_p}{(1-\varepsilon_p) \frac{q_m c_{p,i}}{(K_d + c_{p,i})^2} + \varepsilon_p} \frac{1}{r^2} \frac{\partial}{\partial r} \left(r^2 \frac{\partial c_{p,i}}{\partial r} \right) \quad (4.8)$$

The isotherm relationship between the adsorbed solute and pore-liquid at each of particle radial position is found to be nonlinear, i.e., Langmuir isotherm, with Section 4.3.2 reports the best-fitted parameters from previous adsorption equilibrium studies, a numerical solution for Eqs. 4.5 and 4.7 is thus required. To solve the coupled equations, a homogeneous von Neumann condition is introduced at the particle centre ($r=0$) (Eq. 4.9), in which a finite concentration, i.e., derivative is zero is assumed. On the other hand, the particle surface ($r=r_p$) takes the form of Robin boundary condition (Eq. 4.10). These conditions subjected to the initial conditions (Eq. 4.11), for spherical particles of radius r_p , in a closed batch system.

$$\left. \frac{\partial c_{p,i}}{\partial r} \right|_{r=0} = 0 \quad (4.9)$$

$$D_p \left. \frac{\partial c_{p,i}}{\partial r} \right|_{r=r_p} = k_f \left(c_i - c_{p,i} \right) \Big|_{r=r_p} \quad (4.10)$$

$$c_i = c_i \Big|_{t=0} = c_o \quad (4.11)$$

$$c_{p,i} = c_{p,i} \Big|_{t=0,r} = c_{p,o}$$

Previous studies which incorporated the numerical Crank-Nicholson method to solve Eqs. 4.6 and 4.8 reported stability problems when resolving Eq. 4.8 (McKay 1984, 294). A more stable method evolved and applied in this study by using a dimensionless solution of Eq. 4.8, hence avoiding a direct numerical solution of Eq. 4.8. The independent variables in the above equations are transformed into dimensionless variables (Eq. 4.12).

$$\varphi_m = \frac{q_m}{c_o} \quad \omega = \frac{K_d}{c_o} \quad \tau = \frac{D_p t}{r_p^2} \quad \xi = \frac{r}{r_p} \quad (4.12)$$

$$\varphi = \frac{c_i}{c_o} \quad \varphi_p = \frac{c_{p,i}}{c_o} \quad \varphi_p \Big|_{\xi=1} = \frac{c_{p,i} \Big|_{r=r_p}}{c_o}$$

Subsequent change of variable and rearrangement yielded the dimensionless pore diffusion equations (Eqs. 4.13 and 4.14) subjected to the dimensionless conditions (Eqs. 4.15 to 4.17).

$$\frac{\partial \varphi_p}{\partial \tau} = \frac{1}{\Gamma(\varphi_p)} \frac{1}{\xi^2} \frac{1}{\partial \xi} \left(\xi^2 \frac{\partial \varphi_p}{\partial \xi} \right) \quad (4.13)$$

$$\Gamma(\varphi_p) = (1 - \varepsilon_p) \frac{\varphi_m \omega}{(\omega + \varphi_p)^2} + \varepsilon_p \quad (4.14)$$

$$\frac{\partial \varphi_p}{\partial \xi} \Big|_{\xi=0} = 0 \quad (4.15)$$

$$\frac{\partial \varphi}{\partial \tau} = \varepsilon \frac{3D_p V_s}{r_p V} \frac{\partial \varphi_p}{\partial \tau} \Big|_{\xi=1} \quad (4.16)$$

$$D_p \frac{\partial \varphi_p}{\partial \xi} \Big|_{\xi=1} = k_f \left(\varphi - \varphi_p \Big|_{\xi=1} \right) \quad (4.17)$$

The $\chi = \xi^2$ transformation is applied to eliminate Eq. 4.13 as well as the two-point nature of the boundary condition (Eq. 4.16) (Pedersen et al. 1985, 961). These equations are reduced (Eqs. 4.18 and 4.19) and solved with the given boundary conditions (Eqs. 4.16 and 4.17).

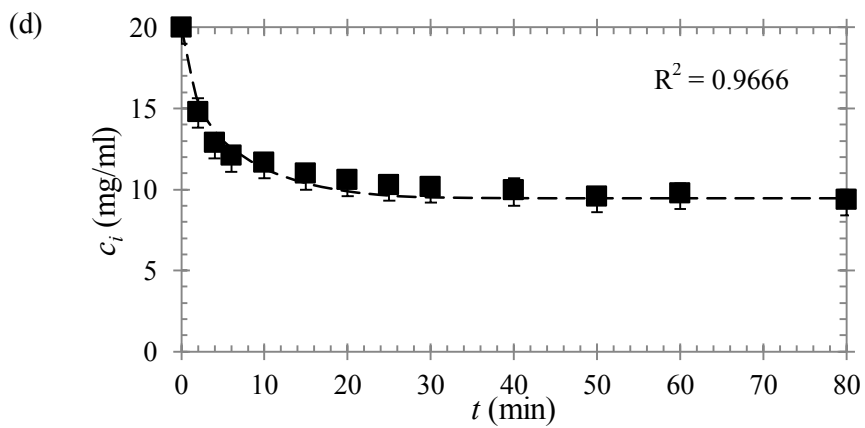
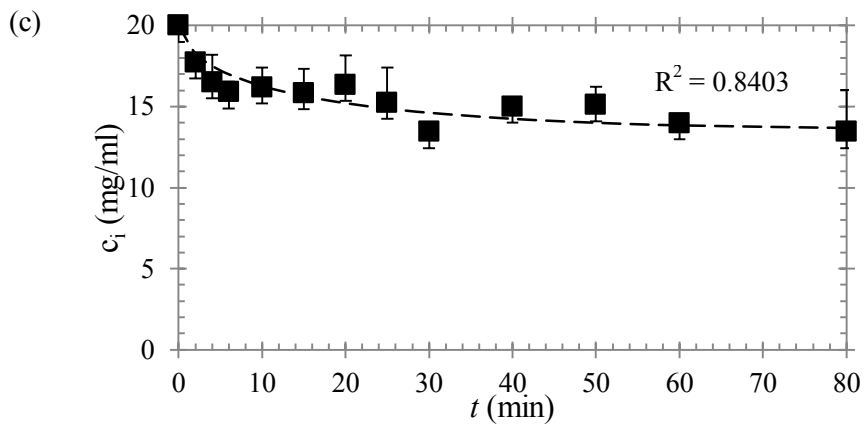
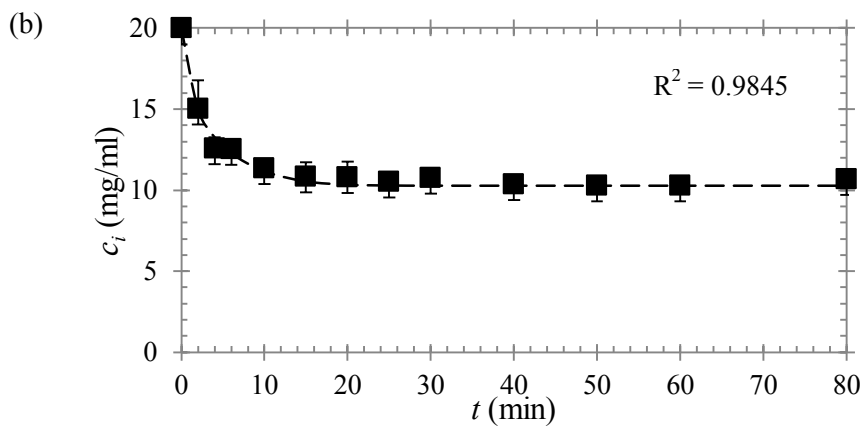
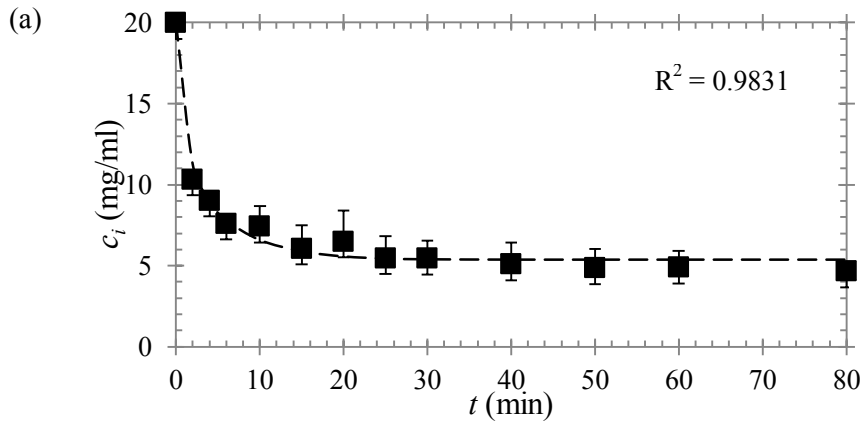
$$\Gamma(\varphi_p) \frac{\partial \varphi_p}{\partial \tau} = 6 \frac{\partial \varphi_p}{\partial \chi} + 4 \frac{\partial^2 \varphi_p}{\partial \chi^2} \quad (4.18)$$

$$\left. \frac{\partial \phi}{\partial \tau} = \varepsilon \frac{3D_p V_s}{r_p V} \frac{\partial \phi_p}{\partial \tau} \right|_{\chi=1} \quad (4.19)$$

The system (Eqs.4.18 and 4.19) are coupled partial differential equations that could be resolved numerically by first discretizing in space by using finite difference method, to transform the partial differential equations into a large set of ordinary differential equations. This is carried out by dividing the particle radius domain into a number of discretization points sufficiently large that changing the number would not have any impact on the numerical results, in particular 100 discretization points are used in the particle radius domain. The discretization is based on second-order central difference approximation method. Following this, a computer program is developed on MATLAB[®] R2010a (MathWorks, Inc.) to execute the time integration method for the resulting ordinary differential equations to advance in the time domain. A multistep ordinary differential equation solver, ODE15S, an implicit variable order solver in MATLAB[®], is used. The spherical diffusion model is coupled with a fitting routine which determined the value of the effective pore diffusion coefficient, D_p external film mass transfer coefficient, k_f and external volume fraction of particle, ε_p . The fitting routine details are discussed in Section 4.2.4.

The diffusion model (Eqs. 4.18 and 4.19) are solved to fit the experimental adsorption data. Parameters are determined with a nonlinear regression method, described in Section 4.2.4. These parameters are used to describe the kinetics of kafirin adsorption on ion exchangers with the best-fitting results summarised in Table 4.3. The linear and nonlinear regression error analyses results for the pore-diffusion parameters indicated that the fit of experimental data is good. In detail, the error functions of the pore-diffusion based model gives coefficient of determination 0.952 and 0.998. The best-fitted ion exchanger is Relisorb QA-400 while the worst is Toyopearl SuperQ-650M. The kinetics of kafirin adsorption on ion exchangers at initial bulk phase concentration of 20 mg/ml is plotted in Figure 4.3.

From the previous analysis UNOsphere Q is found to have the best adsorption performance. The pore diffusion model could help in further understanding the pore-



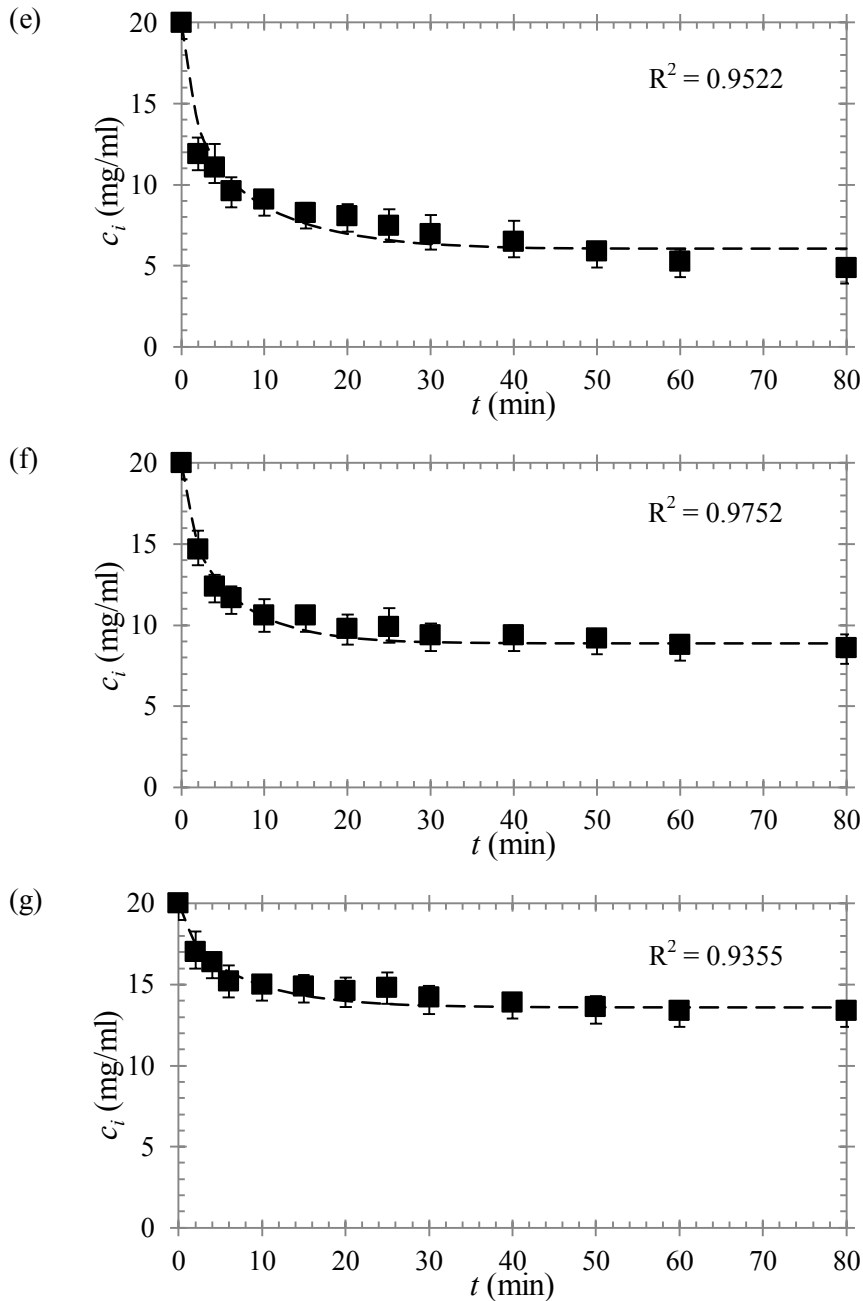


Figure 4.3 Experimental and theoretical results for kafirin adsorption to (a) UNOsphere Q, (b) ReliSorb QA-400, (c) Tulsion A-36MP, (d) Toyopearl QAE-550C, (e) Toyopearl SuperQ-650M, (f) Toyopearl SP-550C, (g) Toyopearl SP-650M. Symbols and solid line correspond to experimental and theoretical curve, respectively.

liquid concentrations profiles inside a particle. Theoretical temporal evolution of kafirin concentration in the adsorbed- and pore-liquid-phase in a single UNOsphere Q ion-exchange particle at different radial positions is shown in Figure 4.4. It could be observed that the concentration of kafirin on the particle surface increases rapidly towards the pore-liquid phase concentration. When saturation on the particle surface

occurs, the concentrations in the inner particle region began to rise progressively until an equilibrium concentration is achieved. Theoretically the diffusion model assumed the adsorbed kafirin to be in equilibrium with the inner particle pore-liquid, which is best represented by the Langmuir isotherm. The pore-liquid concentration is thus related to its adsorbed concentration on the pore surface. Theoretical concentration profile of kafirin adsorbed phase of UNOsphere Q at different time points is shown in Figure 4.5. A very steep intraparticle concentration gradient existed in the beginning but reduced gradually as time advanced when more kafirin becomes available for adsorption in the inner particle region. Complete saturation of the particle surface is observed within 25 minutes.

As indicated in Table 4.3, the relationship between the pore diffusivity, D_p values computed for an initial 20mg/ml kafirin concentration are found to inversely correlate to the external film resistance, k_f values. This complied with the stagnant film theory which proposed a hypothetical stagnant film near the liquid-particle interface within which the mass transport is governed essentially by diffusion (Beck and Schultz 1972, 273). This is supported by some authors that reported though the k_f is included in diffusion models, its effects on the uptake curves are often negligible in almost all practical cases since, in practical, the Biot number, $Bi = r_p k_f / D_p$ (Eq. 4.20), computed is typically very large (Do and Rice 1990, 1419; Wright, Muzzio, and Glasser 1998, 9113). This is justified by referring to the large Biot numbers ($Bi > 10$) reported in Table 4.3, indicative of the high contribution of D_p on the uptake kinetic curves. The estimated D_p and k_f values are 1.911×10^{-8} cm²/s and 5.940×10^{-5} cm/s for UNOsphere Q, 1.757×10^{-8} cm²/s and 4.049×10^{-5} cm/s for Relisorb QA-400, 9.230×10^{-9} cm²/s and 3.088×10^{-5} cm/s for Toyopearl QAE-550C, 3.525×10^{-9} cm²/s and 1.760×10^{-5} cm/s for Toyopearl SuperQ-650M, 9.087×10^{-9} cm²/s and 1.820×10^{-5} cm/s for Toyopearl SP-550C. Highest D_p and k_f values are found for UNOsphere Q, in accord with the highest kafirin adsorption capacity observed from experiments. Further analyses of these parameters are conducted to understand the potential factor that affects the adsorptive uptake. Particle size, for instance, is found to have significantly affected D_p and k_f values. High values of these parameters are found for large particle sizes. This, however, proves that kafirin adsorption is not controlled by diffusion. For diffusion-based adsorption, smaller particles contain less intraparticle volume through which the adsorbing molecules must diffuse. It is construed that

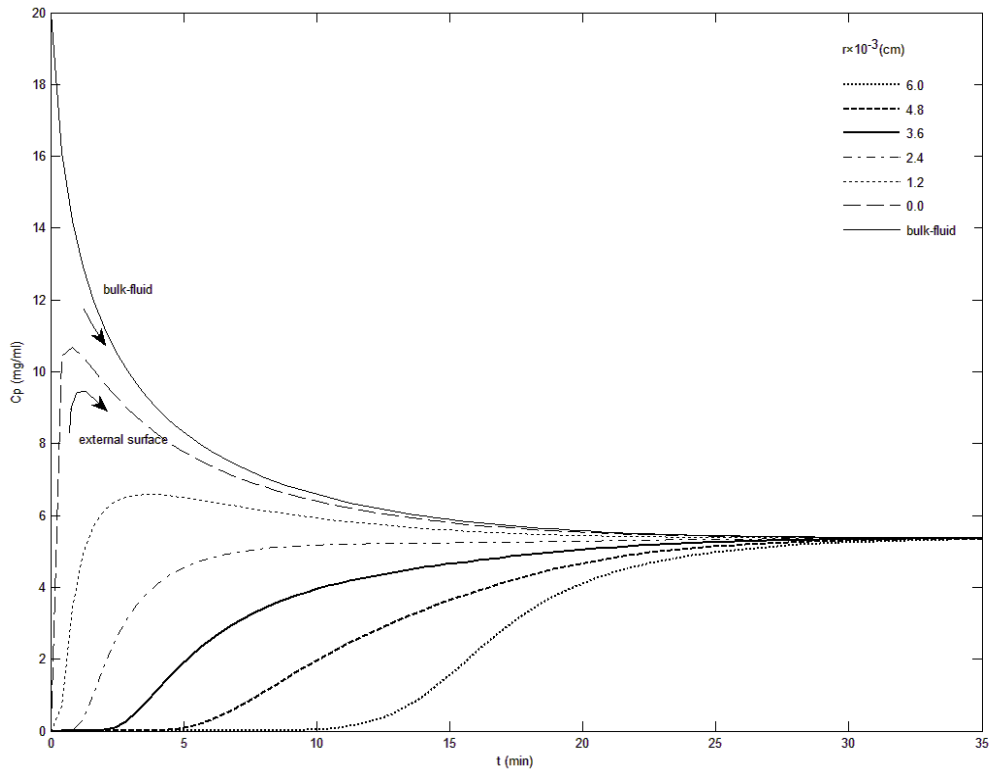


Figure 4.4 Pore-liquid concentration profiles for kafirin adsorption at different radial position in UNOsphere Q particle.

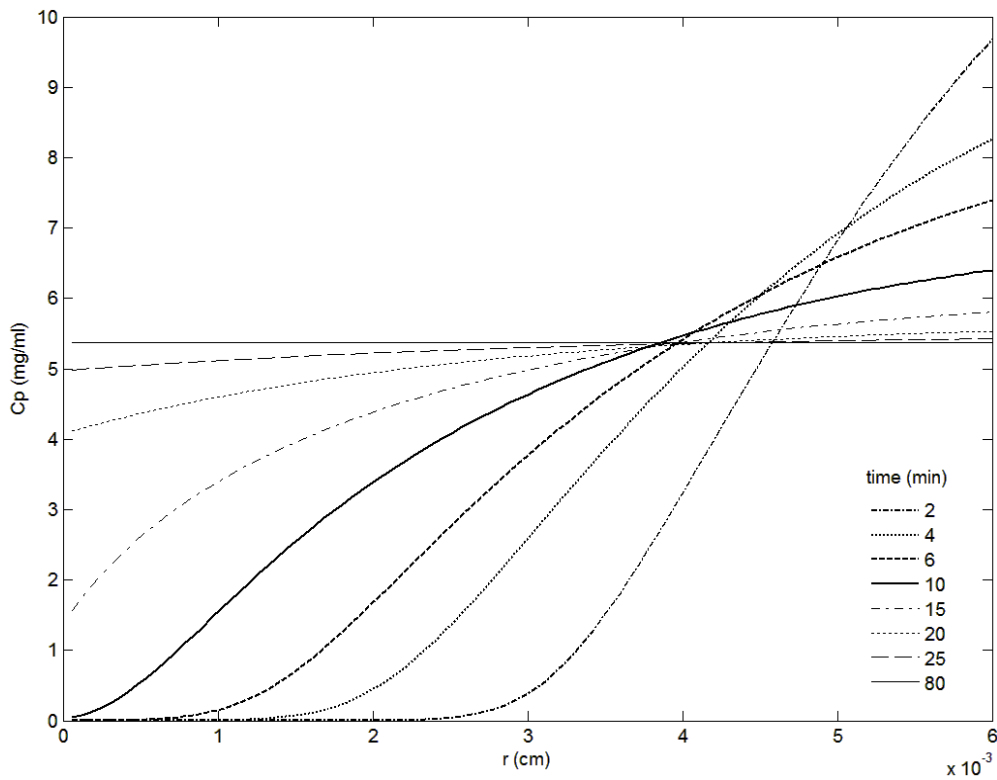


Figure 4.5 Pore-liquid concentration profiles for kafirin adsorption on UNOsphere Q at different time step.

Table 4.3 Summary of results from film-pore diffusion model for adsorption kinetics experiments.

	UNOsphere Q	ReliSorb QA-400	Tulsion A-36MP	Toyopearl QAE-550C	Toyopearl SuperQ-650M	Toyopearl SP-550C	Toyopearl SP-650M
Pore diffusion model							
Pore diffusivity, D_p (cm ² /s)	1.911×10^{-8}	1.757×10^{-8}	9.813×10^{-8}	9.230×10^{-9}	3.525×10^{-9}	9.087×10^{-9}	2.468×10^{-9}
Film resistance, k_f (cm/s)	5.940×10^{-5}	4.049×10^{-5}	9.997×10^{-5}	3.088×10^{-5}	1.760×10^{-5}	1.820×10^{-5}	9.997×10^{-6}
Particle porosity, ε_p	0.650	0.500	0.500	0.550	0.600	0.550	0.600
Extraparticle porosity, ε	0.600	0.350	0.350	0.330	0.500	0.500	0.310
Biot's number, Bi	18.653	13.829	38.200	16.730	16.178	10.013	13.160
Delta factor, δ	0.8570	0.9500	3.1700	0.9390	0.8240	0.4920	0.7340
Coefficient of determination, R_2	0.9831	0.9845	0.8403	0.9666	0.9522	0.9752	0.9355

kafirin adsorption is limited by surface reaction-based kinetic process because larger particle size provides more adsorption sites and hence higher kinetic rate.

4.4 CONCLUSION

In the present study, the binding and mass transfer of kafirin on ion exchangers with different pore structure and surface chemistry is investigated. Differences in particle chemistry, its hydrodynamic design and surface charge of kafirin with respect to the environment in batch equilibrium experiments and uptake kinetic experiments are found to contribute significantly in the adsorption behavior. Five strong basis anion-exchangers and two strong acidic cation-exchangers are studied. Modified Landry method using an ultraviolet-visible spectrophotometer is used to measure the kafirin concentration in the supernatant solutions before and after adsorption. It is found that the Langmuir adsorption isotherm and the film-pore diffusion model described the experimental data well with high regression constants. The film mass transfer has a significant effect on kafirin uptake rate specifically on UNOSphere Q and Toyopearl SuperQ-650M. The values of pore diffusivity and film resistance agree well with the published literature for nonviscous solutions. The best adsorbing ion exchangers are found to be UNOSphere Q and Toyopearl SuperQ-650M. The data presented here is essential for designing and scale up of adsorptive chromatographic purification systems or processes for kafirin.

CHAPTER 5

LIQUID-SOLID CIRCULATING FLUIDISED BED SYSTEM: MODELING CONTINUOUS KAFIRIN PURIFICATION

5.1 INTRODUCTION

Detailed equilibrium and kinetic analyses have been performed on the adsorption and desorption of kafirin in Chapter 4. It is the purpose of this study to introduce the concepts of using an LSCFB for continuous purification of kafirin and to apply the validated LSCFB model in Chapter 3 to predict the behaviour of the system. Simplified mass transfer models are proposed: lumped adsorption model and second-order desorption model, using parameters derived either from empirical correlations or batch equilibrium and kinetic experiments. Model predictions for kafirin purification in the LSCFB ion-exchange system are conducted under different operating conditions, including the degree of mixing, the solids circulation rate, the liquid velocities in circulating fluidised beds, and the feed concentration. The kafirin production rate, the fraction of kafirin recovered, and the ion exchanger inventory required, are indicative of the LSCFB performance. This model allows the use of various forms of ion-exchange kinetic models and can simulate different hydrodynamic behaviours of a continuous ion-exchange LSCFB. It is also useful for providing insights for the design and optimisation of LSCFB systems for recovery and purification processes of other proteins.

5.2 SIMULATION OF LSCFB FOR CONTINUOUS KAFIRIN PURIFICATION

5.2.1 Modeling Basis

Different operating regions exist in the LSCFB ion exchange system. Each of the riser, downer, standpipes etc. can have different residence time distribution as well as flow configuration. Moreover, adsorption, desorption, mass transfer, and hydrodynamics all have disparate time and length scales. A unified model to simultaneously accommodate all these phenomena is therefore difficult and

computationally intensive. A modular and highly configurable dynamic model to simulate protein purification in LSCFB systems is reported in Chapter 3. A similar modeling approach is used in this chapter. Briefly, each different operating region of the LSCFB is modelled as a set of ideal tanks connected in series. The solid phase and the liquid phase are individually modelled and their interaction is considered via interphase mass transfer. Based on this concept, the LSCFB is divided into two major parts, the downer and the riser, as shown in Figure 5.1 and Figure 5.2, respectively. Ion-exchange particles are envisioned as point particles with adsorbed concentration equal to the volume average concentration over the particles. Also, from experiments, it is observed that the particles mix more extensively in contrast to the fluidising liquid. To mimic this behaviour, the solid phase is divided into M number of tanks. Each of the M tanks is further divided into N number of liquid phase subtanks to achieve lower degree of mixing in the liquid phase.

5.2.2 Model Equations and Solution

Balance equations are written for each individual tank in the network using the assumptions listed in Chapter 3. A material balance is applied to the kafirin carried by the liquid phase in the i_d -th liquid subtank, including lumped mass transfer resistance, K_L at the solid-liquid interface (Eq. 5.1). The equilibrium is represented by a Langmuir isotherm. The material balance equation is applied to the kafirin adsorbed in solid phase for the j_d -th solid tank, assuming instantaneous equilibrium between the liquid phase and the adjacent solid phase (Eq. 5.2).

$$\frac{dc_{i,d}}{dt} = \frac{U_{ld}(c_{i-1,d} - c_{i,d})}{h_{ld}\varepsilon_d} - \frac{K_L a(1 - \varepsilon_d)(c_{i,d} - c_{eq})}{\varepsilon_d} \quad (5.1)$$

$$\frac{dq_{j,d}}{dt} = \frac{U_{sd}(q_{j+1,d} - q_{j,d})}{h_{sd}(1 - \varepsilon_d)} + \sum \frac{K_L a(1 - \varepsilon_d)(c_{i,d} - c_{eq})}{\varepsilon_d} \quad (5.2)$$

Desorption of kafirin from the ion-exchanger particles is often very fast compared to adsorption. For simplification, kafirin desorption kinetics in the riser fluidised bed is represented by the second-order forward rate model. The riser is divided into two hydrodynamically different regions. For the j_r -th solid tank, the mass balance is applied to the adsorbed kafirin carried over by the solid phase (Eq. 5.3) where k_r represents $k_{r,1}$ in the distributor region and $k_{r,2}$ in the upper dilute

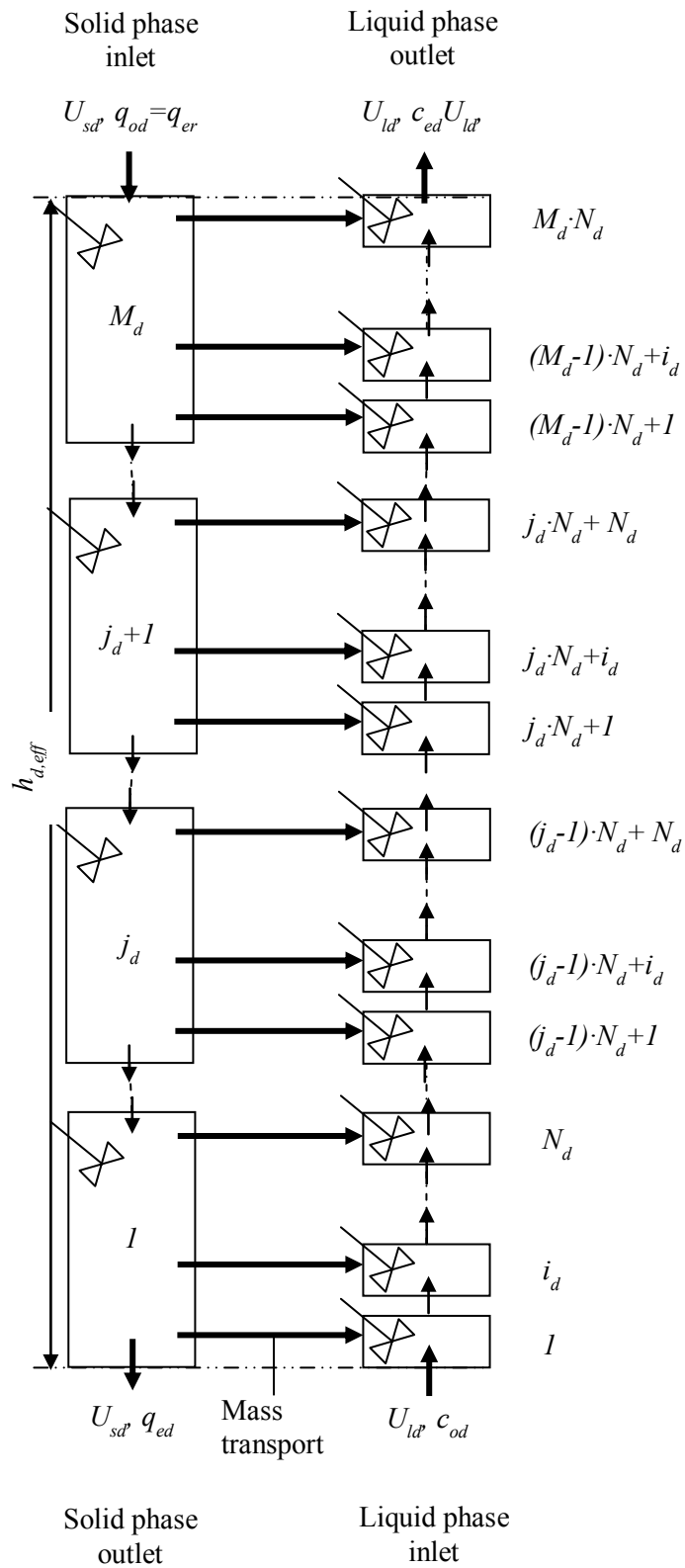


Figure 5.1 Flow diagram of the liquid-solid circulating fluidised beds. Segregation of the downer in M_d number of solid phase tanks and N_d number of liquid phase sub-tanks per solid tank.

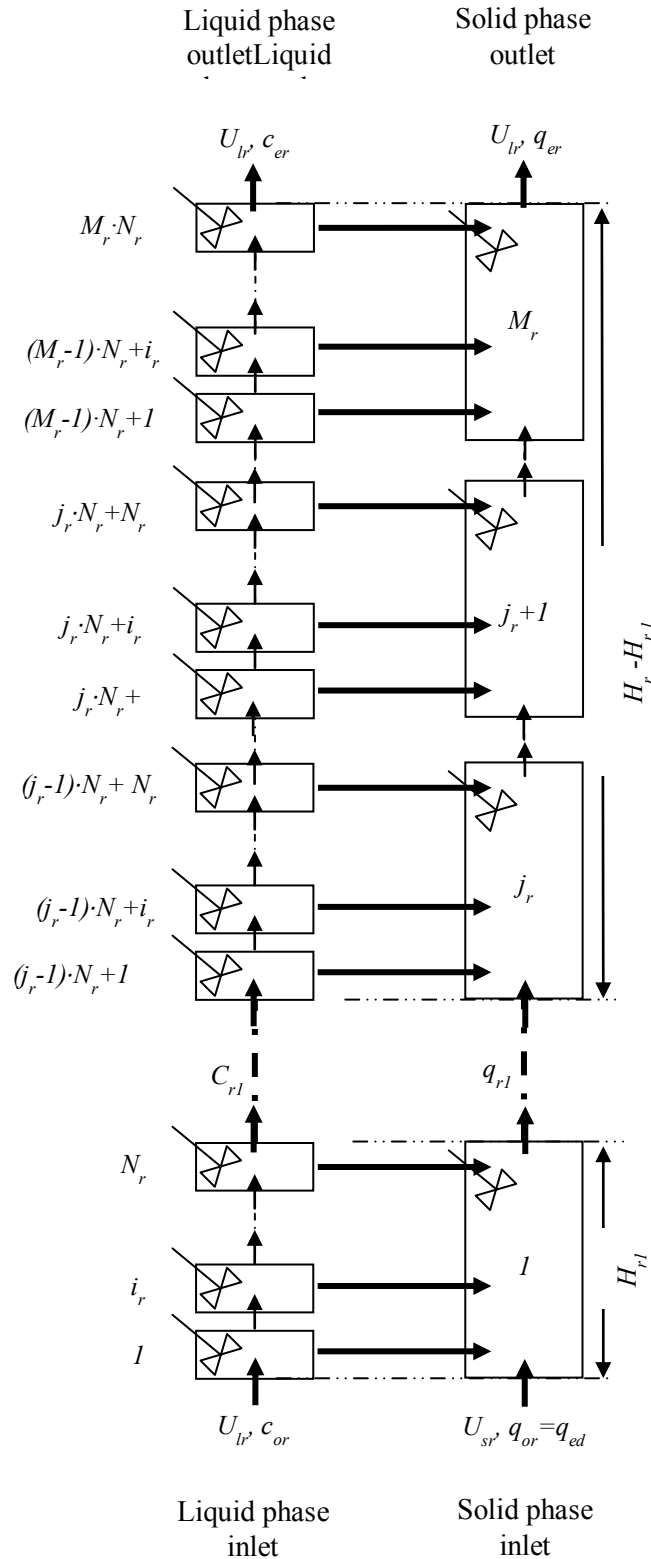


Figure 5.2 Flow diagram of the liquid-solid circulating fluidised beds. Segregation of the riser in $M_{r,l}$ number of solid phase tanks and $N_{r,l}$ number of liquid phase subtanks per solid tank in freeboard region, and $M_{r,2}$ number of solid phase tanks and $N_{r,2}$ number of liquid phase subtanks per solid tank in upper dilute region.

region. Similarly, for the i_r -th liquid subtank, the material balance equation is applied to the kafirin eluted to the liquid adjacent to the solid phase (Eq. 5.4).

$$\frac{dc_{i,r}}{dt} = \frac{U_{lr}(c_{i-1,r} - c_{i,r})}{h_{lr}\varepsilon_r} + \frac{k_r q_{j,r}^2 (1 - \varepsilon_r)}{\varepsilon_r} \quad (5.3)$$

$$\frac{dq_{j,r}}{dt} = \frac{U_{sr}(q_{j-1,r} - q_{j,r})}{h_{sr}(1 - \varepsilon_r)} - \sum \frac{k_r q_{j,r}^2 (1 - \varepsilon_r)}{\varepsilon_r} \quad (5.4)$$

Together, these equations result in a system of simultaneous first order ordinary differential equations (ODEs). The system of ODEs is solved using MATLAB[®] R2010b. Appropriate initial conditions are applied to these equations and the ODEs are solved repeatedly until the convergence criteria are met.

5.2.3 Isotherm and Kinetic Data

For realistic model predictions, it is essential to obtain accurate equilibrium and kinetic data between the kafirin and the ion-exchange particles. The application of adsorption isotherm is very useful to evaluate interactions between kafirin and the ion-exchange particles. The Langmuir (1916, 2221) isotherm equation (Eq. 5.5) is used to analyse the equilibrium kafirin adsorption data (Lau et al. 2013b, 113). The Langmuir isotherm model, initially developed to explain the gas-solid dual-phase adsorption on activated carbon, has traditionally been used for quantification and assessment of the performance of various adsorbents (Foo and Hameed 2010, 4). The parameters obtained from the Langmuir isotherm equation, q_m and K_d relate to the maximum adsorption capacity and dissociation coefficient, respectively, and provide important information on the adsorption mechanisms and the surface properties and affinities of the ion-exchange particles.

$$q_{eq} = \frac{q_m c_{eq}}{K_d + c_{eq}} \quad (5.5)$$

To understand the systems dynamic behaviour as well as to examine the mechanism and rate-controlling steps, lumped kinetic equation and second-order rate equation are used to model the kafirin adsorption and desorption kinetic data, respectively. In the linear driving force model (Eq. 5.6), the lumped parameter K_L (Eq. 5.7) is related to intraparticle diffusion through k_f and dispersion effects, Ψ .

$$\frac{dq}{dt} = K_L a (c - c_{eq}) \quad (5.6)$$

$$K_L = k_f \psi \quad (5.7)$$

Empirical correlation (Eq. 5.8), reported by Fan, Yang and Wen (1960, 484), is for the chosen k_f as this correlation accounts for changes in the film mass transfer as a function of bed voidage, ε_d , and solution viscosity, μ , and does not need adjustable proportionality constants that may be system specific. The film mass transfer parameter, k_f (Eq. 5.8) is in close agreement with previous results obtained from batch adsorption simulation of the ion-exchangers (Lau et al. 2013b, 133).

$$k_f = \frac{D_m \left[2 + 1.03 (\varepsilon_{sd} Re_p)^{0.5} (Sc)^{0.33} \right]}{d_p} \quad (5.8)$$

As observed from the desorption experiment, the desorption of kafirin is very fast and the rates of desorption from ion-exchangers are assumed to obey a simple second-order rate equation (Eq. 5.9). Second-order rate equations are originally developed to describe mineral sorption and desorption by soils (Griffin and Jurinak 1973, 869). The second-order model assumes that there is only one type of site on the adsorbent surface and that the rate is proportional to the square of the number of adsorbate filled sites.

$$\frac{dq}{dt} = -k_2 q^2 \quad (5.9)$$

All model parameters are estimated by employing the non-linear least-squares method. Following McCullough (2012, 150), the least square method is done by the minimisation of sum of squares of the residuals (RSS) between the experimental data and predicted values. Firstly the model equations are simulated to obtain theoretical data points according to the sample intervals of the experimental data points. This is followed by model parameter estimations employing the non-linear least-squares method on MATLAB[®] R2010b.

5.3 RESULTS AND DISCUSSION

5.3.1 Selection of Ion Exchangers

All ion exchangers used are of commercial grades, with details given in Table 5.1. Strong basic anion exchangers (SBA) used are as follows: UNOsphere Q from Bio-Rad Laboratories (Gladesville, NSW Australia), Relisorb QA-400 from Mitsubishi Chemical India (Gurgaon, HAR India), Toyopearl QAE-550C and Toyopearl SuperQ-650M from Kinesis Australia (Redland Bay, QLD Australia). Toyopearl SP-550C bought from Kinesis Australia is the only strong acidic cation exchanger (SAC) tested.

These ion exchangers are selected for their adsorption capacities for kafirin, fluid flow characteristics, and pH conditions required. The maximum kafirin adsorption capacities, q_m of the ion exchangers is tested to be satisfactory (58.20 – 87.08 mg/mL) for this system, with reference to Chapter 4. Although, the ion-exchange particles had different sizes, d_p (65 – 120 μm) and wet densities, ρ_w (1.26 – 1.96 g/mL), their terminal velocities, U_t (0.002 – 0.003 m/s) are sufficient enough to operate the kafirin purification LSCFB system. Kafirin has an isoelectric point (pI) of 6, the selected SBAs allowed the kafirin to be purified from an aqueous solution adjusted to pH around 9 hence reducing usage of acidic solvent at pH 1.5 associated with use of cation exchangers (Anyango, de Kock, and Taylor 2011, 2132). The SAC is used to examine the effects of pH on the LSCFB efficiency.

5.3.2 Estimation of Model Parameters

The parameters for the Langmuir isotherm and desorption kinetics are obtained by batch experiments described in Chapter 4, correspondingly. The comparison between the experimental data and model for batch adsorption and desorption on UNOsphere Q is shown in Figure 5.3. Concentration points measured at equilibrium for various concentrations of kafirin aqueous solution at experimental onset are plotted in Figure 5.3(a) whereas the elution profile is shown in Figure 5.3(b). Both adsorption and desorption are very closely predicted by the model with coefficient of determination of 0.999 and 0.984 respectively. Similar close fit is observed for all other ion exchangers. The kinetic data for all other ion exchangers is summarised in Table 5.2. The kafirin adsorption capacities followed the reference protein adsorption capacities given by the manufacturers. The adsorption capacity of ion-exchange is affected by the particle surface area available for ionic interaction. Larger pore sizes contributed to higher adsorption capacities. Consequently, ion-

Table 5.1 Characteristics of the commercial ion exchangers evaluated.

	UNOsphere Q	ReliSorb QA-400	Toyopearl QAE-550C	Toyopearl SuperQ-650M	Toyopearl SP-550C
Type	SBA	SBA	SBA	SBA	SAC
Matrix structure	Crosslinked polystyrene divinylbenzene	Crosslinked poly-methacrylate	Crosslinked poly-methacrylate	Crosslinked poly-methacrylate	Crosslinked poly-methacrylate
Functional group	Quaternary amine	Quaternary amine	Quaternary amine	Quaternary amine	Quaternary amine
Particle size (μm)	120	120	100	65	100
Pore size (\AA)	>2000	4500	500	400	500
Ion exchange capacity ($\mu\text{eq/ml}$)	120	300	360	240	130
BSA adsorption capacity (mg/ml)	125-180	n.a.	60-80	105-155	120-140
Kafirin adsorption capacity (mg/ml)	87.08	58.20	71.27	78.57	81.36
Terminal velocity (mm/s)	3.00	3.07	3.10	2.10	3.20
Bed expansion index, n	4.47	4.47	4.48	4.51	4.47

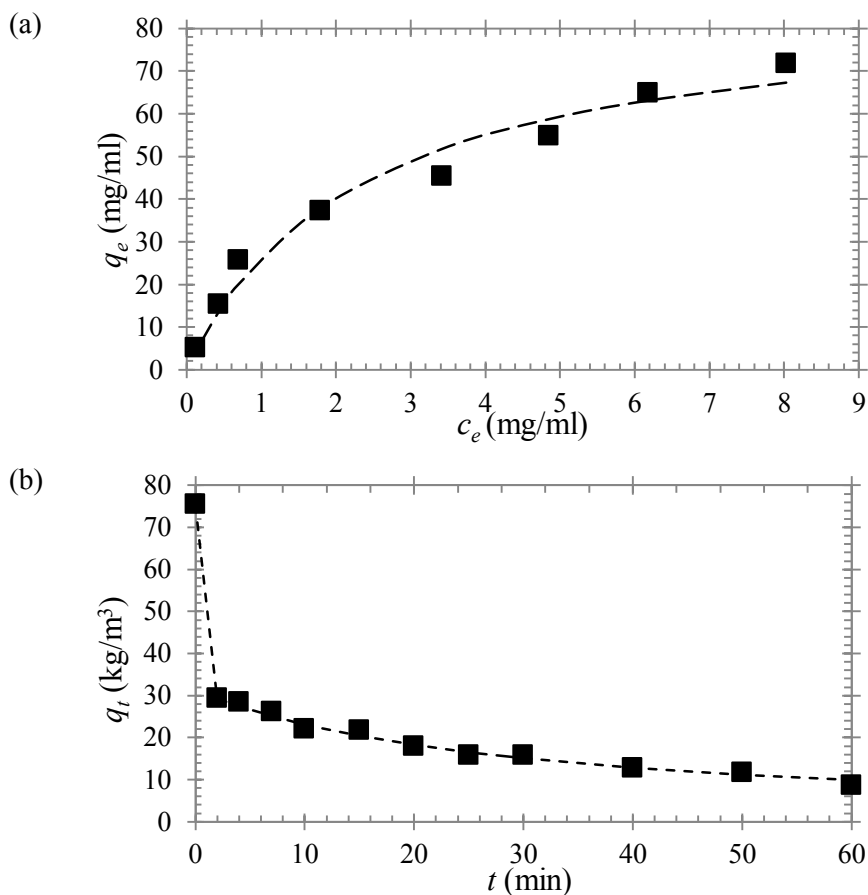


Figure 5.3 Concentration profiles analysis of the kafirin purification data on UNOsphere Q (a) equilibrium data, (b) desorption data. Symbols and solid line correspond to experimental and predicted curve, respectively.

exchangers with macropores (500-2000Å) showed greater adsorption capacity compared to ion exchangers with mesopores (60 – 500Å). The dissociation constant ($1/K_d$) is higher for SBAs than SAC due to the pH difference between anion- and cation-chromatography where the ionic interaction between the kafirin and SBAs are suggested to be more intense than interaction with SAC.

Two distinct regions are observed in the elution profile in Figure 5.3(b), initially, a very fast desorption, followed by a slow region. A single rate constant model tends to overestimate desorption rate initially and underestimate desorption rate in slow region. Thus the two distinct regions are fitted with two different desorption rate constants k_{r1} and k_{r2} independently. These constants are given in Table 5.2. The rate constant for the fast region is an order of magnitude higher than the slow region.

Table 5.2 Parameter estimates used in the isotherm and second-order equations.

	UNOsphere Q	ReliSorb QA-400	Toyopearl QAE-550C	Toyopearl SuperQ-650M	Toyopearl SP-550C
Langmuir isotherm					
Kafirin adsorption capacity, q_m (kg/m ³)	87.08	58.2	71.27	78.57	81.36
Dissociation constant, $1/K_d$ (kg/m ³)	0.4052	0.3419	0.5299	0.5592	0.1017
Second-order forward rate model					
Desorption constant at $t \leq 120s$, k_{r1} (m/s)	4.4673×10^{-4}	4.7339×10^{-4}	6.0480×10^{-4}	2.8236×10^{-4}	3.9968×10^{-4}
Desorption constant at $t > 120s$, k_{r2} (m/s)	1.9235×10^{-5}	3.3577×10^{-5}	4.5383×10^{-5}	2.1229×10^{-5}	2.6824×10^{-5}

Table 5.3 Process conditions for base case steady-state simulation runs.

	Value
Feed concentration, c_{od} (kg/m ³)	2.00
Solids circulation rate, G_s (kg/m ² /s)	1.24
Downer superficial liquid velocity, U_{ld} (mm/s)	0.60
Riser superficial liquid velocity, U_{lr} (mm/s)	5.28
Downer solid-phase tanks in dense region, M_d	20
Downer liquid-phase subtank per solid tank in dense region, N_d	1
Riser solid-phase tanks in distributor region, M_{r1}	1
Riser liquid-phase subtank per solid tank in distributor region, N_{r1}	2
Riser solid-phase tanks in upper dilute region, M_{r2}	9
Riser liquid-phase subtank per solid tank in upper dilute region, N_{r2}	2

5.3.3 Performance of Ion Exchangers in LSCFB

Before investigating the operational aspects of the LSCFB, ion exchanger selection is made by comparing the performance of the ion exchanges in the LSCFB model. The model output for different ion exchangers is compared on basis of the production rate, P (Eq. 5.10), fraction of recovery, R (Eq. 5.11), and the solids inventory required, S (Eq. 5.12). These simulations are performed at constant operating, design and model parameters as given in Table 5.3.

Protein production rate, P

$$= \text{Extract flowrate} \times \text{Kafirin concentration in extract} = U_{lr} A_r c_{er} \quad (5.10)$$

Overall protein recovery, R

$$= \text{Protein production rate} / \text{Kafirin loading rate} = U_{lr} A_r c_{er} / U_{ld} A_d c_{od} \quad (5.11)$$

Solids inventory required, S

= Sum of solids inventory in different sections of LSCFB

$$= h_{d,eff} A_d \varepsilon_{sd} + h_r A_r \varepsilon_{sr} + h_{r2} A_r \varepsilon_{sr2} + V_p (1 - \varepsilon_p) \quad (5.12)$$

The detailed results are given in Table 5.4. It is found that Toyopearl QAE-550C produced and recovered most kafirin from feed, than the other ion exchangers. This is attributed by the maximum adsorption capacity, q_m , lumped mass transfer coefficient, $K_L a$, and desorption coefficients, k_{r1} and k_{r2} . Albeit Toyopearl SP-550C has similar solids holdup in the LSCFB as Toyopearl QAE-550C, it produced and

Table 5.4 Steady-state liquid-solid circulating fluidised bed performance of different ion exchangers at base case conditions.

	UNOsphere Q	ReliSorb QA-400	Toyopearl QAE-550C	Toyopearl SuperQ-650M	Toyopearl SP-550C
Downer solids holdup, ε_{sd}	0.2276	0.2328	0.2461	0.1289	0.2539
Riser distributor region solids holdup, ε_{sr1}	0.1912	0.1911	0.1752	0.1492	0.1749
Riser upper dilute region solids holdup, ε_{sr2}	0.1639	0.1639	0.1639	0.1760	0.1633
Lumped mass transfer constant, $10^3 K_L a$ (s^{-1})	8.430	8.457	9.545	17.96	9.590
Downer raffinate concentration, c_{ed} (kg/m^3)	0.3362	0.6166	0.2233	0.2393	0.5368
Riser extract concentration, c_{er} (kg/m^3)	1.3582	1.1301	1.7119	0.8970	1.4646
Protein production rate, P (g/h)	29.17	24.27	36.77	19.27	31.46
Fraction of protein recovery, R	0.5976	0.4972	0.7533	0.3947	0.6444
Solids inventory required, S (kg)	2.019	2.487	2.399	2.064	2.474

recovered less kafirin than the latter because of the significantly larger mass transfer coefficients of the latter, which governed the LSCFB performance. UNOsphere Q followed Toyopearl SP-550C closely in terms of production and recovery. Due to its higher q_m for kafirin, it has better adsorption in the downer than the Toyopearl SP-550C despite its slightly smaller K_La and downer solids holdup, ϵ_{sd} values. Nonetheless, since Toyopearl SP-550C has a higher desorption coefficient k_{r2} , it performed better in eluting kafirin. Therefore, higher production rate and fraction of recovery are obtained with Toyopearl SP-550C compared to UNOsphere Q. Amongst all the ion exchangers tested, Relisorb QA-400 has the highest desorption coefficients. Thus one would expect better performance from these ion exchangers. However, these ion exchangers have smaller ϵ_{sd} , K_La , and q_m hence they show very poor mass transfer characteristics affecting their performance. On the other hand, Toyopearl SuperQ-650M has a high value of K_La , however, it has lowest solids holdup and low desorption coefficients therefore its performance is the poorest. In the following discussion, we use UNOsphere Q as a sample ion exchanger as it provides an average of all the ion exchangers tested in terms of performance.

5.3.4 Start-Up Dynamics of LSCFB

To understand the start-up dynamics of the LSCFB, the model is solved for process conditions and model parameters listed in Table 5.3. UNOsphere Q is used as the ion exchanger. The adsorption parameters are estimated from experiments and listed in Table 5.2. Figure 5.4 shows the liquid phase kafirin concentration profile in the downer as well as in the riser for different cycles starting from the initial conditions. The first portion of each cycle is the liquid phase kafirin concentration profile in the downer while the second portion is the riser profile. The ending of the downer concentration profile is the raffinate concentration, expressed as c_{ed} , while the ending of the riser profile is the extract concentration, expressed as c_{er} . The value of both c_{ed} and c_{er} increased with cycles because the amount of kafirin being adsorbed in downer would not be equivalent to the amount eluted in the riser, and thus kafirin remained bound to binding sites on the particle surface. This reduced the adsorption and desorption capacities of the ion-exchange particles. Nonetheless, the system arrived to a pseudo steady state value after about 7 cycles of operation, which is approximately 4 h for G_s equivalent to $1.24 \text{ kg/m}^2/\text{s}$.

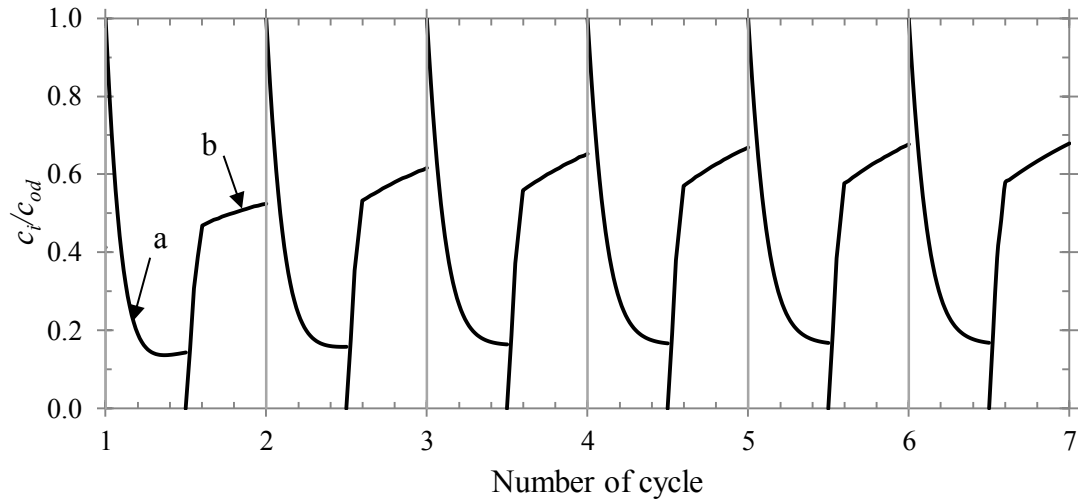


Figure 5.4 Dynamic profiles of kafirin concentration during liquid-solid circulating fluidised bed start-up. (a) Downer dynamic profile, (b) Riser dynamic profile of dimensionless kafirin concentration for UNOsphere Q.

5.3.5 LSCFB Flow Configuration

In a LSCFB, the flow behaviour in various section is designed to mimic ideal (plug flow or mixed) behaviour. However, in reality, the extent of mixing deviates between these flow patterns. The tanks-in-series model readily allows adjusting the degree of mixing. By changing the number of M solid phase tanks, and N liquid sub tanks per solid tank the present model can easily change the flow behaviour of various sections in the LSCFB. In order to tailor the flow, it is essential to understand the effects of flow patterns on the LSCFB kafirin purification process. Base case values reported in Table 5.3 are used to simulate and compare various flow patterns. Kafirin production rate (Eq. 5.10) and fractional kafirin recovery (Eq. 5.11) are calculated from the simulation results.

Downer Mixing Behaviour

The effect of the flow pattern is simulated at different combinations between perfect mixing and plug flow for the solid and liquid phase in downer. The results are presented in Table 5.5 and are compared on the basis of equal residence time in each phase and total height ($h_{d,eff}=0.8$ m). When both the liquid phase ($N_d=1$) and the solid phase ($M_d=1$) are perfectly mixed, a production rate of 19.71 g/h and a fractional recovery of 0.4037 are found. Improved production rate and fractional recovery (29.17 g/h and 0.5976 respectively) are obtained when both solid and liquid phases

Table 5.5 Steady-state performance of UNOsphere Q at different hydraulics of downer dense region.

Solid-phase flow configuration	Perfect mixing $M_d=1$	Perfect mixing with backmixing $M_d=1$	Plug flow $M_d=20$	Plug flow with backmixing $M_d=20$
Liquid-phase flow configuration	Perfect mixing $N_d=1$	Plug flow $N_d=20$	Plug flow $N_d=1$	Plug flow $N_d=20$
Downer raffinate conc., c_{ed} (kg/m ³)	0.8762	1.8764	0.3362	1.875
Downer solid outlet conc., q_{ed} (kg/m ³)	21.08	37.62	28.34	38.98
Riser extract conc., c_{er} (kg/m ³)	0.9175	1.9487	1.3582	2.0394
Riser solid outlet conc., q_{er} (kg/m ³)	8.91	11.66	10.29	11.84
Protein production rate, P (g/h)	19.71	41.86	29.17	43.81
Fraction of protein recovery, R	0.4037	0.9139	0.5976	0.9572

are near plug flow behaviour without involving solids backmixing ($M_d=20$; $N_d=1$). Nonetheless, keeping the solid phase completely mixed with backmixing by the near plug flow behaviour of the liquid phase ($M_d=1$, $N_d=20$) resulted in obvious increase in production rate and fractional recovery (41.86 kg/h and 0.9139 respectively). It should be noted that the values of c_{ed} is higher despite more kafirin being carried over into the riser, for consistent feeding rate and solids circulation rate in the system. This showed although the LSCFB is more efficient with backmixing, the existing feed loading rate is too rapid for the solid particles to adsorb the kafirin from feed. Changing the flow behaviour for solids to near plug flow with backmixing by plug flow liquid ($M_d=20$, $N_d=20$) only marginally improved production rate and fractional recovery (43.81 g/h and 0.9572 respectively). It should be noted that when there is no solids backmixing, even with near plug flow behaviour of solid phase, the production rate and fractional recovery are comparatively poorer. For a fixed number of solid tanks, increasing solids backmixing performed better in LSCFB. In fact, the configuration of plug flow liquid and solids phases incorporating solids backmixing provided the most efficient LSCFB kafirin recovery.

Table 5.6 Steady-state performance of UNOsphere Q at different hydraulics of riser distributor region.

Solid-phase flow configuration	Perfect mixing $M_{r,l}=1$	Perfect mixing with backmixing $M_{r,l}=1$	Plug flow $M_{r,l}=20$	Plug flow with backmixing $M_{r,l}=20$
Liquid-phase flow configuration	Perfect mixing $N_{r,l}=1$	Plug flow $N_{r,l}=20$	Plug flow $N_{r,l}=1$	Plug flow $N_{r,l}=20$
Downer raffinate conc., c_{ed} (kg/m ³)	0.4866	0.2068	0.4044	0.0911
Downer solid outlet conc., q_{ed} (kg/m ³)	30.58	26.06	29.4	23.45
Riser extract conc., c_{er} (kg/m ³)	2.137	0.351	2.346	0.311
Riser solid outlet conc., q_{er} (kg/m ³)	14.15	6.60	12.09	3.00
Protein production rate, P (g/h)	45.89	7.53	50.39	6.67
Fraction of protein recovery, R	0.9401	0.1543	0.9999	0.1367

Riser Mixing Behaviour

The circulating fluidised bed riser comprises of the distributor region, and upper dilute region. Different flow configurations are simulated for riser. Generally, the distributor region has high solids holdup and behaves like a perfectly mixed tank, while in the upper dilute region, both the solid and liquid phases are in near plug flow configuration. The various flow patterns of the two phases in riser examined are summarised in Table 5.6 for the distributor region and Table 5.7 for upper dilute region. The simulation results are compared for these combinations on basis of equal phase residence time and height for riser distributor region ($h_{r,l}=0.3$ m) and upper dilute region ($h_{r,2} = 2.7$ m). Well-mixed solid phase ($M_{r,l}=1$) performed better than plug-flow solid phase ($M_{r,l}=10$) in the riser distributor region. The best overall combination in the riser distributor region is the well-mixed liquid and solid phase, with no solids backmixing configuration, resulting in the highest values of production rate and fractional recovery. This is because of the small values of desorption coefficients of UNOsphere Q requiring for longer residence time in the riser for sufficient elution. It should also be noted that for configuration with solids backmixing, for well-mixed and plug flow of solids, the LSCFB behaved poorly in

Table 5.7 Steady-state performance of UNOsphere Q at different hydraulics of riser upper dilute region.

Solid-phase flow configuration	Perfect mixing $M_{r1}=1$	Perfect mixing with backmixing $M_{r1}=1$	Plug flow $M_{r1}=20$	Plug flow with backmixing $M_{r1}=20$
Liquid-phase flow configuration	Perfect mixing $N_{r1}=1$	Plug flow $N_{r1}=20$	Plug flow $N_{r1}=1$	Plug flow $N_{r1}=20$
Downer raffinate conc., c_{ed} (kg/m ³)	0.3840	0.2295	0.3796	0.1835
Downer solid outlet conc., q_{ed} (kg/m ³)	29.10	26.46	29.03	25.55
Riser extract conc., c_{er} (kg/m ³)	1.4120	1.1364	1.4260	1.1062
Riser solid outlet conc., q_{er} (kg/m ³)	11.56	7.28	11.44	5.91
Protein production rate, P (g/h)	30.33	24.41	30.63	23.76
Fraction of protein recovery, R	0.6213	0.5000	0.6274	0.4867

relative to those without backmixing. This can be explained as the adverse result of incorporating solids backmixing without first modifying the extracting buffer flowrate and solids circulation rate. With the latter remained constant, the increase in backmixing degree though improved the interphase mass transfer, the c_{er} deteriorated. This can be explained as the effect of loading the extracting buffer too rapidly into the riser which causes the kafirin outlet concentration to decrease, and also excess of the extracting buffer. Overall, the well-mixed liquid and solid phase configuration with no solids backmixing is the most efficient configuration.

Well-mixed solid phase ($M_{r2}=1$) for both perfect mixing ($N_{r1}=1$) and plug flow ($N_{r2}=10$) of liquid phase are more efficient than that of plug-flow-like solids ($M_{r2}=10$), in the riser upper dilute region. This is as shown in Table 5.7. The M_{r2} and N_{r2} affected the overall performance of LSCFB similarly to that of M_{r1} and N_{r1} , although the effects of mixing parameters are less evident than the former because the desorption coefficient in the riser upper dilute region, k_{r2} is smaller than the desorption coefficient in the riser distributor region, k_{r1} . The best flow pattern

obtained for the upper dilute region is well-mixed solid phase with no backmixing, with well-mixed liquid phase for highest production rate and fractional recovery of the LSCFB system.

5.3.6 Effects of LSCFB Operating Parameters

Four important parameters, namely, the solids circulation rate, G_s , downer liquid velocity, U_{ld} , riser liquid velocity, U_{lr} and feed concentration, c_{od} affect the performance of LSCFB significantly. The effect of these parameters on the LSCFB performance using UNOsphere Q as the ion exchanger is investigated. Performance ratings such as the kafirin production rate, P , fraction of kafirin recovered, R , and solids inventory required, S , are calculated from the simulation results. These analyses are performed by keeping the other process conditions at base case steady-state values reported in Table 5.3.

Solids Circulation Rate

Solids circulation rate, G_s is an indication of the mass flow rate of the ion-exchange particles circulating between the fluidised beds of LSCFB under steady-state conditions. The effect of G_s on the LSCFB performance is shown in Figure 5.5. G_s are varied between 1.06 to 1.36 kg/m²/s for these simulations. The G_s directly affects the residence time of the solid phase in the circulating fluidised beds. This in turn affects the solids holdup in the fluidised beds as the holdup is closely correlated to the solid phase velocity in the downer, U_{sd} and the riser, U_{sr} .

The value of c_{ed} is an indication of the amount of kafirin lost into the raffinate at the outlet of downer. As depicted in Figure 5.5(a), steeper concentration profiles are observed in the downer for higher values of G_s . This may be due to higher lumped mass transfer coefficients at higher G_s , refer to Table 5.8, causing more kafirin to be adsorbed and hence reduced c_{ed} . Thus, with higher G_s , effectively smaller downer bed is required before the system approaches equilibrium. Figure 5.5(b) illustrates the concentration profiles in the riser simulated for various G_s values. From Table 5.8, the solids holdup in the riser increased with G_s . However, the increase in solids holdup is compensated by the slow desorption rates in the two hydrodynamically different regions. For t less than or at the fast desorption period, the k_{r1} is used as desorption constant spanning over the riser distributor region and a small portion of

Table 5.8 Steady-state performance of UNOsphere Q at various solids circulation rate, G_s ($c_{od}=2\text{kg/m}^3$; $U_{ld}=0.6\text{mm/s}$; $U_{lr}=5.28\text{mm/s}$; $h_{d,\text{eff}}=0.8\text{m}$).

Solids circulation rate, G_s (kg/m ² /s)	1.06	1.24	1.36
Downer solids holdup, ε_{sd}	0.2407	0.2276	0.218
Riser distributor region solids holdup, ε_{sr1}	0.1723	0.1912	0.203
Riser upper dilute region solids holdup, ε_{sr2}	0.1458	0.1639	0.176
Lumped mass transfer constant, $10^3 K_L a$ (s ⁻¹)	4.361	8.43	13.08
Downer raffinate concentration, c_{ed} (kg/m ³)	0.4735	0.3362	0.3112
Riser extract concentration, c_{er} (kg/m ³)	1.5093	1.3582	1.2112
Downer solid outlet concentration, q_{ed} (kg/m ³)	35.06	24.11	24.17
Riser solid outlet concentration, q_{er} (kg/m ³)	10.85	5.59	9.746
Protein production rate, P (g/h)	32.42	29.17	26.01
Fraction of protein recovery, R	0.6641	0.5976	0.5329
Solids inventory, S (kg)	2.012	2.019	2.018

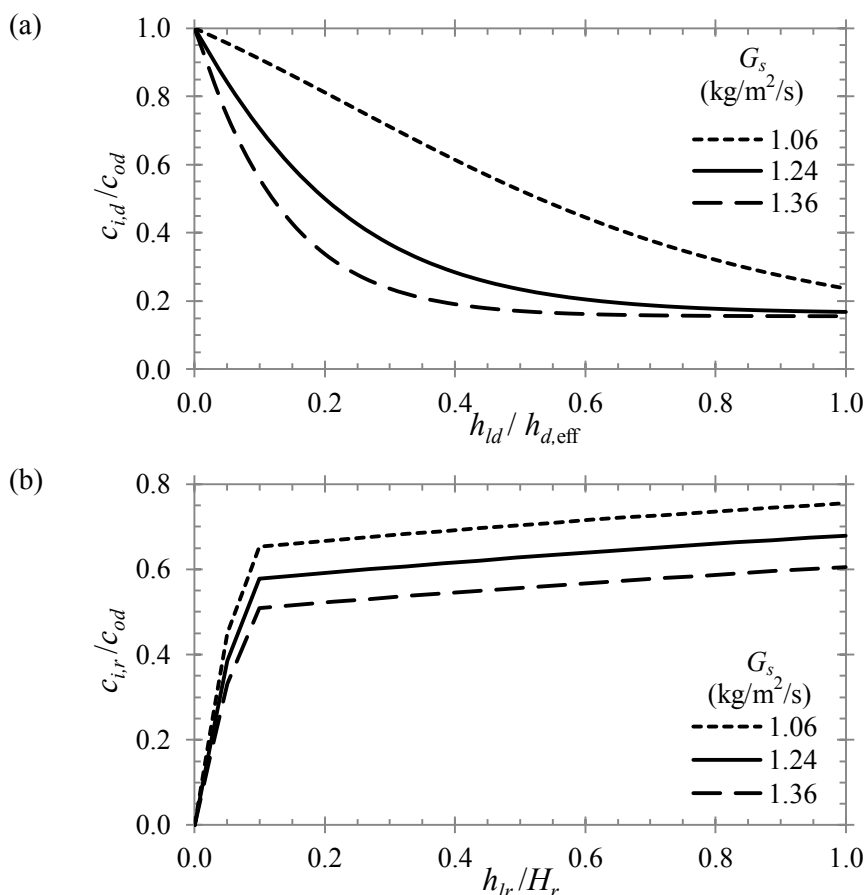


Figure 5.5 Concentration profiles analysis of (a) downer steady-state adsorption profile, (b) riser steady-state desorption profile for UNOsphere Q on the effects of changes in the solids circulation rate, G_s ($c_{od}=2\text{kg/m}^3$; $U_{ld}=0.6\text{mm/s}$; $U_{lr}=5.28\text{mm/s}$; $h_{d,\text{eff}}=0.8\text{m}$).

the upper dilute region. The k_{r2} is used in the remaining portion of the riser. The slow desorption rate in riser led to longer residence time required for solids phase to elute the adsorbed kafirin into the eluent. Consequently, lower amount of kafirin is eluted at higher G_s and higher concentration of kafirin is observed at smaller G_s , thus yielding higher production rate and recovery at lower solids inventory. Therefore, smaller G_s is beneficial to the LSCFB overall performance.

Downer Liquid Velocity

The effects of liquid velocity in the downer, U_{ld} are shown in Figure 5.6. Similar to the solids circulation rate, the influence of U_{ld} on the LSCFB can be identified in many aspects. First of all, U_{ld} directly affects the residence time of the liquid phase in downer. Secondly, it influences the downer solids holdup, ϵ_{sd} . Thirdly, for a given solids circulation rate, a change in the U_{ld} modifies the kafirin feeding rate to the LSCFB and thus changes the mass balance of kafirin in the downer. As depicted in Figure 5.6(a), steeper profiles are observed with U_{ld} increase; yet, the difference between the outlet concentrations, c_{ed} is not significant. From Table 5.9, it can be noted that the c_{ed} increases slightly with U_{ld} . This is affected by the change in residence time and solids holdup in the downer with different U_{ld} . Though the changes in the downer liquid velocity, U_{ld} on the effects of lumped mass transfer increases slightly with U_{ld} this increase is offset by more significant changes in other factors mentioned previously. Figure 5.6(b) illustrates the kafirin concentration profiles in riser at various U_{ld} . When U_{ld} is increased, the profiles became much steeper yielding greater amount of kafirin in eluent, c_{er} . Since the kafirin feeding rate increases with U_{ld} , much more kafirin is carried to the riser via kafirin-loaded solid particles. The U_{ld} does not affect the riser performance where the solids holdup remains constant. Taking all these into account, the highest kafirin production and recovery are obtained for the largest U_{ld} . Also, solids amount required decreases with U_{ld} supporting that higher U_{ld} are beneficial to kafirin purification on LSCFB.

Riser Liquid Velocity

The effect of liquid velocity in the riser, U_{lr} is shown in Figure 5.7. U_{lr} affects the system by altering the liquid phase residence time in riser, solids holdup in riser distributor region, ϵ_{sr1} and riser upper dilute region, ϵ_{sr2} . For a fixed solids circulating rate, U_{lr} also controls the eluent entering flowrate to the riser and thus the kafirin

Table 5.9 .Steady-state performance of UNOsphere Q at various downer liquid velocity, U_{ld} ($c_{od}=2\text{kg/m}^3$; $G_s=1.24\text{kg/m}^2/\text{s}$; $U_{lr}=5.28\text{mm/s}$; $h_{d,\text{eff}}=0.8\text{m}$).

Downer superficial liquid velocity, U_{ld} (mm/s)	0.40	0.50	0.60
Downer solids holdup, ε_{sd}	0.29	0.2573	0.2276
Riser distributor region solids holdup, ε_{sr1}	0.1912	0.1912	0.1912
Riser upper dilute region solids holdup, ε_{sr2}	0.1639	0.1639	0.1639
Lumped mass transfer constant, $10^3 K_L a$ (s^{-1})	8.08	8.29	8.43
Downer raffinate concentration, c_{ed} (kg/m^3)	0.2748	0.307	0.3362
Riser extract concentration, c_{er} (kg/m^3)	0.8686	1.1288	1.3582
Downer solid outlet concentration, q_{ed} (kg/m^3)	20.25	24.61	24.11
Riser solid outlet concentration, q_{er} (kg/m^3)	8.73	9.622	5.59
Protein production rate, P (g/h)	20.25	24.24	29.17
Fraction of protein recovery, R	0.5733	0.596	0.5976
Solids inventory, S (kg)	2.388	2.194	2.019

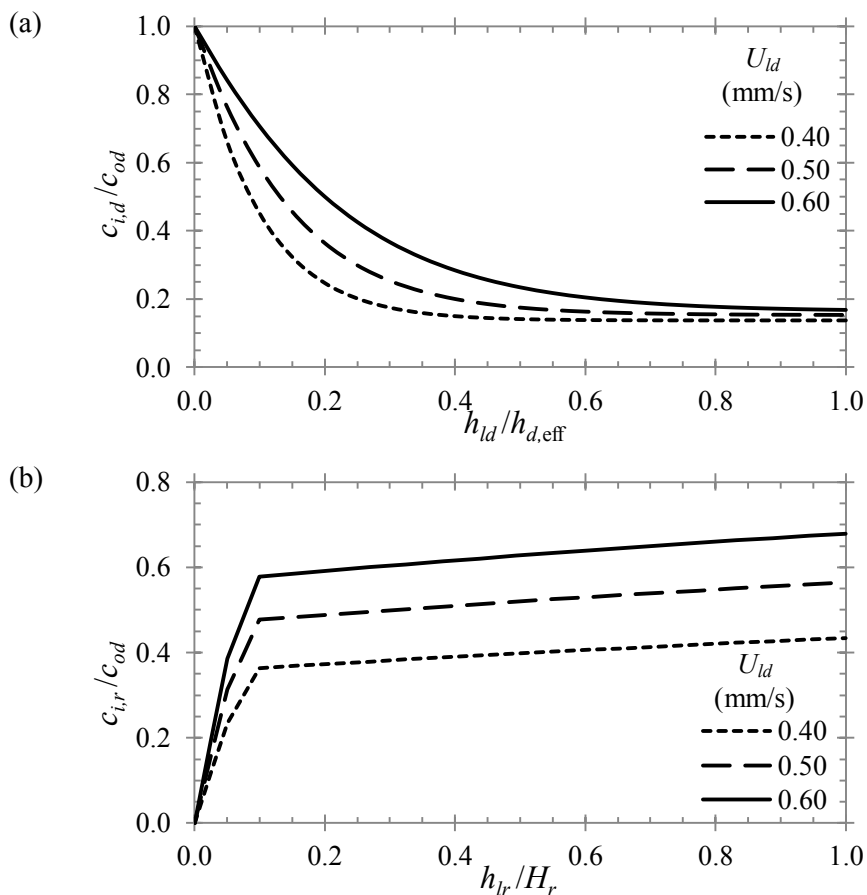


Figure 5.6 Concentration profiles analysis of (a) downer steady-state adsorption profile, (b) riser steady-state desorption profile for UNOsphere Q on the effects of changes in the downer liquid velocity, U_{ld} ($c_{od}=2\text{kg/m}^3$; $G_s=1.24\text{kg/m}^2/\text{s}$; $U_{lr}=5.28\text{mm/s}$; $h_{d,\text{eff}}=0.8\text{m}$).

Table 5.10 Steady-state performance of UNOsphere Q at various riser liquid velocity, U_{lr} ($c_{od}=2\text{kg/m}^3$; $G_s=1.24\text{kg/m}^2/\text{s}$; $U_{ld}=0.60\text{mm/s}$; $h_{d,\text{eff}}=0.8\text{m}$).

Riser superficial liquid velocity, U_{lr} (mm/s)	5.28	6.96	8.64
Downer solids holdup, ε_{sd}	0.2276	0.2276	0.2276
Riser distributor region solids holdup, ε_{sr1}	0.1912	0.1502	0.1228
Riser upper dilute region solids holdup, ε_{sr2}	0.1639	0.0897	0.0603
Lumped mass transfer constant, $10^3 K_L a$ (s^{-1})	8.43	8.43	8.43
Downer raffinate concentration, c_{ed} (kg/m^3)	0.3362	0.4503	0.5354
Riser extract concentration, c_{er} (kg/m^3)	1.3582	1.0054	0.7839
Downer solid outlet concentration, q_{ed} (kg/m^3)	24.11	30.01	31.22
Riser solid outlet concentration, q_{er} (kg/m^3)	5.59	13.26	15.32
Protein production rate, P (g/h)	29.17	28.47	27.55
Fraction of protein recovery, R	0.5976	0.5831	0.5644
Solids inventory, S (kg)	2.019	1.861	1.796

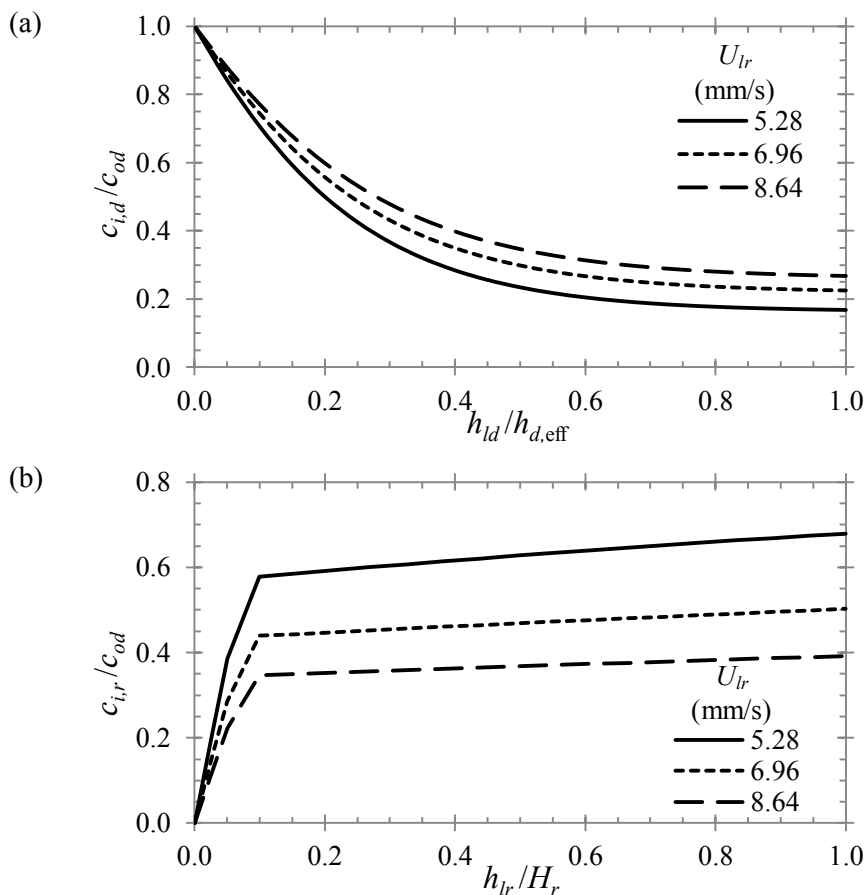


Figure 5.7 Concentration profiles analysis of (a) downer steady-state adsorption profile, (b) riser steady-state desorption profile for UNOsphere Q on the effects of changes in the riser liquid velocity, U_{lr} ($c_{od}=2\text{kg/m}^3$; $G_s=1.24\text{kg/m}^2/\text{s}$; $U_{ld}=0.60\text{mm/s}$; $h_{d,\text{eff}}=0.8\text{m}$).

Table 5.11 .Steady-state performance of UNOsphere Q at various initial feed concentration, c_{od} ($G_s=1.24\text{kg/m}^2/\text{s}$; $U_{ld}=0.60\text{mm/s}$; $U_{lr}=5.28\text{mm/s}$; $h_{d,\text{eff}}=0.8\text{m}$).

Initial feed concentration, c_{od} (kg/m^3)	1	2	3
Downer solids holdup, ε_{sd}	0.2276	0.2276	0.2276
Riser distributor region solids holdup, ε_{sr1}	0.1912	0.1912	0.1912
Riser upper dilute region solids holdup, ε_{sr2}	0.1639	0.1639	0.1639
Lumped mass transfer constant, $10^3 K_L a$ (s^{-1})	8.43	8.43	8.43
Downer raffinate concentration, c_{ed} (kg/m^3)	0.2401	0.3362	0.4075
Riser extract concentration, c_{er} (kg/m^3)	0.6214	1.3582	2.1098
Downer solid outlet concentration, q_{ed} (kg/m^3)	15.91	24.11	40.19
Riser solid outlet concentration, q_{er} (kg/m^3)	7.675	5.59	11.98
Protein production rate, P (g/h)	13.35	29.17	45.32
Fraction of protein recovery, R	0.5469	0.5976	0.6189
Solids inventory, S (kg)	2.019	2.019	2.019

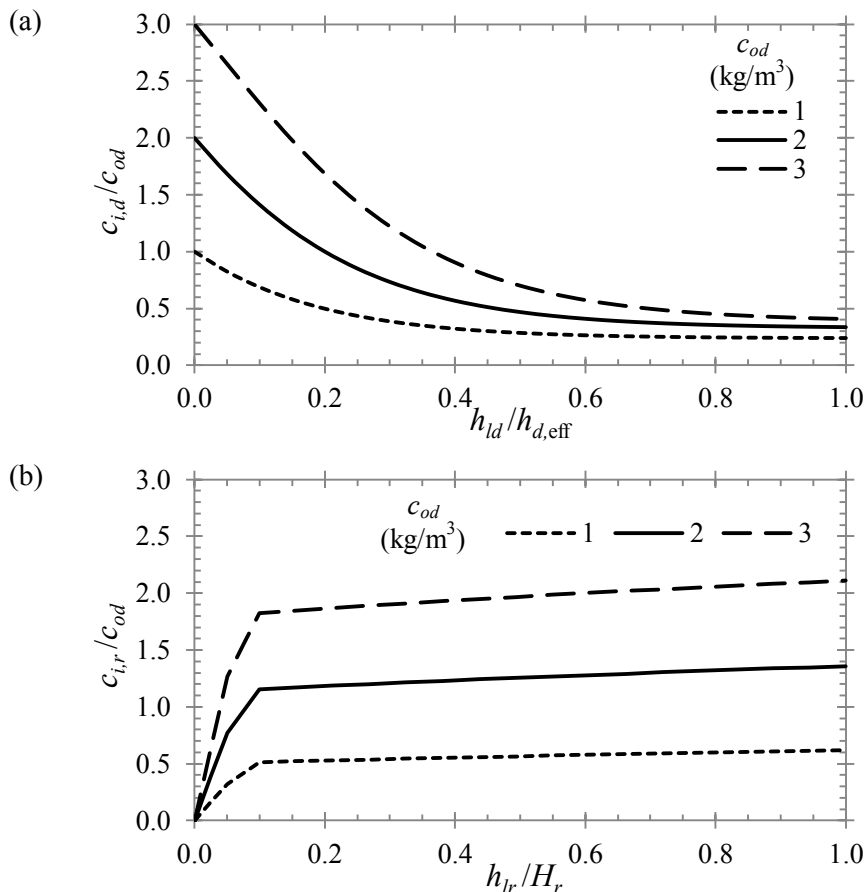


Figure 5.8 Concentration profiles analysis of (a) downer steady-state adsorption profile, (b) riser steady-state desorption profile for UNOsphere Q on the effects of changes in the initial feed concentration, c_{od} ($G_s=1.24\text{kg/m}^2/\text{s}$; $U_{ld}=0.60\text{mm/s}$; $U_{lr}=5.28\text{mm/s}$; $h_{d,\text{eff}}=0.8\text{m}$).

production and mass balance in the riser. The concentration profiles of riser at different U_{lr} are shown in Figure 5.7(b). The steepest increase in concentration is found for the lowest U_{lr} in simulation. This is especially apparent for distributor region. Much more kafirin is desorbed from solid particles into the eluent at smaller U_{lr} value since the solid phase residence time allows sufficient time for desorption. Desorption capacity of solid particles reduces as U_{lr} increased as more kafirin remain inside them due to less residence time for elution process in the riser. This can be observed from Figure 5.7(b) in which at low U_{lr} values, steeper concentration profiles are obtained. Hence, for a given downer dense region height, the c_{ed} values increases with U_{lr} to indicate greater adsorption for smaller U_{lr} , as given in Table 5.10. Thus, smaller values of U_{lr} are required for higher production rate and recovery of kafirin with a slight increase in the solids inventory requirement.

Feed Concentration

As illustrated in Figure 5.8, the simulation results show that the kafirin concentration in the extract increases with the initial kafirin concentration at the downer inlet, c_{od} . But, an increase of the c_{od} without being balanced by decrease of the downer liquid flowrate, U_{ld} causes an increase in loading rate of kafirin to the LSCFB. From Table 5.11, the kafirin production rate increases almost proportionally with the increase in c_{od} . However, a higher c_{od} values, kafirin recovery does not increase as significantly as the kafirin production rate. For this, it is critical to operate the LSCFB at kafirin loading rate below the adsorption capacity of system to reduce loss of kafirin into raffinate.

5.4 CONCLUSION

A first-principle model employing the tanks-in-series approach is developed for a continuous purification of kafirin in the LSCFB. Batch experiments are conducted for a five commercially available ion exchangers to obtain equilibrium and kinetic data for kafirin adsorption and desorption on these ion exchangers. The Langmuir isotherm showed the best fit for describing the equilibrium relationship of solid-liquid interaction for all ion exchangers. Kafirin adsorption rate is expressed by a lumped mass transfer coefficient correlated to the previously validated intraparticle

diffusion and dispersion factor to closely represent the adsorption rate. Kafirin desorption is rapid and the rate is modelled by a second-order equation.

The performance of the LSCFB is compared using the five ion exchangers. It is observed that mass transfer as well as desorption kinetics plays an important role in dictating the performance of the ion exchanger. Toyopearl QAE-550C is the most efficient in recovering kafirin from feed solution, while Toyopearl SuperQ-650M is least efficient. To obtain a fair overview of the behaviour of ion exchangers in the system, an average performing ion exchanger, the UNOsphere Q, is selected for further analysis.

Unsteady state simulations are carried out to understand the dynamics of the LSCFB system. It is observed that the system arrives at pseudo steady state condition after 7 cycles, approximately 4 h of operation. The tanks-in-series model provides great flexibility in manipulating the flow behaviour of individual sections in LSCFB. The flow behaviour of the solid phase and liquid phase, with and without incorporating the solids backmixing is examined. Better performance is obtained with solid backmixing w.r.t. liquid phase in the downer. In the riser, however, the well-mixed liquid-solid flow with no backmixing effect in both the riser distributor and upper dilute regions are the most efficient. These results are valuable in designing new LSCFB systems.

Effects of critical operating parameters namely, solid circulation rate, riser and downer liquid velocities, and initial kafirin concentration in the feed are assessed. Both the production rate and fractional recovery of kafirin in the LSCFB deteriorated with the increase in solids circulation rate and riser liquid velocity, while the recovery and production rate increased with downer liquid velocity and initial kafirin concentration in feed. A close scrutiny of the simulation results showed that each operating parameters affected the system in different manners, and that there exist optimum values of the process conditions. This work not only provides useful insights for multi-parameter optimisation of the LSCFB of kafirin, but also for other protein recovery operations.

CHAPTER 6

LIQUID-SOLID CIRCULATING FLUIDISED BED SYSTEM: MULTIOBJECTIVE OPTIMISATION FOR CONTINUOUS KAFIRIN PURIFICATION

6.1 INTRODUCTION

Multiobjective optimisation (MOO) is used increasingly to optimize chemical engineering applications for conflicting objectives such as conversion, selectivity and yield besides economic criteria. In Chapter 5, the previously validated LSCFB model is successfully applied for continuous purification of kafirin. A close scrutiny of the sensitivity study in Chapter 5 also reveals that some of the operating parameters such as the solids circulation rate, liquid velocity in the downer, liquid velocity in the riser, and feed concentration have significant effects on kafirin recovery and production rate. In some circumstances, these also act in a conflicting manner. It is thus the aim of this chapter to perform MOO to maximise both the production rate and fractional recovery of kafirin. Five process decision variables are studied, specifically downer liquid velocity, solids circulation rate, riser liquid velocity, kafirin concentration of feed and effective height of the downer. The MOO problems of the LSCFB model are solved by the MATLAB® multiobjective function GAMULTIOBJ function, which is a variant of the Non-dominated Sorting Genetic Algorithm-II (NSGA-II). In particular, the MOO is performed to find a range of better operating conditions for improving kafirin purification process in LSCFB, and also to provide insights on the interaction between the different decision variables of the system.

6.2 FORMULATION OF MULTIOBJECTIVE PROBLEMS

The MOO problem is solved for the experimentally validated LSCFB model for continuous kafirin purification. In Chapter 5, the effects of different operating conditions on the LSCFB are evaluated for anion exchanger UNOsphere Q on basis of kafirin production rate, P , and fraction of kafirin recovered, R . Results of these sensitivity studies shown that each of these operating parameters affected the ion-

exchange LSCFB differently, and that there exist a set of optimal process conditions. This study is a continuation of the Chapter 5, and is focused on the maximisation of P (Eq. 6.1) and R (Eq. 6.2) for two-objective optimisation.

$$\begin{aligned} & \text{Maximise protein production rate, } P \\ & = \text{Extract flowrate} \times \text{Kafirin concentration in extract} = U_{lr} A_r c_{er} \end{aligned} \quad (6.1)$$

$$\begin{aligned} & \text{Maximise overall protein recovery, } R \\ & = \text{Protein production rate} / \text{Kafirin loading rate} = U_{lr} A_r c_{er} / U_{ld} A_d c_{od} \end{aligned} \quad (6.2)$$

For optimising the performance of the LSCFB model for continuous purification of kafirin, five process decision variables are available. These and their bounds are as listed in Eqs. 6.3 to 6.7, as followed.

$$0.6 \text{ kg/m}^2\text{s} \leq G_s \leq 1.5 \text{ kg/m}^2\text{s} \quad (6.3)$$

$$0.40 \text{ mm/s} \leq U_{ld} \leq 0.94 \text{ mm/s} \quad (6.4)$$

$$5.0 \text{ mm/s} \leq U_{lr} \leq 11.0 \text{ mm/s} \quad (6.5)$$

$$0.5 \text{ kg/m}^3 \leq c_{od} \leq 2.0 \text{ kg/m}^3 \quad (6.6)$$

$$0.4 \text{ m} \leq h_{d,eff} \leq 1.0 \text{ m} \quad (6.7)$$

The lower and upper bounds of these decision variables are selected based on the feasibility of parameters in the mass transfer equations as well as experimental stability of the LSCFB system as reported by Lan et al. (2000, 858; 2001, 157; 2002b, 252). Solids circulation rate, G_s is the mass flow rate of the ion-exchange particles circulating between the downer and riser. G_s is an important parameter as kafirin desorption decreased with the increase in G_s because the relatively slow desorption rate in the riser led to longer residence time required for the solid particles for efficient elution of the adsorbed kafirin into the extracting buffer. From the sensitivity analysis in Chapter 5, it is revealed that G_s is a non-conflicting operation parameter. Both production rate and fractional recovery decreased with the increase in G_s . Therefore, the lower the G_s value, the better the performance of the LSCFB would be. Nevertheless, the influence of G_s on the solids holdups in the distributor and upper dilute regions of riser restricted the minimum value to be used. The lower bound of the G_s is chosen to ensure sufficient voidage in all regions of the riser. The liquid velocity in the downer, U_{ld} directly affected the feed residence time in downer, and hence the feed loading rate to the LSCFB. U_{ld} also influenced the downer solids

holdup, ε_{sd} , thus changed the kafirin mass balance in downer. From sensitivity study, increased production rate and fractional recovery resulted with the increase in U_{ld} . However, the increase in fractional recovery almost reached a plateau at higher value of U_{ld} , despite the consistent increase in P . More kafirin is carried over to the riser at higher kafirin loading rate, thus the increased P . Nonetheless, the increase in U_{ld} , without being balanced by G_s , caused more kafirin remained unadsorbed and therefore the R has reached a plateau as U_{ld} increased to certain boundary. The lower bound of U_{ld} is chosen to achieve sufficient voidage in the downer dense phase region. The upper bound of U_{ld} is limited by the ion-exchange particles terminal settling velocity, U_t at 3.00 mm/s as the downer operated in conventional fluidisation region. It should be emphasised that the U_{ld} should be in such a magnitude to maintain a freeboard region above the dense phase region to prevent the loss of ion-exchange particles through the raffinate outlet.

The liquid velocity in riser, U_{lr} affected the LSCFB performance by altering the residence time of extracting buffer in the fluidised bed, the solids holdup in the riser distributor region, ε_{sr1} and the upper dilute region, ε_{sr2} . For a given G_s the U_{lr} also controlled the flowrate of extracting buffer in riser and thus the riser mass balance. The U_{lr} is learnt to be a non-conflicting parameter. Both the production rate and fractional recovery decreased with the increase in U_{lr} . Thus, the lower the U_{lr} value, the better the performance of the LSCFB would be. It is critical that U_r is kept above the U_t so the G_s became independent of the liquid velocity. An operating hydrodynamic region known as the fully developed circulating fluidisation region is thus attained in the riser (Lan et al. (2002, 252). The upper bound of the U_{lr} is chosen as such to provide sufficient voidage in the riser. The kafirin concentration in feed, c_{od} is kept at lower range as the protein content in biological broth is usually very low. The bounds of the downer dense region height, $h_{d,eff}$ are chosen considering the height of the downer up to the top return pipe and the extent of the dilute phase in the downer bed.

The aim is to gain a set of equally good solutions, i.e., a set of Pareto optimal solutions. This captured the trade-off between the objective functions over a broad range of non-dominated solutions, in which none of the objective function values could be raised without degrading some of the other objective values. Two-objective

functions optimisation problem is formulated and solved to locate the optimal LSCFB system operating conditions. Through narrowing down the choices, the Pareto set offered a useful guidance in deciding the best solution, amongst the set of Pareto optimal solutions, rather than from an extensive number of possibilities. Other than that, the MOO is useful in providing useful insights on the interaction between the different decision variables of the system. The MOO procedure used in this work is generic and can find application in either designing or revamping of LSCFB systems.

6.3 ELITIST NON-DOMINATED SORTING GENETIC ALGORITHM SOLVER

All decision variables selected in Section 6.2 affected the LSCFB performance in different manners. For example, production rate and fractional recovery decreased with the increase in G_s and U_{lr} , whereas the increase in fractional recovery reached a plateau at higher value of U_{ld} and production rate increased consistently with U_{ld} . With these decision variables influencing the LSCFB differently, it can be expected that the system to have discontinuous, or non-smooth performance for the production rate and overall recovery. Traditional derivative-based optimisation methods are designed to solve smooth problems as they use derivatives to determine the direction of descent. But, these often are not effective when problems lack smoothness, such as problems with discontinuous objective functions. When faced with solving non-smooth problems, like the LSCFB system in our study, the genetic algorithm (GA) is an effective alternative. The LSCFB model is coupled with the multiobjective GA solver GAMULTIOBJ of MATLAB® to solve the problem formulated with two-objective functions described in Section 6.2. The GAMULTIOBJ solver uses a controlled elitist genetic algorithm, a variant of the elitist non-dominated sorting genetic algorithm (NSGA-II) to solve non-smooth MOO problems (Deb et al. 2002, 182). The main difference between the controlled elitist GA and GA is that it sorts individuals, in this context these are the candidate solutions, according to their level of non-domination, so that the non-dominated individuals are always sorted above dominated individuals, and elite individuals are therefore selected automatically. In GA, non-domination refers to an individual being better in at least one objective than the other individual (Mazumder et al. 2009b, 873). The non-dominating sorting is

Table 6.1 Parameters used in elitist non-dominated sorting genetic algorithm solver and their values.

NSGA-II parameter	Value	
Population options	Double vector	Population type
	50	Population size
	Uniform	Creation function
Selection options	Stochastic uniform	Selection function
Reproduction options	0.7	Crossover fraction
Mutation options	Adaptive feasible	Mutation function
Migration options	Forward	Migration direction
	20	Migration interval
	0.2	Migration fraction
Multiobjective options	Distance crowding	Distance measure function
	0.35	Pareto fraction
Stopping criteria options	50	Generations

done by assigning non-dominance ranks to each individual in the population. Higher ranking individuals are chosen such that they dominate over the remaining individuals of the population but do not dominate one another. Individuals belonging to inferior rank are chosen such that they do not dominate individuals ranked higher than them, but dominate the others. This ranking process is continued until all individuals in the population are exhausted. For diversity, the elitist GA adapts multiobjective parameters called the distance measure function and Pareto fraction (MathWork 2013; Deb et al. 2002, 182). The distance function assigns a distance measure to each individual with respect to its neighbours. As will be clear later in the next section, the further the individual on the front, the better its chances are to be selected into the next generation. The other parameter, the Pareto fraction is a number between 0 and 1 that specifies the fraction of the population on the best Pareto frontier to be kept during the MOO.

6.3.1 Input Parameters

All input parameters to the elitist GA performed onto the LSCFB model are listed in Table 6.1 (MathWorks 2013). Parameters of the population such as the population type, population size, creation function, and initial population are specified to generate the initial population randomly at the onset of MOO simulation. The

population type is set to double vector for the MOO problems. 50 individuals are generated in each generation, instead of a smaller population size in order to obtain global optimum instead of local optimum values. The same number of individuals is used in the MOO study of an industrial styrene reactor with the results covered extensive range of optimal operating conditions (Yee, Ray and Rangaiah 2003, 111). A random initial population of 50 with a uniform distribution is then created with the default bounds shifted and scaled to match the existing upper and lower bounds of the decision variables. The selection function elects individuals to be parents. The default selection stochastic uniform is applied. The reproduction parameters control the mechanism to create the next generation. Specifically, a crossover fraction of 0.7 is specified to create fraction of individuals in the next generation that are made up of crossover, while the rest generated by mutation. Mutations are applied to create small random changes in individuals in the existing population to create mutation children. It provided genetic algorithm and increased possibility of obtaining global optimal. The adaptive feasible mutation function is specified to randomly generate directions adaptive to the previous successful or unsuccessful generations.

Crossover parameters are important GA operator that has the basic function of forming a crossover child in a reproduction process (MathWorks 2013). Intermediate crossover function is selected to create children by taking a weighted average of the parents. Migration parameters gave the movement of individuals between subpopulations, a form of parallel processing for the GA. In subpopulations, each worker hosted a number of individuals. These individuals are a subpopulation. The worker evolved the subpopulation independent of other workers, with the exception when migration caused some individuals to travel between the workers. Migration took place toward the last subpopulation, and wrapped at the subpopulation ends. For an interval of 20, migration took place every 20 generations. Besides, the fraction of individuals migrating between subpopulations is determined at 0.20, so the product of the migration fraction and the number of individuals of the smaller of the two subpopulations would migrate into denser subpopulation. Finally, the optimisation criterion of 50 generations is specified. The optimisation criteria are referred to as stopping criteria in the GA algorithm.

6.3.2 Flow Diagram

Figure 6.1 is a flow diagram for the NSGA-II through which the model of LSCFB from previous chapter and the elitist GA solver operated to find an optimal solution. The MOO process began with specifying the input parameters in the GA solver, shown in Table 6.1. Following this, a random set of parent population with 50 individuals is generated without violating the upper and lower bounds in the decision variable space (Eqs. 6.3 to 6.7). All the individuals are analysed by the LSCFB model. The estimated kafirin concentration profiles from the downer and riser are computed by the LSCFB model. The kafirin production rate, P (Eq. 6.1) and fraction of kafirin recovered, R (Eq. 6.2) values are returned to the GA solver. The population is then sorted into different non-domination ranks based on their objective function values. Once the ranks are assigned, the population underwent the GA processes of selection, crossover and mutation to generate the child population. These processes are similar to GA except that the selection is performed using the ranks instead of their scaled objective fitness values (Deb et al. 2002, 182; Mittal 2010, 26).

Following mutation, the elitist GA differed from traditional GA by the invocation of elitism to choose the new population of individuals out of the parents and their mutated children. For elitism, the elitist GA took the parent and the child population and combined them into a single population with the total size of the child and parent population. The new population is then sorted into different non-domination ranks, following this; new individuals out of the combined population are selected. First all individuals belonging to higher rank are chosen followed by individuals from slightly inferior rank, and this continued until a stage is reached where all members belonging to the given rank could not be accommodated to fill up the rest of the remaining slots. To fill up the remaining of the individuals of the given rank, they are chosen in descending order of their distance measure function values. Thus, the individuals that are further away at the front are first selected and so on until all the slots are completely filled up. These are limited by the Pareto fraction set at the elitist GA onset. Gaining a new set of population out of the combined population via elitism is called the advancement of the population from one generation to the next. Once the new generation is created, it again went through the selection, crossover, mutation and elitism processes, and these repeated until a pre-defined stopping criterion, namely the number of generation, is reached. Note that the non-dominated

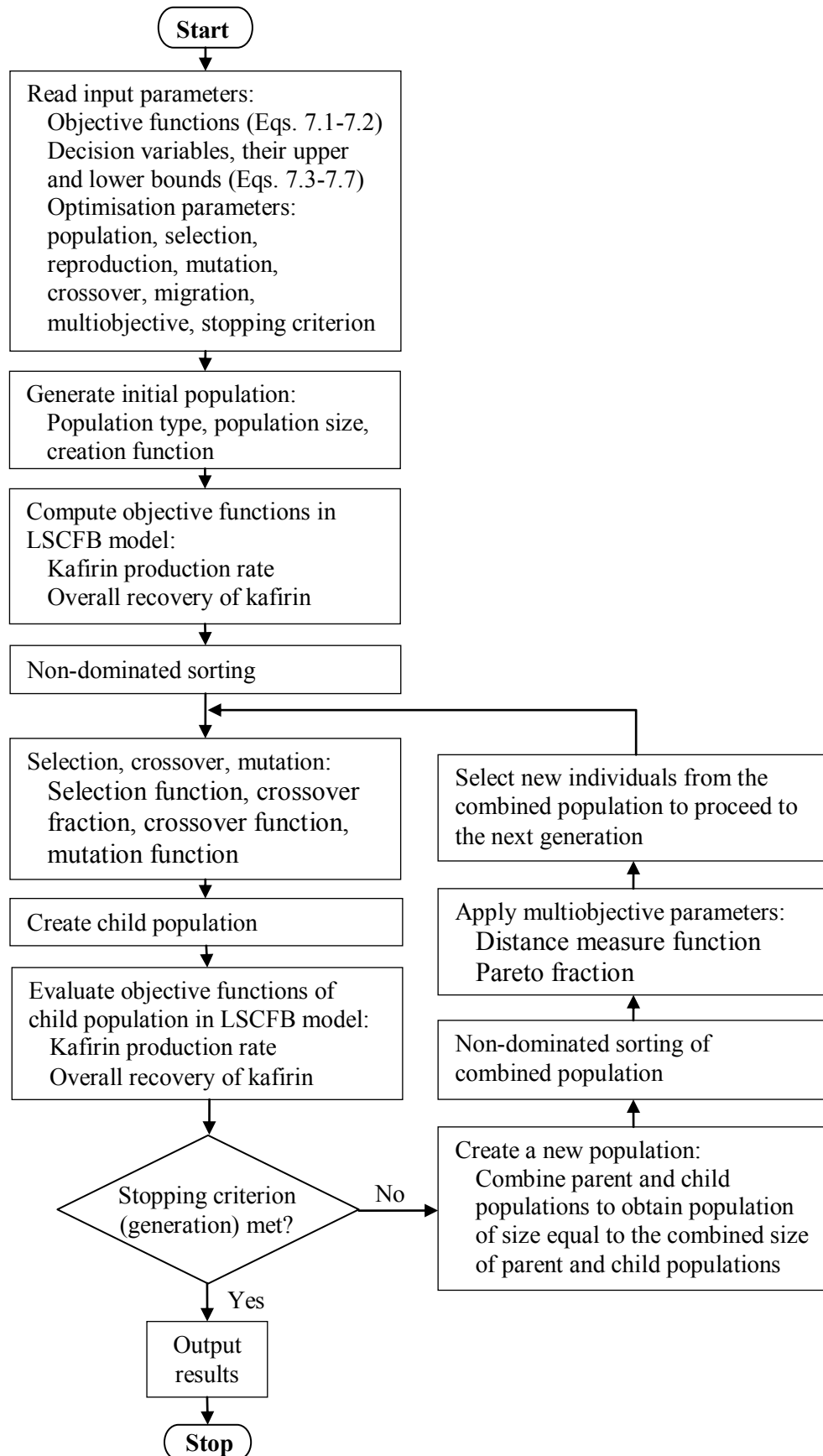


Figure 6.1 Flowchart explaining the multiobjective optimisation process by elitist non-dominated sorting genetic algorithm solver.

Table 6.2 Decision variables and objective functions for point *A* to *C* in the Pareto-optimal frontier plot.

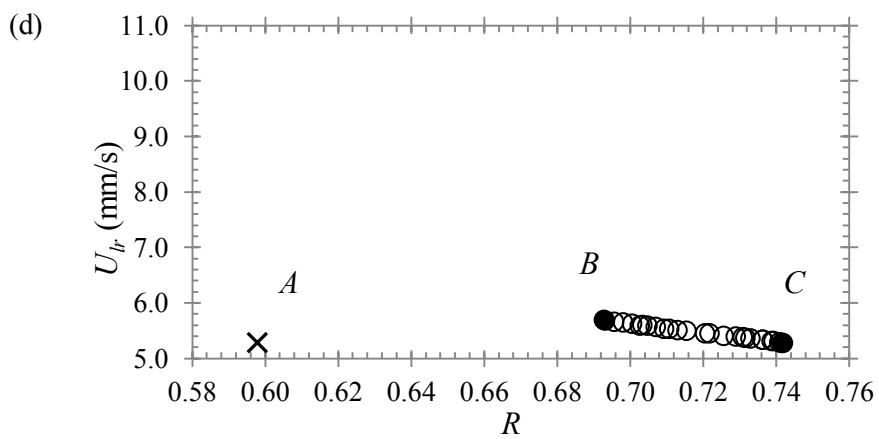
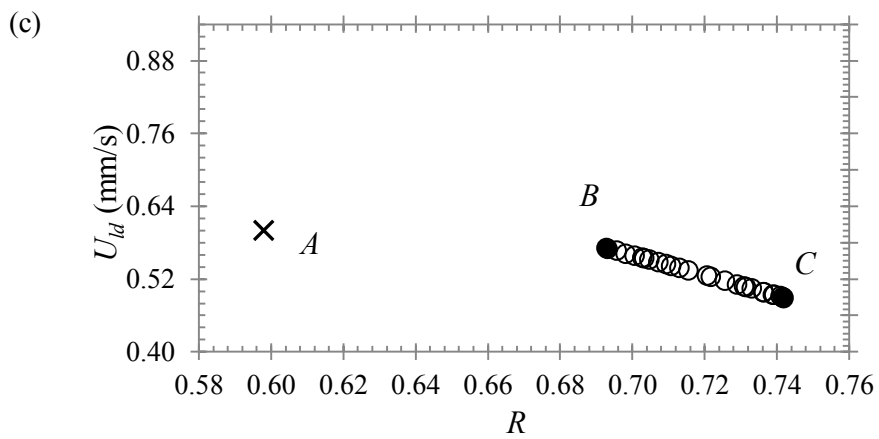
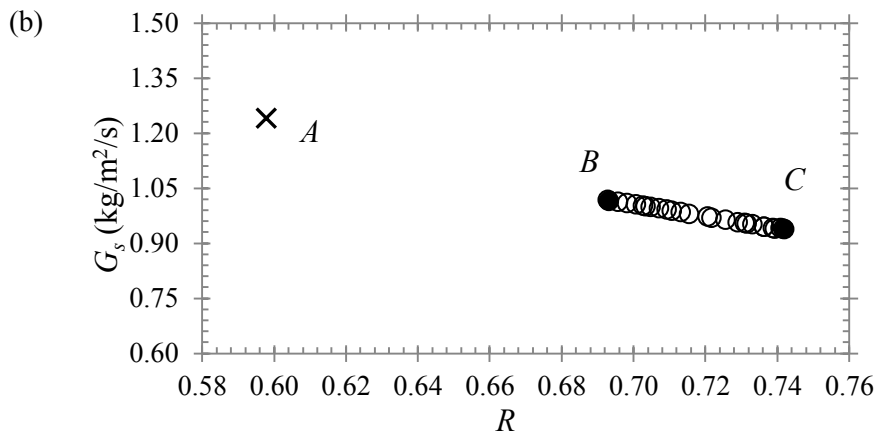
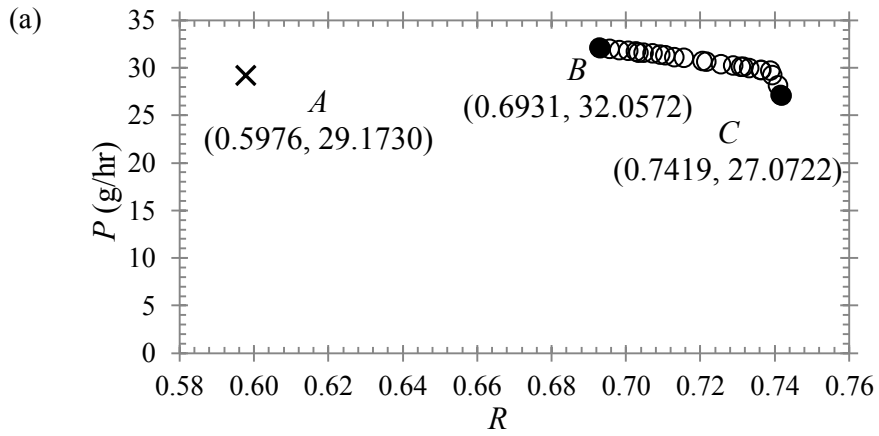
Optimal solution	Point <i>C</i>	Point <i>B</i>	Point <i>A</i>
Protein production rate, P (g/hr)	27.0722	32.0572	29.173
Protein overall recovery, R	0.7419	0.6931	0.5976
Solids inventory required, S (kg)	2.4857	2.3616	2.0189
Solids circulation rate, G_s (kg/m ² /s)	0.9379	1.0155	1.24
Downer superficial liquid velocity, U_{ld} (mm/s)	0.489	0.5698	0.6
Riser superficial liquid velocity, U_{lr} (mm/s)	5.2766	5.6847	5.28
Feed concentration, c_{od} (kg/m ³)	1.8329	1.9937	2
Downer effective bed height, $h_{d,eff}$ (m)	0.9414	0.9892	0.8

sorting and assigning ranks to each individual and computing the distance function as well as the fraction of population at the best Pareto frontier are primary mechanisms that NSGA-II controlled in the estimation of the Pareto-optimal set of solutions. The non-dominated sorting ensured that the best set of solutions is spread through the generations, and at the same time, the distance function attempted to maintain diversity within these solutions so that a premature convergence is avoided.

6.4 RESULTS AND DISCUSSION

In this section, optimisation results of the LSCFB system for continuous kafirin purification are presented and discussed. The objective functions and the associated decision variables are plotted, and compared with the corresponding base case values previously computed in Chapter 5. Figure 6.2(a) shows the Pareto-optimal set obtained for simultaneous maximisation of the kafirin production rate, P and overall fraction of kafirin recovery, R . Table 6.2 reports the values of the decision variables and the two objective functions for the base case solution, point *A* and two extreme points of the non-dominated solutions, point *B* (at maximum production rate) and point *C* (at maximum fractional recovery). Shifting from left to right from point *B* to point *C* in Figure 6.2(a) shows conflicting behaviour between R and P , in which fractional recovery increased at the cost of reduced production rate.

Figure 6.2(a), thus, represents a set of non-dominated solutions, with equally good points in which the preferred LSCFB operating point would have to be decided



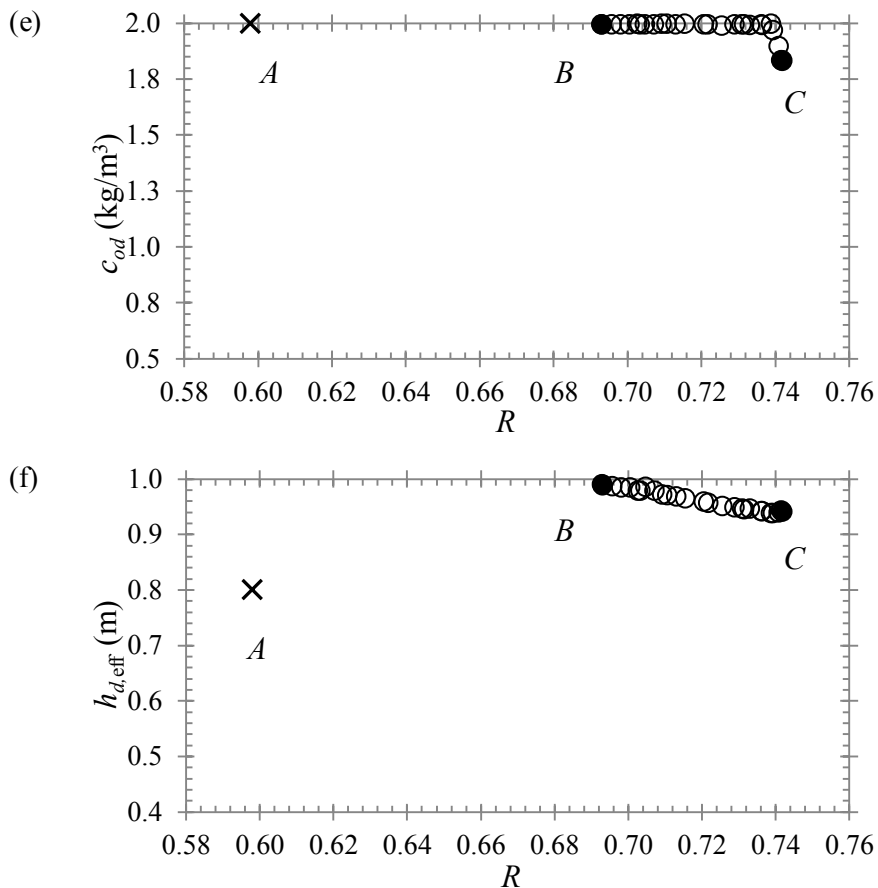


Figure 6.2 Results for maximisation of P and R . (a) Set of Pareto-optimal solutions, (b-f) Values of decision variables corresponding to the Pareto-optimal solutions shown in (a). Symbol \times indicates base case operating point.

by the process designer from among these points. The maximum possible production rate is around 32 g/hr while the maximum possible overall recovery is about 0.74; however, both did not occurred simultaneously. Each point on the Pareto-optimal frontier plot corresponds to a set of decision variables, which are plotted in Figure 6.2(b-f) against the overall recovery. The maximum and minimum values of the vertical axis in these figures are associated to the boundaries of the respective decision variables. It is noteworthy to mention that the MOO results presented in this study differed from the sensitivity analysis carried out earlier in Chapter 5. The latter predicted the effect of one parameter at a time in a steady-state LSCFB setup. Nevertheless, it has not described the interaction between the system parameters, an aspect which is critical because in a real-life situation there would be unforeseeable changes in multiple operating parameters. So this study is meant to illustrate the interaction of these parameters in their corresponding ranges of operability.

It is clear from Figure 6.2(b) that as the solids circulation rate, G_s , decreased from point B to C , the overall recovery of kafirin improved but with a reduced production rate. This is because of the effects of G_s which adsorbed and hence eluted more kafirin at higher G_s , but on the other hand the reduced solids residence time in riser has reduced the extent of kafirin desorption for a given amount of kafirin loading rate hence the decline overall recovery. As G_s shifted from point B to C , the superficial liquid velocity in downer, U_{ld} also reduced accordingly as depicted in Figure 6.2(c). The U_{ld} is known to have an effect on the feed loading rate into the LSCFB as well as the residence time of the feed liquor in downer. As the system shifted from point B and moved towards point C , the U_{ld} has decreased to prevent more kafirin loss into the raffinate due to the limited adsorption capability of the ion exchange particles at lower G_s values. Figure 6.2(d) illustrates the superficial liquid velocity in the riser, U_{lr} of points in the Pareto-optimal frontier. As G_s and U_{ld} operated at higher values, point B in particular, it is anticipated that more kafirin is being carried over into the riser for elution. To achieve maximum possible production rate and recovery, the riser desorption capacity must be increased. This is achievable via increasing the extracting buffer flowrate, i.e. the superficial liquid velocity in the riser, U_{lr} . As the system shifted from point B towards point C , lesser kafirin is being adsorbed and hence carried over into the riser. Therefore the U_{lr} is adjusted to a lower operating point. Similarly as the decision variables discussed earlier changed their operating ranges, the initial feed concentration, c_{od} into the LSCFB has to be adjusted as shown in Figure 6.2(e).

When operated at point B with comparatively higher kafirin mass transfer capabilities in the riser and downer, the system is capable of recovering as much kafirin as possible. Nevertheless as the system switched to point C , the other extreme operating point, the system adsorption and desorption capabilities is reduced. Smaller c_{od} is thus required to cope with the reduced desorption capacity of the riser. Though this might have reduced the production rate, smaller c_{od} is needed as the reduced desorption capacity would lead to reduced adsorption capacity in the downer. So to minimise the kafirin lost into the raffinate, smaller c_{od} is used. Similar trend is observable for the effective height of downer, $h_{d,eff}$ in Figure 6.2(f). This variable is responsible in providing for adsorption in the downer, where higher $h_{d,eff}$ meant greater length for adsorption and longer residence time for liquid and solid phases. It

Table 6.3 Process conditions for base case steady-state simulation runs.

	Value
Solids circulation rate, G_s (kg/m ² /s)	1.24
Downer superficial liquid velocity, U_{ld} (mm/s)	0.6
Riser superficial liquid velocity, U_{lr} (mm/s)	5.28
Feed concentration, c_{od} (kg/m ³)	2
Effective height in downer, $h_{d,eff}$ (m)	0.8

It is found that higher $h_{d,eff}$ is needed when the LSCFB operated at point *B*, but reduced to accommodate the operation changes at point *C*. This is due to the greater adsorption capacity required at the former operating condition where more kafirin is loaded into the LSCFB.

Figure 6.2(a-f) also shows the current operating point at point *A* at base case conditions, as reported in Table 6.3. All the points on the Pareto frontier in Figure 6.2(a) are much better than the current operating point. Also, to see the amount of solids inventory required, S corresponding to the Pareto frontier plot, the production rate and overall recovery are plotted against the calculated values of S in Figure 6.3. To operate the LSCFB at its maximum production rate at 32.06 g/hr (point *B*), a feed of 46.25 g/hr is required. Taking the base case as the calculation basis, this indicates an increase of 5.33% feeding rate to the downer to achieve 9.90% increase in production and 15.90% decrease in recovery. Comparing to the base case, higher solid inventory is required, meaning increased capital cost with a slightly reduced pumping cost of the auxiliary stream to achieve the desirable G_s , feed and extract. On the other hand, for the LSCFB to operate at its maximum recovery (point *C*) means a decrease of 25.31% in feed loading requirement, and increase of 24.07% recovery. A total of 7.19% decrease in production is also resulted though. With this set of operating condition, a great reduction in the pumping cost can be achieved through the reduced auxiliary flowrate, feed loading rate, and extracting buffer flowrate. Considering all these factors, it can be understood that the selection of a operating cost, which depends on the site and time. Therefore the more important objective function between the production rate and overall recovery depends on these factors. Nevertheless Figure 6.2(a-f) provides a wide range of competing options for the improvement over the base case operating conditions of the LSCFB.

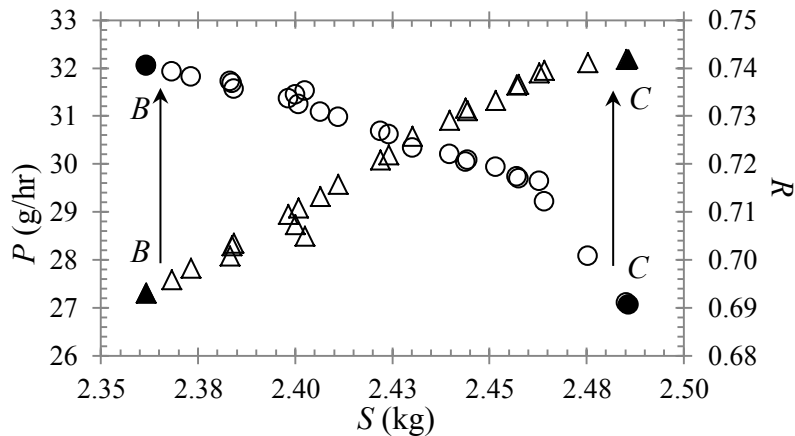


Figure 6.3 Calculated amount of the solids inventory required corresponding to the Pareto-optimal solutions for maximisation of kafirin production rate and overall recovery. Kafirin production rate (o) and recovery (Δ) against amount of the solids required.

6.5 CONCLUSION

MOO studies of the LSCFB model for continuous kafirin purification are performed using an adaptation of the NSGA-II. The validated LSCFB model from Chapter 5 is implemented in this study. The MOO involved five decision variables and the upper and lower bounds of these decision variables are selected based on the model stability and sensitivity. A two-objective function optimisation is carried out using the most important objectives in kafirin purification process, i.e. production rate and fractional recovery, which are contradictory in the sense that the optimal of these two could not occurred simultaneously. From the decision variables values, the interaction between the decision variables are explained, and the complex nature of the LSCFB is revealed. This is because of the non-smooth nature of the objective functions in which changing one decision variable will alter the value of the other variables to arrive at the maximum achievable production rate or overall recovery. One point corresponding for maximum production rate but minimal recovery, and another at minimum production rate but maximum recovery from the Pareto frontier are also selected for detailed analysis. It is shown that operating at the former will induce extra capital and material cost but achieving better production rate, while the latter will reduce in terms of material and operating cost and higher recovery but at a lower production rate. The optimal operating point of the LSCFB depends on these factors, which are location and site specific. Therefore, one must choose carefully in order to draw the optimal performance out of the system.

CHAPTER 7

CONCLUSIONS AND RECOMMENDATION

7.1 CONCLUSIONS

The concepts of LSCFB system is introduced for the recovery sorghum protein kafirin using viable protein extraction and purification process scheme. Specifically phenomenological modeling and optimisation methods are applied to develop and optimise the purification process on LSCFB. The LSCFB protein purification system is described while a phenomenological model based on compartmental framework is developed, and validated with the experimental results reported for a model protein extraction in the literature. Both isotherm and kinetic studies of kafirin adsorption are carried out on anion and cation exchangers for practical applications in preparative-scale chromatography. These serve as the substance for selection of ion exchanger to use in kafirin purification. This is followed by simulation of the previously validated phenomenological model to predict the performance of kafirin purification in LSCFB under different flow configurations and operating conditions of critical parameters in the LSCFB. Finally, maximisation of both production rate and fractional recovery of the kafirin are carried out by manipulating critical decision variables that affected the LSCFB performance most significantly. The sections below gives conclusions from each individual chapters in the thesis.

7.1.1 Liquid-Solid Circulating Fluidised Bed System: Description and Modeling

An LSCFB ion-exchange system, is basically consists of a pair of fluidised beds, liquid-solids separator, washing section below the separator, top solids return pipe between the separator and the downer, washing section below the downer, and bottom solids return pipe between the riser and the downer at the bottom, equipped with ion-exchange particles. The most significant advantages associated with the LSCFB system include the following:

- capability of operating with small ion-exchange particles for better utilization of particle surface area hence high effectiveness factors, increased contact efficiency between particle surface area and solvent due to increased phase-slip.

- ability to withdraw and input ion-exchange particles continuously
- high velocities operations give higher product throughput and rapid mass transport between different phases.
- has been rapidly applied in adsorption based chromatographic processes recently.

A general purpose, extensible and dynamic theoretical model based upon a tanks-in-series framework incorporating the equilibrium and hydrodynamics of liquids and ion-exchange particles has been developed for LSCFB continuous protein recovery system. The model is used to simulate the recovery of BSA from feed solution onto surface of Diaion HPA25 particles. The model is developed based on simplification assumptions such as diffusion mass transfer and first-order reaction kinetic for protein adsorption and desorption, respectively. The design equations are derived from practical guidelines for the design of an LSCFB system.

The simulated results compare well with the experimental results obtained from a laboratory-scale BSA recovery in LSCFB with 84% recovery at a throughput of 21.5 g/hr. Systematic study of the effects of key operating parameters such as the downer liquid velocity, riser operating velocity, solids circulation rate and feed concentration is performed. The analysis revealed that both the BSA production rate and recovery increase with increasing solids circulation rate, while both decrease with increasing superficial liquid velocity in the riser. With the increase in superficial liquid velocity in the downer and feed BSA concentration, the rate of BSA production increases, but the overall recovery decreases.

7.1.2 Kafirin Adsorption Chromatography: Isotherm and Kinetic Analysis

Mass transfer parameters in the first-principle model are essential for designing and upscale of kafirin adsorptive chromatography systems. Kafirin binding and mass transfer on ion exchangers with different pore structure and surface chemistry is investigated. Differences in particle chemistry, its hydrodynamic design and surface charge of kafirin with respect to the environment in batch equilibrium experiments and uptake kinetic experiments are found to contribute significantly to the kafirin adsorption behavior onto the surface of ion-exchange particles. Five basic anion-exchangers and two acidic cation-exchangers are studied.

Data-fitting with Langmuir adsorption isotherm model gave high coefficients of determination for all ion exchangers. The fitted dissociation coefficients have values between 10^{-8} M and 10^{-2} M, indicating reversible binding between kafirin molecules and ligands on the ion-exchange particle surface suitable kafirin desorption without denaturation. Of all the ion exchangers investigated, UNOsphere Q and Toyopearl SuperQ-650M showed highest adsorption efficiency. The film-pore diffusion model described the batch uptake experimental results well. Effects film mass transfer are significant on kafirin uptake rates for UNOsphere Q and Toyopearl SuperQ-650M. Fitted values of both pore diffusivity and film resistance agree well with literature data.

7.1.3 Liquid-Solid Circulating Fluidised Bed System: Modeling Continuous Kafirin Purification

First-principle model of the LSCFB continuous ion-exchange system previously validated with BSA recovery data is modified to model kafirin purification system. Simplification assumptions are made about the system mass transfer, for instance, the Langmuir isotherm model for equilibrium relationship of liquid-solid interaction, the lumped mass transfer coefficient accounted for intraparticle diffusion and dispersion effect for kafirin adsorption, and second-order reaction kinetic for kafirin desorption. Five ion exchangers are compared for their performances in LSCFB. It is observed that the mass transfer parameters affect the extents of adsorption and desorption of kafirin much. The most efficient ion exchanger in recovery of kafirin is Toyopearl QAE-550C. Nevertheless further analysis is carried out on an average performing ion exchanger, i.e. UNOsphere Q, for judicious overview of ion exchanger performance in the system. In unsteady state simulations, the dynamics of the LSCFB continuous kafirin purification system is observed to achieve a pseudo steady-state condition after approximately 4 operational hours.

Liquid-solid flow configurations in the LSCFB ion-exchange system with and without backmixing are examined. Solid backmixing with respect to the liquid phase in the downer gives better performance. In the riser, however, the well-mixed liquid-solid flow with no backmixing effect in riser distributor and upper dilute regions are the most efficient in recovery kafirin. Effects of critical operating parameters namely, solid circulation rate, riser and downer liquid velocities, and initial kafirin feed

concentration are assessed. Both kafirin production rate and fractional recovery of the system deteriorate with increase in solids circulation rate and riser liquid velocity, while both increase with increase in initial kafirin concentration in feed and downer liquid velocity.

7.1.4 Liquid-Solid Circulating Fluidised Bed System: Multiobjective Optimisation for Continuous Kafirin Purification

Sensitivity analysis revealed that some parameters affect the system performance in conflicting and different manners. To solve the non-smooth system performance problem, the MOO studies on the first-principle model for LSCFB ion-exchange system for kafirin purification are carried out using an adaptation of the NSGA-II. Five process decision variables are included, while the upper bound and lower bound values are selected on basis of the model stability and sensitivity. A two-objective function optimisation is carried out using the two most important objectives, i.e., maximisation of kafirin production rate and maximisation of kafirin fractional recovery, These are contradictory in the sense that the optimal of these two could not occurred simultaneously.

Interaction between the decision variables are explained from the values of the decision variables. In other words, changing one decision variable will alter the value of the other variable to arrive at the maximum production rate or fractional recovery due to the non-smooth nature of the objective functions. Different points indicative of the system performance are highlighted on the Pareto frontier for detailed analysis. A point produces maximum production rate but minimum recovery at the expense of additional capital and material costs. Another point gives minimum production rate but maximum recovery saves material and operational costs but at the expense of the process production rate. Operational points of the LSCFB continuous ion-exchange system subject to the interaction between decision variables. One must thus choose operating points carefully to draw the optimal performance out of the system.

7.2 RECOMMENDATIONS FOR FUTURE WORK

This study provides comprehensive systematic understanding on the concepts of recovering sorghum protein using viable protein extraction and purification process scheme on LSCFB system. In particular, model development, mass transfer and

kinetics, model adaptation, followed by sensitivity studies and optimisation are performed. Nevertheless, there are still some areas where further research is needed.

The LSCFB system modelled is rated on three major performance parameters, namely the production rate, overall recovery, and solids inventory requirement. With the currently available simulation data of the downer and riser concentration profiles, the purity of the kafirin produced could be included into the sensitivity and optimisation studies. Other than that, this study validated the model by the literature data on BSA recovery. It would be recommended to conduct kafirin purification on a LSCFB in the laboratory to obtain the profiles in the fluidised beds in order to examine the credibility of the model. Finally, the study only focused on the macro scale modeling of the LSCFB. To examine the effects of hydrodynamics parameters, it would be useful to perform a computational fluid dynamic simulation and incorporate the result into the phenomenological model of LSCFB.

REFERENCES

- Ahmed, H. 1959. *Principles and Reactions of Protein Extraction, Purification, and Characterization*. Boca Raton, Florida: CRC Press.
- Andersson, J., and B. Mattiasson. 2006. "Simulated Moving Bed Technology with A Simplified Approach for Protein Purification: Separation of Lactoperoxidase and Lactoferrin from Whey Protein Concentration." *J. Chromatogr. A*. 1107(1-2): 88-95.
- Anspach, F.B., D. Curbelo, R. Hartmann, G. Garke, and W.-D. Deckwer. 1999. "Expanded-Bed Chromatography in Primary Protein Purification." *J. Chromatogr. A*. 865(1-2): 129-144.
- Anyango, J.O., H.L. de Kock, and J.R.N. Taylor. 2011. "Evaluation of the Functional Quality of Cowpea-Fortified Traditional African Sorghum Foods using Instrumental and Descriptive Sensory Analysis." *LWT-Food Sci. Technol.* 44(10): 2126-2133.
- Balt, B.C., V.M. Yabannavar, and V. Singh. 1995. "Expanded Bed Adsorption Process for Protein Recovery from Whole Mammalian Cell Culture Broth." *Bioseparation* 5(1): 41-52.
- Barnfield Frej, A.-K., R. Hjorth, and A. Hammarstrom. 1994. "Pilot Scale Recovery of Recombinant Annexin V from Unclarified Escherichia coli Homogenate Using Expanded Bed Adsorption." *Biotechnol. Bioeng.* 44(8): 922-929.
- Bayramođlu, G., G. Ekici, N. Besirli, and M.Y. Arica. 2007. "Preparation of Ion-Exchange Beads Based on Poly(Methacrylic Acid) Brush Grafted Chitosan Beads: Isolation of Lysozyme From Egg White in Batch System." *Colloid Surface A* 310(1-3): 68-77.
- Bean, S.R., B.P. Ioerger, S.H. Park, and H. Singh. 2006. "Interaction between Sorghum Extraction and Precipitation Conditions on Yield, Purity, and Composition of Purified Protein Fractions." *Cereal Chem.* 83(1): 99-107.
- Beck, R.E. and J.S. Schultz. 1972. "Hindrance of Solute Diffusion within Membranes as Measured with Microporous Membranes of Known Pore Geometry." *BBA-Biomembranes* 255(1): 273-303.
- Begovich, J.M. and W.G. Sisson. 1981. "Continuous Ion Exchange Separation of Zirconium and Hafnium." In *American Institute of Mining, Metallurgical and*

- Petroleum Engineers Annual Meeting, Hydrometallurgy-Chemical Processing Committee held in Chicago, Illinois, 22-26 February 1981.* 1-14.
- Begovich, J.M. and W.G. Sisson. 1983. "Continuous Ion Exchange Separation of Zirconium and Hafnium using An Annular Chromatograph." *Hydrometallurgy* 10(1): 11-20.
- Belton, P.S., I. Delgadillo, N.G. Halford, and P.R. Shewry. 2006. "Kafirin Structure and Functionality." *J. Cereal Sci.* 44(4): 272-286.
- Bermejo, R., E. Ruiz, and F.G. Acien. 2007. "Recovery of B-phycoerythrin Using Expanded Bed Adsorption Chromatography: Scale-Up of the Process." *Enzyme Microb. Tech.* 40(4): 927-933.
- Bio-Rad. 2014. *UNOsphere Q Anion Exchange Support Product Information Sheet, Rev. D.* Gladesville, N.S.W.: Bio-Rad Laboratories.
- Blehaut, J. and R.-M. Nicoud. 1998. "Recent Aspects in Simulated Moving Bed." *Analysis* 26(7): 60-70.
- Bloomington, G.F., J.S. Bauer, G. Carta, and C.H. Byers. 1991. "Continuous Separation of Proteins by Annular Chromatography." *Ind. Eng. Chem. Res.* 30(5): 1061-1067.
- Boardman, N.K. and S.M. Partridge. 1955. "Separation of Neutral Proteins in Ion-Exchange Resins." *Biochem. J.* 59(4): 543-552.
- Bonnerjea, J., J. Jackson, M. Hoare, and P. Dunnill. 1988. "Affinity Flocculation of Yeast Cell Debris by Carbohydrate-Specific Compounds." *Enzyme Microb. Technol.* 10(6): 357-360.
- Boyer, P.M. and J.T. Hsu. 1990 "Adsorption Equilibrium of Proteins on A Dye-Ligand Adsorbent." *Biotech. Tech.* 4(1): 61-66.
- Broughton, D.B. 1968. "Molex: Case History of a Process." *Chem. Eng. Progr.* 64(8): 60-65.
- Broughton, D.B. 1984. "Production-Scale Adsorptive Separations of Liquid Mixtures by Simulated Moving-Bed Technology." *Sep. Sci. Technol.* 19(11-12): 723-736.
- Bruce, L.J. and H.A. Chase. 2002. "The Combined Use of In-Bed Monitoring and an Adsorption Model to Anticipate Breakthrough during Expanded Bed Adsorption." *Chem. Eng. Sci.* 57(15): 3085-3093.
- Buchacher, A., G. Iberer, A. Jungbauer, H. Schwinn, and D. Josic. 2001. "Continuous Removal of Protein Aggregates by Annular Chromatography." *Biotechnol. Prog.* 17(1): 140-149.

- Buchner, S. 2006. "Coating of Pears (Var. 'Packhams Triumph') with Kafirin Protein and its Effect on Postharvest Physiology and Shelf-Life." Master's thesis, University of Pretoria.
- Buffo, R.A., C.L. Weller, and A. Gennadios. 1997. "Films from Laboratory-Extracted Sorghum Kafirin." *Cereal Chem.* 74(4): 473-475.
- Byaruhanga, Y.B., C. Erasmus, M.N. Emmambux, and J.R.N. Taylor. 2007. "Effect of Heating Cast Kafirin Films on Their Functional Properties." *J. Sci. Food Agric.* 87(1): 167-175.
- Byers, C.H., W.G. Sisson, J.P. De Carli, and G. Carta. 1989. "Pilot-Scale Studies of Sugar Separations by Continuous Chromatography." *Appl. Biochem. Biotechnol.* 20-21(1): 635-654.
- Chairat, M., S. Rattanaphani, J.B. Bremmer, and V. Rattanaphani. 2005. "An Adsorption and Kinetic Study of Lac Dyeing on Silk." *Dyes and Pigm.* 64(3): 231-241.
- Chase, H.A. 1994. "Purification of Proteins by Adsorption Chromatography in Expanded Beds." *Trends Biotechnol.* 12(8): 296-303.
- Chen, L., G.E. Remondetto, M. Rouabhia, and M. Subirade. 2008. "Kinetics of the Breakdown of Cross-Linked Soy Protein Films for Drug Delivery." *Biomaterials* 29(27): 3750-3756.
- Chen, L., G.E. Remondetto, and M. Subirade. 2006. "Food Protein-Based Materials as Nutraceutical Delivery Systems." *Trends Food Sci. Tech.* 19(5): 272-283.
- Chen, W.-D., X.-D. Tong, X.-Y. Dong, and Y. Sun. 2003. "Expanded Bed Adsorption of Protein with DEAE Spherodex M." *Biotech. Prog.* 19(3): 880-886.
- Chu, K.H. and Y.-T. Hung. 2010. "Modeling of Biosorption Processes." In *Handbook of Environmental Engineering*, edited by L.K. Wang, J.-H. Tay, S.T.L. Tay, and Y.-T. Hung, 351-374. New York: Humana Press.
- Clift, R., J.R. Grace and M.E. Weber. 1978. "Slow Viscous Flow Past Spheres." In *Bubbles, Drops, and Particles*, 30-66. New York: Academic Press.
- Corthier, G., E. Boschetti, and J. Charley-Poulain. 1984. "Improved Method for IgG Purification from Various Animal Species by Ion Exchange Chromatography." *J. Immunol. Meth.* 66(1): 75-79.
- Couriol, C., S. le Quellec, L. Guihard, D. Molle, B. Chaufer, and Y. Prigent. 2000. "Separations of Acid Whey Proteins on the Preparative Scale by Hyperdiffusive Anion Exchange Chromatography." *Chromatographia* 52(7): 465-472.

- Cowan, G.H., I.S. Gosling and W.P. Sweetenham. 1989. "Modeling Methods to Aid the Design and Optimisation of Batch Stirred-Tank and Packed-Bed Column Adsorption and Chromatography Units." *J. Chromatogr.* 484(1): 187-210.
- Crittenden, J.C. and W.J. Weber. 1978. "Predictive Model for Design of Fixed-Bed Adsorbers: Parameter Estimation and Model Development." *J. Environ. Eng.* 104(2): 185-197/
- Crittenden, J.C., N.J. Hutzler, D.G. Geyer, J.L. Oravitz, and G. Friedman. 1986. "Model Development and Parameter Sensitivity." *Water Resour. Res.* 22(3): 271-284.
- Cui, Y., G. Nakhla, J. Zhu, and A. Patel. 2004. "Simultaneous Carbon and Nitrogen Removal in Anoxic-Aerobic Circulating Fluidising Bed Biological Reactor (CFBBR)". *Environ. Technol.* 25(6): 699-712.
- Cuq, B., N. Gontard, and S. Guillbert. 1998. "Proteins as Agricultural Polymers for Packaging Production." *Cereal Chem.* 75(1): 1-9.
- Da Silva, L.S. 2003. "Transgenic Sorghum: Effects of Altered Kafirin Synthesis on Kafirin Polymerisation, Protein Quality, Protein Body Structure and Endosperm Texture." PhD thesis. University of Pretoria.
- Da Silva, L.S. and J.R.N. Taylor. 2005. "Physical, Mechanical, and Barrier Properties of Kafirin Films from Red and White Sorghum Milling Fractions." *Cereal Chem.* 82(1): 9-14.
- De Mesa-Stonestreet, N.J., S. Alavi, and S.R. Bean. 2010. "Sorghum Proteins: The Concentration, Isolation, Modification, and Food Applications of Kafirins." *J. Food Sci.* 75(5): 90-104.
- De Wit, J.N. 2001. "Processing of Whey Ingredients." In *Lecturer's Handbook on Whey and Whey Products*, 24-35. Belgium: European Whey Products Association.
- Deb, K., A. Pratap, S. Agarwal, and T. Meyarivan. 2002. "A Fast Elitist Genetic Algorithm: NSGA-II." *IEEE T. Evolut. Comput.* 6(2): 182-197.
- DeRose, R.T., D.P. Ma, I.S. Kwon, S.E. Hasnain, R.C. Klassy, and T.C. Hall. 1989. "Characterisation of the Kafirin Gene Family from Sorghum Reveals Extensive Homology with Zein from Maize." *Plant Mol. Biol.* 12(3): 245-256.
- Do, D.D. and R.G. Rice. 1990. "Applicability of the External-Diffusion Model in Adsorption Studies." *Chem. Eng. Sci.* 45(5): 1419-1421.

- Draeger, N.M. and H.A. Chase. 1990. "Modeling of Protein Adsorption in Liquid Fluidised Beds." In *Separations for Biotechnology 2*, edited by D.L. Pyle, 325-334. Netherlands: Springer.
- Duodu, K.G., J.R.N. Taylor, P.S. Belton, and B.R. Hamaker. 2003. "Factors Affecting Sorghum Protein Digestibility." *J. Cereal Sci.* 38(2): 117-131.
- Eldyasti, A., N. Chowdhury, G. Nakhla, and J. Zhu. 2010. "Biological Nutrient Removal from Leachate using a Pilot Liquid-Solid Circulating Fluidised Bed Bioreactor (LSCFB)." *J. Hazard. Mater.* 181(1-3): 289-297.
- Elkhalifa, A.E.O., D.M.R. Georget, S.A. Barker, and P.S. Belton. 2009. "Study of the Physical Properties of Kafirin during the Fabrication of Tablets for Pharmaceutical Applications." *J. Cereal Sci.* 50(2): 159-165.
- Emmambux, M.N. and J.R.N. Taylor. 2003. "Sorghum Kafirin Interaction with Various Phenolic Compounds." *J. Sci. Food Agr.* 83(5): 402-407.
- Emmambux, M.N., M. Stading, J.R.N. Taylor. 2004. "Sorghum Kafirin Film Property Modification with Hydrolysable and Condensed Tannins." *J. Cereal Sci.* 40(2): 127-135.
- Erasmus, C. 2003. *Extraction of Cereal Biopolymers*. Pretoria, South Africa: Division of Food, Biologica and Chemical Technologies (CSIR).
- Fair, G.M. and J.C. Geyer. 1954. *Water Supply and Waste-water Disposal*. New York: John Wiley & Sons.
- Fan, L.-T., Y.-C. Yang, and C.-Y. Wen. 1960. "Mass Transfer in Semifluidised Beds for Solid-Liquid System." *AIChE J.* 6(3): 482-487.
- Feng, X., S. Jing, Q. Wu, J. Chen, and C. Song. 2003. "The Hydrodynamic Behaviour of the Liquid-Solid Circulating Fluidised Bed Ion Exchange System for Cesium Removal." *Powder Technol.* 134(3): 235-242.
- Feuser, J., J. Walter, M.-R. Kula, and J. Thommes. 1999. "Cell/Adsorbent Interactions in Expanded Bed Adsorption of Proteins." In *Expanded Bed Chromatography*, edited by B. Maltiasson, 99-109. Netherlands: Springer.
- Flemmer, R.L.C. and C.L. Banks. 1986. "On the Drag Coefficient of a Sphere." *Powder Technol.* 48(3): 217-221.
- Foo, K.Y. and B.H. Hameed. 2010. "Insights into the Modeling of Adsorption Isotherm Systems." *Chem. Eng. J.* 156(1): 2-10.
- Finette, G.M.S., Q.-M. Mao, and M.T.W. Hearn. 1997. "Comparative Studies on the Isotherm Characteristics of Proteins Adsorbed under Batch Equilibrium

- Conditions to Ion-Exchange, Immobilised Metal Ion Affinity and Dye Affinity Matrices with Different Ionic Strength and Temperature Conditions.” *J. Chromatogr. A* 763(1-2): 71-90.
- Freundlich, H.M.F. 1906. “Over the Adsorption in Solution.” *J. Phys. Chem.* 57(1): 385-470.
- Garside, J. and Al-Dibouni, M.R. 1977. “Velocity-Voidage Relationships for Fluidisation and Sedimentation in Solid-Liquid Systems.” *Ind. Eng. Chem. Process Des. Dev.* 16(2): 206-213.
- GE Healthcare. 2013. *Protein and Peptide Purification: Technique Selection Guide*. Rydalmere, N.S.W.: GE Healthcare Australia.
- Gennadios, A. and C.L. Weller. 1990. “Edible Films and Coatings from Wheat and Corn Proteins.” *Food Technol.* 44(1): 63-69.
- Gerberding, S.J. and C.H. Byers. 1998. “Preparative Ion-Exchange Chromatography of Proteins from Dairy Whey.” *J. Chromatogr. A.* 808(1-2): 141-151.
- Giles, C.H., T.H. MacEwan, S.N. Nakhwa, and D. Smith. 1960. “Studies in Adsorption. Part XI.* A System of Classification of Solution Adsorption Isotherms, and its Use in Diagnosis of Adsorption Mechanisms and in Measurement of Specific Surface Areas of Solids.” *J. Chem. Soc.* 56(0): 3973-3993.
- Goldstein, S. 1929. “The Steady Flow of Viscous Fluid Past a Fixed Spherical Obstacle at Small Reynolds Numbers.” *Proc. R. Soc. Lond. A* 123(791): 225-235.
- Gordon, N.F., C.M.V. Moore, and C.L. Cooney. 1990. “Overview of Continuous Protein Purification Processes.” *Biotech. Adv.* 8(4): 741-762.
- Gordon, N.F. and C.L. Cooney. 1990. “Impact of Continuous Affinity – Recycle Extraction (CARE) in Downstream Processing.” In *Protein Purification: From Molecular Mechanisms to Large-Scale Processes*, edited by M.R. Ladisch, R.C. Willson, C.C. Painton, and S.E. Builder, 118-138. Washington DC: American Chemical Society.
- Gottschlich, N. and V. Kasche. 1997. “Purification of Monoclonal Antibodies by Simulated Moving-Bed Chromatography.” *J. Chromatogr. A.* 765(2): 201-206.
- Grace, J.R. 1990. “High-Velocity Fluidised Bed Reactors.” *Chem. Eng. Sci.* 45(8): 1953-1966.

- Griffin, R.A. and J.J. Jurinak. 1973. "Test of A New Model for The Kinetics of Adsorption-Desorption Processes." 1973. *Soil Sci. Soc. Amer. Proc.* 37(6): 869-872.
- Gueorguieva, L., S. Palani, U. Rinas, G. Jayaraman, A. Seidel-Morgenstern. 2011. "Recombinant Protein Purification using Gradient Assisted Simulated Moving Bed Hydrophobic Interaction Chromatography. Part II: Process Design and Experimental Validation." *J. Chromatogr. A.* 1218(37): 6402-6411.
- Guerrero-German, P., R.M. Montesinos-Cisneros, and A. Tejada-Mansir. 2012. "Simulation of Frontal Protein Affinity Chromatography using MATLAB." *J. Chem. Eng. Process Technol.* 3(3): 1-6.
- Guiochon, G., A. Felinger, D.G. Shirazi, and A.M. Katti. 2006. "Linear Chromatography." In *Fundamentals of Preparative and Nonlinear Chromatography*, 281-346. 2nd ed. San Diego, C.A.: Elsevier.
- Haider, A. and O. Levenspiel. 1989. "Drag Coefficient and Terminal Velocity of Spherical and Non-Spherical Particles." *Powder Technol.* 58(1): 63-70.
- Haikerwal, M. and A.R. Mathieson. 1971. "Extraction and Fractionation of Proteins of Sorghum Kernels." *J. Sci. Food Agric.* 22(3): 142-145.
- Haghseresht, F. and G. Lu. 1998. "Adsorption Characteristics of Phenolic Compounds onto Coal-Reject-Derived Adsorbents." *Energy Fuels* 12(6): 1100-1107.
- Hahn, R., P.M. Schulz, C. Schaupp, and A. Jungbauer. 1998. "Bovine Whey Fractionation Based on Cation-Exchange Chromatography." *J. Chromatogr. A.* 795(2): 277-287.
- Hamaker, B.R., A.A. Mohamed, J.E. Habben, C.P. Huang, and B.A. Larkins. 1995. "Efficient Procedure for Extracting Maize and Sorghum Kernel Proteins Reveals Higher Prolamin Contents Than the Conventional Method." *Cereal Chem.* 62(6): 583-588.
- Haq, A. P.I. Lobo, M. Al-Tufail, N. R. Rama, and ST. Al-Sedairy. 1999. "Immunomodulatory Effect of Nigella sativa Proteins Fractionated by Ion Exchange Chromatography." *Int. J. Immunopharmacol.* 21(4): 283-295.
- Hartman, M., D. Trnka, and V. Havlin. 1992. "A Relationship to Estimate the Porosity in Liquid-Solid Fluidised Beds." *Chem. Eng. Sci.* 47(12): 3162-3166.
- Hinz, C. 2001. "Description of Sorption Data with Isotherm Equations." *Geoderma* 99(3): 225-243.

- Ho, Y.-S. 2006. "Isotherms of the Sorption of Lead Onto Peat: Comparison of Linear and Non-Linear Methods." *Pol. J. Environ. Stud.* 15(1): 81-86.
- Ho, Y.S. and G. McKay. 2000. "Kinetics of Pollutant Sorption by Biosorbents: Review." *Separ. Purif. Method* 29(2): 189-232.
- Hooper, N.M.1999. "Drugs and Inhibitors as Affinity Ligands." In *High Resolution Chromatography: A Practical Approach* edited by P. Millner, 217-232. Oxford, New York: Oxford University Press.
- Horvath, J., E. Boschetti, L. Guerrier, N. Cooke. 1994. "High-Performance Protein Separations with Novel Strong Ion Exchangers." *J. Chromatogr. A.* 679(1): 11-22.
- Huang, S.Y., C.K. Lin, W.H. Chang, and W.S. Lee. 1986. "Enzyme Purification and Concentration by Simulated Moving Bed Chromatography: An Experimental Study." *Chem. Eng. Comm.* 45(1-6): 291-309.
- Hunter, A.K. and G. Carta. 2000. "Protein Adsorption on Novel Acrylamido-Based Polymeric Ion Exchangers: II. Adsorption Rates and Column Behavior." *J. Chromatogr. A* 897(1-2): 81-97.
- Jambunathan, R. and E.T. Mertz. 1973. "Relationship between Tannin Levels, Rat Growth, and Distribution of Proteins in Sorghum." *J. Agric. Food Chem.* 21(4): 692-696.
- Johansson, H.J., C. Jagersten, and J. Shiloach. 1996. "Large Scale Recovery and Purification of Periplasmic Recombinant Protein from E. coli Using Expanded Bed Adsorption Chromatography Followed by New Ion Exchange Media." *J. Biotechnol.* 48(1-2): 9-14.
- Johns, C.O. and J.F. Brewster. 1916. "Kafir, an Alcohol-Soluble Protein from Kafir, *Andropogon Sorghum*." *J. Biol. Chem.* 28(1): 59-65.
- Jones, R.W. and A.C. Beckwith. 1970. "Proximate Composition and Proteins of Three Grain Sorghum Hybrids and Their Dry-Mill Fractions." *J. Agric. Food Chem.* 18(1): 33-36.
- Jonsson, J.A. 1996. "Nomenclature for Non-Linear Chromatography." *Pure Appl. Chem.* 68(8): 1591-1595.
- Jungbauer, A. and C. Machold. 2004. "Chromatography of Proteins." In *Chromatography: Fundamentals and Applications of Chromatography and Related Differential Migration Methods*, edited by E. Heftmann, 669-738. Amsterdam, Netherlands: Elsevier.

- Kalil, S.J., F. Maugeri-Filho, and M.I. Rodrigues. 2005. "Ion Exchange Expanded Bed Chromatography for the Purification of an Extracellular Inulinase from *Kluyveromyces marxianus*." *Process Biochem.* 40(20): 581-586.
- Karamanev, D. and L.N. Nikolov. 1992. "Bed Expansion of Liquid-Solid Inverse Fluidisation." *AIChE J.* 38(12): 1916-1922.
- Karau, A., C. Benken, J. Thommes, and M.-R. Kula. 1997. "The Influence of Particle Size Distribution and Operating Conditions on the Adsorption Performance in Fluidised Beds." *Biotechnol. Bioeng.* 55(1): 54-64.
- Karri, R.S.B. and T.M. Knowlton. 1991. "A Practical Definition of the Fast Fluidisation Regime." In *Circulating Fluidised Bed Technology III*, edited by P. Basu, M. Hario, and M. Hasatani, 67-72, Kidlington, Oxford: Pergamon Press.
- Kaser, F. 2003. *Environment-Friendly Packaging Solutions for Enhanced Storage and Quality of Southern Africa's Fruit and Nut Exports: 18-Month Activity Report*. Sweden: The Swedish Institute for Food and Biotechnology (SIK), Italy: Institute of Composite Materials Technology (IMCB), United Kingdom: Institute of Food Research (IFR), South Africa: Division of Food, Biological and Chemical Technologies (CSIR), South Africa: University of Pretoria (UP), Mozambique: University of Eduardo Mondlane (UEM), and Mauritius: University of Mauritius (UOM).
- Khan, A.R. and J.F. Richardson. 1989. "Fluid-Particle Interactions and Flow Characteristics of Fluidised Beds and Settling Suspensions of Spherical Particles." *Chem. Eng. Commun.* 78(1): 111-130.
- Khan, A.R. and J.F. Richardson. 1987. "The Resistance to Motion of a Solid Sphere in a Fluid." *Chem. Eng. Commun.* 62(1-6): 135-150.
- Khan, H.U. 2012. "The Role of Ion Exchange Chromatography in Purification and Characterization of Molecules." In *Ion Exchange Technologies*, edited by A. Kilislioglu, 331-342. Croatia: InTech.
- Khan, M. 2004. *Report on the Selection and Optimisation of Suitable Coating Techniques for Fruits and Nuts on Pilot Scale*. Marseille, France: European Research Council.
- Kinniburgh, D.G. 1986. "General Purpose Adsorption Isotherms." *Environ. Sci. Technol.* 20(9): 895-904.

- Krochta, J.M. 2002. "Proteins as Raw Materials for Films and Coatings: Definitions, Current Status, and Opportunities." In *Protein-Based Films and Coatings*, edited by A., Gennadios, 1-42. Florida: CRC Press.
- Kwauk, M. 1963. "Generalised Fluidisation I, Steady-State Motion". *Scientia Sinica* 12(4): 587-612.
- Lagergren, S. 1898. "About the Theory of So-Called Adsorption of Soluble Substances." *Kungl. Sven. Vetén. Akad. Handl.* 24(1): 1-39.
- Lan, Q., A.S. Bassi, J.-X. Zhu, and A. Margaritis. 2002a. "Continuous Protein Recovery from Whey Using Liquid-Solid Circulating Fluidised Bed Ion-Exchange Extraction." *Biotechnol. Bioeng.* 78(2): 157-163.
- Lan, Q., A.S. Bassi, J.-X. Zhu, and A. Margaritis. 2002b. "Continuous Protein Recovery with a Liquid-Solid Circulating Fluidised-Bed Ion Exchanger." *AIChE J.* 48(2): 252-261.
- Lan, Q., J.-X. Zhu, A.S. Bassi, A. Margaritis, Y. Zheng, and G.E. Rowe. 2000. "Continuous Protein Recovery Using a Liquid-Solid Circulating Fluidised Bed Ion Exchange System: Modeling and Experimental Studies." *Can J. Chem. Eng.* 78(5): 858-866.
- Lan, Q., A. Bassi, J.-X. Zhu, and A. Margaritis. 2001. "Continuous Protein Recovery from Whey Using Liquid-Solid Circulating Fluidised Bed Ion-Exchange Extraction." *Biotechnol. Bioeng.* 78(2): 157-163.
- Landry, J., J.W. Paulis, and J.S. Wall. 1987. "Chromatographic and Electrophoretic Analysis of Zein Heterogeneity." *J. Cereal Sci.* 5(1): 51-60.
- Langmuir, I. 1916. "The Constitution and Fundamental Properties of Solids and Liquids. Part I. Solids." *J. Am. Chem. Soc.* 38(11): 2221-2295.
- Langmuir, I. 1917. "The Constitution and Fundamental Properties of Solids and Liquids. II. Liquids." *J. Am. Chem. Soc.* 39(9): 1848-1906.
- Lasztity, R. 1996. "Sorghum Protein." In *The Chemistry of Cereal Proteins*, edited by R. Lasztity, 227-248. Boca Raton, Florida: CRC Press.
- Lau, E.T.L., S.J. Giddings, S.G. Mohammed, P. Dubois, S.K. Johnson, R.A. Stanley, P.J. Halley, and K.J. Steadman. 2013. "Encapsulation of Hydrocortisone and Mesalazine in Zein Microparticles." *Pharm.* 5(2): 277-293.
- Lau, E.T.L., S.K. Johnson, D. Mikkelsen, P.J. Halley, and K.J. Steadman. 2012. "Preparation and in vitro Release of Zein Microparticles Loaded with Prednisolone for Oral Delivery." *J. Microencapsul.* 29(7): 706-712.

- Lau, P.W., R. Utikar, V. Pareek, S. Johnson, S. Kale, and A. Lali. 2013a. "Modeling and Numerical Simulation of Liquid-Solid Circulating Fluidised Bed System for Protein Purification." *Chem. Eng. Res. Des.* 91(9): 1660-1673.
- Lau, P.W., P. Kumar, R. Utikar, V. Pareek, S. Kale, A. Lali, and S. Johnson. 2013b. "Kinetics of Kafirin Sorption and Desorption Using Chromatography." In *Chemeca 2013: Challenging Tomorrow: 29 September – 2 October 2013, Brisbane Convention and Exhibition Centre, Queensland/Chemical College, Engineers Australia*. Brisbane, Q.L.D.: Chemeca 2013 and Institution of Engineers, Australia.
- Lawton, J.W. 2002. "Zein: a History of Processing and Use." *Cereal Chem.* 79(1): 1-18.
- Li, P., G. Xiu, and A.E. Rodrigues .2007. "Proteins Separation and Purification by Salt Gradient Ion-Exchange SMB." *AIChE J.* 53(9): 2419-2431.
- Liang, M.-T., R.-C. Liang, S. Yu, and R. Yan. 2013. "Separation of Resveratrol and Emodin by Supercritical Fluid-Simulated Moving Bed Chromatography." *J. Chromat. Separation Techniq.* 4(3): 1-5.
- Liang, W., Z. Yu, Y. Jin, Z. Wang, and Q. Wu. 1995. "The Phase Holdups in A Gas-Liquid-Solid Circulating Fluidised Bed." *Chem. Eng. J. Biochem. Eng. J.* 58(2-3): 259-264.
- Liang, W., Z. Yu, Y. Jin, Z. Wang, Y. Wang, M. He, E. Min. 1995. "Synthesis of Linear Alkylbenzene in a Liquid-Solid Circulating Fluidised Bed Reactor." *J. Chem. Tech. Biotechnol.* 62(1): 98-102.
- Lundblad, R.L. 2012. "Albumin" In *Biotechnology of Plasma Proteins*. 83-182. Boca Raton, Florida: CRC Press.
- Ma, Z., R.D. Whitley, N.-H. Wang. 1996. "Pore and Surface Diffusion in Multicomponent Adsorption and Liquid Chromatography Systems." *AIChE J.* 42(5): 1244-1262.
- MathWorks. 2013. "Multiobjective Genetic Algorithm Options." Accessed January 3, <http://www.mathworks.com.au/products/global-optimisation/code-examples.html?file=/products/demos/shipping/globaloptim/gamultiobjoptionsdemo.html>.
- Mao, Q.M. and M.T.W. Hearn. 1996. "Optimisation of Affinity and Ion-Exchange Chromatographic Processes for the Purification of Proteins." *Biotechnol. Bioeng.* 52(2): 204-222.

- Martin, A.J.P. and R.L.M. Synge. 1941. "A New Form of Chromatogram Employing Two Liquid Phases." *Biochem. J.* 35(12): 1358-1368.
- Masamune, S., J.M. Smith. 1964. "Adsorption Rate Studies – Significance of Pore Diffusion." *AIChE J.* 10(2): 246-252.
- Masamune, S., and J.M. Smith. 1965. "Adsorption of Ethyl Alcohol on Silica Gel." *AIChE J.* 11(1): 41-45.
- Mazumder, J., J. Zhu, A.S. Bassi, and A.K. Ray. 2009a. "Modeling and Simulation of Liquid-Solid Circulating Fluidised Bed Ion Exchange System for Continuous Protein Recovery." *Biotechnol. Bioeng.* 104(1): 111-126.
- Mazumder, J., J. Zhu, A.S. Bassi, and A.K. Ray. 2009b. "Multiobjective Optimisation of the Operation of A Liquid-Solid Circulating Fluidised Bed Ion-Exchange System for Continuous Protein Recovery." *Biotechnol. Bioeng.* 103(5): 873-890.
- McCreath, G.E., H.A. Chase, D.R. Purvis, and C.R. Lowe. 1992. "Novel Affinity Separations Based on Perfluorocarbon Emulsions. Use of a Perfluorocarbon Affinity Emulsion for the Purification of Human Serum Albumin from Blood Plasma in a Fluidised Bed." *J. Chromatogr.* 597 (1-2): 189-196.
- McCreath, G.E., R.O. Owen, D.C. Nash, and H.A. Chase. 1997. "Novel Affinity Separations Based on Perfluorocarbon Emulsion Reactor for Continuous Affinity Separation and Its Application in the Purification of Human-Serum Albumin from Blood-Plasma." *J. Chromatogr. A.* 773(2): 73-83.
- McCullough, B.D. 2012. "Assessing the Reliability of Statistical Software: Part II." *Am. Stat.* 53(2): 149-159.
- McHugh, T.H. and J.M. Krochta. 1994. "Permeability Properties of Edible Films." In *Edible Coatings and Films to Improve Food Quality*, edited by E.A., Baldwin, H. Robert, J. Bai, and J.M. Krochta, 139-188. Florida: CRC Press.
- McKay, G. 1984. "Two-Resistance Mass Transfer Models for The Adsorption of Dyestuffs From Aqueous Solutions Using Activated Carbon." *J. Chem. Technol. Biot.* 34(6): 294-310.
- McNaire, H.M. and J.M. Miller. 1998. "Introduction." In *Basic Gas Chromatography*, edited by H.M. McNaire and J.M. Miller, 1-13. New York: John Wiley and Sons.
- Mittal, A. 2010. "Optimisation of the Layout of Large Wind Farms Using A Genetic Algorithm." Master's thesis. Case Western Reserve University.

- Monazam, E.R. and L.J. Shadle. 2004. "A Transient Method for Characterizing Flow Regimes in A Circulating Fluid Bed." *Powder Technol.* 139(1): 89-97.
- Nfor, B.K., T. Ahamed, G.W.K., van Dedem, L.A.M. van der Wielen, E.J. van de Sandt, M.H.M. Eppink, and M. Ottens. 2008. "Review Design Strategies for Integrated Protein Purification Processes: Challenges, Progress and Outlook." *J. Chem. Technol. Biotechnol.* 83(2): 124-132.
- Nicoud, R.-M. 1996. "Large Scale Fraction of Optical Isomers by Simulated Moving Bed Chromatography." In *Proceedings of Chiral Europe held in Strasbourg, France, 14-15 October 1996.* 117-119. Stockport, Manchester: Spring Innovations.
- Osborne, T.B. and L.B. Mendel. 1914. "Nutritive Properties of Proteins of the Maize Kernel." *J. Biol. Chem.* 19(1): 1-16.
- Oseen, W. 1910. "Ueber Die Stokessche Formel Und Die Verwandte Aufgabe in Der Hydrodynamik." *Arkiv for Matematik, Astronomi och Fysik* 6(29): 1-20.
- Owen, R.O. and H.A. Chase. 1999. "Modeling of the Continuous Counter-Current Expanded Bed Adsorber for the Purification of Proteins." *Chem. Eng. Sci.* 54(17): 3755-3781.
- Özdural, A.R., A. Alkan, and P.J.A.M. Kerkhof. 2004. "Modeling Chromatographic Columns: Non-Equilibrium Packed-Bed Adsorption with Non-Linear Adsorption Isotherms." *J. Chromatogr. A* 1041(1-2): 77-85.
- Pall Corporation. 2013. *Overview of Chromatography in Biopurification.* Washington, N.Y.: Pall Corporation.
- Park, H.J., J.W. Rhim, C.L. Weller, A. Gennadios, and M.A. Hanna. 2002. "Films and Coatings from Proteins of Limited Availability." In *Protein-Based Films and Coatings*, edited by A. Gennadios, 305-327. Boca Raton, Florida: CRC Press.
- Park, J.-H. and S.R. Bean. 2003. "Investigation and Optimisation of the Factors Influencing Sorghum Protein Extraction." *J. Agric. Food Chem.* 51(24): 7050-7054.
- Park, J.W. R.F. Testin, H.J. Park, P.J. Vergano, and C.L. Weller. 1994. "Fatty Acid Concentration Effect of Tensile Strength, Elongation, and Water Vapor Permeability of Laminated Edible Films." *J. Food Sci.* 59(4): 916-919.
- Park, S.H., S.R. Bean, J.D. Wilson, and T.J. Schober. 2006. "Rapid Isolation of Sorghum and Other Cereal Starches using Sonication." *Cereal Chem.* 83(6): 611-616.

- Parris, N., P. Cooke, K. Hicks. 2005. "Encapsulation of Essential Oils in Zein Nanospherical Particles." *J. Agric. Food Chem.* 53(12): 4788-4792.
- Patel, M., A.S. Bassi, J. J.-X. Zhu, and H. Gomaa. 2008. "Investigation of a Dual-Particle Liquid-Solid Circulating Fluidised Bed Bioreactor for Extractive Fermentation of Lactic Acid." *Biotechnol. Progr.* 24(4): 821-831.
- Paulis, J.W. and J.S. Wall. 1979. "Distribution and Electrophoretic Properties of Alcohol-Soluble Proteins in Normal and High-Lysine Sorghums." *Cereal Chem.* 56(1): 20-23.
- Pedersen, H., L. Furler, K. Venkatasubramanian, J. Prenosil, and E. Stuker. 1985. "Enzyme Adsorption in Porous Supports: Local Thermodynamic Equilibrium Model." *Biotechnol. Bioeng.* 27(7): 961-971.
- Pérez-Gago, M.B. 2012. "Protein-Based Films and Coatings." In *Edible Coatings and Films to Improve Food Quality*, edited by Baldwin, E.A., R.D. Hagenmaier, and J. Bai, 13-77. Boca Raton, Florida: CRC Press.
- Pignatello, J.J. and B. Xing. 1996. "Mechanisms of Slow Sorption of Organic Chemicals to Natural Particles." *Environ. Sci. Technol.* 30(1): 1-11.
- Pfund, N.E. 1987. *The Wheat from the Chaff: The Separations Industry Comes of Age*. New York: Hambrecht and Quist.
- Prince, A., A.S. Bassi, C. Haas, J.-X. Zhu, and J. Dawe. 2012. "Soy Protein Recovery in a Solvent-Free Process using Continuous Liquid-Solid Circulating Fluidised Bed Ion Exchanger." *Biotechnol. Tech.* 28(1): 157-162.
- Richardson, J.F. and W.N. Zaki. 1954. "Sedimentation and Fluidisation (Part I)." *Trans. Inst. Chem. Eng.* 32(1): 35-53.
- Polykarpon, E. 2011. "Optimisation of Chromatography for Downstream Protein Processing." PhD thesis. University College London.
- Proudman, I. and J.R. Pearson. 1957. "Expansion at Small Reynolds Number for the Flow past a Sphere and a Circular Cylinder." *J. Fluid Mech.* 2(3): 237-262.
- Przybycien, T.M., N.S. Pujar, and L.M. Steele. 2004. "Alternative Bioseparation Operations: Life Beyond Packed-Bed Chromatography." *Curr. Opin. Biotechnol.* 15(5): 469-478.
- Reissner, K., A. Prior, J. Wolfgang, H.J. Bart, and C.H. Byers. 1997. "Preparative Desalting of Bovine Serum Albumin by Continuous Annular Chromatography." *J. Chromatogr. A*: 763(1-2): 49-56.

- Resindion. 2011. *ReliSorb QA Highly Porous Hydrophilic Packing Material*. Gurgaon, Haryana, India: Resindion.
- Rhodes, M., ed. 2008. *Introduction to Particle Technology*. 2nd ed. West Sussex: John Wiley & Sons.
- Rhone-Poulenc Industries. 1978. Method of Separating Proteins by Ion Exchange. US Patent US4100149 A, filed August 16, 1976, and issued July 11, 1978.
- Rhone-Poulenc Industries. 1980. Process for Extracting Proteins from Milk using Silica and Anion Exchange Resins. US Patent US4229342 A, filed May 5, 1978, and issued October 21, 1980.
- Richardson, J.F., and W.N. Zaki. 1954. "Sedimentation and Fluidisation: Part I." *Trans. Inst. Chem. Engrs.* 32(0): 35-53.
- Righetti, P.G. and G. Tudor. 1981. "Isoelectric Points and Molecular Weights of Proteins: A New Table." *J. Chromatogr.* 220(11): 115-194.
- Rodrigues, A.E., J.M. Loureiro, C. Chenou, M. Rendueles de la Vega. 1995. "Bioseparations with Permeable Particles." *J. Chromatogr. B Biomed. Sci. Appl.* 664(1): 233-240.
- Rowe, P.N. 1961. "Drag Force in a Hydraulic Model of a Fluidised Bed – Part II." *Trans. Instn. Chem. Engrs.* 39(1): 175-180.
- Roos, P.H. 1999. "Ion Exchange Chromatography" in *Protein Liquid Chromatography*, edited by M. Kastner, 3-88. Amsterdam, Netherlands: Elsevier.
- Ruthven, D.M. 1984. "Dynamics of Adsorption Columns: Single-Transition Systems." In *Principles of Adsorption and Adsorption Processes*, 220-273. New York: John Wiley and Sons.
- Schiller, L. and A. Naumann. 1933. "Über Die Grundlegenden Berechnungen Bei der Schwekraftaubereitung." *Zeitschrift des Vereines Deutscher Ingenieure* 77(12): 318-320.
- Schmidt-Traub, H. and J. Strube. 1996. "Dynamic Simulation of Simulated-Moving-Bed Chromatographic Processes." *Comput. Chem. Eng.* 20(1): 641-646.
- Seely, J. and C.W. Richey. 2001. "Use of Ion-Exchange Chromatography and Hydrophobic Interaction Chromatography in the Preparation and Recovery of Polyethylene Glycol-Linked Proteins." *J. Chromatogr. A.* 908(1-2): 235-241.
- Sengupta, S. and A.K. Sengupta. 2001. "Trace Heavy Metal Separation by Chelating Ion Exchangers." In *Environmental Separation of Heavy Metals: Engineering Processes*, edited by A.K. Sengupta, 45-96. Boca Raton, Florida: CRC Press.

- Shewry, P.R. and A.S. Tatham. 1990. "The Prolamin Storage Proteins of Cereal Seeds: Structure and Evolution." *Biochem. J.* 267(1): 1-12.
- Shull, J.M., J.J. Watterson, and A.W. Kirleis. 1991. "Proposed Nomenclature for the Alcohol-Soluble Proteins (Kafirins) of Sorghum Bicolor (L. Moench) Based on Molecular Weight, Solubility, and Structure." *J. Agric. Food Chem.* 39(1): 83-87.
- Silva, V.M.T.M., G.K. Gandi, and A.E. Rodrigues. 2007. "Development of Simulated Moving Bed Reactor Using a Cation Exchange Resin as A Catalyst and Adsorbent for the Synthesis of Acetals." In *Ion Exchange and Solvent Extraction: A Series of Advances* vol. 17, edited by A. K. Sengupta, 45-102. Boca Raton, Florida: CRC Press.
- Silverston, P.L., K. Hashimoto, and M. Kawase. 2012. "Chromatographic Reactors." In *Periodic Operation of Chemical Reactors*, edited by P.L. Silverston and R.R. Hudgins, 569-593. Kidlington, Oxford: Butterworth-Heinemann.
- Skogh, L.V., C.W. Deyoe, F.K. Shoup, J. Bathurst, and D. Liang. 1970. "Protein Fractionation of Sorghum Grain." *Cereal Chem.* 47(4): 472-481.
- Sober, H.A., F.J. Gutter, M.M. Wyckoff, and E.A. Peterson. 1956. "Chromatography of Proteins. II. Fractionation of Serum Protein on Anion-Exchange Cellulose." *J. Biol. Chem.* 78(1): 756-763.
- Stanton, P. 2004. "Ion-Exchange Chromatography." In *HPLC of Peptides and Proteins: Methods and Protocols*, edited by M.-I. Aguilar, 23-43. New York: Humana Press.
- Stokes, G.G. 1851. "On the Effect of the Internal Friction of Fluids on the Motion of Pendulums." *Trans. Cambridge* 9(8): 8-106.
- Suvarov, P., A.V. Wouwer, and A. Kienle. 2012. "A Simple Robust Control for Simulated Moving Bed Chromatographic Separation." In *8th IFAC International Symposium on Advanced Control of Chemical Processes..Held in Furama Riverfront, Singapore, 10-13 July 2012.* 137-142. Red Hook, N.Y.: Curran Associates.
- Takahashi, Y. and S. Goto. 1992. "Continuous Separation and Concentration of Proteins using An Annular Chromatography." *J. Chem. Eng. Jpn.* 25(4): 403-407.
- Taylor, J. and J.R.N. Taylor. 2013. Process for Producing Protein Microparticles. US Patent US8541040 B2, filed February 6, 2013, and issued September 24, 2013.

- Taylor, J., J.R.N. Taylor, M.F. Dutton, and S. de Kock. 2005. "Glacial Acetic Acid – A Novel Food-Compatible Solvent for Kafirin Extraction." *Cereal Chem.* 82(5): 485-487.
- Taylor, J. J.R.N. Taylor, P.S. Belton, and A. Minnaar. 2009b. "Kafirin Microparticle Encapsulation of Catechin and Sorghum Condensed Tannins." *J. Agric. Food Chem.* 57(16): 7523-7528.
- Taylor, J., J.R.N. Taylor, P.S. Belton, and A. Minnaar. 2009a. "Formation of Kafirin Microparticles by Phase Separation from an Organic Acid and Their Characterisation." *J. Cereal Sci.* 50(1): 99-105.
- Taylor, J.R.N., L. Schüssler, and W.H. van der Walt. 1984. "Fractionation of Proteins from Low-Tannin Sorghum Grain." *J. Agric. Food Chem.* 32(1): 149-154.
- Thermax. 2013. *Basics of Ion Exchange Resins*. Doha, Qatar: Thermax.
- Thermax. 2014. *Tulsion A-36MP Macroporous Strong Base, Type-II Anion Exchange Resin*. Pune, India: Thermax.
- Tong, X.-D., B. Xue, and Y. Sun. 2003. "Modeling of Expanded-Bed Protein Adsorption by Taking Into Account the Axial Particle Size Distribution." *Biochem. Eng. J.* 16(3): 265-272.
- Tong, X.-D., X.-Y. Dong, and Y. Sun. 2002. "Lysozyme Adsorption and Purification by Expanded Bed Chromatography with a Small-Sized Dense Adsorbent." *Biochem. Eng. J.* 12(2): 117-124.
- Tosoh Bioscience. 2011a. *Product Specification Sheet- Toyopearl QAE-550*. Redland Bay, Queensland, Australia: Tosoh Bioscience.
- Tosoh Bioscience. 2011b. *Product Specification Sheet- Toyopearl SuperQ-650M*. Redland Bay, Queensland, Australia: Tosoh Bioscience.
- Tosoh Bioscience. 2011.c *Product Specification Sheet- Toyopearl SP-550C*. Redland Bay, Queensland, Australia: Tosoh Bioscience.
- Tosoh Bioscience. 2011d. *Product Specification Sheet- Toyopearl SP-650M*. Redland Bay, Queensland, Australia: Tosoh Bioscience.
- Trivedi, U., A. Bassi, and J.-X. Zhu. 2006. "Continuous Enzymatic Polymerization of Phenol in a Liquid-Solid Circulating Fluidised Bed." *Powder Technol.* 169(2): 61-70.
- Turton, R. and O. Levenspiel. 1986. "A Short Note on the Drag Correlation for Spheres." *Powder Technol.* 47(1): 83-86.

- Universal Oil Products. 1962. Continuous Sorption Process Employing Fixed Bed of Sorbent and Moving Inlets and Outlets. US Patent US2985589 A, filed May 22, 1957 and issued May 23, 1961.
- Uretschlager, A., A. Einhauer, and A. Jungbauer. 2001. "Continuous Separation of Green Fluorescent Protein by Annular Chromatography." *J. Chromatogr. A.* 908(1-2): 243-250.
- USDA (United States of Department of Agriculture). 2014a. *U.S. Supply and Disappearance – Sorghum: Supply and Disappearance*. Washington, D.C.: United States of Department of Agriculture.
- USDA (United States Department of Agriculture). 2014b. *Grain: World Markets and Trade*. Washington: D.C.: United States of Department of Agriculture.
- Virupaksha, T.K. and L.V.S. Sastry. 1968. "Studies on the Protein Content and Amino Acid Composition of Some Varieties of Grain Sorghum." *J. Agr. Food Chem.* 16(2): 199-203.
- Wallace, J.C., M.A. Lopes, E. Paiva, and B.A. Larkins. 1989. "New Methods for Extraction and Quantitation of Zeins Reveals a High Content of γ -Zein in Modified *Opaque-2* Maize." *Plant Physiol.* 92(1): 191-196.
- Wang, Y., M. Tilley, S. Bean, X.S. Sun, and D. Wang. 2009. "Comparison of Methods for Extracting Kafirin Proteins from Sorghum Distillers Dried Grains with Solubles." *J. Agric. Food Chem.* 57(18): 8366-8372.
- Ward, W. 2012. "The Art of Protein Purification." In *Protein Purification*, edited by R. Ahmad, 1-29. Croatia: InTech.
- Weber, T.W. and R.K. Chakravorti. 1974. "Pore and Solid Diffusion Models for Fixed-Bed Adsorbers." *AIChE J.* 20(2): 228-238.
- Wen, C.Y. and Y.H. Yu. 1966. "Mechanics of Fluidisation." *Chem. Eng. Prog. Symp. Ser.* 62(62): 100-111.
- Wheaton, R.M., L.J. Lefevre. 1981. "Ion Exchange." In *Kirk-Othmer Encyclopaedia of Chemical Technology*, 678-705. New York: Wiley.
- Wiblin, D.J., S.D. Roe, and R.G. Myhill. 1995. "Computer Aided Desk-Top Scale-Up and Optimisation of Chromatographic Processes." *J. Chromatogr. A* 702(1-2): 81-87.
- Wright, P. and B.J. Glasser. 2001. "Modeling Mass Transfer and Hydrodynamics in Fluidised-Bed Adsorption of Proteins." *AIChE J.* 47(2): 474-488.

- Wright, P.R., F.J. Muzzio, and B.J. Glasser. 1998. "Batch Uptake of Lysozyme: Effect of Solution Viscosity and Mass Transfer on Adsorption." *Biotechnol. Prog.* 14(6): 913-921.
- Wu, Y.V. and J.S. Wall. 1980. "Lysine Content of Protein Increased by Germination of Normal and High-Lysine Sorghums." *J. Agric. Food Chem.* 28(2): 455-458.
- Xu, Z., J.-G. Cai, and B.-C. Pan. 2013. "Mathematically Modeling Fixed-Bed Adsorption in Aqueous Systems."
- Yamamoto, S. and T. Ishihara. 1999. "Ion-Exchange Chromatography of Proteins near the Isoelectric Points." *J. Chromatogr. A.* 852(1): 31-36.
- Yang, H. 2008. "Characterization of Hexamer Peptides for Immunoglobulin G Isolation as Affinity Media." In *Fc-Binding Hexamer Peptide Ligands for Immunoglobulin Purification*. 78-110. Ann Arbor, M.I.: ProQuest.
- Yang, Y.L., Y. Jin, Q. Yu, J.X. Zhu, H.T. Bi. 1993. "Local Slip Behaviour in the Circulating Fluidised Bed." *AIChE Symp. Ser.* 89(296): 81-90.
- Yee, A.K.Y., A.K. Ray, and G.P. Rangaish. 2003. "Multiobjective Optimisation of An Industrial Styrene Reactor." *Comput. Chem. Eng.* 27(1): 111-130.
- Yun, J. D.-Q. Lin, and S.-J. Yao. 2005. "Predictive Modeling of Protein Adsorption Along the Bed Height by Taking into Account the Axial Nonuniform Liquid Dispersion and Particle Classification in Expanded Beds." *J. Chromatogr. A.* 1095(1-2): 16-26.
- Zhao, R., S.R. Bean, B.P. Ioerger, D. Wang, and D.L. Boyle. 2008. "Impact of Mashing on Sorghum Proteins and Its Relationship to Ethanol Fermentation." *J. Agric. Food Chem.* 56(3): 946-953.
- Zheng, Y., J.-X. Zhu, J. Wen, S.A. Martin, A.S. Bassi, and A. Margaritis. 1999. "The Axial Hydrodynamic Behaviour in A Liquid-Solid Circulating Fluidised Bed." *Can. J. Chem.* 77(2): 284-290.
- Zhong, Q. and M. Jin. 2009. "Nanoscalar Structures of Spray-Dried Zein Microcapsules and in vitro Release Kinetics of the Encapsulated Lysozyme as Affected by Formulations." *J. Agric. Food Chem.* 57(9): 2886-2894.
- Zhu, J.-X., D.G. Karamanev, A.S. Bassi, and Y. Zheng. 2000. "(Gas-)Liquid-Solid Circulating Fluidised Beds and Their Potential Applications to Bioreactor Engineering." *Can. J. Chem.* 78(1): 82-94.

Every reasonable effort has been made to acknowledge the owners of the copyright material. I would be pleased to hear from any copyright owner who has been omitted or incorrectly acknowledged.

CURRICULUM VITAE

Name: Pei Wen Lau

Post-Secondary Education: Doctor of Philosophy (November 2011 – Present)
Department of Chemical Engineering, Curtin University, Bentley Campus

B.Eng. (2006-2010)
Department of Chemical Engineering, Curtin University, Bentley Campus

Foundation in Engineering (2005-2006)
Foundation Programme, Curtin University, Miri Campus

Honours and Awards: Curtin Postgraduate Research Scholarship (2011-2014)
Vice-Chancellor's List (2006-2007)
B.Eng. Dean's List (2006-2008)
Curtin First Year Degree Scholarship (2006-2007)
Curtin Foundation Scholarship (2005-2006)
Foundation Program Dean's List (2005-2006)

Related Work Experience: Teaching Assistant/Tutor (2012-Present)
Department of Chemical Engineering, Curtin University, Bentley

Publications: Lau, P.W., R. Utikar, V. Pareek, S. Johnson, S. Kale, and A. Lali. 2013. "Modeling and Numerical Simulation of Liquid-Solid Circulating Fluidised Bed System for Protein Purification." *Chem. Eng. Res. Des.* 91(9): 1660-1673.

Kumar, P., P.W. Lau, S. Kale, S. Johnson, V. Pareek, R. Utikar, and A. Lali. 2014. "Kafirin Adsorption on Ion-Exchange Resins: Isotherm and Kinetic Studies." (Paper accepted by *J. Chromatogr. A*).

Kumar, P., P.W. Lau, S.B. Kale, A.M. Lali, V. Pareek, S. Johnson, and R.P. Utikar. 2014. "Investigations in Adsorption-Desorption Phenomena of Kafirin on Ion-Exchange Matrix." (Paper submitted to *Prep. Biochem. Biotechnol.*).

Lau, P.W., P. Kumar, R.P. Utikar, V.K. Pareek, S.B. Kale, A.M. Lali, S.K. Johnson. 2014. "Modeling and Simulation of LSCFB for Large Scale Purification of Kafirin." (To be submitted to *Chemical Engineering Journal*).

Lau, P.W., P. Kumar, V. Pareek, S. Johnson, S. Kale, and A. Lali. 2014. "Multi-Objective Optimisation (MOO) of Liquid-Solid Circulating Fluidised Bed (LSCFB) for Continuous Kafirin Purification using Ion-Exchange Chromatography." (Manuscript under preparation).

Publications:
(continued)

Lau, P.W., R. Utikar, V. Pareek, S. Johnson, S. Kale, and A. Lali. 2012. "Modelling and Numerical Simulation of Liquid-Solid Circulating Fluidised Bed Systems." In Chemeca 2012: Quality of Life Through Chemical Engineering, Wellington, New Zealand, 23-26 September 2012, 139-149. Barton, A.C.T.: Engineers Australia. (Conference Oral Presentation)

Lau, P.W., P. Kumar, R. Utikar, V. Pareek, S. Kale, and S. Johnson. 2013. "Kinetics of Kafirin Sorption and Desorption using Chromatography." In Chemeca 2013: Challenging Tomorrow 2013, Brisbane Convention and Exhibition Centre, Queensland/ Chemical College, Engineers Australia, 29 September – 2 October 2013, 30342. Brisbane, Q.L.D.: Chemeca 2013. (Conference Poster Presentation)

Lau, P.W., P. Kumar, R. Utikar, V. Pareek, S. Kale, A. Lali, and S. Johnson. "Modeling Continuous Kafirin Purification in LSCFB." In Bioprocessing India 2013, Indian Institute of Technology Delhi, India, 5-7 December 2013. New Delhi, India. (Conference Poster Presentation)